THE BELL SYSTEM TECHNICAL JOURNAL

Wideband, Bidirectional Lightguide Communication With an Optically Powered Audio Channel

By R. C. MILLER, B. C. De LOACH, T. S. STAKELON, and R. B. LAWRY

(Manuscript received December 29, 1981)

The feasibility of bidirectional speech-television communication over a single-strand lightguide, with emergency optical powering of the remote station telephone, has been demonstrated. The remote circuits drew ~250 µA at 0.9 volt from a double-heterostructure photovoltaic detector at 0.65 mW of received optical power; the detector low-pass response into 50 ohms was down 6 dB at 60 MHz. The optical packages featured GRIN-lens bidirectional couplers and, at the remote station, a low-threshold-current, buried-heterostructure laser.

I. INTRODUCTION

Lightguides connecting remote customer stations to a central switching office would make wideband telecommunications available to large markets. A two-wavelength, bidirectional link utilizing single-strand optical fiber might be economical compared to rechargeable batteries or auxiliary metallic conductors, particularly if used with an optical detector capable of powering the telephone channel during electric utility outage at a remote station. The feasibility of incorporating emergency optical powering into a wideband, two-way optical link is described below.

Both wideband and optically powered services can be realized with the GaAlAs photovoltaic diode used in previous demonstrations of

optically powered speech signalling[1] and sound alerting[2] at a remote station. This detector provides efficient photovoltaic conversion[3] along a high-resistance (3-kilohm) load line and short-circuit frequency response extending into the television carrier range. Since their capacitances are at least an order of magnitude larger than those of reverse-biased p-i-n diodes of comparable area, these devices must be used with low-input-impedance circuits at large bandwidths. This reduced high-frequency sensitivity is compensated for, at least in part, by the high light levels used in photovoltaic applications.

II. SIGNAL FORMAT AND OPTICAL METHODS

The block diagram of Fig. 1 identifies major components of the demonstration signalling stations. Each station transmitted and received a complete television channel and an audio bandwidth FM channel via a single-strand fiber lightguide. The local station depended entirely on electric utility power and the remote station only partly so. If utility power failed at the remote station, bidirectional speech and sound-alert capabilities were automatically maintained by photovoltaic conversion of optical power arriving from the local station. The local-station laser was continuously operated at high enough powers to ensure these capabilities regardless of how the remote station was being powered.

The remote-station laser was a low-operating-current, GaAs, buried-stripe heterostructure (BSH), producing 50 to 100 microwatts of single-ended power at wavelength $\lambda_2 = 0.885$ μm, predominately in the lowest-order spatial modes; the local-station laser was a planar stripe GaAlAs double heterostructure emitting up to 3 mW at wavelength $\lambda_1 = 0.84$ μm. The FM and TV signals, produced by microphone (MIC)-modulated variable-frequency oscillators (VFOS) and video-cassette recorders (TV-3) or color-bar generators (TV-4), were superimposed on adjustable laser bias currents. The laser emissions were focussed into short fiber pigtails by high-refractive-index glass microlenses and delivered to the transmission lightguide by GRIN-lens bidirectional couplers.[4] Each coupler utilized colinear quarter-period lenses, separated by a dielectric multilayer of high reflectivity at λ_1 and high transmission at λ_2, to obtain the wavelength combinations shown by the dashed line in Fig. 1.

Light of wavelength λ_1 was directed onto a GaAs double-hetero-structure photodetector in the remote station. High-frequency photo-current was capacitor-coupled to the FM and TV receivers, while the photovoltaic dc component provided steady-state operation of the FM receiver and of a low-duty-factor, pulse-amplitude-modulation (PAM) transmitter. In the absence of electric utility power, speech transmission switched automatically to this PAM standby channel. The micro-
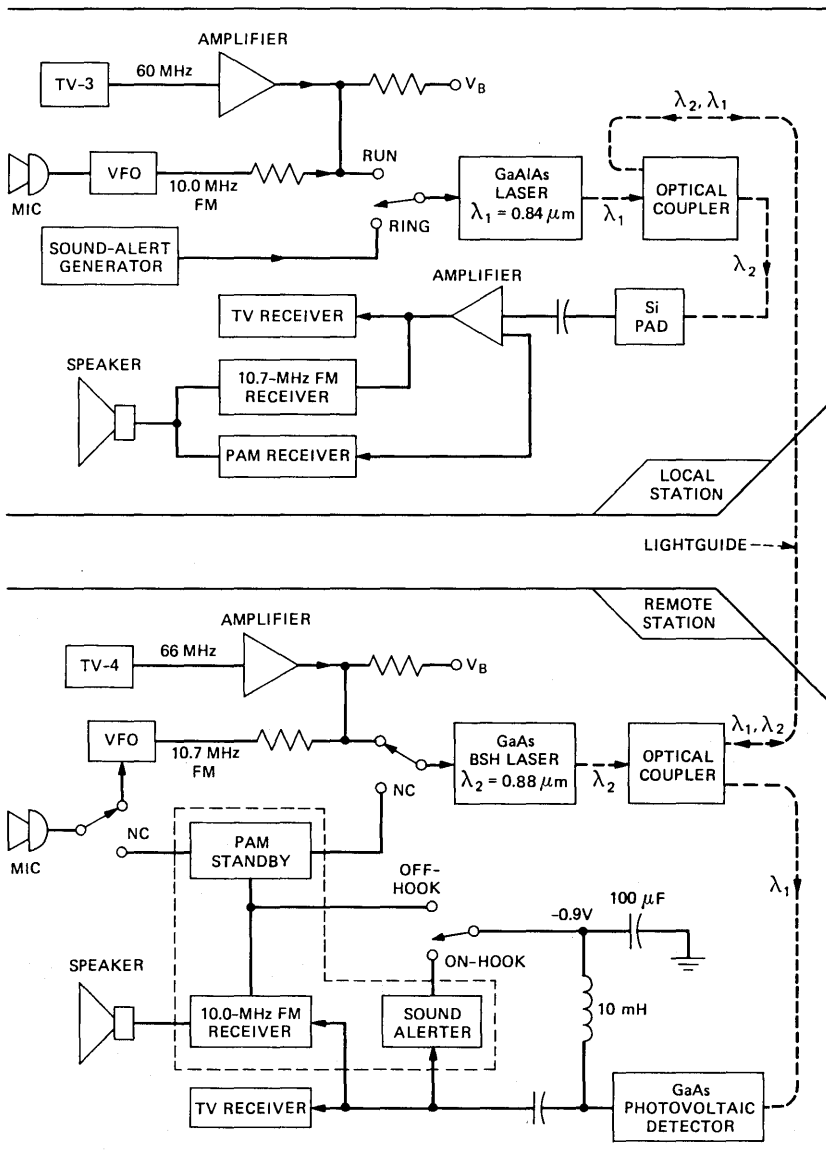
Fig. 1—Block diagram of optics and circuits in local and remote stations.

phone and speaker were housed in a telephone handset. When the handset was on-hook, a photovoltaic-powered sound alert could be activated by a manually controlled switch in the local station. Optical signals of wavelength λ_2 arriving at the local station were directed onto

a silicon avalanche photodetector (APD) connected via an impedance-matching transistor to the TV, FM, and PAM receivers.

III. IMPLEMENTATION

The quantum efficiencies and photovoltaic form factors measured at low frequencies for remote-station detectors were comparable with values reported[3] for similarly processed devices of the same nominal layer dopings and thicknesses. Design variations in the p-side contact diameter and in the diameter and depth of the proton-bombarded region produced device capacitances ranging between 30 and 1000 pF. Detectors near the lower end of this capacitance range had the typical small-signal frequency response illustrated in Fig. 2 and also exhibited short-circuit, pulsed-current decay times of 5 to 10 ns, consistent with reported[5,6] electron lifetimes. Although photovoltaic double-hetero-structure diodes are not optical detectors of choice in low-light-level, wideband applications, they provided acceptable reception of TV channels 3 and 4 at prevailing light levels when connected to untuned 75-ohm loads. Dispersion was not a factor in limiting the quality of television reception for the 0.5-km to 1.5-km-length graded-index light-guides used during various phases of this work.

Frequency modulation at 10.0 MHz was chosen for the telephony channel to maintain compatibility with simultaneous television recep-
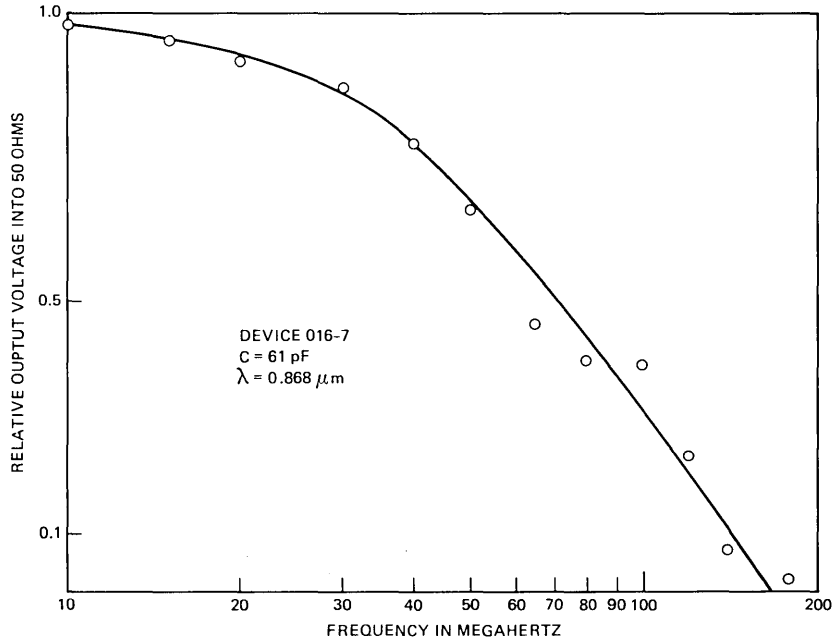
Fig. 2—Frequency response of GaAs photovoltaic detector with 50-ohm load.

tion, and particularly to avoid audio-frequency cross modulation of the TV displays. Strong FM limiting was provided at the local-station, variable-frequency oscillator in lieu of expending photovoltaic power to achieve amplitude limiting at the remote-station receiver. The receiver utilized a one-transistor FM → AM slope detector to obtain linear demodulation over a ±50 kHz range, followed by a two-transistor audio amplifier which produced comfortable sound volume (approximately 0.3 volt peak-to-peak) in a 600-ohm earphone. The receiver drew about 70 μA at 0.90 volt from the photovoltaic detector. During optically powered operation, the PAM transmitter produced 25- to 40-mA current pulses of 100-ns duration in the remote station laser at 12-kHz repetition rate.

The quarter-period graded-refractive-index (GRIN) lenses* used in the bidirectional couplers were 4.0 mm long and 1.5 mm in diameter. They were aligned along a common optical axis and cemented to a 1.1-mm-thick glass flat on which a long-wavelength-pass, sharp-transition, dielectric-multilayer filter had been deposited. (The filters were supplied by Optical Coating Laboratories, Inc. Design procedures for this type of edge filter are summarized by H. A. MacLeod.[7]) Three 100-cm-long, connectorized, lightguide pigtails were manipulated into optimum coupling position in a sequence that allowed some compensation for previous component misalignment, and were affixed to the GRIN-lens faces with ultraviolet-curing cement. The insertion losses versus wavelength of a typical bidirectional coupler, epoxied into an aluminum housing for protection, are shown in Fig. 3; combined losses of the coupler pair used in the present work were 1.5 dB or less in either channel. Crosstalk protection was particularly important at the local station where the power at λ_1 was much larger than at λ_2. The coupler provided approximately 30 to 35 dB of cross-talk protection, and a GaAlAs band-edge filter[1] cemented to the APD added an additional 17 dB. No crosstalk effects were observed at either station.

Graded-index, cabled lightguide of 50-μm core diameter and 0.22 numerical aperture was used throughout the final assembly. At either station the laser emission injected into the lightguide link was enhanced by thermally forming[8] a glass lens on the end of an optical fiber pigtail. Substantially hemispherical, 125-μm-diameter lenses in the refractive index range 1.9 to 2.1, made from low-melting-temperature glasses of high lead-oxide content, refracted 70 per cent of the laser output-facet emission into the optical guided modes. The lensed pigtail was epoxied into position relative to the laser to deliver maximum output power.

---

* These lenses were of the SLW type supplied by Orient Glass, Inc.
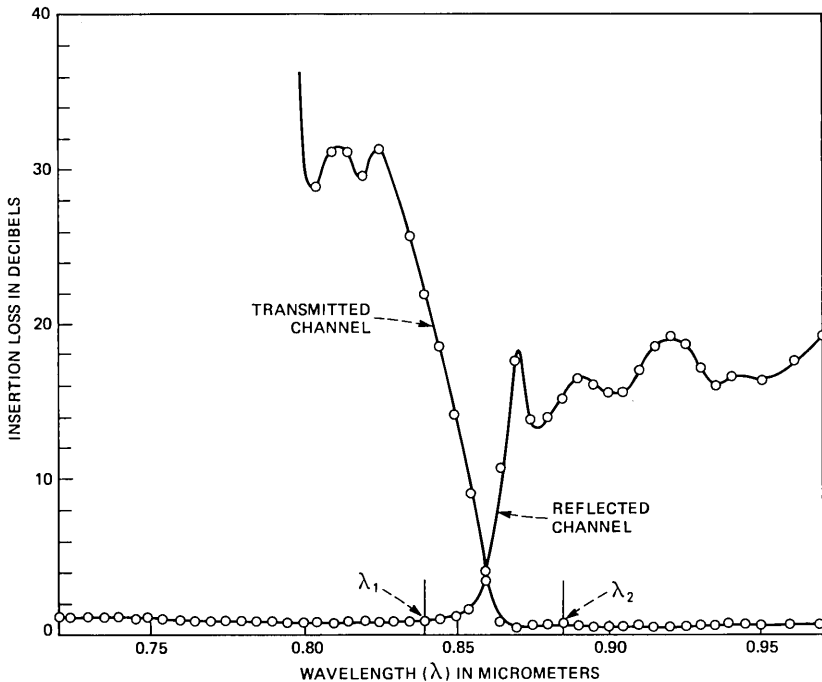
Fig. 3—Bidirectional characteristic of GRIN-lens coupler.

IV. PERFORMANCE

The local-station laser bias current was adjusted to produce a 0.90-volt dc level at the remote station, a photovoltage at which the optically powered circuits of Fig. 1 drew currents in the range of 220 to 280 μA. The optical power incident on the photovoltaic detector at wavelength $\lambda_1 = 0.84$ μm was 0.65 mW, yielding a 1.0-volt open-circuit voltage, 330-μA short-circuit current, and a photovoltaic power conversion efficiency of 0.34 at the circuit operating point. (Substantially larger efficiencies have been reported[3] for optimum loading at higher optical powers.) The cabled lightguide link was 0.5 km long. The loss at λ_1 was 4.7 dB, comprised of 1.5-dB laser-to-lightguide coupling loss, 1.2-dB bidirectional-coupler-pair insertion loss, and 2.0-dB lightguide transmission loss. Hence 2.0 mW of local-station laser emission were needed to power the remote station optically. This power was increased to 3 mW for sound alerting. Alerting relied on charge storage during silent portions of the sound-alert format to lessen the laser power requirements compared to an earlier[2] method; acoustic power bursts of about 0.3-mW peak and 0.5-second duration were generated at 1.4 kHz, the alerter resonant frequency.

Television reception via the optical link was subjectively indistin-

guishable from that obtained by connecting the receivers via 75-ohm cable to the TV-4 color-bar generator or to the video cassette TV-3 output. Speech reception of good commercial telephone quality was observed subjectively at either station under both electrically and optically powered conditions, and the transition between electrical and optical powering of the remote station occurred without significant alteration in audio quality.

V. CONCLUSIONS

The ability of double-heterostructure photovoltaic devices to detect high-frequency optical modulations, while providing efficient photovoltaic generation of dc power, has been established. The feasibility of bidirectional speech-television communication over a lightguide link, with speech communication capability during utility power outages at the remote station, was demonstrated.

VI. ACKNOWLEDGMENTS

REFERENCES

1. R. C. Miller and R. B. Lawry, "Optically Powered Speech Communication Over a Fiber Lightguide," B.S.T.J., *58,* No. 7 (September 1979), pp. 1735–41.
2. B. C. De Loach, Jr., R. C. Miller, and S. Kaufman, "Sound Alerter Powered Over an Optical Fiber," B.S.T.J., *57,* No. 9 (November 1978), pp. 3309–16.
3. R. C. Miller, B. Schwartz, L. A. Koszi, and W. R. Wagner, "A High-Efficiency GaAlAs Double-Heterostructure Photovoltaic Detector," Appl. Phys. Lett., *33* (October 15, 1978), p. 721.
4. S. Sugimoto et al., "High-Speed Digital-Signal Transmission Experiments by Optical Wavelength-Division Multiplexing," Elec. Lett., *13* (October 27, 1977), pp. 680–2.
5. R. J. Nelson and R. G. Sobers, "Minority-Carrier Lifetime and Internal Quantum Efficiency of Surface-Free GaAs," J. Appl. Phys., *49* (December 1978), p. 6103.
6. G. A. Acket, W. Nijman, and H. 't Lam, "Electron Lifetime and Diffusion Constant in Germanium-Doped Gallium Arsenide," J. Appl. Phys., *45* (July 1974), p. 3033.
7. H. A. MacLeod, *Thin-Film Optical Filters,* New York: American Elsevier, 1969.
8. L. D'Auria, Y. Combemale, C. Maronvalle, and A. Jacques, "High Index Microlenses for GaAlAs Laser-Fibre Coupling," Elec. Lett., *16* (April 24, 1980), pp. 322–4.

Equalization of Multimode Optical Fiber Systems

By B. L. KASPER

Decision feedback equalization (DFE) may provide a simple way to dramatically increase the bit rate on multimode optical systems. Computer simulations of digital multimode systems with tapped delay-line linear equalization and/or DFE are described. Results indicate that with relatively simple hardware it may be possible to increase by many times the usable bit rate on dispersion-limited optical channels, with a power penalty less than that for multilevel transmission and without the latter's complexity. For example, one could double the bit rate of a two-level system by paying an equalization power penalty of about 3 dB with DFE, whereas doubling the bit rate by going to four levels requires a penalty of 4.8 dB.

I. INTRODUCTION

It has been recognized for some time[1] that conventional linear equalization is of limited benefit in improving the performance of multimode optical fiber channels. The major reason is the rapid falloff in the equivalent baseband frequency response of the optical channel, which results in considerable noise enhancement when linear equalization is attempted using a filter which emphasizes the high frequencies.

However, for data rates above 100 Mb/s, multimode systems are generally modal dispersion rather than loss-limited[2] and some form of equalization is highly desirable. This is particularly true considering that index-grading imperfections in presently manufactured fibers produce a wide spread in fiber bandwidths and that equalization could improve the yield of usable fibers.

Decision feedback equalization (DFE) is known to be superior to linear equalization for channels which exhibit amplitude distortion.[3,4] Previous theoretical investigations[5,6] of DFE for fiber transmission systems have shown that power penalties are significantly lower than

those using linear equalization, with the improvement becoming greater as the amount of dispersion increases.

This paper gives the results of computer simulation of fiber optic channels for cases having no equalization, linear equalization via transversal filtering, and DFE both with and without a preceding stage of transversal equalization. We show that for pulses with either Gaussian or cosine-squared dispersion, decision feedback alone does a remarkably good job. A single DFE tap is adequate over a wide range of fiber bandwidths. A discussion of the effect of timing phase on DFE performance is included. The use of a transversal filter with minimum mean-square error (mse) tap weights preceding the DFE stage is found to produce little improvement in performance.

II. SYSTEM MODEL

To investigate the performance of various equalizers, the model shown in Fig. 1 was chosen. The input and output parameters of the model are shown and are explained below.

2.1 Transmitter

The input data sequence, $\{a_n\}$, consists of elements which are assumed to be independent identically distributed discrete random variables. These discrete amplitudes modulate the power of the transmitted pulse $p_t(t)$ at a rate $B = 1/T$ to produce the transmitted signal. Optical detectors produce an output current proportional to received power that is always positive; therefore, $p_t(t)$ which defines the pulse shape and the elements of $\{a_n\}$ which determine the pulse amplitudes must always be greater than or equal to zero. Input data sequence,
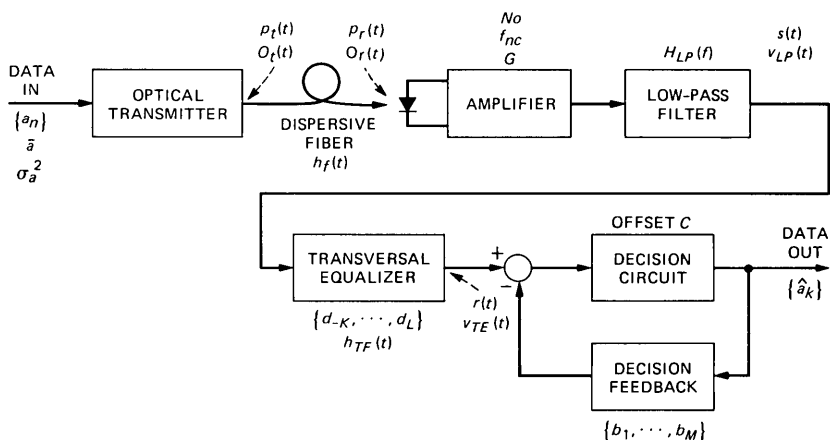
Fig. 1—Block diagram of optical system model showing important parameters.

$\{a_n\}$, has an expected value $\bar{a}$ and a variance σ_a^2. For the binary case, $a_n = 0$ or 1, we have $\bar{a} = 0.5$ and $\sigma_a^2 = 0.25$.

The transmitted optical signal is thus

$$O_t(t) = \sum_{n=-\infty}^{\infty} a_n p_t(t - nT),$$

where $O_t(t)$ is in units of optical power. The average transmitted power is

$$\langle O_t(t) \rangle = \bar{a} \int_{-\infty}^{\infty} p_t(t) dt.$$

The optical signal can be constrained by a limit in either average power or peak power.

2.2 Channel

The optical fiber has an impulse response $h_f(t)$ such that the received optical signal power is

$$O_r(t) = \int_{-\infty}^{\infty} O_t(\tau) h_f(t - \tau) d\tau.$$

The average received power will be

$$\langle O_r(t) \rangle = \int_{-\infty}^{\infty} O_r(t) dt$$

$$= \int_{-\infty}^{\infty} \int_{-\infty}^{\infty} O_t(\tau) h_f(t - \tau) dt d\tau$$

$$= \int_{-\infty}^{\infty} O_t(\tau) \int_{-\infty}^{\infty} h_f(t - \tau) dt d\tau$$

$$= \int_{-\infty}^{\infty} O_t(\tau) d\tau \int_{-\infty}^{\infty} h_f(t) dt$$

$$= \langle O_t(t) \rangle \cdot H_f(0),$$

where $H_f(0) = \int_{-\infty}^{\infty} h_f(t) dt$ is the dc or steady-state fiber loss.

The shape of an isolated received pulse will be

$$p_r(t) = p_t(t) * h_f(t),$$

where $*$ denotes convolution, hence the received signal can be expressed as

$$O_r(t) = \sum_{n=-\infty}^{\infty} a_n p_r(t - nT).$$

2.3 Detector and amplifier

The detector and amplifier together produce an output voltage $v_d(t)$ proportional to the received optical power, plus added noise $n(t)$,

$$v_d(t) = G[O_r(t) + n(t)],$$

where G is a gain constant.

In general,[7] the noise spectrum of receivers referred to the input can be characterized by a noise corner frequency, f_{nc}, above which the noise power increases at 6 dB/octave. Hence

$$N(f) = N_0[1 + (f/f_{nc})^2],$$

where N_0 is the low-frequency noise spectral density. This characterization is a good approximation for receivers employing either avalanche photodiode or p-i-n detectors, and either high impedance (integrating) or transimpedance amplifiers. It is assumed that $1/f$ noise can be neglected for bit rates of 100 Mb/s or more.

2.4 Low-pass filter

The amplifier in Fig. 1 is followed by a low-pass filter $H_{LP}(f)$ which attempts to maximize the s/n by eliminating high-frequency noise and by performing phase equalization on the received pulses. If linear equalization or DFE is employed following this filter, its optimum form[4] is known to be a whitening matched filter for the noise spectrum $N(f)$ and received pulse shape $p_r(t)$. Such a filter produces perfect phase equalization but does not perform amplitude equalization, hence intersymbol interference (ISI) will generally be present between pulses at its output, if the channel exhibits amplitude distortion. If additional equalization does not follow, then the low-pass filter should be used to reduce ISI through amplitude, as well as phase equalization. The desired goal is often a raised-cosine pulse which has zero-crossings at all other sampling instants. However, amplitude equalization results in the enhancement of noise at frequencies which are "bumped up," limiting the attainable s/n improvement.

In a practical repeater, $H_{LP}(f)$ will generally be some nonoptimum fixed filter. If subsequent equalization is included, the filter will be near-optimum as long as it passes frequencies where $p_r(t)$ has significant energy and rejects noise at frequencies where $p_r(t)$ has little energy. Phase equalization, if necessary, should be done here or by a following transversal equalizer. If phase equalization is not attempted, $H_{LP}(f)$ should have a linear phase characteristic to prevent the addition of phase distortion.

In this paper, no attempt is made to optimize $H_{LP}(f)$. A fixed filter is chosen with the optimization being left to later equalization stages.

2.5 Transversal equalizer

The transversal equalizer is illustrated in Fig. 2. The output $v_{TE}(t)$ consists of the weighted sum of delayed versions of the input $v_{LP}(t)$. The weighting coefficients are $\{d_k\}$ and the delay interval is T. Hence

$$v_{TE}(t) = \sum_{k=-K}^{L} d_k v_{LP}(t + kT).$$

A number of papers have been written about transversal equalizers, and their characteristics are well known. The design problem consists of choosing the number of leading and trailing taps L and K, and the weighting coefficients $\{d_k\}$. If $H_{LP}(f)$ is a whitening matched filter, then a synchronous equalizer with tap spacing, T, is known to be optimum.[4] If $H_{LP}(f)$ is suboptimum, then a fractionally spaced equalizer[8] with more frequent taps can be used to advantage. The extra degrees of freedom provided by more taps are used to approach the matched filter condition.

If decision feedback is used following the transversal equalizer, then it has been shown[4] that trailing taps which correspond to decision feedback taps can be eliminated. With enough DFE taps to cancel all pulse postcursors, only leading transversal taps are necessary. The coefficients $\{d_k\}$ are commonly chosen to either minimize peak distortion (the zero-forcing equalizer) or mse.[9]

The transversal equalizer can be viewed as an extension of the low-pass filter $H_{LP}(f)$. To eliminate ISI, it must shape the pulse spectrum to that of a Nyquist pulse. Frequencies attenuated by the channel, usually the higher frequencies, must be enhanced with the consequent penalty of increased noise. The advantage of using a transversal structure to accomplish this filtering is ease of adjustability, especially when the equalizer must be adapted to an originally unknown or slowly time-varying channel characteristic. However, as mentioned in the introduction, linear equalization of this type is known to be of little benefit for optical channels because of exorbitant noise enhancement.
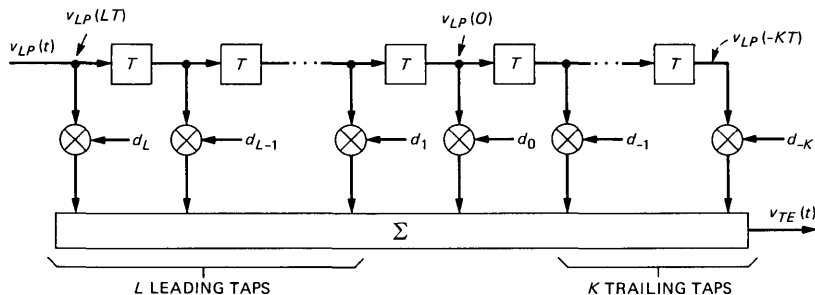
Fig. 2—Block diagram of transversal equalizer stage.

2.6 Decision feedback

The decision feedback stage is diagrammed in Fig. 3. A decision circuit or comparator produces estimates $\{\hat{a}_k\}$ of the transmitted data. A weighted sum of past decisions is subtracted from the incoming signal, with the weights $\{b_m\}$ being exactly equal to the amplitude of corresponding pulse postcursors at each sampling instant. Thus, if the decisions $\{\hat{a}_k\}$ are correct, then ISI from already-detected pulses is completely removed with no enhancement whatsoever of the noise.

An offset C is included to allow optimization of the decision threshold.

III. COMPUTER SIMULATIONS

The objective of the computer simulations is to compare the power penalties of different equalizers for various amounts of fiber dispersion. Inputs to the model include the number of DFE taps M, the number of leading and trailing transversal filter taps L and K, the low-pass filter response $H_{LP}(f)$, the receiver noise corner frequency f_{nc}, and the received pulse shape $p_r(t)$. Outputs consist of the receiver low-frequency noise level N_0 for an error probability of 10^{-9}, the optimum transversal tap weights $\{d_k\}$ and DFE tap weights $\{b_k\}$, and the equalized pulse shape $r(t)$.

3.1 Error probability bounds

The calculation of exact error probabilities in the presence of ISI plus noise is very complex, hence one generally resorts to various bounds. One common worst-case bound compares eye opening for the most adverse message sequence to the noise standard deviation. The criterion Q is defined as
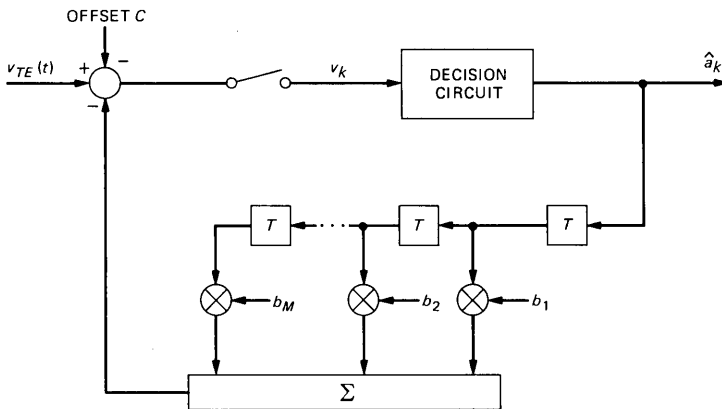
Fig. 3—Block diagram of decision feedback stage.

$$Q = \frac{0.5\left(r_o - \sum_{\substack{n \notin S \\ n \neq 0}} |r_n|\right)}{\sigma},$$

where

r_o = pulse height at sampling instant

r_n = pulse height (ISI) in other time slots

S = set of time slots equalized by decision feedback

σ = noise standard deviation.

This bound is relatively good if the ISI is large relative to the noise and is limited to only a few symbols, but it is pessimistic if ISI is small and extended over time, as the worst-case bit sequence will then occur only rarely. For this case, a better bound is obtained by approximating ISI by a normal distribution and adding its variance to the noise variance, giving the usual mse bound.[4,5]

Tighter bounds than either of these can be found at the expense of various degrees of computational complexity.[10]

The impulse response of optical fibers is typically found to resemble a Gaussian or a cosine-squared pulse.[11] Therefore, the ISI is limited to only a few adjacent symbols. In this situation, the worst-case eye opening or Q bound is a reasonably good choice.

3.2 Offset and decision feedback optimization

The optimum mse DFE for fiber optic systems has been analyzed by Messerschmitt.[5] Let the shape of an isolated pulse at the transversal filter output be denoted by $r(t)$:

$$r(t) = G[\,p_r(t) * h_{LP}(t) * h_{TF}(t)\,],$$

where

G = amplifier gain

$h_{LP}(t)$ = low-pass filter impulse response

$h_{TF}(t)$ = transversal filter impulse response

$$= \sum_{k=-K}^{L} d_k \delta(t + kT).$$

The decision threshold can be optimized by an offset C given by[5]

$$C = \lambda_0 G H_{LP}(0) H_{TF}(0) + \bar{a}\left[\sum_{n=-\infty}^{\infty} r_n - \sum_{m \in S} b_m - 1\right],$$

where λ_0 is the detector dark current and S is the set of DFE taps 1, $\cdots$, M. Also, the decision feedback tap weights are optimized by setting

$$b_m = r_m, \, m \in S.$$

The values r_m are sampled versions of $r(t)$, with r_o corresponding to the instant at which the pulse is sampled for detection. With the above choice of DFE tap weights, we have

$$C = \lambda_0 G H_{LP}(0) H_{TF}(0) + \bar{a} \left[\sum_{n \notin S} r_n - 1 \right].$$

With the above choices of C and $\{b_m\}$, and assuming correct decisions, the mse is shown to be[5]

$$\text{mse} = E[(v_k - \hat{a}_k)^2]$$

$$= \sigma_a^2 \left[\sum_{n \notin S} r_n^2 - 2r_o + 1 \right] + \sigma^2,$$

where

$$\sigma^2 = \text{noise variance}$$

$$= E[[Gn(t) * h_{LP}(t) * h_{TF}(t)]^2].$$

As before, $n(t)$ is the receiver noise (thermal plus shot noise) referred to the receiver input. Note that only terms r_n, $n \in S$ (i.e., no corresponding DFE taps) contribute to mse.

3.3 Transversal filter optimization

The problem of determining optimum transversal filter tap weights $\{d_k\}$ when decision feedback is used was first solved by Austin.[12] In matrix form, the solution can be expressed as

$$\mathbf{D} = \mathbf{A}^{-1}\alpha,$$

where

$$\mathbf{D} = \text{vector of tap weights}$$

$$= [d_{-K}, d_{-K+1}, \cdots, d_L]^T$$

$$\mathbf{A} = \psi + \frac{1}{\sigma_a^2} \phi$$

$$\phi = \text{noise covariance matrix of terms } \phi_{km}$$

$$\phi_{km} = \phi_{k-m} = \int_{-\infty}^{\infty} N(f) H_{LP}(f) e^{-j(k-m)2\pi fT} df$$

ψ = modified signal autocorrelation matrix of terms ψ_{km}

$$\psi_{km} = \sum_{n \notin S} s_{n+k} s_{n+m}$$

$$\alpha = [s_{-K}, s_{-K+1}, \cdots, s_L]^T$$

s_k = sample of isolated pulse at low-pass filter output

$$= s(kT)$$

$$s(t) = G[p_r(t) * h_{LP}(t)].$$

The matrix

$$\mathbf{A} = \psi + \frac{1}{\sigma_a^2} \phi$$

is symmetric and positive semidefinite, hence it is invertible, except in extreme cases unlikely to be encountered in practice. The above solution for the tap weight vector $\mathbf{D}$ minimizes mse. This criterion may not produce the best bound on the probability of error, but is used here because it is the only bound for which optimum tap weights are known to have been formulated.

3.4 Power penalty calculation

Equalization power penalties are computed by assuming that the received pulse $p_r(t)$ has unit area (i.e., unit energy) and solving for the receiver noise level N_0 which will produce an error probability of 10^{-9}. Because the transversal filter coefficients $\mathbf{D}$ are dependent upon the noise covariance matrix ϕ, which is itself proportional to N_0, an iterative solution is necessary. The simulation program allows the operator to enter an initial value for N_0, and Newton-Raphson iteration is then used to converge to a final solution for both N_0 and $\mathbf{D}$.

An error probability of less than 10^{-9} is assured by making Q equal to 5.99781. The eye opening E in the presence of decision feedback is calculated as

$$E = r_o - \sum_{\substack{n \notin S \\ n \neq 0}} |r_n|,$$

while the noise standard deviation is

$$\sigma = [N_0 \mathbf{D}^T \phi \mathbf{D}]^{1/2}.$$

Iteration proceeds by assuming a value for N_0 and calculating the corresponding tap weights $\mathbf{D}$. The eye opening and σ, plus their derivatives with respect to N_0, can then be found, allowing new values of N_0 to be calculated until the ratio $Q = 0.5E/\sigma$ converges to 5.99781.

3.5 Timing phase optimization

When decision feedback with no transversal equalizer was analyzed, or when only leading or anticausal transversal taps were specified, the power penalties were found to depend heavily upon timing phase. Optimization was carried out by simply advancing the sampling time (i.e., delaying the pulse) and finding the delay which resulted in the lowest power penalty.

IV. RESULTS

4.1 Gaussian dispersion and equalizing filter

Fibers with perfect mode mixing exhibit Gaussian dispersion and have an impulse response given by

$$h_f(t) = \frac{1}{\sqrt{2\pi}\alpha T}\, e^{-[t^2/2(\alpha T)^2]}.$$

The baseband frequency response is

$$H_f(f) = e^{-[(2\pi\alpha Tf)^2/2]},$$

and the 6-dB electrical bandwidth is

$$f_{6\,\mathrm{dB}} = \frac{1}{2\pi\alpha T}\,\sqrt{2\ln 2}$$

$$= 0.1874/\alpha T.$$

Figures 4, 5, and 6 show power penalties for rectangular nonreturn to zero (NRZ) pulses transmitted over such a fiber. An NRZ pulse is defined by

$$x(t) = \begin{cases} 1, -\dfrac{T}{2} \le t \le \dfrac{T}{2} \\[2mm] 0, \text{ elsewhere} \end{cases}$$

$$X(f) = \frac{1}{\pi f}\sin \pi f T.$$

The low-pass filter $H_{LP}(f)$ is chosen to produce a Nyquist output pulse with a raised cosine characteristic[7] and an excess bandwidth of $\beta = 0.5$ for an NRZ input pulse. The output pulse spectrum is

$$Y(f) = \begin{cases} 1, 0 \le |f| \le \dfrac{B}{2}(1-\beta) \\[3mm] \dfrac{1}{2}\left[1 - \sin\dfrac{\pi}{\beta}\left(\dfrac{f}{B} - \dfrac{1}{2}\right)\right], \dfrac{B}{2}(1-\beta) < |f| < \dfrac{B}{2}(1+\beta) \\[3mm] 0, \text{ elsewhere}, \end{cases}$$

hence the required low-pass filter characteristic is

$$H_{LP}(f) = \begin{cases} \dfrac{Y(f)}{X(f)}, \ |f| < \dfrac{B}{2}(1+\beta) \\ 0, \text{ elsewhere}. \end{cases}$$

For zero fiber dispersion, this low-pass filter produces a Nyquist output pulse with no ISI. The ISI will be produced by fiber dispersion and will increase as the fiber bandwidth decreases.

Power penalties in the following results are calculated relative to ideal matched-filter detection of an isolated NRZ pulse with zero dispersion.

4.1.1 White noise ($f_{nc} > B$)

An actual optical receiver will not generally have a white noise spectrum. With a high-gain APD, for example, the noise is proportional to the received signal and so is time dependent. However, as a worst-case situation, one may assume stationary white noise with a level equal to that for the most adverse message sequence.

Figure 4 shows power penalties for a white receiver noise spectrum. The four curves are for A—no additional equalization; B—11-tap transversal equalizer; C—five DFE taps plus 11-tap transversal equalizer; and D—five taps of decision feedback with optimized timing
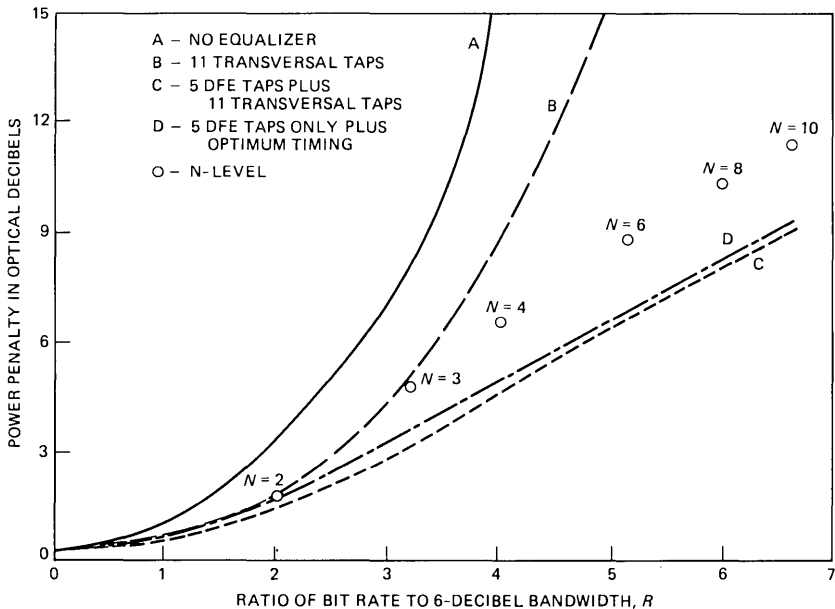
Fig. 4—Power penalties versus ratio of bit rate to fiber bandwidth for Gaussian dispersion, equalizing low-pass filter, and white noise.

phase but no transversal equalizer. Also shown are power penalties for multilevel signaling which are discussed in Section 4.5.

The horizontal axis values are in terms of a variable R given by

$$R = \frac{\text{bit rate } B}{6\text{-dB electrical bandwidth (3-dB optical)}}.$$

As the 6-dB channel bandwidth becomes less than the Nyquist frequency (i.e., $R > 2$), DFE plus linear equalization (curve C) begins to perform much better than linear equalization alone (curve B). Most notable, however, is that DFE only (curve D) does nearly as well as DFE plus linear, and beyond $R = 4.5$ remains within 0.2 dB. The addition of a transversal equalizer stage prior to DFE produces almost no improvement. The reason for this is that the transversal tap weights have been chosen to minimize mse, whereas the criterion of goodness is the ratio of eye opening to noise standard deviation. The problem is that almost all of the ISI is due to one large immediate precursor. The mse algorithm seeks to minimize the sum of the square of this precursor and the noise variance. To reduce the ISI, it must allow the noise to increase, which it does to such a degree that according to the eye opening criterion very little has been gained.

Prior to adoption of the eye opening criterion, an attempt was made to use mse as the power penalty measure. However, this criterion proved to be extremely pessimistic in the absence of a transversal equalizer. The mse is dominated by a few large ISI values and indicated very high-power penalties. However, the eye opening criterion showed the actual penalties to be much smaller.

4.1.2 Colored noise ($f_{nc} = B/3$)

The curves in Fig. 5 were obtained assuming a receiver noise spectrum which increases with frequency. The noise corner frequency is chosen as $f_{nc} = B/3$, and is based upon parameters of a typical p-i-n/FET receiver operating at 100 Mb/s as described in the Appendix.

In comparing Figs. 5 and 4, note the difference of 1.12 dB in the 0-dB reference levels (i.e., matched-filter detection is 1.12 dB worse for colored noise than for white noise). Disregarding this baseline shift, curves A and D in both figures are identical, as should be expected, because with no transversal equalizer the error rate depends only on the noise variance and not on the shape of the noise spectrum. The addition of a transversal equalizer does not help as much as in the white noise case. The reason is that a linear equalizer works by enhancing high frequencies which now contain more noise than they did for white noise.

Comparing curves C and D, we see that the addition of a transversal
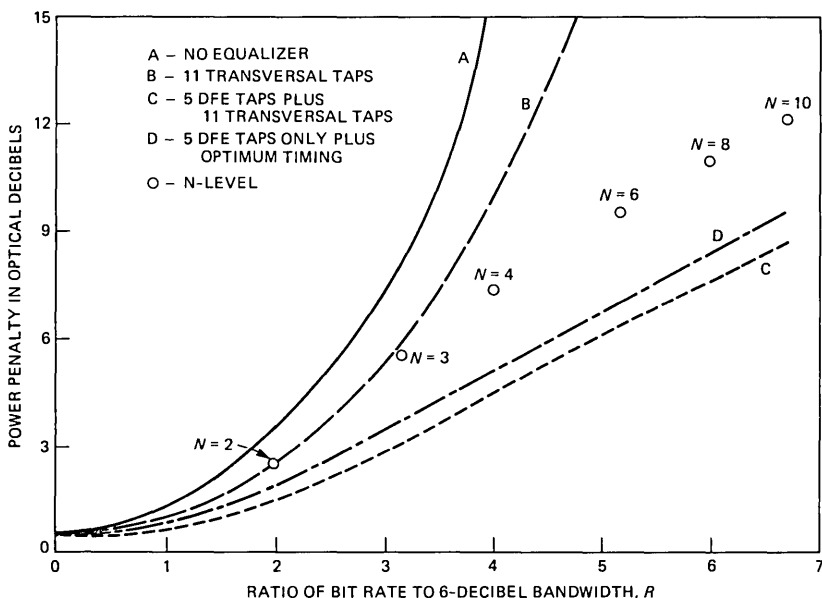
Fig. 5—Power penalties for Gaussian dispersion, equalizing low-pass filter and colored noise with $f_{nc} = B/3$. Receiver noise spectrum corresponds to a p-i-n FET receiver as described in the Appendix.

equalizer improves the power penalty by about 1 dB over DFE alone. As DFE removes much of the ISI, the transversal stage is able to decrease the mse by acting to reduce high-frequency noise. It can be expected that the choice of a fixed low-pass filter $H_{LP}(f)$ with a lower 3-dB frequency than $B/2$ would produce similar power penalty improvements for DFE only. A narrower $H_{LP}(f)$ would not affect ISI significantly if the channel bandwidth is already less than the low-pass filter bandwidth.

For cases where f_{nc} is lower than $B/3$ as assuméd here, the choice of a minimum $H_{LP}(f)$ bandwidth becomes more crucial because the amount of high-frequency noise increases. Decision feedback equalization is very important in such cases as it provides a way of noiselessly eliminating the ISI introduced by a narrow low-pass filter.

4.1.3 One decision feedback tap

The curves in Fig. 6 are for white noise with five DFE taps plus optimum timing phase and one DFE tap plus optimum timing phase. Up to a bit rate of 3.5 times the 6-dB bandwidth, the curves remain within 0.4 dB of one another. Hence, a single DFE tap with no transversal equalizer, which in hardware would require one flip-flop, a summer and a weighting network, does a remarkably good job of
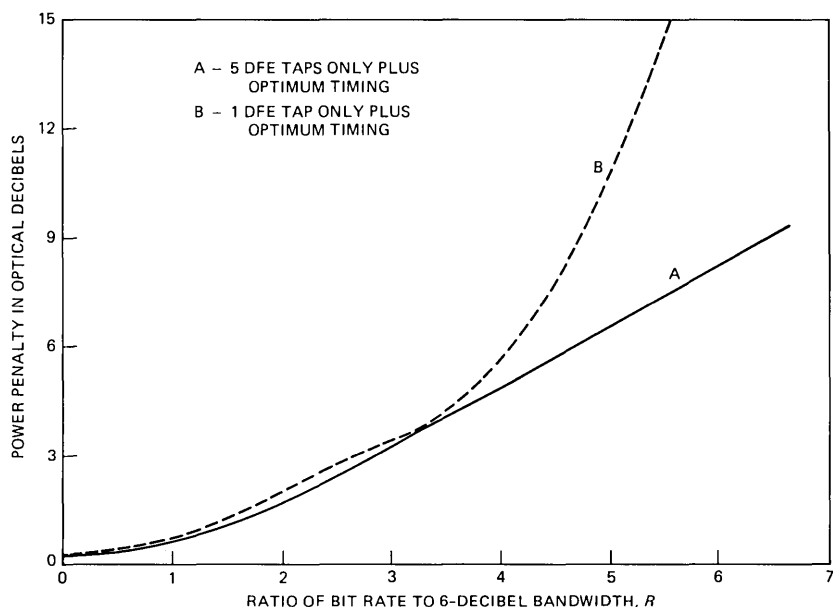
Fig. 6—Power penalties for decision feedback alone. Gaussian dispersion, equalizing low-pass filter and white noise.

equalization for Gaussian dispersion. The reason for this success is that up to $R = 3.5$, almost all of the ISI is due to one large postcursor (provided sampling is done before the pulse peak), and one DFE tap can remove this ISI completely.

4.2 Gaussian dispersion and Bessel filter

The raised cosine low-pass filter used in the previous cases could be difficult to design in practice. Therefore, it is of interest to see what happens with an ordinary realizable filter, in this case a 5th order maximally linear phase or Bessel filter, with a 3-dB bandwidth of $B/2$. The exact low-pass filter response is

$$H_{LP}(f) = \cfrac{1}{\left[1 - 10.47\left(\frac{f}{B}\right)^2 + 8.832\left(\frac{f}{B}\right)^4\right] + j\frac{f}{B}\left[4.855 - 12.70\left(\frac{f}{B}\right)^2 + 2.859\left(\frac{f}{B}\right)^4\right]}.$$

Results for white receiver noise and Gaussian dispersion are shown in Fig. 7.

Compared to Fig. 4, the power penalty for no equalization is higher
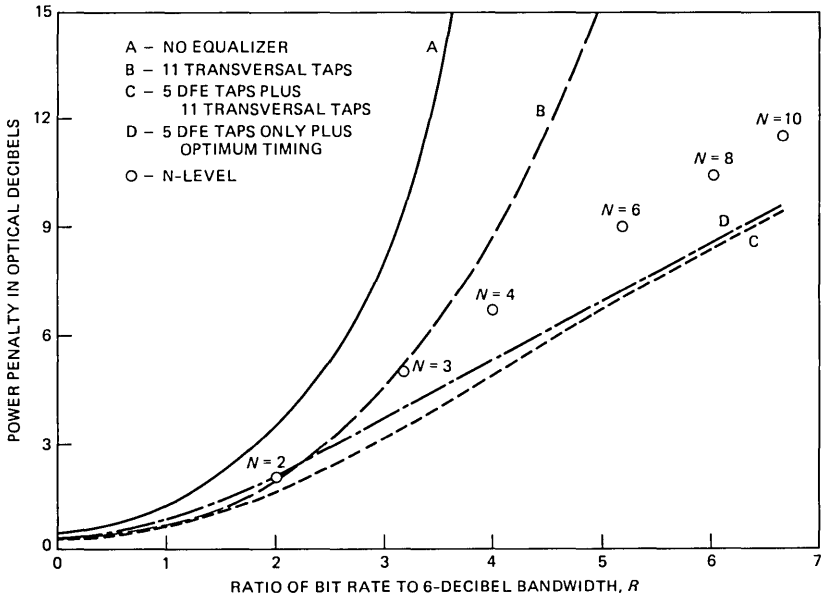
Fig. 7—Power penalties for Gaussian dispersion, Bessel low-pass filter and white noise. The low-pass filter is a 5th order maximally linear phase Bessel filter with a 3-dB bandwidth of $B/2$.

after $R = 2.5$ as expected because the Bessel filter does a poorer job of equalization than the previous low-pass filter. The linear equalization curves are identical because the transversal filter can compensate for a poorer choice of $H_{LP}(f)$. Both decision feedback curves show penalties less than 0.3 dB greater than those in Fig. 4, which would indicate that the choice of low-pass filter is not too critical.

4.3 Cosine-squared dispersion and equalizing filter

Measurements of actual fibers indicate that a cosine-squared pulse shape is often more representative of the actual impulse response than a Gaussian.[11] Power penalties for NRZ pulses transmitted over a fiber with cosine-squared dispersion are shown in Fig. 8. The receiver noise spectrum is white and the low-pass filter produces $\beta = 0.5$ raised cosine equalization for an NRZ pulse with zero dispersion.

Compared to Fig. 4, we see that linear equalization is much less effective for cosine-squared dispersion than for Gaussian dispersion. The reason for this is found by considering the channel's bandpass characteristic. If its impulse response $h(t)$ is given by

$$h_f(t) = \begin{cases} 2/\tau \cos^2 \dfrac{\pi t}{\tau}, & -\tau/2 \le t \le \tau/2 \\ 0, & \text{elsewhere}, \end{cases}$$
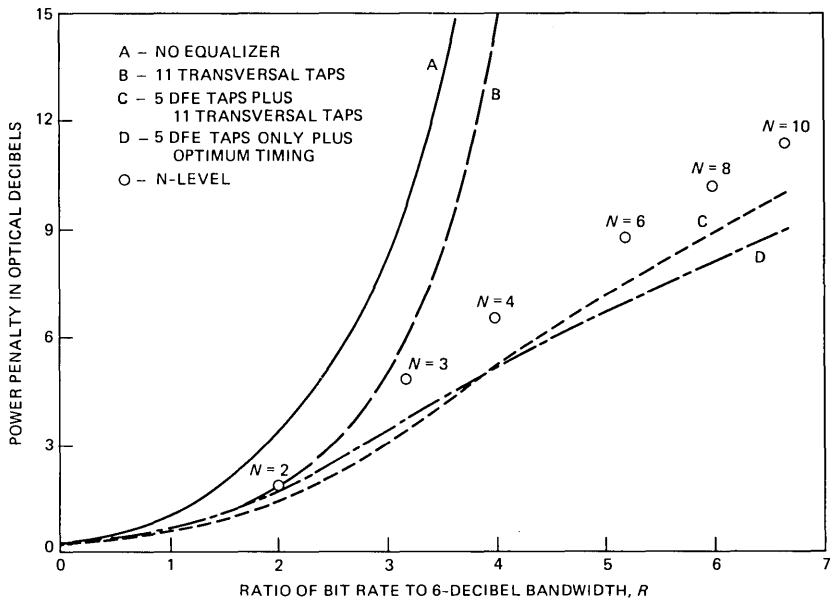
Fig. 8—Power penalties for cosine-squared dispersion, equalizing filter, and white noise.

then the baseband frequency response is

$$H_f(f) = \frac{\sin \pi f \tau}{\pi f \tau} \left[\frac{1}{1 - f^2 \tau^2} \right].$$

The channel will have nulls wherever $\sin \pi f \tau = 0$ (except at $f = 0$ and $f = 1/\tau$). As is well known, a linear equalizer would need infinite gain to correct for such nulls, resulting in infinite noise enhancement.

The DFE alone is able to perform equally as well for cosine-squared dispersion as for Gaussian. However, DFE plus linear equalization is somewhat worse than DFE alone above $R = 4.0$. The choice of minimum mse tap weights appears to be particularly bad for cosine-squared dispersion.

4.4 Dependence on timing offset

To increase the effectiveness of decision feedback in eliminating ISI, one should arrange to have as much of the ISI as possible come from pulses which have already been received (postcursors) and for as little as possible to come from future pulses (precursors). The simplest way to do this is to advance the sampling instant such that decisions are made on the leading edge of the pulse rather than on the center of the pulse. Because optical pulses are generally quite limited in duration
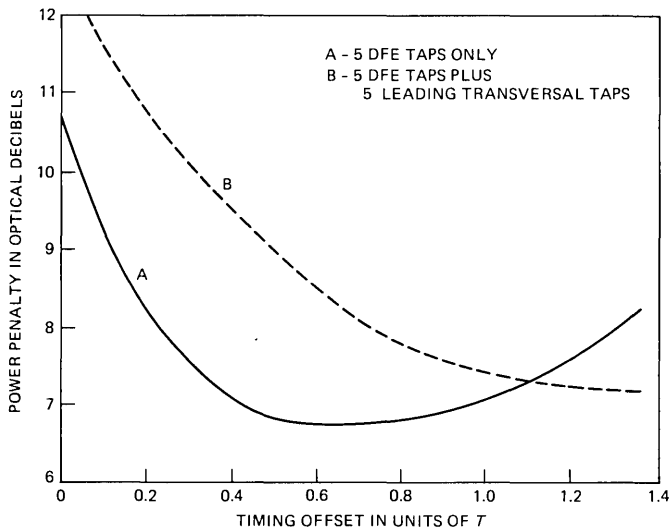
Fig. 9—Power penalties versus sampling time advance for cosine-squared dispersion. Ratio of bit rate to fiber 6-dB bandwidth is $R = 5.0$. Equalizing low-pass filter and white noise are assumed.

and do not have extensive post- and precursors, this simple technique combined with DFE may offer a substantial improvement in performance.

Figs. 9 and 10 show calculated power penalties versus timing offset for cosine-squared and Gaussian dispersion when $R = 5.0$. The receiver noise is white, and an equalizing low-pass filter is assumed. The solid curves are for five DFE taps only, whereas the dashed curves are for five DFE taps plus five leading transversal taps.

For DFE only, advancing the sampling time by 0.6 of a bit interval improves the power penalty by 4.0 and 2.6 dB in these two cases. Improvements are also produced for DFE plus linear equalization, with the optimum timing advance being greater than one bit interval.

To illustrate the effect of offset sampling, consider the example in Fig. 11. The pulses are produced by convolving a rectangle of width T with a Gaussian having a standard deviation of 0.937 T, equivalent to a channel bandwidth of $B/5$. With DFE, only precursor ISI is important. The eye openings for (a) a centrally sampled pulse and (b) a pulse-sampled 0.5 T earlier will be

(a)
$$E = r_0 - \sum_{\substack{n \notin s \\ n \neq 0}} |r_n|$$

$$= 1.0 - 0.58 - 0.10 = 0.32$$

(b)
$$E = 0.87 - 0.29 - 0.02 = 0.56.$$
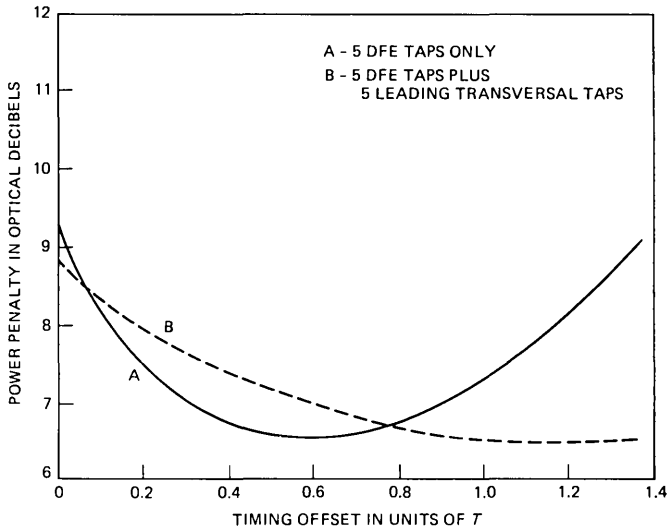
Fig. 10—Power penalty versus sampling time advance for Gaussian dispersion.
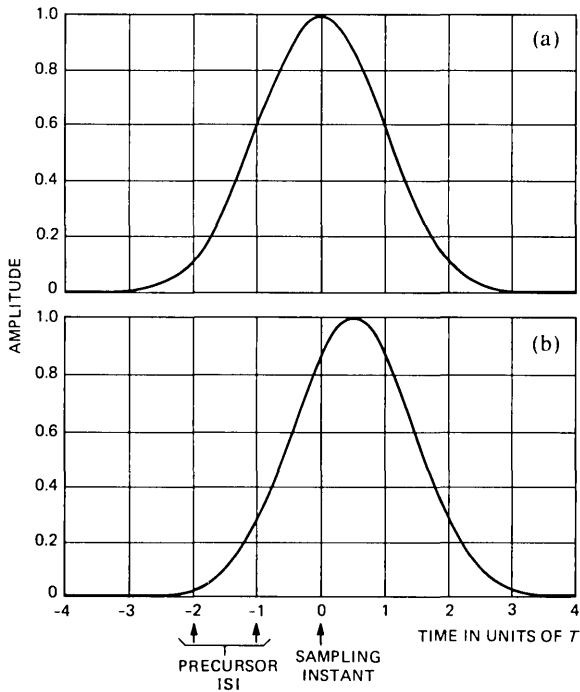
Fig. 11—Pulse waveforms with Gaussian dispersion to illustrate the advantages of sampling prior to the center of the pulse. (a) Central sampling. (b) Sampling advanced by 0.5 T.

The larger eye opening with advanced sampling produces a 2.4 dB-optical power penalty improvement, as σ is the same in both cases.

One disadvantage of advancing the sampling time is that it will increase the likelihood of DFE error propagation. This likelihood is dependent upon the DFE tap weights, and will increase with timing advance because the postcursors become both larger in amplitude and more extended in duration. Therefore, the improvement in power penalty will not be as large in practice as indicated above. However, the gains can be expected to be much greater than the losses, because doubling the size of the eye opening through DFE can reduce the probability of error by perhaps four orders of magnitude, whereas the increase in the error rate because of error propagation cannot be more than 2^M where M is the number of DFE taps.[13]

A most interesting point is that theoretical derivations of the optimum transversal filter for use with decision feedback have always concluded that a one-sided transversal filter is optimal and that no taps following the peak of a matched-filter pulse are necessary.[3,4,14] This implies a timing phase such that sampling coincides with the peak of the pulse. However, the simulation results herein show that advanced sampling leads to better performance. One way to obtain the necessary optimal timing phase is to have a few trailing transversal taps which can delay the pulse relative to the sampling instant. Hence, 11 transversal taps with five leading and five trailing were found to perform much better than five leading taps only.

4.5 Comparison of DFE and multilevel signaling

The use of DFE more closely approximates the use of partial-response[9] or multilevel signaling than the use of traditional linear equalization. Binary signals transmitted at a rate greater than twice the optical-channel, 6-dB bandwidth will always contain ISI when received. The received level, however, is a predictable function of the transmitted message sequence. Decision feedback provides a simple way of decoding the multiple received levels back into the transmitted binary digits.

It is useful to compare the previous DFE power penalties to those which one could expect for multilevel signaling. Consider the case of Gaussian dispersion and white receiver noise. For two-level transmission, one might operate at a symbol rate equal to twice the channel's 6-dB bandwidth (i.e., $R = 2$). Very good linear equalization would be needed to prevent ISI, hence from curve B of Fig. 4 the power penalty for two-level transmission would be 1.8 dB. For N-level transmission, there is an additional power penalty of $10 \log_{10}(N - 1)$ dB, with a factor of $\log_2 N$ increase in R. Total power penalties for multilevel transmission for the various combinations of receiver noise spectra,

low-pass filters, and fiber impulse responses considered previously are included in Figs. 4, 5, 7, and 8. In all cases, both DFE plus transversal equalization and DFE only show better performance than multilevel signaling at the same bit rate. For example, by using DFE doubling R from 2 to 4 results in a penalty of about 3 dB in all cases, whereas doubling R by using 4-level signaling results in a penalty of 4.8 dB. For tripling to $R = 6$, DFE is consistently better than 8-level signaling by at least 2 dB.

Hence, DFE may offer a way of obtaining the performance of multilevel optical transmission without many of the latter's disadvantages. For instance, only two-level (on-off) transmitter modulation is needed. Also, complex linear equalization to prevent ISI is unnecessary. The hardware to implement DFE is extremely simple.

V. CONCLUSIONS

The main conclusion is that DFE offers substantial benefits for multimode optical fiber systems. Channels which are presently dispersion-limited could potentially be operated at many times the existing bit rate with a power penalty less than that for multilevel signaling. The hardware required to implement the necessary equalization can be extremely simple as transversal filters are not a necessary component and no special filtering need be included. In addition, the characteristics of an optical channel are very stable, making circuitry for continuous adaptability unnecessary.

A good deal of theoretical work remains. For transversal equalizers, a new technique of selecting tap weights besides the traditional zero-forcing or minimum mse algorithms must be developed. For decision feedback, further investigation of error propagation is needed. Attention should be given to optimizing the sampling time and to its effects on the probability of error propagation. Sensitivity to errors in the sampling time should also be considered.

Experimental confirmation of the simulation results described above is also very desirable, and work along these lines is now proceeding.

APPENDIX

P-i-n FET Receiver Parameters and Noise Corner Frequency

According to Smith and Personick,[7] the noise corner frequency is given by

$$f_{nc} = \frac{1}{2\pi C_T} \left[\frac{d\langle i^2(\omega)\rangle_{eq}/df}{d\langle e_a^2(\omega)\rangle/df} + \frac{1}{R_{in}^2} \right]^{1/2}.$$

For a p-i-n FET receiver, we have

$$\frac{d}{df} \langle i^2(\omega) \rangle_{\text{eq}} = \text{equivalent input shunt}$$
$$\text{current noise source}$$

$$= \frac{4kT}{R_L} + 2qI_{\text{gate}} + 2qI_{\text{dark}}$$

$$\frac{d}{df} \langle e_a^2(\omega)() \rangle = \text{equivalent input series}$$

$$\text{voltage noise source}$$

$$= \frac{4kT\Gamma}{g_m}.$$

Some typical parameter values for a good p-i-n FET receiver at a bit rate of $B = 100$ Mb/s are

$$R_{\text{in}} = R_L = 1 \text{ M}\Omega$$

$$C_T = 1 \text{ pF}$$

$$g_m = 50 \text{ ms}$$

$$\Gamma = 1.75$$

$$I_{\text{gate}} = 10 \text{ nA}$$

$$I_{\text{dark}} = 10 \text{ nA}.$$

With the above values, one obtains a noise corner frequency of $f_{nc} = 31.7$ MHz $\simeq B/3$.

REFERENCES

1. S. D. Personick, "Receiver Design for Digital Fiber Optic Communication Systems I," B.S.T.J., *52* (July–August 1973), pp. 843–74.
2. K. Ogawa et al., "System Experiments Using 1.3 μm LEDs," Electronics Letters, *17,* No. 2 (January 1981), pp. 71–2.
3. J. Salz, "Optimum Mean-Square Decision Feedback Equalization," B.S.T.J., *52,* No. 8 (October 1973), pp. 1341–73.
4. M. S. Mueller and J. Salz, "A Unified Theory of Data-Aided Equalization," B.S.T.J., *60,* No. 9 (November 1981), pp. 2023–38.
5. D. G. Messerschmitt, "Optimum Mean-Square Equalization for Digital Fiber Optic Systems," Proc. Int. Conf. Commun., June 1975, pp. 43.2–5.
6. D. G. Messerschmitt, "Minimum MSE Equalization of Digital Fiber Optic Systems," IEEE Trans. Commun., *Com-26,* No. 7 (July 1978), pp. 1110–8.
7. R. G. Smith and S. D. Personick, "Receiver Design for Optical Fiber Communication Systems," *Semiconductor Devices for Optical Communication,* H. Kressel, ed., New York: Springer-Verlag, 1980, Chapter 4.
8. R. D. Gitlin and S. B. Weinstein, "Fractionally Spaced Equalization: An Improved Digital Transversal Equalizer," B.S.T.J., *60,* No. 2 (February 1981), pp. 275–96.
9. R. W. Lucky, J. Salz, and E. J. Weldon, Jr., *Principles of Data Communication,* New York: McGraw-Hill, 1968.

10. B. R. Saltzberg, "Intersymbol Interference Error Bounds with Application to Ideal Bandlimited Signaling," IEEE Trans. Inform. Theory, *IT-14*, No. 4 (July 1968), pp. 563–8.
11. M. J. Buckler, private communication.
12. M. E. Austin, "Decision-Feedback Equalization for Digital Communication Over Dispersive Channels," M.I.T. Research Laboratory of Electronics, Technical Report 461, August 11, 1967.
13. D. L. Duttweiler, J. E. Mazo, and D. G. Messerschmitt, "Error Propagation in Decision-Feedback Equalizers," Rec. Int. Conf. Commun., Minneapolis, July 1974, Paper No. 25E.
14. P. Monsen, "Feedback Equalization for Fading Dispersive Channels," IEEE Trans. Inform. Theory, *IT-17* (January 1971), pp. 56–64.

Frequency-Hopped Single-Sideband Modulation for Mobile Radio

By V. K. PRABHU and R. STEELE

A frequency-hopped single-sideband (SSB) modulation with pilot tone (FH-SSB-PT) transmission scheme is described for mobile radio. The single-sideband signal changes its carrier frequency every τ seconds, and the sequence of carrier frequencies is controlled by a suitable scrambling code. Co-channel cells using the same frequency band in the mobile radio system use different scrambling codes with the result that co-channel interference is altered from cross-talk to random noise if τ is small. In the presence of Rayleigh fading, frequency hopping improves reception for stationary vehicles, and does not degrade the performance for moving vehicles. Further, the technique of frequency hopping may offer communications privacy. Expressions for s/n are derived for SSB, SSB plus pilot tone, and FH-SSB-PT in the presence of Rayleigh fading. Co-channel interference effects are also considered.

I. INTRODUCTION

Mobile radio telephone systems are required to operate in a hostile environment compared to radio systems using terrestrial and satellite links. The transmission channel is time varying in a manner dependent on the vehicle speed and location, distribution of buildings and terrain, siting of fixed antennas relative to the mobile, the effect of other mobiles, to mention but a few. Paramount of the design objectives is a high user density with good uninterrupted communication at a reasonable cost. To achieve these goals, a number of system concepts have been advocated,[1,2] and a developmental system to provide Advanced Mobile Phone Service (AMPS) is currently being operated by Illinois Bell Telephone Company in the Chicago Area.[3]

Unlike conventional telephony where extra demand on communication capacity can be accommodated by additional links, the mobile

radio spectrum is limited. To increase capacity, the area must be divided into cells and the RF band must be reused. Although mobiles in adjacent cells can be arranged not to interfere, co-channel interference caused by frequency reuse must be controlled in these systems. Thus, the mobile radio engineer increases capacity, not by using extra frequency assignments but by re-using the spectrum and taking care to reduce co-channel interference by adequate spacing between cells using the same frequencies.

For urban mobile radio, the hexagonal cell structure giving complete coverage of an area has been extensively studied and is the one currently in vogue. In a cell there is either an omnidirectional antenna at the center of the cell site (start-up mode), or three directional antennas at alternate corners (fully operational mode). Assuming that mobiles in a cell do not interfere with others in the same cell, the main source of signal impairment results from fading of the received signal because of multipath effects present in an urban environment. The fading is statistically described by the Rayleigh distribution,[3] and is not instantaneously correlated across the frequency band of interest— an effect known as selective fading. Some other sources of signal degradation, in addition to co-channel interference, are ignition and receiver noise.

The choice of type of modulation is very important if we are to attain our design objectives. Various proposals have been made, and can be separated into two basic groups, those advocating digital modulation methods, and others arguing for the relatively well-known analog techniques.[4-7] In this paper, we specifically consider the use of single-sideband modulation (SSB) for mobile radio telephony. We do this because SSB does not result in any expansion of the occupied bandwidth, merely in its linear frequency translation. Single-sideband modulation has been exhaustively investigated at HF, and some proposals[8,9] have been made for its introduction in mobile radio. However, no complete work appears to have been done in connection with its use in cellular structures. The AMPS system opted for frequency modulation (FM) rather than SSB, exploiting the ability of FM to capture the wanted signal in the presence of an interfering signal, provided the latter is below a certain threshold level. There is no capture effect inherent in SSB, and for a given annoyance in cross-talk the interfering signal level must be significantly reduced compared to FM. With its nonconstant envelope, SSB is also more vulnerable to fading than FM. However, FM requires significantly more bandwidth than SSB, and it is this fact that has prompted us to have a closer look at SSB to see if we can mitigate its inherent weaknesses.

We describe quantitatively how well SSB performs when subjected to frequency selective fading and co-channel interference in a mobile

radio environment. The effect of using pilot carriers to combat fading is considered in detail.

We then propose a new SSB system which we have called frequency-hopped SSB (FH-SSB). We attempt to ensure that a particular channel is never continuously in a fade, and that two co-channel signals (i.e., two signals occupying the same band in a single duration τ) being scrambled by different codes will produce an effect on each other equivalent to that of additive noise. This technique compensates for some deficiencies in SSB, and, being a scrambling method, may offer communication privacy.* The effect of applying space diversity reception to frequency-hopped SSB with pilot tone is then considered. We conclude with a discussion that contains a summary and suggestions for further research.

II. PERFORMANCE OF FREQUENCY-HOPPED MODULATION IN MOBILE RADIO ENVIRONMENT

To mitigate the effects of multipath and co-channel interference in the mobile radio environment, we propose a frequency-hopping system that ensures that adjacent voice signal segments are in noncontiguous RF bands after modulation. The basic scheme of frequency hopping can be applied to any modulation as illustrated in this section. Its operation and performance using SSB are treated in succeeding sections of this paper.

Consider the transmission of a set of N single-channel voice signals over an RF bandwidth of B Hz. The RF bandwidth occupancy B_c of each voice channel is, therefore,

$$B_c = \frac{B}{N}. \tag{1}$$

Let the complex envelope of the kth speech signal $s_k(t)$, be represented by $m_k(t)$, namely,

$$m_k(t) = s_k(t) + j\hat{s}_k(t), \tag{2}$$

where $\hat{s}_k$ is the Hilbert transform of $s_k(t)$,

$$s_k(t) = \frac{1}{\pi} \int_{-\infty}^{\infty} \frac{s_k(x)}{t - x} \, dx. \tag{3}$$

The speech signals are band-limited to W Hz and divided into a set of nonoverlapping intervals of τ seconds. Parameter τ is determined by switching transients, vehicular speeds and available technology, and

---

* It may be argued that to offer communication privacy, τ has to be small compared to typical syllabic durations and scrambling codes should be changed frequently.

may therefore differ considerably depending on whether the environment is urban or rural. The kth speech signal is represented by

$$m_k(t) = m_k(t) \sum_{l=-\infty}^{\infty} \text{rect}\left(\frac{t - l\tau}{\tau}\right)$$

$$= \sum_{l=-\infty}^{\infty} m_k(t)\text{rect}\left(\frac{t - l\tau}{\tau}\right). \tag{4}$$

In eq. (4), rect($\cdot$), the rectangular window function, is defined by

$$\text{rect}(x) = \begin{cases} 1 & -\frac{1}{2} < x \leq \frac{1}{2} \\ 0, & \text{otherwise.} \end{cases} \tag{5}$$

Suppose that in any time slot $(l - 1)\tau < t \leq l\tau$, a segment of the speech signal $m_k(t)$ is modulated on a carrier to occupy an RF bandwidth of B_c and that this frequency band is directed to a subband p, $1 \leq p \leq N$. The subband p changes its location in the spectrum every τ seconds according to a scrambling code.[10]

The kth modulated voice channel can, therefore, be represented as

$$y_k(t) = \sum_{l=-\infty}^{\infty} F\{m_k(t), f_k(l, \omega)\}\text{rect}\left(\frac{t - l\tau}{\tau}\right), \tag{6}$$

where $F\{\cdot\}$ denotes the modulator output, $f_k(l, \omega)$ represents the carrier frequency ω during the lth time slot chosen for the kth speech channel by the scrambling code.

Because the scrambling code is known at the receiver, we can detect $m_k(t)$, $(l - 1)\tau < t \leq l\tau$.

Assuming the modulated RF bandwidth B_c is much smaller than the "coherence bandwidth"[1] of the multipath interference, we denote the kth received RF signal as

$$z_k(t) = \sum_{l=-\infty}^{\infty} r_l(t)\exp[j\phi_l(t)]F\{m_k(t), f_k(l, \omega)\}\text{rect}\left(\frac{t - l\tau}{\tau}\right), \tag{7}$$

where $r_l(t)\exp[j\phi_l(t)]$ is the complex envelope of the Rayleigh fading imposed by the transmission medium. This is the only type of multipath interference considered here; we justify this on the grounds that it is usually the major source of degradation in mobile radio systems.[1]

III. FREQUENCY-HOPPED SSB IN MOBILE RADIO ENVIRONMENT

We now consider SSB in a frequency-hopping system. The kth modulated voice channel can be represented as

$$v_k(t) = \sum_{l=-\infty}^{\infty} \left\{ \frac{1}{2} s_k(t)\cos[f_k(l, \omega)t]\text{rect}\left(\frac{t - l\tau}{\tau}\right) \right.$$

$$\left. - \frac{1}{2} \hat{s}_k(t)\sin[f_k(l, \omega)t]\text{rect}\left(\frac{t - l\tau}{\tau}\right) \right\}, \quad (8)$$

where $s_k(t)$ is the speech signal in the kth channel. Further, the complex envelope of the kth modulated voice channel in the lth time slot is

$$u_k(t) = m_k(t)\exp[jf_k(l, \omega)t]. \quad (9)$$

Note that the carrier frequency changes every τ seconds according to a scrambling code and $f_k(l, \omega)$ represents the carrier frequency for the kth channel during the lth time slot. Since the RF bandwidth occupancy B_c of each voice channel in SSB is γW, where γ is slightly higher than unity, (typically 1.1), the total number N of radio channels that can be accommodated in the RF bandwidth B is

$$N = \frac{B}{\gamma W}. \quad (10)$$

As in Section II, we assume that the scrambling code is such that successive modulated voice signal elements are in noncontiguous RF bands, no two voice channels are in the same band, and all channels are accommodated in a given band B. A typical time-frequency characteristic of the kth voice channel is shown in Fig. 1.
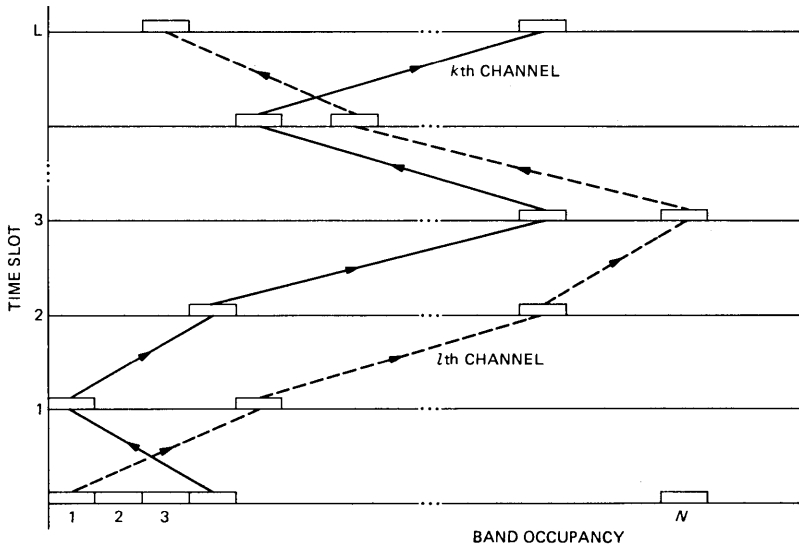
Fig. 1—Frequency hopping of kth and lth channels during successive time slots.

Our intention is to demonstrate that by frequency hopping the speech channels as described, the performance of SSB will not be degraded and its co-channel interference characteristics will be improved. As a prelude, we calculate the s/n of single channel SSB signal, that is *not* accompanied by a pilot tone, and is subject to Rayleigh fading. We show that its performance is too low to be of any practical value. The s/n of SSB with pilot carrier is next examined and a significant improvement observed. We further show that frequency hopping does not degrade the performance of SSB with pilot carrier.

3.1 Effects of Rayleigh fading on a SSB signal

Consider a SSB signal subject to rapid Rayleigh fading of the type found in mobile radio systems. No pilot carrier transmission or frequency hopping is used. Assuming that the modulation bandwidth B_c is much smaller than the coherence bandwidth (typically 250 kHz in an urban environment), the fading of the SSB signal is frequency flat over the signal band, and the envelope of recovered speech signal impaired by fading is

$$\mu(t) = r(t)s(t).$$ (11)

As $r(t)$ is Rayleigh distributed, the probability density function (pdf) of r is given by

$$p_r(x) = \begin{cases} \dfrac{x}{\sigma^2} e^{-\frac{x^2}{2\sigma^2}}, & x \geq 0 \\ 0, & \text{otherwise} \end{cases},$$ (12)

where the parameter σ^2 is a function of the transmission medium.

We now proceed to determine the s/n of (11). In Ref. 9, s/n is defined as

$$\text{s/n} = \frac{\langle s^2(t)\rangle_t}{\langle(\mu(t) - s(t))^2\rangle_{r,t}},$$ (13)

where $\langle \cdot \rangle_r$ represents the average with respect to r and

$$\langle x^2(t)\rangle_t \triangleq \lim_{T\to\infty} \frac{1}{2T} \int_{-T}^{T} x^2(t)dt.$$ (14)

However, Ref. 1 uses

$$\text{s/n} = \frac{\langle(\langle\mu(t)\rangle_r)^2\rangle_t}{\langle(\mu(t) - \langle\mu(t)\rangle_r)^2\rangle_{r,t}}.$$ (15)

The cross-correlation of the noise and signal as defined by eq. (13) is nonzero, although the fading and signal are statistically independent. In (15), the signal is defined as

$$\alpha(t) = \langle\mu(t)\rangle_r$$ (16)

and the noise as

$$n(t) = \mu(t) - \langle \mu(t) \rangle_r, \tag{17}$$

yielding the desired result that the signal and noise are uncorrelated. Consequently, we opt for the definition of s/n given by eq. (15).

From (11) and (16) the recovered signal is

$$\alpha(t) = \langle \mu(t) \rangle_r = \langle r(t) \rangle_r s(t) \tag{18}$$

and

$$n(t) = [r(t) - \langle r(t) \rangle] s(t), \tag{19}$$

$$\langle n(t) \rangle_r = 0 \tag{20}$$

and

$$\langle n^2(t) \rangle_r = \langle s^2(t) \rangle \{ \langle r^2(t) \rangle_r - \langle r(t) \rangle_r^2 \}. \tag{21}$$

With the aid of eq. (12),

$$\langle r^2(t) \rangle_r = 2\sigma^2 \tag{22}$$

and

$$\langle r(t) \rangle_r^2 = \frac{\pi}{2} \sigma^2, \tag{23}$$

resulting in a noise power of

$$\langle n^2(t) \rangle_r = \langle s^2(t) \rangle (2 - \pi/2) \sigma^2. \tag{24}$$

The s/n becomes

$$\text{s/n} = 1 \left/ \left(\frac{4}{\pi} - 1 \right) \right. = 3.66 \; or \; 5.63 \; \text{dB}. \tag{25}$$

We note that this s/n of 5.63 dB is too low to be viable in a mobile radio environment, unless we mitigate the effects of fading.

3.2 Effects of Rayleigh fading on a SSB signal with pilot carrier (SSB + PT)

The first step to reduce the distortion in the recovered speech, caused by fading of the SSB signal, is to add a pilot tone $p(t)$ of known magnitude and frequency f_p.[1,9] The spectral arrangement is shown in Fig. 2. The frequency f_p is selected to reside outside the bandwidth B_c of the SSB signal, but sufficiently close for it to experience similar fading conditions. The receiver, on examining the magnitude of the pilot tone, can estimate the degree of fading of the SSB signal, make appropriate compensation, and thereby improve s/n.

The received SSB signal is not the desired $m(t)$, but $r(t)m(t)$, where $r(t)$ is Rayleigh-distributed. The pilot tone is used to correct the

distorted demodulated signal to a value

$$\hat{\mu}(t) = \frac{r(t)m(t)}{r_p(t)} \exp\{j[\phi(t) - \phi_p(t)]\}, \tag{26}$$

where ϕ and ϕ_p are the phase angles of the complex fading signals $r(t)\exp[j\phi(t)]$ and $r_p(t)\exp[j\phi_p(t)]$, respectively. Clearly the pdf of

$$A(t) = \frac{r(t)}{r_p(t)} \tag{27}$$

is of importance in determining how closely $\hat{\mu}(t)$ approaches the original complex envelope of the speech signal $m(t)$. It has been shown[1] that the pdf of $A(t)$ is

$$p_A(x) = \frac{2x(1 - \lambda^2)(1 + x^2)}{[(1 + x^2)^2 - 4\lambda^2 x^2]^{3/2}}, \tag{28}$$

where λ, the correlation between $r(t)$ and $r_p(t)$, is

$$\lambda = \frac{1}{[1 + (2\pi f_d T_o)^2]^{1/2}}. \tag{29}$$

In eq. (29), T_σ is a measure of the time-delay spread caused by multipath effects in the transmission medium. Parameter f_d is the frequency separation between the pilot tone f_p and a frequency f in the SSB signal. Hence, it follows that there is a minimum and a maximum value of f_d for a given pilot tone f_p (see Fig. 2).

As the noise signal is

$$n(t) = \hat{\mu}(t) - \langle \hat{\mu}(t) \rangle_A, \tag{30}$$

where

$$\langle \hat{\mu}(t) \rangle_A = \langle A(t) \rangle m(t) \exp\{j[\phi(t) - \phi_p(t)]\} \tag{31}$$

and has infinite variance, unless $\lambda = 1$, it is possible for $\langle \hat{\mu}(t) \rangle_A$ to swamp the average output signal as $r_p(t)$ can be zero. This situation is similar to that for AM,[1] and can be prevented by ensuring that the compensating term $r_p(t)$ cannot fall beyond a value r_o. A block diagram of such a system is shown in Fig. 3. The demodulated signal is now

$$\hat{\mu}(t) = A_L(t)m(t)\exp\{j[\phi(t) - \phi_p(t)]\}, \tag{32}$$

where

$$A_L(t) = \begin{cases} \dfrac{r}{r_p} & \text{if } r_p \geq r_o \\ \dfrac{r}{r_o} & \text{if } r_p < r_o \end{cases} = r\min\left(\frac{1}{r_p}, \frac{1}{r_o}\right). \tag{33}$$

Parameter r_o can be selected to maximize the system performance. By imposing this limit on r_p, the signal $\langle \hat{\mu}(t) \rangle_{A_L}$ can be shown to be[1]

$$\langle \hat{\mu}(t) \rangle_{A_L} = \langle A_L(t) \rangle m(t) \exp\{j[\phi(t) - \phi_P(t)]\}, \tag{34}$$

where

$$
\langle A_L(t) \rangle = \int_0^\infty dr \int_{r_o}^\infty dr_p \frac{r^2}{\sigma^4(1-\lambda^2)} \exp\left[-\frac{r^2 + r_p^2}{2\sigma^2(1-\lambda^2)}\right]
$$

$$
\cdot I_o\left(\frac{rr_p}{\sigma^2}\frac{\lambda}{1-\lambda^2}\right)
$$

$$
+ \int_0^\infty dr \int_0^{r_o} dr_p \frac{r^2 r_p}{r_o \sigma^4(1-\lambda^2)} \exp\left[-\frac{r^2 + r_p^2}{2\sigma^2(1-\lambda^2)}\right]
$$

$$
\cdot I_o\left(\frac{rr_p}{\sigma^2}\frac{\lambda}{1-\lambda^2}\right)
$$

$$
= E(\lambda) - \sqrt{\pi}\frac{r_o}{\sqrt{2\sigma^2(1-\lambda^2)}} \exp\left[\left(\frac{\lambda^2}{2}-1\right)\frac{r_o^2}{2\sigma^2(1-\lambda^2)}\right]
$$

$$
\cdot \left[\frac{\lambda^2}{2} I_1\left(\frac{\lambda^2 r_o^2}{4\sigma^2(1-\lambda^2)}\right) + \left(1-\frac{\lambda^2}{2}\right) I_o\left(\frac{\lambda^2 r_o^2}{4\sigma^2(1-\lambda^2)}\right)\right]
$$

$$
+ \frac{\sqrt{\pi}}{\lambda^2} \sum_{k=0}^\infty (2^k k!)^{-2}
$$

$$
\cdot \left\{ \frac{\sqrt{2\sigma^2(1-\lambda^2)}\,\Gamma\left(2k+1, \left(\frac{\lambda^2}{2}-1\right)\left\{r_o^2/[2\sigma^2(1-\lambda^2)]\right\}\right)}{r_o\left(\frac{2}{\lambda^2}-1\right)^{2k+1}} \right.
$$

$$
\left. - \frac{2^{3/2}(1-\lambda^2)\Gamma\left\{2k+\frac{3}{2}, \left(\frac{\lambda^2}{2}-1\right)[\Gamma_o^2/\{2\sigma^2(1-\lambda^2)\}]\right\}}{\lambda\left(\frac{2}{\lambda^2}-1\right)^{2k+3/2}} \right\} \tag{35}
$$

In this equation, $I_n(\cdot)$ is the modified Bessel function of the first kind and of order n, $E(\lambda)$ is the complete elliptic integral of the second kind given by

$$
E(\lambda) = \frac{\pi}{2}\left[1 - \sum_{n=1}^\infty \left\{\frac{(2n-1)!!}{2^n n!}\right\}^2 \frac{\lambda^{2n}}{2n-1}\right], \tag{36}
$$

$$
(2n-1)!! \triangleq 1.3.5 \cdots (2n-1), \tag{37}
$$

and $\Gamma(p, x)$ is the incomplete gamma function,[7]
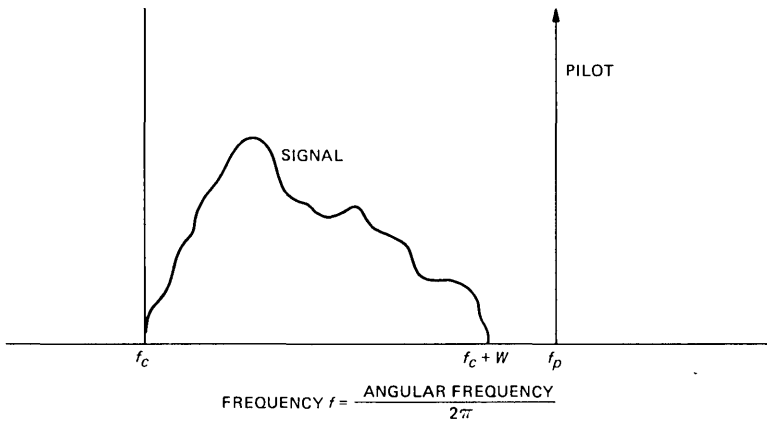
Fig. 2—Spectral arrangement of SSB signal with pilot tone.

$$\Gamma(p, x) = \sum_{n=0}^{\infty} \frac{(-1)^n x^{p+n}}{n!(p + n)}. \tag{38}$$

Knowing the average output signal $\langle \hat{\mu}(t) \rangle_{A_L}$ we determine the variance of the noise $n(t)$, namely,

$$\langle n^2(t) \rangle = \{ \langle A_L^2 \rangle - \langle A_L \rangle^2 \} | m(t) |^2, \tag{39}$$

where $\langle A_L \rangle$ is given in eq. (35) and

$$\langle A_L^2 \rangle = \int_0^{\infty} dr \int_{r_o}^{\infty} dr_p \frac{r^3}{r_p \sigma^4 (1 - \lambda^2)} \exp\left[-\frac{r^2 + r_p^2}{2\sigma^2(1 - \lambda^2)} \right]$$

$$\cdot I_o\left(\frac{rr_p}{\sigma^2} \frac{\lambda}{1 - \lambda^2} \right)$$

$$+ \int_0^{\infty} dr \int_0^{r_o} dr_p \frac{r^3 r_p}{r_o^2 \sigma^4 (1 - \lambda^2)} \exp\left[-\frac{r^2 + r_p^2}{2\sigma^2(1 - \lambda^2)} \right]$$

$$\cdot I_o\left(\frac{rr_p}{\sigma^2} \frac{\lambda}{1 - \lambda^2} \right)$$

$$= (1 - \lambda^2) E_1\left(\frac{r_o^2}{2\sigma^2} \right) + \frac{1 - \exp\left(-\frac{r_o^2}{2\sigma^2} \right)}{r_o^2 / (2\sigma^2)}. \tag{40}$$

In eq. (40), $E_1(x)$ is the exponential integral[11]

$$E_1(x) = \int_x^{\infty} \frac{\exp(-t)}{t} dt \qquad x > 0. \tag{41}$$
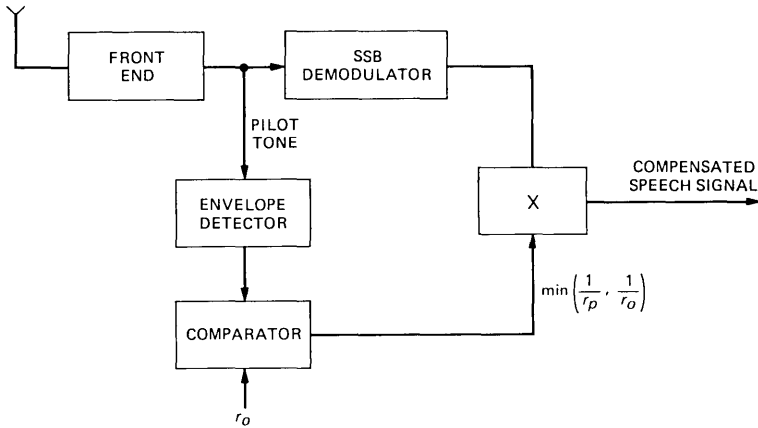
Fig. 3—Pilot correction scheme.

From eqs. (32), (34), (35), and (39), the s/n is given by

$$\text{s/n} = \frac{\langle A_L \rangle^2}{\langle A_L^2 \rangle - \langle A_L \rangle^2}, \tag{42}$$

where $\langle A_L \rangle$ and $\langle A_L^2 \rangle$ are given by eqs. (35) and (40), respectively.

The s/n of eq. (42) is plotted in Fig. 4 as a function of $(r_o^2/2\sigma^2)$, where r_o is the smallest value of $r_p(t)$ and $2\sigma^2$ is the variance of $r(t)$ [or of $r_p(t)$] for various correlation amplitudes λ. This figure is similar to Fig. 4.1-23 of Ref. 1. When r_o is too small, the speech signal may occasionally be over-corrected, resulting in poor s/n. If r_o is too large, the signal compensation may be insufficient, even for high values of λ, a condition of false pilot fade. Thus, for a given σ^2 and λ, there is a broad optimum for r_o, the limit of permissible gain control. The dotted curve in Fig. 4 is the locus of $r_o^2/2\sigma^2$ for optimum gain limiting to ensure peak s/n for a given λ.

The figure also shows that λ needs to be large if the noise is to be low and high s/n achieved. For example, with optimum gain limiting and $\lambda = 0.999$, the output s/n is approximately 20 dB. For a time-delay spread T_d of 1 μs and $\lambda = 0.999$, the maximum frequency separation of the pilot from any part of the SSB signal must be less than

$$f_d = \frac{\sqrt{1 - \lambda^2}}{2\pi T_d \lambda} = 7.12 \text{ kHz}, \tag{43}$$

a value that is attainable in SSB speech systems. Thus, an s/n of better than 20 dB can be achieved with the transmission of a pilot carrier and fast-acting automated gain control.

3.3 Effects of Rayleigh fading on a single frequency-hopped SSB signal transmitted with a pilot carrier

After considering the effects of Rayleigh fading on a SSB signal and
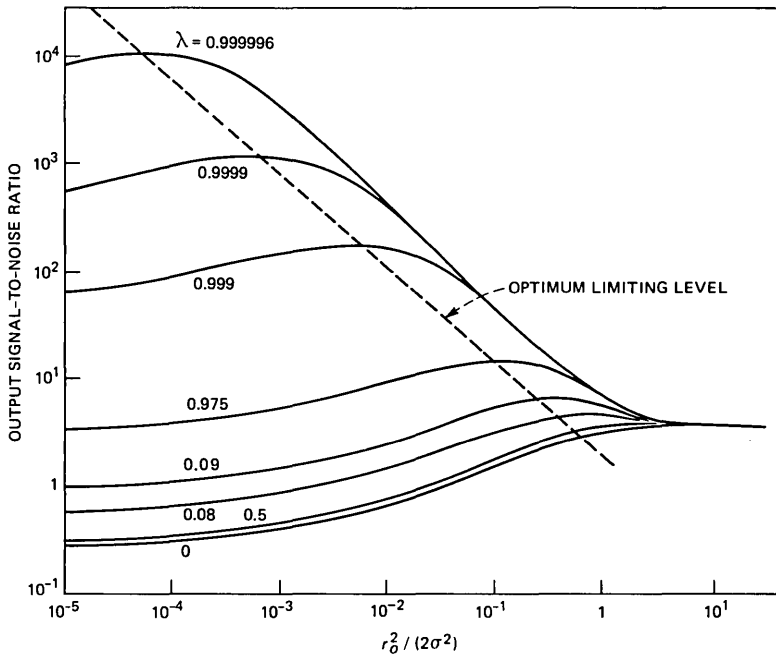
Fig. 4—Signal-to-noise ratio as a function of $r_o^2/2\sigma^2$ for various frequency correlation values.

how its reception is improved with the aid of a pilot carrier, we now examine the effect of frequency-hopping the SSB, plus pilot tone signal in the presence of Rayleigh fading. The frequency-hopping strategy has already been outlined in Section II.

The recovered speech signal in frequency-hopped SSB with pilot tone (FH-SSB-PT) is found by proceeding as in Section 3.2, but modifying eq. (26) to allow for the time segmentation, namely,

$$\hat{\mu}(t) = \sum_{l=-\infty}^{\infty} \hat{\mu}_l(t)\text{rect}\left(\frac{t-l\tau}{\tau}\right), \tag{44}$$

where $\hat{\mu}_l(t)$ from eqs. (32) and (33) is

$$\hat{\mu}_l(t) = r_l(t)\min\left\{\frac{1}{r_{pl}(t)}, \frac{1}{r_o}\right\}\exp\{j[\phi_l(t) - \phi_{pl}(t)]\}m_l(t). \tag{45}$$

The subscript l refers to the lth time slot, and $\phi_l(t)$ and $\phi_{pl}(t)$ are the phase angles of the complex fading signals $r_l(t)\exp[j\phi_l(t)]$ and $r_{pl}(t)\exp[j\phi_{pl}(t)]$ associated with the signal and pilot tone, respectively. Quantity $m_l(t)$ is the segment of the complex envelope of the original speech in the lth time slot. Equation (44) can be expressed as

$$\hat{\mu}(t) = \sum_{l=-\infty}^{\infty} R_l(t)m_l(t)\exp\{j[\phi_l(t) - \phi_{pl}(t)]\}, \tag{46}$$

where $R_l(t)$ is the composite fading envelope because of the mobile radio environment. Notice that $R_l(t)$, given by

$$R_l(t) = r_l(t)\min\left\{\frac{1}{r_{pl}(t)}, \frac{1}{r_o}\right\}\text{rect}\left(\frac{t - l\tau}{\tau}\right), \tag{47}$$

has similar characteristics to those of $A_L(t)$ [see eq. (33)], except that $R_l(t)$ applies for the lth slot of τ seconds duration.

Before proceeding, we make the following assumptions.

(*i*) Values of $R_l(t)$ for different l, i.e., for different time slots of duration τ, are statistically independent. This implies that the scrambling algorithm controlling the frequency hopping ensures that the carrier frequencies in two contiguous time slots are separated by a frequency band that is larger than the coherence bandwidth of the mobile radio channel.

(*ii*) Over a long period of time, each of the N channel frequency bands is likely to be occupied by each of the N voice signals.

(*iii*) The fading characteristics of all the radio channels are identically distributed.

If we consider any two angular frequencies ω_1 and ω_2, where $\omega_2 - \omega_1$ exceeds the coherence bandwidth, their fading patterns will in general be very different. Figure 5 shows a typical example. Even if
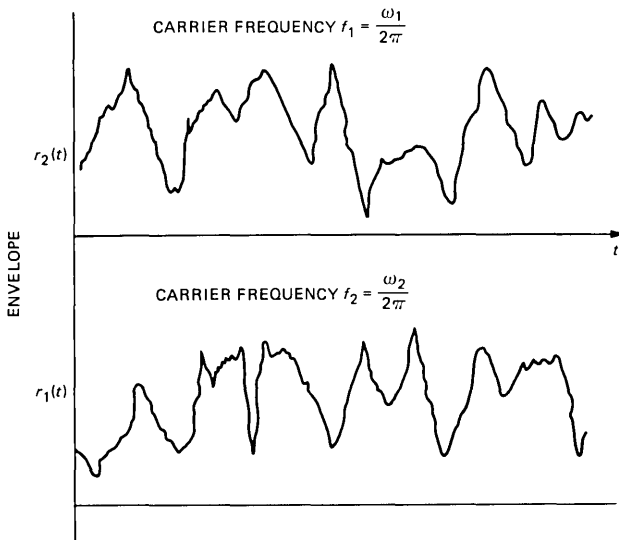
Fig. 5—Fading patterns for angular frequencies ω_1 and ω_2; $\omega_1 - \omega_2$ exceeds the coherence bandwidth.

two mobiles use the same carrier frequency their fading characteristics will generally be different if the vehicles are separated by several wavelengths of the carrier frequency. In our analysis, we assume all fading characteristics are statistically independent.

The recovered signal is found by averaging $\hat{\mu}(t)$ of eq. (46) with respect to the set $\{R_l\} = \{\cdots, R_o, R_1, \cdots, R_l, \cdots\}$

$$\langle \hat{\mu}(t) \rangle_{\{R_l\}} = \sum_{l=-\infty}^{\infty} \langle R_l(t) \rangle m_l'(t)$$

$$= \langle R(t) \rangle \sum_{l=-\infty}^{\infty} m_l'(t),$$

$$m_l'(t) = m_l(t) \exp\{j[\phi_l(t) - \phi_{pl}(t)]\}, \tag{48}$$

where $\langle R_l(t) \rangle$ is assumed to be independent of the time slot l, and is represented by $\langle R(t) \rangle$.

The noise $n(t)$ becomes for the frequency-hopped system

$$n(t) = \sum_{l=-\infty}^{\infty} [R_l(t) - \langle R_l(t) \rangle] m_l'(t), \tag{49}$$

and its variance

$$\langle n_s^2(t) \rangle = \{\langle R^2(t) \rangle - \langle R(t) \rangle^2\} \sum_{l=-\infty}^{\infty} |m_l(t)|^2 \tag{50}$$

as $R_l(t)$ for $-\infty < l < \infty$ are assumed to be independent.

The s/n is, from eqs. (48) and (50),

$$\text{s/n} = \frac{\langle R(t) \rangle^2}{\langle R^2(t) \rangle - \langle R(t) \rangle^2} \frac{\left\langle \left(\left| \sum_{l=-\infty}^{\infty} m_l(t) \right| \right)^2 \right\rangle_t}{< \sum_{l=-\infty}^{\infty} |m_l(t)|^2 >_t}, \tag{51}$$

where

$$\left\langle \left(\left| \sum_{l=-\infty}^{\infty} m_l(t) \right| \right)^2 \right\rangle_t = \langle s^2(t) \rangle_t$$

is the average power in the original speech signal, and

$$\left\langle \sum_{l=-\infty}^{\infty} |\dot{m}_l^2(t)|^2 \right\rangle_t$$

is the sum of the average powers in the segments of the speech signal. For Gaussian signals, it has been shown[12] that

$$\frac{\left\langle \left(\left| \sum_{l=-\infty}^{\infty} m_l(t) \right| \right)^2 \right\rangle_t}{\left\langle \sum_{l=-\infty}^{\infty} |m_l(t)|^2 \right\rangle_t} = 1. \tag{52}$$

Assuming that speech signals have approximately Gaussian characteristics, this result is also true for speech. Hence,

$$\text{s/n} = \frac{\langle R(t) \rangle^2}{\langle R^2(t) \rangle - \langle R(t) \rangle^2}. \tag{53}$$

Since this s/n is the same as eq. (42), frequency hopping does not lead to any degradation in performance of the system. Note further that Fig. 4 can be used to determine the s/n of an FH-SSB-PT system.

IV. EFFECTS OF CO-CHANNEL INTERFERENCE ON A FH-SSB-PT SIGNAL

Consider a mobile radio system which has been allocated an RF bandwidth of B_T Hz, where each cell is assigned a bandwidth of B Hz. Cells B_T/B can use different parts of the B_T spectrum; but if more than B_T/B cells are required to accommodate user demand, some frequency bands must be reused. Let us consider two such cells which are spaced apart as far as possible to restrict mutual interference. Vehicles in each cell communicate via the cell site station using FH-SSB-PT, and let us concentrate on a vehicle in one cell which is subjected to interference, called co-channel interference, from mobiles in the co-channel cell. By arranging for each cell to frequency-hop using different scrambling codes, the co-channel interference will be incoherent. Observe that FH-SSB-PT operates on the interfering signal with the incorrect descrambling code and adds to the wanted speech signal short segments of numerous speech signals in the co-channel cell. The co-channel signal is, therefore, more noise-like and perceptually more acceptable than a single coherent interfering speech signal, provided τ is suitably small. This is the main advantage of using frequency hopping.

An analysis to determine the subjective nature of interference is very difficult and, therefore, we characterize the interference in terms of its mean square value. We proceed as follows.

Since the voice signal associated with a particular frequency slot of width B_c is different from one time slot to the next, we will evaluate the effect of co-channel interference in a single time slot of duration τ. The total input to the receiver consists of the sum of the wanted and interfering components and is given by

$$\alpha_R = r(t)m(t)\exp[j(\omega_c t + \phi)] + r_p(t)\exp[j(\omega_p t + \phi_p)]$$

$$+ \delta\{r_i(t)m_i(t)\exp[j(\omega_i t + \phi_i)] + r_{pi}(t)\exp[j(\omega_{pi}t + \phi_{pi})]\}, \quad (54)$$

where the subscript i refers to the interfering or co-channel signal, subscript p refers to the pilot tone, ω_c and ω_i are the carrier frequencies of the wanted and unwanted signals, and the remaining symbols have their usual meaning. Carrier frequencies, ω_c and ω_i, are equal as eq. (54) applies for one time slot. The relative amplitude δ of the interference determined by antenna and propagation characteristics, and in a nonfading environment the signal-to-interference ratio at RF is $1/\delta^2$.

Suppose that the pilots associated with the wanted and co-channel signals are off-set (say, one above and one below the SSB signal frequency band) with the result that the desired pilot is unaffected by the unwanted pilot. The demodulated speech signal is, therefore,

$$\beta(t) = \frac{r(t)}{r_p(t)} m(t)\exp[j(\phi - \phi_p)] + \delta\frac{r_i(t)}{r_p(t)} m_i(t)\exp[j(\phi_i - \phi_p)]. \quad (55)$$

Hence,

$$\beta(t) = \hat{\mu}(t) + \delta\frac{r_i(t)}{r_p(t)} m_i(t)\exp[j(\phi_i - \phi_p)], \quad (56)$$

where $\hat{\mu}(t)$ is given by eq. (26). Averaging with respect to $r(t)$ and $r_i(t)$, we compute the average signal $\langle\beta(t)\rangle$. The noise signal is $\beta(t) - \langle\beta(t)\rangle$. Hence,

$$\text{s/n} = \frac{\langle A \rangle^2}{\langle A^2 \rangle - \langle A \rangle^2}, \quad (57)$$

where

$$\langle A \rangle = \langle A_L \rangle \quad (58)$$

$$\langle A^2 \rangle = \langle A_L^2 \rangle + \delta^2\langle A_i^2 \rangle \quad (59)$$

and

$$\langle A_i^2 \rangle = \left\langle \left\{\min\left(\frac{r_i}{r_p}, \frac{r_i}{r_o}\right)\right\}^2 \right\rangle_{r_i, r_p}. \quad (60)$$

Note that $\langle A_L \rangle$ and $\langle A_L^2 \rangle$ are given by eqs. (35) and (40), respectively.

Assuming r_i and r_p are statistically independent and both are Rayleigh-distributed with the probability density function of eq. (13),

$$\langle A_i^2 \rangle = \langle r_i^2 \rangle_{r_i}\left\langle \left\{\min\left(\frac{1}{r_p}, \frac{1}{r_o}\right)\right\}^2 \right\rangle_{r_p}. \quad (61)$$

Further,

$$\langle r_i^2 \rangle_{r_i} = 2\sigma^2 \quad (62)$$

and

$$\left\langle \left\{ \min\!\left(\frac{1}{r_p}, \frac{1}{r_o}\right) \right\}^2 \right\rangle_{r_p} = \frac{1}{r_o^2} \int_0^{r_o} \frac{r}{\sigma^2}\, e^{-r^2/2\sigma^2} dr$$

$$+ \int_{r_o}^{\infty} \frac{1}{r^2} \cdot \frac{r}{\sigma^2}\, e^{-r^2/2\sigma^2} dr$$

$$= \frac{1 - e^{-r_o^2/2\sigma^2}}{r_o^2} + \frac{1}{2\sigma^2}\, E_1\!\left(\frac{r_o^2}{2\sigma^2}\right), \qquad (63)$$

where $E_1(\cdot)$ is given by eq. (41). Hence,

$$\text{s/n} = \frac{\langle A_L \rangle^2}{\langle A_L^2 \rangle + \delta^2 \langle A_i^2 \rangle - \langle A_L \rangle^2}, \qquad (64)$$

where $\langle A_i^2 \rangle$ is given in eqs. (61) to (63). Notice that if $\delta = 0$, i.e., no co-channel interference, eqs. (64) and (42) are identical. For interference from M co-channel cells, the s/n becomes

$$\text{s/n} = \frac{\langle A_L \rangle^2}{\langle A_L^2 \rangle + \sum_{j=1}^{M} \delta_j^2 \langle A_{ij}^2 \rangle - \langle A_L \rangle^2}, \qquad (65)$$

where δ_j is the relative amplitude, and $\langle A_{i,j}^2 \rangle$ is the appropriate value of $\langle A_i^2 \rangle$ given by eqs. (61) to (63).

V. FH-SSB-PT WITH SPACE DIVERSITY RECEPTION

The impairments associated with FH-SSB-PT in a mobile radio environment can be alleviated by using diversity techniques. As we would like to maximize the number of users in a given RF band, the diversity methods most appropriate are space-diversity techniques.

The simulation analysis provided in Ref. 5 of an equal gain, N branch diversity receiver for conventional SSB-PT is applicable to the FH-SSB-PT system presented here. In the receiver the individual branch pilot signals are phase-corrected and then averaged to provide the envelope correction signal. Amplitude correction is then applied as in the nondiversity case described in Section 3.2.

The improvements in s/n obtained through space-diversity reception are substantial. For example, a two-branch space-diversity receiver with 20 dB ($=10 \log r_o^2/2\sigma^2$) of correction gives 18-dB improvement in s/n when the delay spread T_d is as high as 3 μs. A four-branch diversity receiver provides another 13-dB gain in s/n. Those improvements are obtained in FH-SSB+PT when space-diversity techniques are applied.

VI. COMPARISON OF FH-SSB-PT WITH FM

In this section, we shall present a comparison of user densities obtained with FH-SSB-PT and wide-index FM. Assuming that the use of space diversity mitigates the effects of fading, we consider only degradation from co-channel interference. Consider a mobile radio system based on a cellular structure,[13] where each cell is hexagonal in shape. Figure 6 shows two such cells; cell A is the center of a cluster of U cells that have been allocated an RF bandwidth of B_T Hz and each cell has a bandwidth of B Hz. The value of U is

$$U = i^2 + ij + j^2, \tag{66}$$

where i and j are marked on Fig. 6. There are co-channel cells arranged symmetrically around cell A that will cause interference with mobiles travelling inside this cell. One of these co-channel cells is cell B, spaced a distance D from cell A such that

$$\frac{D}{R} = \sqrt{3U}, \tag{67}$$

where R is the cell radius.

Suppose a mobile in cell A is at the cell boundary on a line connecting the center of cell A to the center of cell B, and that the cell site
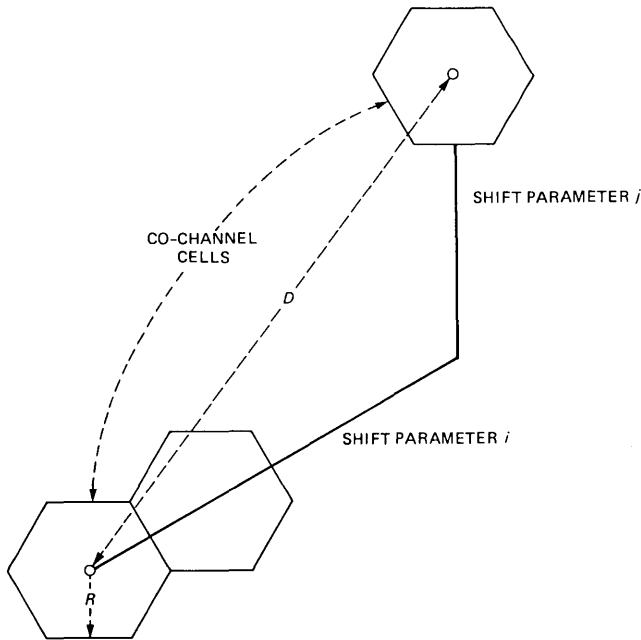
Fig. 6—Co-channel cells for hexagonal cell structure.[8]

antennas are at the cell centers. The ratio δ^2 [see eq. (54)] of the received radiated powers by the mobile from the antennas of cells A and B is approximated by

$$\delta^2 = \left(\frac{R}{D-R}\right)^n, \tag{68}$$

where n varies between 2 and 4. We assume $n = 3.5$. However, there are six co-channel cells[2] at a distance D and other cells spaced kD from A, where $k = 2, 3, \cdots$. We consider only the closest six cells, as they cause the dominant co-channel interference, and assuming each co-channel cell radiates the same power and $D \gg R$,

$$\frac{\text{RF co-channel interference power}}{\text{RF signal power}} = 6\delta^2 = 6[1/(D/R - 1)]^{3.5}. \tag{69}$$

Following demodulation, the s/n values for the SSB and FM systems are

$$\text{s/n}_1 = \frac{1}{6\delta_1^2} \tag{70}$$

and[1]

$$\text{s/n}_2 = \left(\frac{1}{6\delta_2^2}\right) \sqrt{\frac{\pi}{3}} \frac{\chi^3}{0.46}, \tag{71}$$

where the subscripts 1 and 2 refer to the SSB and FM systems, respectively, and χ is the FM modulation index.

Let the comparison be made on the basis that

$$\text{s/n}_1 = \text{s/n}_2, \tag{72}$$

which results in

$$\frac{\delta_1^2}{\delta_2^2} = \sqrt{\frac{3}{\pi}} \frac{0.46}{\chi^3}. \tag{73}$$

Equations (67), (68), and (73) yield

$$\left(\frac{\sqrt{3U_2} - 1}{\sqrt{3U_1} - 1}\right)^{3.5} = \frac{0.45}{\chi^3}. \tag{74}$$

The RF bandwidths allocated to the entire system, to each cell and to each voice channel are B_T, B, and B_c, respectively. The number of available channels is B_T/B_c, and the number of users in each cell is

$$N = \frac{B_T}{B_c U} = \frac{B}{\gamma W} = \frac{B}{B_c}. \tag{75}$$

If the cell sizes are the same in the SSB and FM systems, the user density ρ, i.e., the number of users per unit area, is

$$\rho = \frac{1}{\pi} \frac{B_T}{D^2 B_c}, \tag{76}$$

where D is the co-channel distance [see eq. (67)]; i.e., we approximate the cluster of non-cochannel cells by a circle of radius D. The ratio of user densities in the SSB and FM systems is, therefore,

$$\frac{\rho_1}{\rho_2} = \left(\frac{D_2}{D_1}\right)^2 \left(\frac{B_{c,2}}{B_{c,1}}\right). \tag{77}$$

As an example, let the number of cells in the FM system be 12, and we will assume $\chi = 2.5$. From eq. (74), the number of cells in the SSB scheme becomes 73. For $B_T = 20$ MHz, $B_{c,1} = 4$ kHz, $B_{c,2} = 30$ kHz, $D_1 = R_1\sqrt{3U_1} = 14.8 R_1$, $D_2 = R_2\sqrt{3U_2} = 6R_2$, and as $R_1 = R_2$, $D_2/D_1 = 0.405$. Hence from eq. (76), $\rho_1/\rho_2 = 1.23$, i.e., the user density of SSB is 1.23 times higher than that for FM. From eqs. (69) and (70), the s/n is

$$\text{s/n} = \frac{1}{6} (\sqrt{3U} - 1)^{3.5} = 32 \text{ dB},$$

a value that is more than adequate.

VII. DISCUSSION

Users of a mobile radio system want good service, being completely indifferent to the type of modulation employed. The designer of a mobile radio system, however, is faced with a hostile communications environment. If digital modulation methods are used the speech signals have to be encoded into digital waveforms that have significantly more bandwidth (typically a factor of 6) than that of the speech signal. Unfortunately, narrow-band FM with its small signal expansion is difficult to use for mobile radio because of its vulnerability to co-channel interference, while wideband FM with its acceptable performance requires a bandwidth that is comparable to the bandwidth of digitized speech. However, the bandwidth of the SSB signal is the same as the original speech, and this has encouraged us to innovate new techniques to overcome inability of SSB to perform well in the presence of co-channel interference and fading. We were aware at the inception of this study that many people have analog radio receivers and, therefore, the capability to eavesdrop on mobile radio conversations using analog modulation methods. The outcome of our deliberations is the frequency-hopped SSB with pilot tone (FH-SSB-PT) scheme described in the previous sections.

Although the concept of SSB and its compensation by a pilot tone is well known, we presented in Sections 3.1 and 3.2 new analytical results. For the case of pilot tone compensation of the SSB signal in the presence of Rayleigh fading, we used an alternative definition of s/n from that used in Ref. 9, and further, we expressed it as a function of λ instead of limiting it to the special case of $\lambda = 1$. Our results show that pilot compensation can achieve an s/n of more than 20 dB if $\lambda > 0.999$ and $f_d = 7.1$ kHz. A more relevant value of f_d for speech is probably 3 kHz, and T_d is typically 1 μs, then from eq. (29) $\lambda = 0.9998$, resulting in s/n = 27 dB.

When the SSB signal, plus pilot tone is frequency-hopped, we show that no degradation in s/n occurs. Thus, although frequency hopping does not alter the s/n [compare eqs. (42) and (53)], it does have important perceptual advantages. For example, consider a stationary mobile (e.g. parked, or in congested traffic) operating in an SSB system that does not employ frequency hopping. Suppose the mobile is subjected to a deep fade that defies pilot correction, resulting in a complete disruption of communications. Now imagine that frequency hopping is applied; the probability that communication will be restored increases as the probability of repeatedly hopping into a deep fade condition is small. Of course, if the mobile were not in a deep fade but receiving excellent communications, the effect of frequency hopping would degrade the recovered speech, although the degradation would probably be marginal. What frequency hopping ensures is that no mobile is ever in a permanent deep fade, provided the vehicle is not in a completely hostile environment, such as a tunnel, etc.

Generally, pilot correction can be performed, and the recovered speech will have only occasional segments of duration τ that have been obliterated by the fade. As they are likely to be in juxtaposition with good quality segments, speech enhancement procedures can be used on the degraded segments, particularly if τ is of the order of a pitch period. If τ is small (<5 ms), the model of Rayleigh fading is not applicable and the accuracy of our s/n analysis is unknown. Note that the short-time statistics of fading are also unknown. The choice of τ, therefore, depends on many factors, ease of switching, aid to enhancement, etc. Duration τ also determines how noise-like the co-channel interference will be. From these considerations, a suitable choice of τ is between 10 to 50 ms.

We have derived and discussed in detail the problem of frequency selective fading. By employing space diversity reception (see Section V) the signal deterioration caused by fading can be further reduced. This means that the factor controlling user density is co-channel interference, and it is here that frequency hopping makes its most significant contribution by changing the nature of co-channel interfer-

ence from cross-talk to almost band-limited white noise. Comparing eqs. (64) and (53), we see that the effect of co-channel noise is to introduce the term $\delta^2 \langle A_i^2 \rangle$, where $\langle A_i^2 \rangle$ is noise-like, composed of segments of τ seconds, where adjacent segments contain speech from different speakers in the interfering cell. By frequency hopping we have circumvented, in perceptual terms, the inability of the SSB receiver to capture the wanted signal. What we are left with is the speech signal corrupted by noise, and we envisage that the next phase of the research will involve the development of techniques to strip the noise from the speech signal. By doing this, we will be able to operate with high s/n, or alternatively move the cells closer together, thereby raising the user density.

Frequency hopping is not confined to SSB. When applied to FM, eq. (53) applies with the same advantages as for SSB. In terms of co-channel interference, there would be no need to rely on the capture effect of FM, and further, a measure of privacy could be obtained.

Summarizing: SSB can combat fading if pilot tones are used, and has enhanced quality if space diversity reception is added. By using frequency hopping under the auspices of a scrambling code, improvements occur for stationary and slow-moving vehicles. The most significant advantages accrue from combating co-channel interference, where crosstalk is perceived as random noise. Scrambling codes to satisfy the requirements of the system are trivial to generate and have not been discussed here. When compared to FM, the user density of FH-SSB-PT is marginally higher. Frequency hopping is not confined to SSB, can be applied to FM with advantage, and offers privacy in mobile radio where eavesdropping may be a problem.

Finally, we comment that since SSB demodulation requires recovery of a carrier, linearity of its modulators, etc., it is still possible that SSB user density may not be higher than that of wide-index FM in all situations. Also, since the availability and economics of SSB are not discussed in this paper, we do not imply that current FM modulation used in the AMPS system is not technologically appropriate at this time. We present a new analysis of SSB and point out some directions of research to resolve these questions.

REFERENCES

1. W. C. Jakes, "Microwave Mobile Communications," New York: John Wiley, 1974.
2. W. R. Young, "Advanced Mobile Phone Service: Introduction Background and Objectives," B.S.T.J., *58*, No. 1 (January 1979), pp. 1–14.
3. D. L. Huff, "The Developmental System," B.S.T.J., *58*, No. 1 (January 1979), pp. 249–69.
4. J. C. Feggeler, private communication.
5. D. J. Goodman, P. S. Henry, and V. K. Prabhu, "Frequency-Hopped Multilevel FSK for Mobile Radio," B.S.T.J., *59*, No. 7 (September 1980), pp. 1257–75.
6. G. R. Cooper and R. W. Nettleton, "A Spread Spectrum Technique for High

Capacity Mobile Communication," IEEE Trans. Veh. Tech., *27* (November 1978), pp. 264–75.

7. P. S. Henry, "Spectrum Efficiency of a Frequency-Hopped DPSK Mobile Radio System," IEEE Trans. Veh. Tech., *28* (November 1979), pp. 327–32.

8. R. W. Gibson and R. Wells, "The Potential of SSB for Land Mobile Radio," 29th IEEE Vehicular Technology Conf., Arlington Heights, Illinois (March 27–30), 1979, pp. 90–4.

9. K. W. Leland and N. F. Sollenberger, "Impairment Mechanisms for SSB Mobile Communications at UHF with Pilot Based Doppler/Fading Correction," B.S.T.J., *59,* No. 10 (December 1980), pp. 1923–42.

10. S. C. Kac and N. S. Jayant, "On Speech Encryption using Waveform Scrambling," B.S.T.J., *56,* No. 5 (May–June 1977), pp. 781–808.

11. M. Abramowitz and I. A. Stegun, "Handbook of Mathematical Functions," National Bureau of Standards (1967), pp. 228–54.

12. D. Slepian, "Fluctuations of Random Noise Power," B.S.T.J., *37,* No. 1 (January 1958), pp. 163–84.

13. V. H. MacDonald, "The Cellular Concept," B.S.T.J., *58,* No. 1 (January 1979), pp. 15–41.

Description of Fasnet—A Unidirectional Local-Area Communications Network

By J. O. LIMB and C. FLORES*

Fasnet is an implicit token-passing, local-area network aimed at supporting high data rates and carrying a wide mix of traffic (data, voice, video, and facsimile). Transmission is unidirectional with stations attaching to the medium passively via directional couplers. A link consists of two lines, one to carry traffic in each direction. Unidirectional transmission provides the potential for efficient operation at high data rates, while the passive medium provides the potential for high reliability. We describe the physical configuration and the protocol and give channel utilization for the condition of continuously queued sources. Mechanisms to control the access of various traffic types are described. Finally, the interconnection of multiple Fasnets is studied for one particular configuration, a ring.

I. INTRODUCTION

Local computer networks operating at 1 to 10 Mb/s are being commercially offered and appear to adequately meet current demands for computer communications within the office environment. However, future needs stimulated by both a broader range of services than is now available and changes in system architecture (e.g., the trend towards distributed processing) could increase significantly the demand for digital capacity. For example, one would like to be able to handle video information, voice traffic, and facsimile, as well as computer traffic, in a single digital system. The availability of a cheap, high-capacity communication conduit between computers will itself stimulate increased traffic. For example, processing time can be traded for communication capacity; rather than transmitting a text file and

---

* Department of Electrical Engineering and Computer Science, University of California at Berkeley.

formatting it at a remote location, one may choose to transmit a formatted version or even a bit map. Thus, while today 10 Mb/s may be regarded as an extremely generous bit rate for a local computer network, 200 Mb/s may become limiting for an integrated communications network.

Carrier-sense multiple access with collision detection (CSMA/CD) is reliable and reasonably efficient even under heavy load for most conditions.[1] Shoch and Hupp[2] show that measurements of channel utilization of an Ethernet* yield results that are close to calculations made by Metcalf and Boggs, using a simplified model and assuming that active stations have data continuously queued for transmission. Utilization is reported in Ref. 1: $\eta = \gamma/[\gamma + F(M)]$, where γ is the ratio of packet duration to slot time and $F(M)$ is a slowly varying function of M, the number of active stations. Utilization is plotted as a function of γ in Fig. 1, with M as a parameter. If we assume that slot time is 50 μs,[3] and the transmission rate is 100 Mb/s, then for an average packet length of 1000 bits, $\gamma = 0.2$ and utilization is in the range 7 to 8 percent.† Shorter packets, higher transmission rates, or longer slot times would further decrease efficiency. Also note that the above equation does not incorporate source acquisition and synchronization time which, like slot time, is relatively more significant at higher transmission speeds. Thus, it appears that CSMA/CD is not viable for operation at high data rates.[5]

Fasnet is an implicit token-passing protocol developed to efficiently utilize the channel capacity when the ratio of packet duration to the maximum station-to-station propagation time is small (<1). Information flows in only one direction on the medium, unlike the usual CSMA/CD configurations (although see Refs. 5 and 6), but like CSMA/CD the essential passivity of the medium is retained. The access method is closely related to a ring protocol (e.g., see Ref. 7) and may be regarded as a variant of implicit token passing.

Reliability was an important consideration in the design of Fasnet. Consider both the transmission medium and the control electronics. Reliability of the transmission medium may be enhanced by keeping active electronics in the medium to a minimum. Bus architectures such as Ethernet have occasional repeaters, depending on the length of the signal path. Cable-TV (CATV) type architectures have periodic line amplifiers whose spacing is determined by the number of stations (taps), as well as by cable attenuation. Ring architectures usually have

---

* Ethernet is a trademark of Xerox Corporation.
† Since Ethernet requires $\gamma \geq 1.0$ for collisions to be reliably detected, utilization for values of $\gamma < 1.0$ were obtained by multiplying the utilization for $\gamma = 1$ by the value of γ. This can result in efficiencies much lower than that obtainable by other CSMA protocols, e.g., p-persistent CSMA.[4]
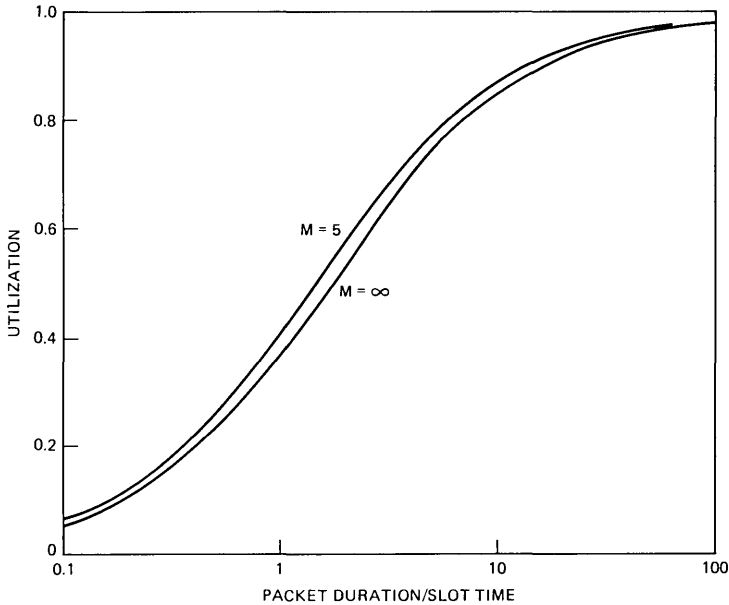
Fig. 1—Plot of efficiency as a function of the ratio of packet duration to slot time. Parameter is the number of simultaneous users. Efficiency changes little as the number of users goes from 5 to ∞.

most electronics in the signal path; digital regeneration is usually provided at each station.[7] Turning to control, reliability considerations tend to favor distributed control. An alternative to a fully distributed system is to permit some stations to perform unique functions but have these functions assumable by any station on the network; however, this can result in a large cost penalty. A further alternative is to have the function performed on a server basis (two or more stations provide the service to all other stations). The Fasnet medium resembles that employed in CATV, and control is primarily distributed with some functions assumable by all stations.

There is considerable attraction in having a single system to handle all forms of traffic in the environment. Indeed, such a system may be regarded as an extension into the local environment of the Integrated Systems Digital Network (ISDN) that is being so vigorously pursued in the long distance and local loop environments by the common carriers.[8] An integrated transmission system simplifies the implementation of services that utilize different types of traffic. Examples are voice-annotated electronic mail[9] and interactive use of voice and facsimile.[10] An integrated transmission system also provides the opportunity to reduce overall transmission needs by taking advantage of the complementary nature of some types of traffic; for example, most electronic

mail can be deferred until after the voice busy hour. Further, one would anticipate cost reductions in having one integrated system over a number of separate systems.

While design of an integrated system offers opportunities, it also presents the need for compromises and trade-offs. Consider terminal costs and transmission efficiency. If a system is to provide economical interconnection for telephones and terminals, it must permit construction of an interface that is cost-effective relative to alternative solutions. This may mean that some interfaces have to be tailored to the specific application to make them competitive.

Virtually any type of traffic should be able to exploit the channel efficiently. For example, environments that generate a large number of short messages (e.g., computer terminal traffic), as well as environments that generate a preponderance of long messages (e.g., file transfers), should be able to operate efficiently. This requires that there be a minimum of structure at the lowest common level of the service. For example, a packet structure which mandated a source-address field, while useful for computer traffic, may be unnecessary overhead for a voice channel where call set-up would establish the identity of the source.

The description of Fasnet starts in Section II with the physical loop; the access protocol is described in Section III. The performance of the basic system is given in Section IV, followed by a discussion of some of the system design issues (in particular, the synchronization and signaling procedures) in Section V. Section VI describes variations of the basic system, including methods for improving efficiency, particularly when the number of users is small. Section VII describes mechanisms to support the efficient management and control of mixtures of different traffic types. Section VIII describes the interconnection of Fasnets, with consideration of the impact of the topology on throughput and ability to handle localized sources of traffic. Section IX summarizes the paper.

II. PHYSICAL CONFIGURATION

The basic link, as shown in Fig. 2, consists of two lines. One line passes all stations carrying traffic in one direction and the other line passes all stations carrying traffic in the other direction. For line A, station S_1 is referred to as the head station and S_n the end station. For line B the assignment is reversed. Together the two lines provide a connection between any pair of stations attached to the link. While the lines may be either twisted pair, coaxial cable, or light fibers, we will be primarily concerned with a coaxial cable implementation. Each station makes two connections to each line. A read tap precedes a
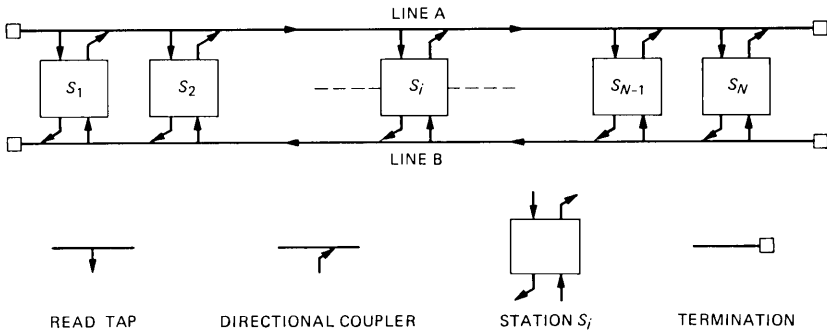
Fig. 2—Physical configuration of a Fasnet link.

passive directional coupler used for writing. The nature of the directional coupler is such that very little energy travels in the reverse direction on the line so that the signal read virtually simultaneously from the read tap will be unaffected by the signal being written on the line via the directional coupler. A station writes on the line by adding energy to the signal already existing on the line. Except for specific fields of the header, the protocol ensures that only one station at a time writes on the line. Thus, once a signal is written on a line, it is not removed or changed by any station. This has certain implications for the line code that is selected (Section 5.2).

Depending on the length of the line, amplifiers are needed to boost and compensate the signal. The technology and design procedures used for CATV systems[11] are directly applicable here, although the noise margin required for a high-quality video signal is somewhat greater than that required for two- or three-level digital transmission.

Links may be joined together to form a network of links. Usually, links will be run in pairs of lines, but this is not always necessary. The advantage of using multiple links is that the traffic-carrying capacity of the network can be increased and reliability may be improved by the use of redundant paths.

An earlier version of Fasnet[12] differs primarily from the system described here in that a link consists of a single unidirectional line that passes each station twice—on the outbound or write side and on the inbound or read side. Each station makes three connections to the line, a read tap for control purposes, and a directional write tap on the write side, and a read tap for recovering data on the read side. The primary advantage of the scheme described here is that the link can carry approximately twice the traffic of the earlier version. A disadvantage is that a station must select the correct line on which to transmit, and this will depend on the relative physical location of the destination.

III. PROTOCOL DESCRIPTION

The data link layer may be divided into two sublayers.[13] One sublayer, the logical link control with which we are less concerned here, provides functions like addressing, windowing, and acknowledgments. The other sublayer, the media access control with which we are more concerned, determines when and how to send information via the physical medium. This is influenced by the media type, the physical configuration, and the technology used.

3.1 Frame format

The frame structure suggested in Ref. 13 and its relation to the data link sublayers is shown in Table I. The information unit is delivered by the network layer. The logical link control appends the source address, the destination address, the link control field for windowing, acknowledgments, and similar functions. We call this unit a packet, and in the work described here we will assume it is of fixed length. The media access control sublayer appends (i) the frame check sequence computed on the previous fields for error detection and (ii) the access control (AC) field which determines how and when each station may access the physical medium. The main objective in the design of this field is to control access among all active stations in an efficient, reliable, and fair manner. The frame start and frame end delimiters are unnecessary, since the stations are kept in tight bit and frame synchronization (see Section 5.1). The duration of the frame is referred to as a slot.

3.2 Access control

Basic access control for Fasnet is as follows. The head station, S_1, initiates a cycle on line A. After a cycle has been initiated, each active station on the line with packets destined in the right direction is allowed to access the line for one slot. To do this, each station monitors the line. When it senses the line idle, it seizes the line for one slot. It has to wait for a new cycle to be initiated before it attempts to access the line again. The exact manner in which this is done efficiently and

Table I—Protocol and frame structures

Protocol Structure		Frame Structure
Data link layer	Logical link control sublayer	DA/SA/LC/IU
	Media access control sublayer	FS/AC/DA/SA/LC/IU/FCS/FE
Physical layer	Physical layer signaling	FS/AC/DA/SA/LC/IU/FCS/FE

FS:	Frame starting delimiter	LC:	Link control field
AC:	Access control field	IU:	Information unit from network layer
DA:	Destination address	FCS:	Frame check sequence
SA:	Source address	FE:	Frame ending delimiter

fairly is described in the next paragraphs. If a station has priority, it is given permission to access the line for an integral number of slots. In this manner, the active stations can access the line for a specified duration in the order in which they are physically located on the line. The operation on line B is identical to that described above with S_N replacing S_1 as head station.

To describe the operation in more detail, let $\{S_1, S_2, \cdots, S_N\}$ be the set of stations in the order of their physical locations as shown in Fig. 2. Let AQ_i and BQ_i be the number of packets queued at station S_i for access to lines A and B, respectively.

When the next packet arrives at S_i from the Network layer interface, if destination address $j > i$, then AQ_i is incremented by 1; if destination address $j < i$, then BQ_i is incremented by 1.

The structure of the AC field is shown in Fig. 3. Let t_{fn} be the start of the nth frame. The AC field is from t_{fn} to t_{bn}. Station S_i gains access to line A in the following manner. Let S_i be permitted access for $p_{\max}$ packets each cycle. At t_{fn}, the start of the nth frame, the read tap reads the START bit of the AC field. The start of cycle is indicated by START = 1. Because of gate delays in the decision circuitry and propagation delays in the tap cables, the outcome of the read operation is only known at t_{sn}. This additional time of duration τ_{dec}, shown in Fig. 3, is of the order of a few bit times for a 100 Mb/s line and nanosecond logic. Next, the station may simultaneously read the BUSY bit via the read tap and write BUSY = 1 via the directional coupler. Again, the outcome of the read operation is only known at t_{bn} after a delay of τ_{dec}. Nonetheless, the write operation does not alter the BUSY bit if it is already set to 1. The nature of the signaling to achieve this is explained in Section 5.2. At t_{bn}, if BUSY = 1, the station defers until the BUSY bit of the next frame. If BUSY = 0, the station accesses the line for the remaining frame duration.

Station S_i is said to be in one of four states:

IDLE —if it has no packets to transmit, i.e., $AQ_i = 0$.

WAIT—if it is waiting for the start of cycle.
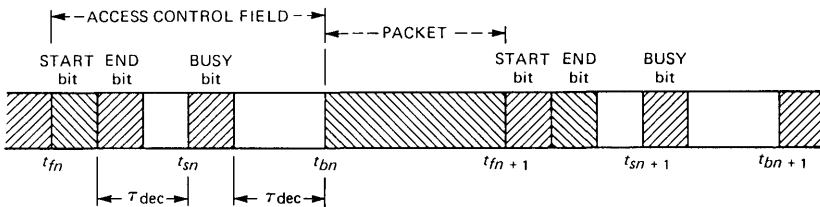
Fig. 3—The frame structure of Fasnet. Each frame consists of (*i*) an access control field containing START, END, and BUSY bits; and (*ii*) the packet as provided by the logical link sublayer.

DEFER —if it is deferring to busy users who are upstream on the line.

ACCESS—if it is accessing the line.

The station makes transitions (denoted as →) between states as follows (Fig. 4): While $AQ_i = 0$, S_i is in IDLE. Upon arrival of a packet for line A, $AQ_i > 0$ and $S_i \to$ WAIT. The station reads the START bit of every frame. When START $= 1$ $S_i \to$ DEFER, and the station simultaneously reads and writes the BUSY bit as described above for every frame. When BUSY $= 0$ $S_i \to$ ACCESS. Now it accesses the line for p_{max} frames and also writes BUSY $= 1$ for each. Then $S_i \to$ WAIT. The station may cease to access the line earlier if $AQ_i = 0$, whereby $S_i \to$ IDLE.

Station S_1 initiates cycles by START $= 1$ in the first frame of each cycle. There is an additional bit, END, in each frame to indicate the end of cycles. This bit can be conveniently located in the blank portion of the frame after the START or BUSY bits. When station S_N reads BUSY $= 0$ on line A (indicating that all active stations have accessed the line), it sets END $= 1$ in the next frame on line B. On receipt of this frame on line B, S_1 then initiates a new cycle on line A. Thus, in the worst case, line A will be silent once every cycle for a time equal
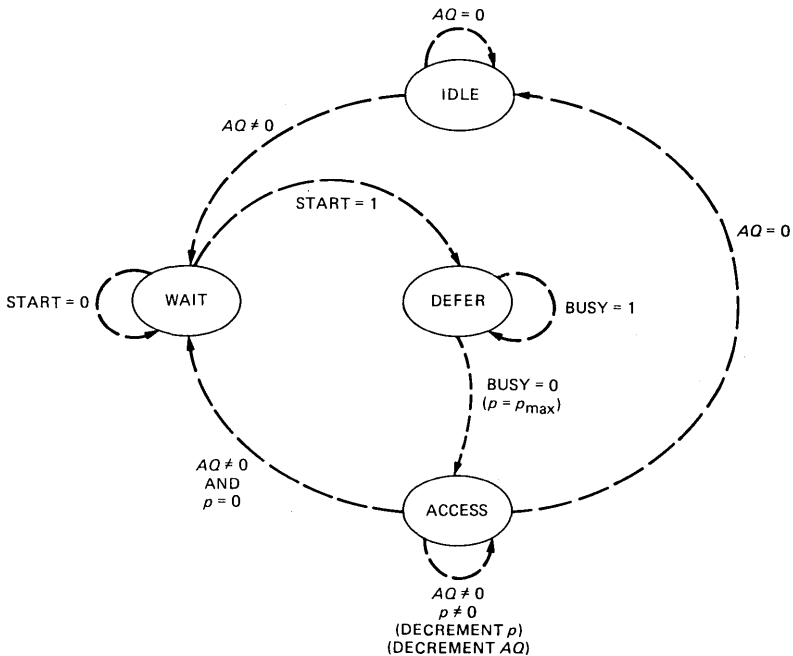
Fig. 4—State transition diagram describing the operation of a Fasnet station.

to twice the end-end propagation delay, plus twice the frame duration, as each end station has to wait until the next frame to set the START or END bits.

The operation on line B is identical, with the roles of S_1 and S_N reversed. Thus, the two lines cycle independently of each other with access being passed between the stations in the same order as their physical locations on each line.

In the protocol described above, the outcome of the read operation on the START bit needs to be known before the BUSY bit is written so that the first frame of a new cycle does not remain idle. Should the START and BUSY bits be adjacent to each other, a station will only learn that START = 1 after the BUSY bit has passed and the frame will not be used. However, for large cycle lengths and short packet lengths, the reduction of one decision interval, τ_{dec}, per frame would be greater than the addition of the extra idle frame.

A further alternative is to have the first frame of each cycle contain only an access field. However, unequal frame sizes complicate synchronization for a very small increase in efficiency.

3.3 Error recovery

The protocol is controlled by the START, BUSY, and END fields. An error in a BUSY field will have no lasting effect; it will result in a packet being overwritten if the busy bit is changed from a 1 to a 0. Alternatively, an empty slot will go unused if the busy bit is changed from 0 to 1. Of more significance is an error in the START and END fields. If a START field is set to 1 in error, two STARTs or a START and an END would be simultaneously present on the loop.

It will be shown that generation of additional STARTs and ENDs will not propagate and have little effect on the operation of the link. We will assume that end stations do not generate STARTs or ENDs that are closer together than the round-trip delay time, τ_r; under normal operation this cannot occur. A false START = 1 will occur either in the active portion of a cycle (including the first empty slot) or in the empty slots occurring at the end of the cycle. If the former, a new cycle will start before, or as, the old one is finishing. Since the additional START = 1 will not generate an END = 1 on the return line (because no transition from busy slot to empty slot is detected), the condition will not propagate. If the false START = 1 occurs in the empty slots, other than the first, the new cycle will start prematurely (actually increasing utilization temporarily). One of two conditions results:

(i) The busy part of the additional cycle terminates at least one slot before the next normally occurring START = 1, in which case the end station will detect an end condition. However, because the period

since the last END $= 1$ is less than τ_r a new END $= 1$ will not be generated.

(*ii*) There is no empty slot before the next normally occurring START $= 1$. As a result, an additional end condition is not detected by the end station.

Thus, a START $= 1$ resulting from a fault condition will not produce additional END $= 1$ bits on the return line. On the other hand, END $= 1$ faults, unless they are closer together than τ_r, will produce additional START $= 1$ slots which as just described, have a transient effect on the operation of the link.

Consider the condition where a START or END bit is changed from a 1 to a 0. A new cycle would fail to initiate. After a time-out greater than the longest permitted cycle time, the head station will issue a START $= 1$, and the link will continue to operate normally. Should a head or end station fail, the station next to the head or end station would assume the functions on detecting loss of timing or after timing out on the arrival of START $= 1$ or END $= 1$.

3.4 Fault diagnosis

The independent lines of the Fasnet link provide the opportunity to localize and mitigate some types of faults. Consider first that a line is severed because of some catastrophic event or something trivial like a cable connector failing. The result will usually be either a short or open circuit leading to a gross impedance mismatch. The fault will most likely terminate all effective communication on the upstream side of the fault because of reflections from the mismatch traveling back into station interface units via the read tap. The downstream segment will be affected very little because the directional couplers will propagate little energy in the direction of the mismatch. Thus, a diagnostic program in the end station can determine between which stations the mismatch lies. This is done by having the end station send a query to each station via the intact line and determining which stations respond to the query.

A difficult type of station fault is to have a station continuously write garbage on a line. Diagnostic programs in the end stations, again by querying each station, can determine the faulty station and remove it from service. The head station on the line with the fault, after being informed of the fault by the end station, via the other line, queries each station in turn. If the station fault is confined only to the write circuit, the faulty station will respond. The next station on the downstream side will not respond, since it will not be able to read the query sent by the head station because of the interference from the faulty station. If both read and write circuits in the faulty station are affected, the last correctly responding station will be the station on the upstream

side of the faulty station. Thus, the fault is isolated to one of two stations. Both stations may then be disconnected by means of a control signal sent via the functioning line. The faulty station may then be uniquely determined by returning one of the stations to service. If the fault condition resumes, the returned station is faulty and is disconnected; otherwise the other station is faulty.

IV. PERFORMANCE

4.1 Sample operation

Typical operation of Fasnet for lines of 2.5-km individual length, 100 Mb/s bandwidth, and 200-bit frame length is shown in Fig. 5. It shows the time-space relation of the frames on each line. The horizontal axis represents time divided into slots A_1, A_2, A_3, $\cdots$ for line A and B_1, B_2, B_3, $\cdots$ for line B. The vertical axis represents the physical locations of the active stations S_1, S_2, S_3, S_4, and S_5 with S_1 and S_5 serving, additionally, as end stations. The electrical line length is five frames. Station S_1 initiates the cycle in frame A_1, and access passes from S_1 to S_2 to S_3 to S_4. When the end station, S_5, senses BUSY = 0 in frame A_5, it sets END = 1 in frame B_9. Receipt of this frame by S_1 causes it to
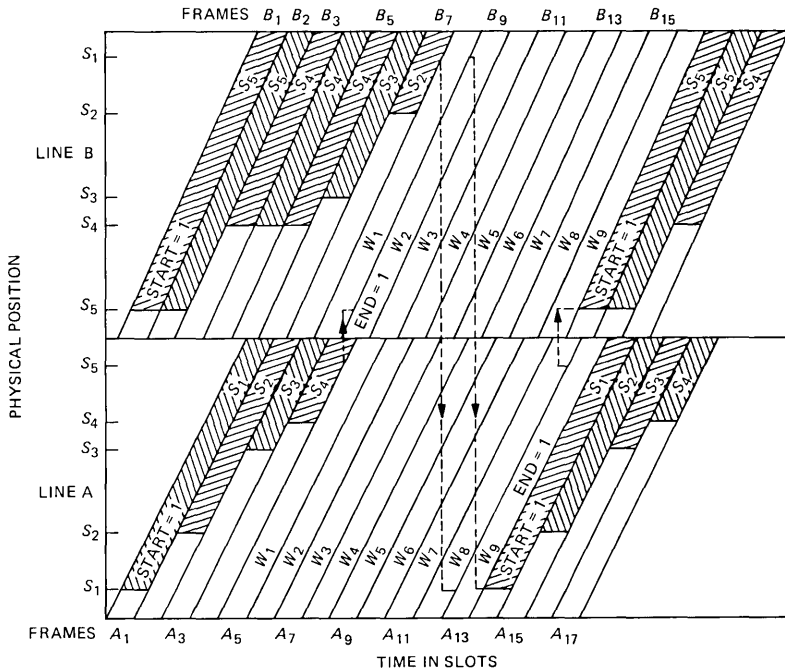
Fig. 5—A graph of activity on a Fasnet link (lines A and B) as a function of time. The dotted lines indicate the flow of information from one line to another.

initiate a new cycle in A_{14}. Similarly, a cycle on line B starts at B_1. Assume that S_5 and S_4 are permitted access for up to two and three packets, respectively. Station S_1 senses BUSY $= 0$ in frame B_8 and sets END $= 1$ in A_{13}. Receipt of this frame by S_5 causes it to start a new cycle in B_{17}.

4.2 Utilization

As there are no collisions, no capacity is lost through collision resolution. However, the utilization is not 100 percent as each line is idle at the end of each cycle. The idle period is nine frames, W_1, W_2, $\cdots W_9$, on each line in Fig. 4. In the worst case, this is equal to twice the end-end propagation delay, plus twice the slot time (one slot time on average) as each end station has to wait until the start of the next slot to set the START or END bits. If

v = speed of propagation on the line (m/s)

W = line capacity (b/s)

L = line length (m)

F = frame size (bits)

M = number of busy stations with downstream traffic,

then if each station is allowed access for only a single packet per cycle,

$$\text{cycle length} = \tau_c = M^*(F/W) + 2^*(L/v) + (F/W) \, ,$$

$$\text{duration of busy frames} = \tau_b = M^*(F/W) \, , \tag{1}$$

and

$$\text{utilization} = \eta = \frac{M^*(F/W)}{M^*(F/W) + 2^*(L/v) + (F/W)} \, . \tag{2}$$

The effective utilization is lower since a fraction of each frame is devoted to access control. However, for large F, it results in only a small reduction in utilization. If $v = 2.5 \times 10^8$ m/s, $W = 100 \times 10^6$ b/s, $L = 2.5 \times 10^3$ m,

$$\eta = \frac{M^*F}{(M + 1)^*F + 2000} \, .$$

For $M = 100$,

$F = 50$	$\eta = 71$ percent
$F = 100$	$\eta = 83$ percent
$F = 200$	$\eta = 90$ percent
$F = 500$	$\eta = 95$ percent
$F = 1000$	$\eta = 97$ percent.

For the same values of ν, W, and L, with $F = 500$[1,2] and assuming an Ethernet slot time $T = 50 \times 10^{-6}$ s,[3] we can compare the performance of Fasnet and Ethernet as the number of stations is varied as shown in Table II.

Unlike Ethernet, Fasnet has the desirable feature that as the load increases, the utilization also increases. The above figures do not reflect the fact that in practice the length of packets is variable and, consequently, the fixed frames of Fasnet frequently will be only partially filled. The effect on η depends on the distribution of packet size, and to some extent is determined by the system design. For example, in a system designed for large amounts of voice traffic, F could be set equal to the size of a voice packet.

V. IMPLEMENTATION CONSIDERATIONS

The design criteria previously stressed in the introduction affect the implementation in important ways. In particular, the requirement to operate at high speeds and the unidirectional operation of the bus affect the design of the synchronization system; in turn, the type of synchronization and the use of directional couplers impact the choice of the line code that is used.

5.1 Synchronization

Bus systems in which signals travel in both directions on the line require the receiving stations to adapt to the signals transmitted by the sending station because the amplitude, dispersion, and phasing of the received signal vary depending upon the position of the transmitting station on the line. Synchronization can be achieved very quickly when the signaling rate is low relative to the bandwidth of the transmission medium. At higher signaling rates, synchronization needs to

Table II—Fasnet versus Ethernet as a function of number of busy stations

M	Fasnet	Ethernet*
	(in percent)	
5	50	4.1
10	67	3.9
50	91	3.7
100	95	3.7

* Note that since the minimum permissible packet length is 5000 bits, η is calculated as 0.1 of η with 5000-bit packets. Other CSMA protocols that do not require collision detection perform better.

be more accurate to achieve good error performance. Ethernet specifies a synchronization preamble of 64 bits and for higher transmission rates an even longer sequence may be required. Thus, for short messages efficiency would be significantly reduced. Using a unidirectional bus, each station can be synchronized to a common clock issued from the head station. Thus, if all stations add signals to the cable in phase with the transmitting clock, stations will receive the signals in correct phase. Similarly, fixed gain and frequency compensation can be employed. The problem of reliability can be overcome by giving each station the ability to supply clock. The clock drive would be inhibited by detection of, and locking to, an incoming clock.

Initial tests have shown that a simple, cost-effective method of synchronization is to synchronize to a continuously injected pilot tone placed at the high end of the signaling band. The synchronizing function then assumes a negligible fraction of the transmission capacity.

In addition to bit synchronization, frame synchronization is also required. This is achieved by sending periodically a synchronizing bit pattern. Design is simplified if this is sent after an integral number of frames, say 64 or 128. With tight bit and frame synchronization, successive frames may be butted together without a gap.

5.2 Signaling

Because synchronization is achieved independently of the data signal, line codes with fewer transitions may be considered. It is particularly convenient if a code is chosen that couples no energy to the line when one of the logic states is continuously transmitted (assume logic 0). Each station at the end of transmission then simply returns to logic 0, and there is no need to "disconnect" the transmitter from the line. The two line codes we are investigating are a bipolar three-level code, Fig. 6a, and a nonreturn to zero (NRZ) two-level code, Fig. 6b. The two-level signal has a greater noise margin; however, one has to contend with the dc signal component.[14]

The Fasnet protocol does not permit subsequent stations to modify a signal already transmitted by an upstream source. In principle, this could be done. For example, a signal from one station could be deleted from the line by a second station writing the complement on the line. In practice, signal levels would have to be matched very accurately for such a scheme to work.

There is one condition in which more than one station may add energy to the same bit in a frame—the BUSY bit of the AC field. As a result, the amplitude of this bit may far exceed the amplitude of the remaining signal. This may lead to errors in adjacent bits of the AC field. To prevent this, guard bands on either side of the BUSY bit
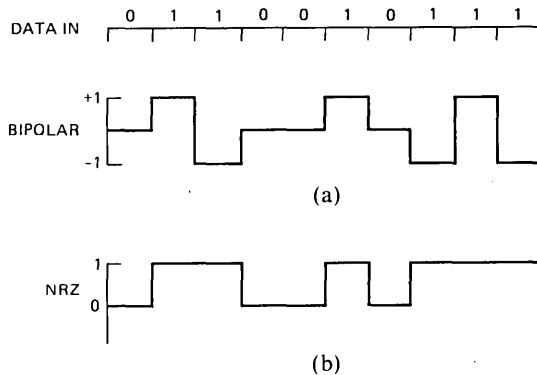
Fig. 6—(a) Bipolar three-level line code. (b) NRZ two-level line code.

should be used. Notice from Fig. 3 that the access field is configured so that the guard bands fall in the intervals τ_{dec} and, in practice, will have a comparable duration.

VI. IMPROVING UTILIZATION

As can be seen from (1), efficiency increases (i) as cycle length increases and (ii) as the idle period at the end of each cycle (intercycle gap) decreases. At the expense of some increase in complexity, techniques may be devised to improve utilization by increasing cycle length or reducing intercycle gap.

6.1 Control of cycle length

Since START $= 1$ may be read by all stations, the length of the last cycle, τ_c, may be determined by any station. As previously described, each station may transmit up to p_{max} packets per access. Thus, by controlling p_{max}, stations may influence the value of τ_c. Station control of τ_c by manipulation of p_{max} is obviously limited. For example, let us assume that p is fixed at 1 and that we have stations each generating packets at a rate $< 1/\tau_c$. Increasing p will not change the cycle length since packets will be transmitted before a queue can form. On the other hand, increasing p for heavily loaded stations will lead to an increase of τ_c, provided τ_c is less than the accepted maximum.

6.2 Reducing inter-cycle gap

Three methods are described for reducing the intercycle gap and hence increasing the line utilization. In the first, stations detecting the END $= 1$ bit seize empty slots on the other line; in the second, stations use the END field as a request field; in the third, the end station
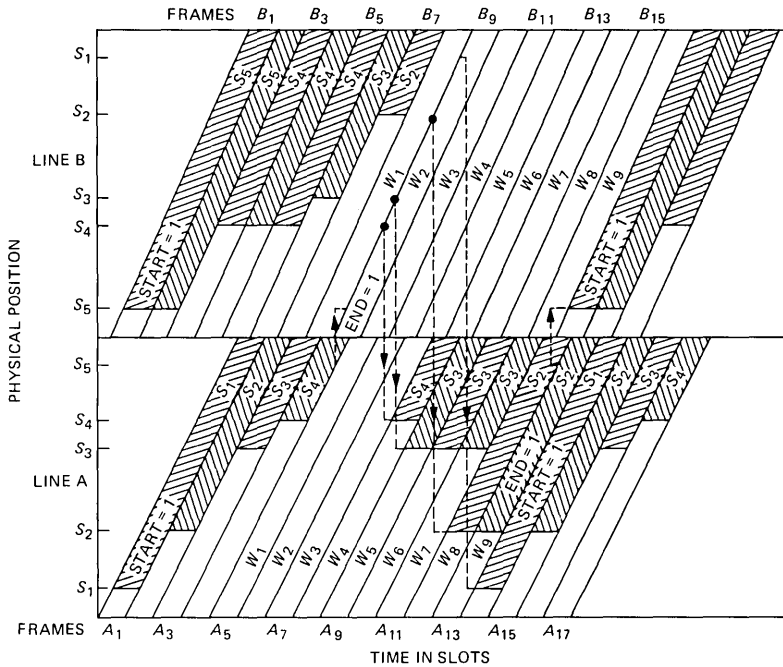
Fig. 7—A graph of activity on a Fasnet link as a function of time. Empty slots encountered on line A by stations that have read END = 1 on line B are utilized. The IDLE period is reduced to three slots. Corresponding use of IDLE slots on line B would also occur but is not shown.

attempts to estimate the end of a cycle, setting END = 1 before BUSY = 0 is received.

Considering the first method, any station S_i in the WAIT state that observes END = 1 may attempt to seize any empty slots on the opposite line.[12] The number of empty slots seized depends on the time the END = 1 frame takes to propagate to the next active station, which then seizes empty slots, thus preempting active stations down-stream.* The intercycle gap now depends on the propagation time from the last active station to the end station and back. (The relative timing of the frame starts in the two lines will also affect the gap size). As shown in the example of Fig. 7, the intercycle gap has been reduced from nine slots to three, shown for line A only.

In the second method, stations in DEFER and ACCESS states write REQUEST (REQ) = 1 on the return line (the END field is now

---

* A station may only transmit a single frame at a time because of the possibility of preemption. This will interfere with construction of "superpackets." Superpackets are used to increase efficiency by reducing the effect of packet overhead. The overhead is attached only to the first packet of the superpacket.[12]

replaced by an REQ field). After all stations have been served, the head station will read REQ = 0 and initiate a cycle. To ensure that at least one REQ = 1 occurs in a cycle for which only one station is active, a station in changing from WAIT to DEFER or ACCESS writes at least one REQ = 1. Approximately speaking, the average intercycle gap is now equal to twice the propagation time from the head station to the last active station, plus half a slot time. Notice that this procedure is more distributed in that the end-station function of recognizing the end-of-cycle END condition and writing END = 1 on the return line is now bypassed. Each station now performs an equivalent operation.

A further refinement is to observe that the head-station function can also be distributed.* Each station with traffic to transmit need not wait for the head station to issue START = 1. Rather, after reading REQ = 0 on the return line, it can switch from WAIT to DEFER or ACCESS mode setting the p register to the allowed number of packets that may be transmitted per cycle. The intercycle gap is virtually eliminated under heavy traffic conditions and for a large number of users as in the first method. For two continuously queued stations, the intercycle gap is twice the delay time between the stations, plus one slot time on average. Notice that even though no START is being issued, or is necessary, the loop cycles. However, as in the first method, packets from a source during one cycle will usually not be consecutive. The station protocol is summarized in Fig. 8 by means of the state diagram. As seen in comparison with Fig. 4, the protocol is more complex; however, the algorithm no longer requires the centralized head or end-station functions. The issue of distributed control versus centralized control is particularly important in efficiently accommodating different types of traffic and is discussed further in Section VII.

In the third method, each active station in the DEFER state indicates its desire to transmit by setting an additional request field to 1 (REQ = 1) in the access field of the line on which it wishes to write, as in Ref. 12. The end station estimates the cycle length and transmits END = 1 timed to arrive at the head station as the last slot to be used in the cycle is leaving the head station. If the estimate was too low, the end station will read REQ = 1 in the last frame in the cycle indicating that the estimate of the length of the last cycle was too short. Therefore, the estimate of the length of the next cycle would be increased. If the estimate is too high, there will be empty slots prior to the arrival of the next START = 1, and the estimate of the length of the next cycle would be decreased. If the estimate is correct, then the

---

* Suggested by Z. L. Budrikis in connection with the earlier single-line version of Fasnet.
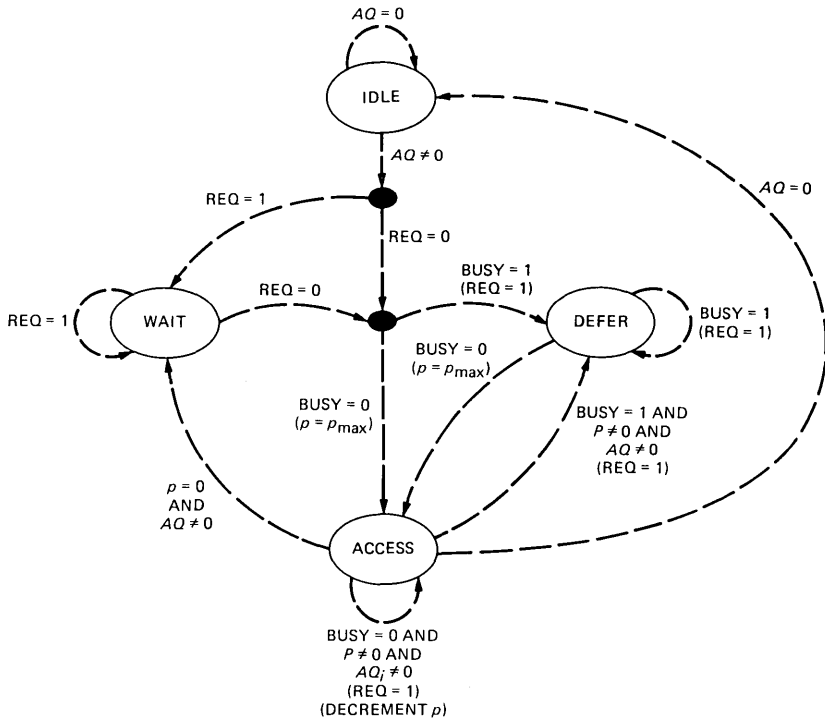
Fig. 8—State transition diagram of a distributed version of the Fasnet protocol in which unique functions in the head and end stations are not employed. Statements in parentheses are actions executed on making the transition. The filled circles denote intermediate states.

last frame before the next START $= 1$ will have REQ $= 0$ and the estimate of cycle length would remain unchanged.

Of the three methods for reducing intercycle gap, the former two are distributed while the latter requires additional intelligence in the end station.

VII. TRAFFIC CONTROL

Different types of traffic have very different transmission require-ments. Voice traffic is an interesting example of where an initial restriction of access (blocking) is preferable to losing voice packets. Real-time traffic such as voice and video requires a guaranteed maxi-mum delay if information is not to be lost. In contrast, some types of computer traffic are rather tolerant of delay. It is not our aim to develop here a comprehensive algorithm for handling different traffic types; it would depend closely on the particular environment and the mix of traffic. However, we would like to indicate the mechanisms that Fasnet can support to control integration of traffic.

We can identify four different types of control mechanisms.

(*i*) Selection of traffic—The ability to individually control a class of traffic.

(*ii*) Request for access—The ability to communicate that service is required.

(*iii*) Blocking of traffic—The ability to prevent traffic of a specific class from gaining access to the system.

(*iv*) Continuation of service—The ability to delay traffic for later transmission. We will take these four control mechanisms in turn and consider how they may be implemented in Fasnet.

(*i*) Selection—We can borrow from the strategy used by Frata et al.[15] and Ulug et al.[6] START, instead of being a single bit, can be expanded to a multibit word. A START code can then be allocated to each class of traffic. A station would then be permitted to transmit only if the START corresponded to the class of traffic it is waiting to transmit. A class of traffic could denote a traffic type, as well as a priority. The term subcycle will be used to denote the period from a START of one class to the next occurring START. Cycle will be reserved for the period between two STARTs of the same class.

(*ii*) Request—The amount of request information can vary from knowing exactly which station wants to send what traffic in one extreme to knowing just that a station somewhere wants to send some type of traffic in the other extreme. A compromise would be to provide a request word adjacent to the END field in each packet on the return line. Each bit in the request word would denote a class of traffic. This information would enable the head station to determine that one or more stations required service of a particular type without indicating the extent of the demand. Information about demand for service would most likely be used to adapt the control strategy in the case where there was a change in the balance between traffic types.

(*iii*) Blocking—The channel capacity allocated to a class can be controlled by the time allocated to that class as suggested in Frata et al.[15] By issuing a different START after a given period, further traffic of the original class type wishing to transmit would be denied access. Blocking is typically used to handle overflow of the type of traffic that generates information periodically, such as real-time voice and video, and synchronous data traffic. In this instance, it is appropriate to speak of connections between source and destination which implies guaranteed access once a connection has been allocated.

To discuss the allocation of connections in a blocking traffic class requires that the previous definitions of WAIT state and ACCESS state be generalized:

WAIT—A station is waiting for permission to seek access to the line.

ACCESS—A station has a connection.

Stations that already have access take the first free slot available to them after the appropriate START. Allocation of freed up slots on a reasonably equitable basis would proceed as follows. Stations would be aware of say n slots becoming free from the position of the END bit on the return line. Note, no END is issued if the class is full. Stations in the DEFER state would be permitted to compete for the n empty slots at the end of the subcycle. This will favor stations close to the head end. However, a large degree of fairness is achieved by permitting stations to switch from the WAIT to DEFER state only when two consecutive ENDS are encountered for that subcycle. This will only occur when all traffic currently in DEFER state has been granted access. At this point, traffic in the WAIT state would switch to DEFER and then vie for empty slots as they become available. This strategy is related to the snapshot algorithm.[16]

(iv) Continuation—In contrast to blocking, continuation requires that traffic not able to access the link in the previous cycle be served before any new traffic is accommodated. This may be achieved in the following manner. Assume that the class type is non-blocking. If the head station should issue a new START before all traffic of the class has been served, the end station will not detect the end of the cycle and hence will not issue END = 1. The absence of an END = 1 would indicate to the head station that the p registers of the stations in that class should not be reset on the next cycle (i.e., the stations would not switch from WAIT to DEFER).[15] Thus, in the following cycle, remaining traffic would be served. For centralized control, the START for this traffic type could contain an additional bit to indicate whether the previous cycle is being continued for deferring traffic or a fresh cycle is being started for new traffic. For distributed control, each station could keep track of the sequence of STARTs and ENDs.

It is important that the control strategy be adaptive to changing traffic conditions. We expect that the traffic mix will change relatively slowly—over a period of seconds rather than ms. Thus, it would be feasible to have the adaptation achieved by a server process.

The control algorithm could be implemented as completely distributed, completely centralized, or somewhere in between. Economics and reliability will dictate, to a large extent, where the control should be placed. Nevertheless, a hybrid strategy would seem more in the spirit of the current design. For example, selection is probably best achieved by having the head station transmit the appropriate START code (centralized, but perhaps assumable), whereas traffic assignment and continuation is probably best achieved by having each station read and operate on the END field (distributed).

VIII. TOPOLOGY

8.1 Introduction

A population of stations may be connected together by either a single link (Fig. 9a) or by several interconnected links (Fig. 9b). The best topology will depend upon physical distribution, traffic patterns, and the particular performance measures that one seeks to optimize. We will not consider the general problem, but restrict ourselves to the linear interconnection of links forming closed loops. Fasnets may be connected as shown in Fig. 10. Packets in Fasnet 1 destined for Fasnet 2 are addressed to station S_N. Station S_N transmits the packets to station S_1 which puts them on Fasnet 2. Similarly, for packets from Fasnet 2 destined for Fasnet 1. To provide reliability against single-station failures, interconnection stations would be provided in pairs. Thus, a similar connection would be provided between S_{N-1} and S_2. A detailed procedure may be specified whereby control of the interconnection passes from the $S_N - S_1$ connection to the $S_{N-1} - S_2$ connection in case of failure of the former. In principle, the secondary connection monitors both Fasnets and assumes the interconnection function after a suitable time-out period in event of failure. Provision can also be made for the primary connection to periodically check that the secondary connection is operational.
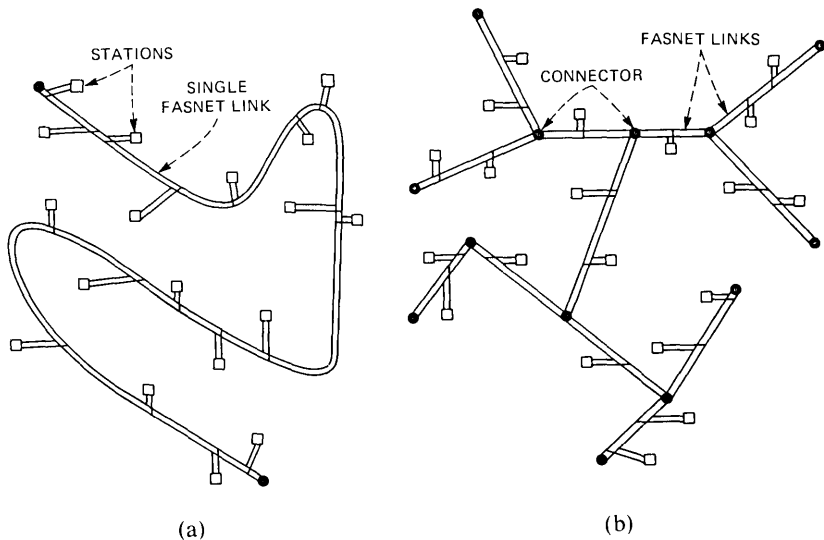
Fig. 9—(a) A cluster of stations being served by a single Fasnet link. (b) The same station population being served by several interconnected links.
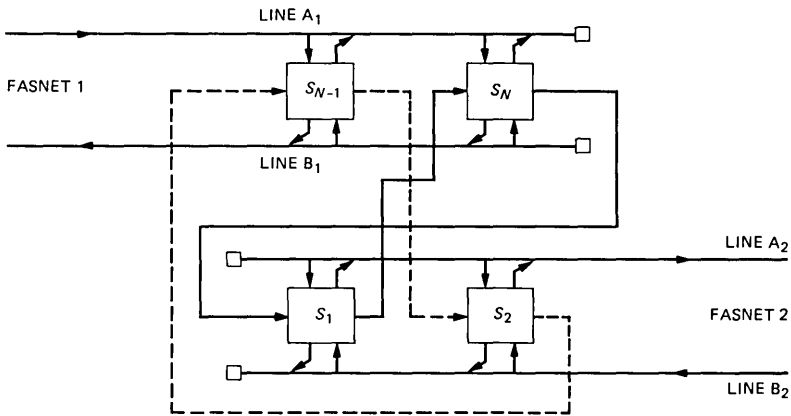
Fig. 10—Structure of a connector used to interconnect two Fasnet links.

Interconnection of Fasnets as shown in Fig. 10 permits traffic to pass from one link to another with a minimum of delay. Since the connection is to the first station on the link, the incoming packet can utilize the next occurring slot. Because of differences in frame timing between two links, it may be necessary to buffer a maximum of one complete packet; this amount of buffering is normally provided in a station interface. In general, interconnection of more than two Fasnets will require larger buffers to be employed to handle the condition where traffic arrives simultaneously for one Fasnet from connecting Fasnets.

8.2 Traffic localization

If stations on a Fasnet have traffic destined only for stations in the immediate vicinity, then total utilization can be significantly improved by dividing the single link into separate links that are connected. Only traffic that has not reached its destination link is allowed to cross the connector.

Consider two Fasnet links connected to form a ring with an inner and outer loop as shown in Fig. 11. The two connectors transfer traffic from one link to the other.

Assume that the ring has a length of unity and that the first link has a length l where $l \leq \frac{1}{2}$. For a given packet, let d be the distance of the destination station from the source station. This distance is measured along the ring with the anticlockwise direction as positive, the clockwise direction as negative, and the source station as the origin. Assume that d is a random variable with a uniform distribution over $[-\frac{1}{2}, \frac{1}{2}]$. When $d \in [-\frac{1}{2}, 0]$, the source station accesses the outer loop; when $d \in [0, \frac{1}{2}]$, the source station accesses the inner loop. Thus, the source station selects the shortest distance to the destination along the ring.
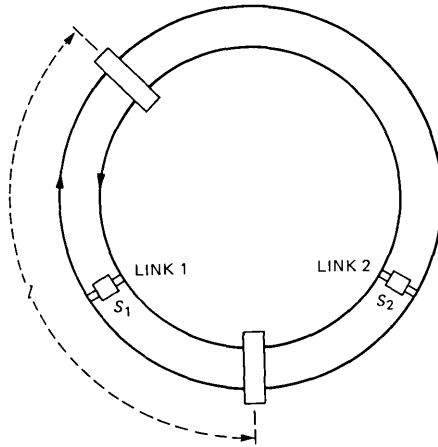
Fig. 11—Two Fasnet links interconnected to form a link using two connectors.

Depending on l and d, the traffic to any destination may have to traverse zero, one, or two connectors before it can be removed.

We first wish to determine the probabilities of the above events when the stations are distributed uniformly on the ring. For station S_j selected at random on link j ($j = 1, 2$), let

p_j = probability that the destination is on the inner loop, and the same link, and the traffic traverses zero connectors,

q_j = probability that the destination is on the inner loop, but the other link, and the traffic traverses one connector,

r_j = probability that the destination is on the inner loop, and the same link, but the traffic traverses two connectors ($r_j \neq 0$ only if the length of the link is $>\frac{1}{2}$ and the shortest path between two stations at the ends of the link is through the other link).

It can easily be shown that

$$p_1 = \frac{l}{2} \qquad p_2 = \frac{1}{2}\left(\frac{3}{4} - l\right)\frac{1}{1 - l}$$

$$q_1 = \frac{1 - l}{2} \qquad q_2 = \frac{1}{2}l$$

$$r_1 = 0 \qquad r_2 = \frac{1}{2}\frac{\left(\frac{1}{2} - l\right)^2}{1 - l}.$$

$$\left(\text{as } l < \frac{1}{2}\right)$$

(3)

Note that $p_j + q_j + r_j = \frac{1}{2}$, $(j = 1, 2)$ as any station accesses the inner loop with probability $\frac{1}{2}$. Now suppose that there are N_1 active stations on link l and N_2 active stations on link 2. If each active station requires unit capacity, then the average traffic $T_i (i = 1, 2)$ in units of capacity on the inner loop in links 1 and 2 is given by

$$T_1 = N_1(p_1 + q_1 + r_1) + N_2(q_2 + r_2) + N_1 r_1$$
$$T_2 = N_2(p_2 + q_2 + r_2) + N_1(q_1 + r_1) + N_2 r_2 \tag{4}$$

because the traffic on a line in any link is the sum of three components: (i) all the traffic generated in that link, (ii) that fraction of the traffic generated in the other link that traverses this link, and (iii) that fraction of the traffic generated in this link that transverses the other link and then returns to the first link. If N_1 and N_2 are very large, then by the law of large numbers we have

$$\text{traffic on link } 1 = T_1 \leq C$$
$$\text{traffic on link } 2 = T_2 \leq C, \tag{5}$$

where C is the line capacity.

It can be shown that $N_1 + N_2$ is maximum when $l = \frac{1}{2}$ and

$$N_1 + N_2 = \frac{8}{3} C.$$

If no connectors were used, we have a single Fasnet link (it can no longer be a closed ring) for which

$$N_1 + N_2 = 2C.$$

Hence the gain $G = (8C/3)/2C = 4/3$. Thus, we are able to obtain a 33 percent increase in the effective network capacity even for uniformly distributed traffic by having two diametrically located connectors.*

We now extend the above analysis to the case of K connectors C_1, C_2 $\cdots C_K$, which are located symmetrically around the ring as shown in Fig. 12.

It can be shown by similar means that

$$G = \frac{4}{1 + \dfrac{4}{K}}. \tag{6}$$

This is plotted in Fig. 13.

We then extend the same analysis to the case with K symmetric connectors C_1, C_2 $\cdots C_K$, but with an arbitrary traffic distribution symmetric about the source station and extending from $-\frac{1}{2}$ to $+\frac{1}{2}$

---

* While this analysis does not pertain to a specific access protocol, the effective gain can be closely realized by the Fasnet protocol and the connector structure of Fig. 10.
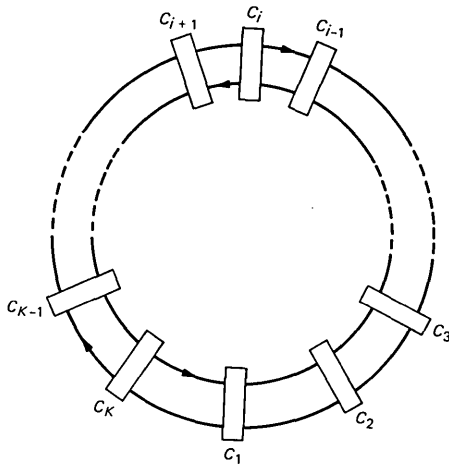
Fig. 12—A Fasnet link with multiple connectors.
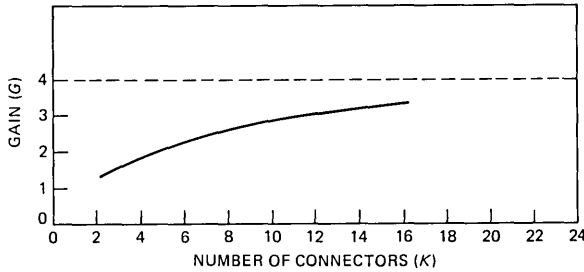
Fig. 13—Plot of the gain in traffic handling capacity of interconnected links relative to a single link as a function of K, the number of connectors.

along the ring. This preserves the shortest path routing, as well as sharing the load equally between the two loops.

It can be shown by similar means that for large K

$$G \approx \frac{K}{1 + KD} = \frac{1}{\dfrac{1}{K} + D}, \tag{7}$$

where D is the expected value of $|d|$, the absolute value of the source-destination distance. The approximation becomes exact if the distribution is uniform or if $K \to \infty$. Note that for the uniform distribution, $D = \frac{1}{4}$ and

$$G = \frac{1}{\dfrac{1}{K} + \dfrac{1}{4}} = \frac{4}{1 + 4/K}$$

as before. For a given traffic distribution, (7) is a good design formula for how capacity costs can be reduced at the cost of extra connectors. However, this trade-off is useful only if accurate estimates of capacity and connector costs are available.

The above analysis highlights certain interesting features. For the uniform traffic distribution, it is seen that the gain, G, does not increase uniformly with K. This is fairly intuitive. Since the traffic is uniform, an extra connector, when K is large, removes the traffic over only a short link and results in only a marginal increase in the gain. On the other hand, as the traffic distribution becomes more localized (i.e., $D \rightarrow 0$)G increases uniformly with K. This is again fairly obvious, as with a high degree of localization the traffic on each link is almost independent of the traffic on the other links.

We have considered here some configurations of interconnected links. There are interesting graph theoretic questions relating to reliability. For example, given a graph like Fig. 9b, what is the minimum number of additional links and their position so that full connectivity is still maintained if any link is cut at a single point? Development of realistic models of the physical traffic and cost structures of local environments still remains. There is a paucity of statistics (except for Ref. 2) on the local network parameters. Future operational local networks will hopefully furnish statistics on which to build more accurate models.

IX. CONCLUSION

The physical configuration of Fasnet consists of two communication lines passing each station. One line carries traffic in one direction, while the other line carries traffic in the opposite direction. Thus, this configuration carries twice the traffic of a previous system in which the two lines were connected at one end so that traffic was written on the outbound line and read from the inbound line. Each station makes two connections to each line, a nondirectional read tap and a directional write tap. Reliability of the physical medium is high because it contains no active electronics. The access protocol is partly centralized in that bit synchronization, framing, and start-of-cycle are provided by the end stations; however, these functions would be assumable by any station upon failure of an end station.

The access protocol is as follows: Upon reading a start-of-cycle, a station may transmit a prespecified number of packets in the first available empty slots. When all stations have transmitted their packets, a signal is sent on the return line to inform the head station to start a new cycle. The efficiency of Fasnet increases as the length of a cycle increases; cycle length depends upon the length of a packet, the number of active stations, and the number of packets, p_{max}, that each

station is permitted to send in a cycle. By adaptively changing p_{max}, efficiency can be maintained at a high level even for a small number of active stations. A number of techniques for further improving efficiency are suggested. A trade-off is necessary between increasing the complexity of the protocol, on one hand, and the resulting small improvements in efficiency on the other.

Bit synchronization of the stations is achieved through adding an out-of-band pilot tone, while framing is achieved through a periodically inserted code word. A three-level bipolar line code is preferred.

The potential of Fasnet for operation at high transmission rates makes it attractive as a conduit for the various types of traffic that may flow in a business environment. Mechanisms have been proposed to implement blocking, delaying, and request-for-service operations that are needed if mixed traffic is to be handled efficiently within a single medium. These operations can be implemented centrally or they can be distributed. The low-level access operations are best distributed while the more complex operations are best centralized.

Fasnets may be interconnected to increase the load that may be carried or to improve reliability. Investigation has been restricted to the connection of Fasnets to form a ring. As the number of segments in the ring increases, the throughput first increases rapidly (assuming uniformly distributed traffic). After about five segments, the increase is very small. Exploration of other topologies presents a challenge.

X. ACKNOWLEDGMENT

REFERENCES

1. R. M. Metcalfe and D. R. Boggs, "Ethernet: Distributed Packet Switching for Local Computer Networks," Commun. of the ACM *19,* 7 (July 1976), pp. 395–404.
2. J. F. Shoch and J. A. Hupp, "Measured Performance of an Ethernet Local Network," Presented at Local Area Communications Network Symposium, Boston (May 1979), pp. 113–34.
3. The Ethernet, A Local Area Network, Data Link Layer and Physical Layer Specifications, DEC, INTEL, XEROX, Version 1.0 (September 30, 1980).
4. F. A. Tobagi, "Multiaccess Protocols in Packet Communication Systems," IEEE Trans. Commun. *COM-28,* 4 (April 1980), pp. 468–88.
5. J. O. Limb, "High Speed Operation of Broadcast Local Networks," Proc. ICC, June 1982.
6. M. E. Ulug, G. M. White, and W. L. Adams, "Bidirectional Token Flow System, Proc. Seventh Data Commun. Symp. (October 1981), pp. 149–55.
7. M. V. Wilkes and D. J. Wheeler, "The Cambridge Digital Communication Ring," Proc. Local Area Commun. Network Symp. (May 1979), pp. 47–61.
8. C. S. Skrzypczak and W. E. Falconer, "Bell System Planning of ISDN," Proc. ICC, June 1981, pp. 19.6.1–6.
9. N. F. Maxemchuk and H. A. Wilder, "Virtual Editing: I. The Concept," Office Information Systems Workshop, St. Maximim, France, October 1981.

10. W. Pferd, L. A. Peralta, and F. X. Prendergast, "Inactive Graphics Teleconferencing," Computer *12* (November 1979), pp. 62–71.
11. W. A. Rheinfelder, *CATV System Engineering*, Third Ed., Blue Ridge Summit, Pa.: TAB Books, 1972.
12. J. O. Limb, "Fasnet: Proposal for a High Speed Local Network," Office Information Systems Workshop, St. Maximim, France, October 1981.
13. IEEE 802 Standards Committee, Interim Report.
14. F. D. Waldhauer, "A 2-Level, 274 Mb/s Regenerative Repeater for T4M," Proc. of the ICC 1975, *3*, pp. 48-13–17.
15. L. Frata, F. Borgonovo, and F. A. Tobagi, "The Express-Net: A Local Area Communication Network Integrating Voice and Data," in *Performance of Data Communication Systems*, G. Pujolle, Ed., Amsterdam: North Holland, 1981, pp. 77–88.
16. R. C. Chen, "Bus Communication Systems," Report No. PB 235-897, Carnegie-Mellon University, January 1974.

On the Distribution Function and Moments of Power Sums With Log-Normal Components

By S. C. SCHWARTZ* and Y. S. YEH

An approximate technique is presented for the evaluation of the mean and variance of the power sums with log-normal components. Exact expressions for the moments with two components are developed and then used in a nested fashion to obtain the moments of the desired sum. The results indicate more accurate estimates of these quantities over a wider range of individual component variances than any previously reported procedure. Coupling our estimates with the Gaussian assumption for the power sum provides a characterization of the cumulative distribution function which agrees remarkably well with a Monte Carlo simulation in the 1 to 99 percent range of the variate. Simple polynomial expressions obtained for the moments lead to an effective analytical tool for various system performance studies. They allow quick and accurate calculation of quantities such as cochannel interference caused by shadowing in mobile telephony.

I. INTRODUCTION

The power sum with K independent components

$$P_K = 10 \log_{10}\left[\sum_{k=1}^{K} 10^{X_k/10} \right] \tag{1}$$

is a random variable which appears in many areas of communications. With X_k Gaussian, the quantity

$$L_k = 10^{X_k/10} \tag{2}$$

is called a log-normal variate. The characterization of the sum of L_k is

---

* Professor Schwartz is currently with the Department of Electrical Engineering and Computer Science, Princeton University.

of importance in multihop scatter systems,[1] log-normal shadowing environments,[2,3] target detection in clutter,[4,5] and the general problem of propagation through a turbulent medium.* Thus, the distribution and moments of P_K are quantities of considerable importance. Unfortunately, these quantities do not appear to be expressible in simple analytical formulae and, as a consequence, approximate procedures have been investigated for some time. Of particular interest is the Wilkinson approach which uses a normal approximation for the distribution of P_K. The problem of characterizing the distribution function then reduces to finding the first two moments of the power sum.

The Wilkinson approach is consistent with an accumulated body of evidence indicating that, for the values of K that are of interest, the distribution of the sum of a finite number of log-normal random variables is well-approximated, at least to first-order, by another log-normal distribution.[1,9-12]† The central question, then, is how to estimate the mean and variance of the approximately Gaussian variate P_K, i.e., the power sum. Knowledge of the mean, m_x, and standard deviation, σ_x, of the Gaussian random variable X_k leads to a complete specification of the log-normal variate L_k, assuming, of course, no location parameter for the log-normal. Yet, the procedure for then estimating the moments of the power sum variable

$$P_K = 10 \log_{10}(L) = 10 \log_{10}(L_1 + L_2 + \cdots + L_K) \tag{3}$$

based on the individual moments m_x, σ_x, is by no means straightforward. As discussed in the next section, the Wilkinson approach leads to useful results only for a limited range of small values of the dB spread σ_x. Unfortunately, this is not the σ_x range of most practical interest.

The purpose of this paper is to outline a procedure that appears to be more accurate and to have a wider range of applicability than previously reported approximations. The new technique can be easily summarized: Analytical formulae are developed to compute the exact mean and variance for the power sum with two components,

$$P_2 = 10 \log(L_1 + L_2). \tag{4}$$

We then suppose P_2 is Gaussian, i.e., it is assumed that $L_1 + L_2 = 10^{P_2/10}$ is log-normal. We then consider

$$P_3 = 10 \log(L_1 + L_2 + L_3) = 10 \log(10^{P_2/10} + L_3) \tag{5}$$

and compute the mean and variance using the derived formulae. In this manner, we iterate until the required moments of P_K are obtained.

---

* Many more applications, including the field of economics and the estimation of crude oil reserves, are noted in Refs. 6, 7, and 8.
† We also confirm this observation here by means of Monte Carlo simulations.

We have compared the results of a Monte Carlo study to the estimates of moments obtained from the new method just described, and permuted versions of it. Our procedure leads to remarkably accurate estimates for the mean of P_K, over a wide range of component variances. The estimate of the standard deviation of P_K is accurate for a somewhat more limited range but, nevertheless, a much wider range than for previously reported approximations.

The rest of this paper is organized as follows. In the next section, we establish additional notation and discuss, in more detail, previous work relating to power sums. The analytical development is presented in Section III, with the details reserved for the Appendix. The development of both accurate and simple expressions for the mean and variance of P_2 is of considerable importance for system performance studies in areas such as shadowing in mobile radio and log-normal fading in microwave radio. In Section III, we also present such an expression in the form of simple polynomials. Simulation results, validating both the Gaussian approximation for P_K and the new estimation technique, are presented in Section IV. Concluding comments are given in Section V.

II. PRELIMINARIES

The power sum, as defined in (1), is measured in decibels. However, rather than use the definition for L_k given in (2), it is more convenient to use the natural logarithm:

$$L_k = e^{Y_k}. \tag{6}$$

The relationship between the two associated normal variates is simply

$$Y_k = \lambda X_k, \tag{7}$$

where

$$\lambda = \tfrac{1}{10}\log_e 10 = 0.23026. \tag{8}$$

When the mean and variance of X_k are specified as, say, m_x and σ_x, in order to use the representation (6), we have the obvious scaling

$$m_y = \lambda m_x, \qquad \sigma_y^2 = \lambda^2 \sigma_x^2. \tag{9}$$

Similarly, we define the quantities

$$L = 10^{P_{K/10}} = e^Z, \tag{10}$$

and the corresponding moments are related by

$$m_z = \lambda m_{P_K}, \qquad \sigma_z^2 = \lambda^2 \sigma_{P_K}^2. \tag{11}$$

The rth moment of a log-normal variate L is given in terms of the moment-generating function of Y:

$$E(L_1^r) = E(e^{rY_1}) = e^{rm_{y_1}+1/2(r^2\sigma_{y_1}^2)}. \tag{12}$$

Note that the moments grow exponentially with the order r^2. This rapid growth of moments may be one of the reasons for the limited range of applicability of the classical Wilkinson approximation (see Ref. 11); dealing with diffferences of large numbers can lead to numerical instability in trying to evaluate the approximate log-normal density of the sum.

Marlow[13] has shown that under quite general conditions, as $K \to \infty$, P_K is asymptotically normally distributed.* For fixed, finite K, and with the X_K independent, identically distributed normal random variables (with mean m_x and standard deviation σ_x), Marlow also derived a small variance normal approximation.[14] As $\sigma_x \to 0$, a scaled version of P_K approaches the distribution function of a unit normal.

In terms of log-normal variates, if we write

$$P_K = 10 \log_{10}(L) = 10 \log_{10}(L_1 + L_2 + \cdots + L_K), \tag{13}$$

Marlow's second result says that, in the finite-component, small-variance case, the sum of log-normal variates is also approximately log-normal. This result forms the analytical basis for the classical Wilkinson approximation, which is the usual normal approximation for the distribution of the power sum.

The Wilkinson approximation proceeds as follows: With

$$L = e^Z, \tag{14}$$

now taken to be log-normal, Z is the associated Gaussian random variable with parameters m_z and σ_z. To find these quantities, one uses (12) and equates the first two moments of both sides of (14). For example, with $K = 2$, and Y_1, and Y_2 identically distributed with mean m_y and variance σ_y^2,

$$E(L) = e^{m_z+1/2\sigma_z^2} = 2e^{m_y+1/2\sigma_y^2}$$

$$E(L^2) = e^{2m_z+2\sigma_z^2} = 2e^{2m_y+2\sigma_y^2} + 2(e^{m_y+1/2\sigma_y^2})^2. \tag{15}$$

Taking logarithms gives a set of linear equations for the two unknowns, m_z and σ_z^2.

Figure 3, which will be discussed in detail later, presents the results of a Monte Carlo simulation and the Wilkinson approximation, employing eq. (15). As indicated, the Wilkinson approach tends to break down for $\sigma_x = \sigma_y/\lambda$ greater than 4 dB. This is consistent with the above-quoted result from Marlow.

---

*For the infinite component case, Marlow also points out that there is asymptotic normality both on the power scale, as well as on the dB scale. That is, both P_K and L are asymptotically normal.

If one is interested in small σ, but larger values of the random variable, i.e., the tails of the power sum distribution, Fenton[1] suggests a better approximation to the equivalent log-normal distribution by utilizing higher-order moments. In this case, eq. (15) is replaced with equality of, say, third and fourth moments. This procedure of using different values of r in different regions results in an approximating distribution which would be a series of connected straight lines when plotted on log-probability graph paper.

At the other end of the σ_x component range, Farley[9] has derived a large variance approximation. With independent, identically distributed variables, as $\sigma_x \to \infty$

$$Pr\left[\frac{1}{\sigma_x}(P_K - m_x) < \alpha\right] = [\Phi(\alpha)]^K, \tag{16}$$

where $\Phi(\alpha)$ is the unit normal distribution function. (Clearly, this is a decidedly non-Gaussian result.) Farley's simulations indicate that the large variance approximation gives better results than Wilkinson's approach for about $\sigma_x > 10$ dB and K fixed.

In this study, we also take K finite, but focus on the midrange, $4 \leq \sigma_x \leq 12$ dB, where neither Marlow's nor Farley's results are applicable. This midrange is of particular interest for the shadowing phenomena in mobile telephony, microwave radio fading, and airborne radar clutter.

III. ANALYTICAL RESULTS

We assume that

$$L = \sum_{k=1}^{K} L_k = \sum_{k=1}^{K} e^{Y_k} = e^Z \tag{17}$$

for finite K is log-normal. The associated Gaussian variate is Z, and the goal is to determine the quantities

$$m_z = E(\ln L)$$

$$\sigma_z^2 = E[(\ln L - m_z)^2] \tag{18}$$

in terms of the mean and standard deviation of the component variates Y_k.

Below, we give exact expressions for m_z and σ_z when there are two components. The procedure for K greater than two combines the log-normal variates in a nested fashion two-by-two, using the exact formulas developed. To illustrate the procedure, suppose we have three log-normal variates: $L = L_1 + L_2 + L_3$. The exact first and second moments of $\ln(L_1 + L_2)$ are computed. We then take

$$Z_2 = \ln(L_1 + L_2) \tag{19}$$

as a normal random variable and write*

$$Z = \ln(L) = \ln(e^{Z_2} + L_3) = \ln(e^{Z_2} + e^{Y_3}). \qquad (20)$$

We then compute the moments of $\ln(L)$, again using the exact expressions developed for two components. This procedure has been tested in a variety of situations and groupings of variates. The results are very encouraging and will be discussed in the next section. Here, we outline the development of the analytical formulae, with the details in the Appendix.

Naus[15] has derived the moment-generating function, and computed the first two moments of the power sum with two independent, identically distributed normal components. (Hamdan[16] generalized Naus' result for correlated variables with unequal variances.) Here, we extend Naus' general approach to the case of two independent variables with unequal means and variances.

For the two components, we have

$$e^Z = L = L_1 + L_2 = e^{Y_1} + e^{Y_2} \qquad (21)$$

or

$$Z = \ln(e^{Y_1} + e^{Y_2}).$$

Define the Gaussian random variable

$$w = Y_2 - Y_1 \qquad (22)$$

$$m_w = \bar{w} = m_{y_2} - m_{y_1} \qquad (23)$$

$$\sigma_w^2 = \sigma_{y_2}^2 + \sigma_{y_1}^2. \qquad (24)$$

Taking the expectation of Z, we have

$$
\begin{aligned}
E\{Z\} &= E[\ln(e^{Y_1} + e^{Y_2})] \\
&= E\{\ln[e^{Y_1}(1 + e^{Y_2 - Y_1})]\} \\
&= E(Y_1) + E[\ln(1 + e^w)]. \qquad (25)
\end{aligned}
$$

The second term is

$$E[\ln(1 + e^w)] = \int_{-\infty}^{+\infty} [\ln(1 + e^w)]f(w)\,dw, \qquad (26)$$

where $f(w)$ denotes the normal density with the above-indicated mean and variance. The logarithmic term is now expanded in a power series. To ensure convergence of both the power series and the series resulting from the subsequent integration, the integral is broken up into the appropriate ranges. Thus,

---

* Equivalently, $L_1 + L_2$ is assumed to be log-normal.

$$\int_{-\infty}^{+\infty} \ln(1 + e^w) f(w) \, dw = \int_{-\infty}^{0} \ln(1 + e^w) f(w) \, dw$$

$$+ \int_{0}^{\infty} [\ln(1 + e^{-w}) + w] f(w) \, dw. \quad (27)$$

The expansion

$$\ln(1 + x) = \sum_{j=1}^{\infty} C_j x^j, \; C_j = \frac{(-1)^{j+1}}{j}, \quad (28)$$

valid for $|x| < 1$, can now be used for each of the above integrals. The result (details are given in the Appendix) for the first moment is

$$m_z = E[\ln(L_1 + L_2)]$$

$$= m_{y_1} - \frac{\sigma_w}{\sqrt{2\pi}} e^{-m_u^2/2\sigma_u^2} + m_w \, \Phi\left(\frac{m_w}{\sigma_w}\right)$$

$$+ \sum_{k=1}^{\infty} C_k e^{k^2 \sigma_u^2/2} \left[e^{km_w} \, \Phi\left(\frac{-m_w - k\sigma_w^2}{\sigma_w}\right) \right.$$

$$\left. + e^{-km_w} \, \Phi\left(\frac{m_w - k\sigma_w^2}{\sigma_w}\right) \right]$$

$$= m_{y_1} + G_1(\sigma_w, m_w), \quad (29)$$

where $\Phi(x)$ is the Gaussian probability distribution function as defined in the Appendix, eq. (39), and G_1 is defined implicitly. It is not difficult to show that the series in (29) converges. Our computer experience indicates that about 40 terms are required for the 4th significant digit.

As might be expected, the formula for the second moment is more complicated and is given by eq. (72) in the Appendix. The basic idea however, remains the same: When expansions of logarithmic functions are used, the expectation is broken up into integration ranges which provide convergent series.

Although the formulae as developed involve infinite series and are complicated, their application is relatively simple. We can write [see eqs. (49) and (73) in the Appendix]:

$$m_z = m_{y_1} + G_1(\sigma_w, m_w)$$

$$\sigma_z^2 = \sigma_{y_1}^2 - G_1^2(\sigma_w, m_w) - 2\rho^2 G_3(\sigma_w, m_w) + G_2(\sigma_w, m_w), \quad (30)$$

where the $G_i(\sigma_w, m_w)$ are defined in the Appendix and

$$\rho = -\sigma_{y_1}/\sigma_w. \quad (31)$$

Observe that the G_i functions, $i = 1, 2, 3$, depend only on the two parameters m_w, σ_w. Consequently, we can evaluate $G_i(\sigma_w, m_w)$ as a

Table Ia—Coefficients of the approximating polynomials—Region I

$$[-20 < m_w < 0, 0 < \sigma_w < 15]$$

	Functions		
Coefficients	G1	G2	G3
A00	−0.1153239E 00	0.4012876E-01	−0.3958699E 01
A01	−0.5667912E 01	−0.4483259E 01	−0.5454983E 01
A02	0.1151279E 02	0.7391760E 01	0.1139280E 02
A03	−0.7162489E 01	−0.3772190E 01	−0.7116366E 01
A04	0.1312986E 01	0.5262268E 00	0.1315218E 01
A10	−0.1611385E 00	−0.1579114E 01	0.6839918E 01
A11	0.2084215E 02	0.1637249E 02	0.1962529E 02
A12	−0.4499768E 02	−0.2994901E 02	−0.4314091E 02
A13	0.2756210E 02	0.1337812E 02	0.2647795E 02
A14	−0.5109783E 01	−0.1747459E 01	−0.4940592E 01
A20	0.1345124E 00	0.2174588E 01	−0.4717296E 01
A21	−0.2670183E 02	−0.2114152E 02	−0.2486802E 02
A22	0.5919191E 02	0.3976749E 02	0.5618572E 02
A23	−0.3695334E 02	−0.1776890E 02	−0.3501815E 02
A24	0.6912766E 01	0.2195322E 01	0.6560938E 01
A30	0.8057054E-01	−0.7525302E 00	0.1819360E 01
A31	0.1429709E 02	0.1147157E 02	0.1323538E 02
A32	−0.3225969E 02	−0.2189501E 02	−0.3050022E 02
A33	0.2055628E 02	0.1006767E 02	0.1937757E 02
A34	−0.3888684E 01	−0.1224983E 01	−0.3658379E 01
A40	−0.3145306E-01	0.8447987E-01	−0.2817493E 00
A41	−0.2730047E 01	−0.2222839F 01	−0.2518272E 01
A42	0.6244253E 01	0.4289557E 01	0.5893337E 01
A43	−0.4048245E 01	−0.2035757E 01	−0.3809492E 01
A44	0.7746786E 00	0.2499568E 00	0.7260144E 00

function of these two parameters and store the results in three lookup tables. An alternative is suggested by Fig. 5, which gives the three G_i's as a function of σ_w with m_w as a parameter. Since the curves are smooth, we can fit low-order polynomials to them and use the resulting expressions in (30) for the evaluation of the moments m_z and σ_z. The advantage of utilizing these analytical expressions in system performance studies is clear and, indeed, is what we have implemented.

A least-squares fit was performed to determine the polynomial coefficients. After some experimentation, we chose the polynomial

$$\log_{10} G_i(\sigma_w, m_w) = \sum_{j=0}^{J} \sum_{k=0}^{K} A_{jk}(i)\sigma_w^{j/2} |m_w|^{k/2}, \quad i = 1, 2, 3, \quad (32)$$

with $J = K = 4$. The coefficients $A_{jk}(i)$ were obtained for two regions of the parameter space. The results for Region I ($-20 \le m_w \le 0, 0 \le \sigma_w \le 15$) and Region II ($-40 \le m_w \le -20, 0 \le \sigma_w \le 15$) are presented in Tables Ia and Ib. Over these regions of interest, the maximum error produced by using the polynomial approximations was found to be about 1 percent as compared to the exact calculations based on eqs. (49) and (73).

Before discussing the results of the simulation study, we digress to note how the analytical results can be extended. First, the development

Table Ib—Coefficients of the approximating polynomials—Region II

$[-40 < m_w < -20, 0 < \sigma_w < 15]$

Coefficients	Functions		
	G1	G2	G3
A00	−0.3354792E 03	0.8942737E 02	−0.3596955E 03
A01	0.5281230E 03	−0.1521976E 03	0.5576596E 03
A02	−0.3085414E 03	0.9734654E 02	−0.3242909E 03
A03	0.7895054E 02	−0.2744724E 02	0.8271772E 02
A04	−0.7518427E 01	0.2756644E 01	−0.7863267E 01
A10	0.1354559E 04	−0.3688427E 03	0.1443269E 04
A11	−0.2133838E 04	0.6287175E 03	−0.2250748E 04
A12	0.1245491E 04	−0.4077784E 03	0.1307118E 04
A13	−0.3191052E 03	0.1148104E 03	−0.3336339E 03
A14	0.3036738E 02	−0.1161187E 02	0.3167827E 02
A20	−0.1865732E 04	0.4966108E 03	−0.1986007E 04
A21	0.2941369E 04	−0.8514775E 03	0.3106047E 04
A22	−0.1718295E 04	0.5574036E 03	−0.1804377E 04
A23	0.4403198E 03	−0.1588548E 03	0.4603419E 03
A24	−0.4188256E 02	0.1624075E 02	−0.4366067E 02
A30	0.1059090E 04	−0.2684747E 03	0.1128759E 04
A31	−0.1671264E 04	0.4638312E 03	−0.1768423E 04
A32	0.9776851E 03	−0.3061915E 03	0.1028409E 04
A33	−0.2507169E 03	0.8842364E 02	−0.2624284E 03
A34	0.2384698E 02	−0.9152624E 01	0.2487490E 02
A40	−0.2121206E 03	0.5077676E 02	−0.2264791E 03
A41	0.3350888E 03	−0.8833020E 02	0.3553536E 03
A42	−0.1963238E 03	0.5876009E 02	−0.2069294E 03
A43	0.5040234E 02	−0.1717538E 02	0.5284466E 02
A44	−0.4795980E 01	0.1799387E 01	−0.5008795E 01

is valid when the random variables Y_1 and Y_2 are correlated as well as having different means and variances. With a simple modification in eq. (24) to account for the correlation [and another in (52)],

$$\sigma_w^2 = \sigma_{y_2}^2 + \sigma_{y_1}^2 - \rho_{12}\sigma_{y_1}\sigma_{y_2}, \tag{33}$$

the results remain unchanged. Furthermore, in principle, the underlying component variables do not have to be Gaussian. The proviso, of course, is that the integration with the non-Gaussian $f(w)$ be tractable, and it must fall off fast enough so that the resulting series is convergent. (Clearly, the components are no longer log-normal.)

Finally, we observe that the results can be extended in yet another direction. By generalizing the procedure outlined above, exact formulae for moments of more than two components can be obtained. However, the resulting expressions are very complicated and, given the high accuracy of our new method, the added complexity does not appear to be warranted.

IV. SIMULATION RESULTS

We use the definitions introduced earlier:

$$L_k = 10^{X_k/10} \tag{34}$$

$$P_K = 10 \log_{10}(L) = 10 \log_{10}\left[\sum_{k=1}^{K} L_k\right]. \tag{35}$$

In the following discussion, by m_p and σ_p, we shall mean the first moment and standard deviation of the random variable P_K. The value of K should be clear from the context. We focused our Monte Carlo study on three issues:

   (i) How good is the assumption that $L = L_1 + L_2 + \cdots + L_K$ is approximately log-normal or, equivalently, how well is the cumulative distribution function (cdf) of $P_K = \log_{10}(L)$ described by a Gaussian cdf? Furthermore, how closely does the Gaussian cdf (based on the calculated m_p and σ_p) match the true cdf of the power sum?

   (ii) How accurate is the new analytical method in estimating the resultant mean m_p and standard deviation σ_p and for what range of dB spread σ_x and component number K is the technique accurate?

   (iii) Is the nested procedure we have described numerically robust, or are the estimates of m_p and σ_p sensitive to the order in which we combine the log-normal components?

The results of our Monte Carlo simulation confirmed the observation of a number of other investigators, that the cdf of P_K is well approximated by the Gaussian cdf, particularly in the range of practical interest.* Shown in Fig. 1 is the cdf of the sum of two log-normal variates with $\sigma_x = 6$, 10, and 14 dB. We note that the Monte Carlo simulation agrees quite closely with the assumed Gaussian cdf (based on the calculated m_p and σ_p) in the range of 0.1 to 99 percent. Outside this range, the simulation values start to deviate slightly. The cdf of the sum of a large number of log-normal variates, discussed below in Examples 1 to 3, together with a fourth case (the sum of six equal components with $m_x = 0$ dB and $\sigma_x = 10$ dB), are presented in Fig. 2. Here we observe excellent agreement between the calculated (assumed) and simulated cdf in the range 1 to 99 percent.

Having confirmed the Gaussian approximation for P_K and the fact that the calculated cdf closely represents the true cdf, we turn our attention to the second issue, estimating the moments m_p and σ_p from the moments of the individual log-normal components. In Figs. 3a to 3c, the number of identically distributed components, K, is held fixed and the component variance (dB spread) σ_x^2 is varied. In all cases, the component mean m_x is 0. Figure 3a illustrates the results for two components and serves to verify the Monte Carlo program. Our computed results coincide (as they should) with the simulation. In contrast, the Wilkinson approximation begins to give inaccurate results

---

   * The simulations typically had 10,000 sample points for each value quoted or indicated on the figures.
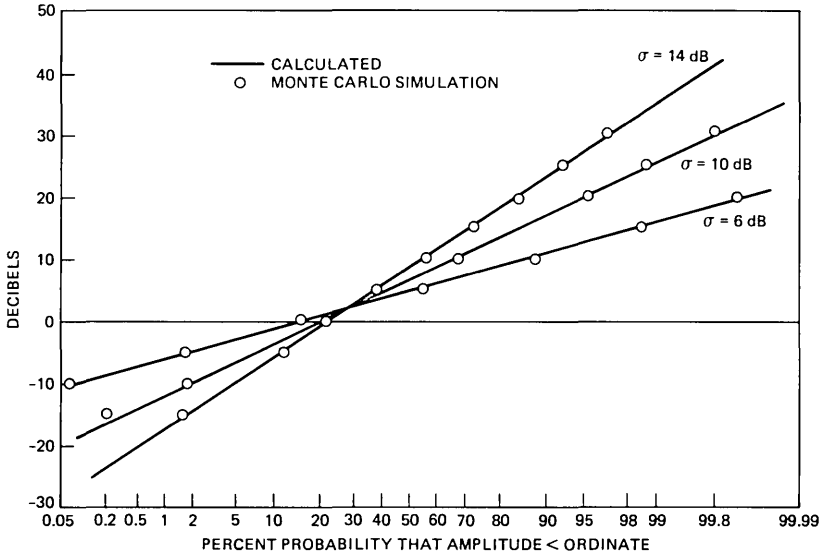
Fig. 1—Cumulative distribution function of sum of two log-normal variates with zero means and variances equal to 6, 10, and 14 dB.
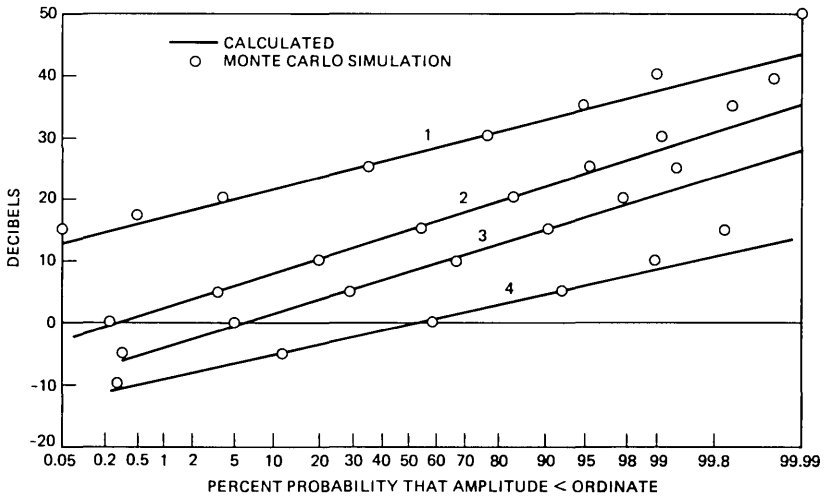
1. THREE VARIATES: $m = 0$, $\sigma = 6, 7, 9.5$.
2. SIX EQUAL COMPONENTS: $m = 0$, $\sigma = 10$.
3. NINE COMPONENTS IN THREE GROUPS: GROUP 1, $m = -10$, $\sigma = 6$; GROUP 2, $m = -18$, $\sigma = 10$; GROUP 3, $m = -38$, $\sigma = 12$.
4. EIGHTEEN COMPONENTS IN THREE GROUPS: GROUP 1, $m = 10$, $\sigma = 10$; GROUP 2, $m = -2$, $\sigma = 10$; GROUP 3, $m = -8$, $\sigma = 10$.

Fig. 2—Cumulative distribution function of the sum of a large number of log-normal variates corresponding to Examples 1 to 3 in Section IV plus an additional case.
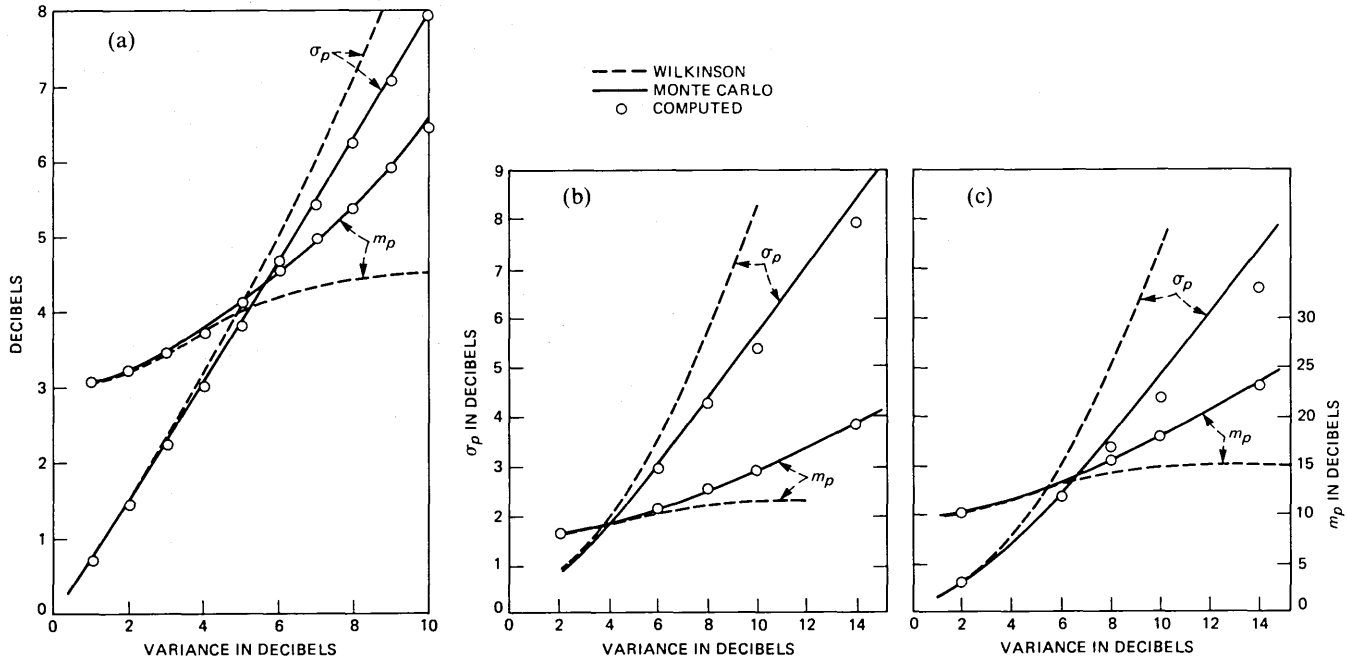
Fig. 3—Mean and standard deviation of power sum with (a) two, (b) 5:x, and (c) ten log-normal comonents as a function of comopnent standard deviation.

at about $\sigma_x = 4$ dB and becomes increasingly worse with increasing σ_x.

Figure 3b illustrates six components, and Fig. 3c illustrates ten. The dB spread ranges from 2 to 14 dB. Our technique gives remarkably accurate estimates of m_p, while the estimate of σ_p is quite close for $\sigma_x < 8$ dB and then tends to underestimate the true standard deviation. By way of contrast, for these ranges and number of components, the Wilkinson approach gives gross inaccuracies and cannot be used.

In Figs. 4a and 4b, we vary the number of components, set $m_x = 0$, and hold the dB spread fixed. Again, our procedure gives very accurate estimates of the mean and, as the number of components increases, the variance is underestimated only slightly for $\sigma_x = 6$ dB (Fig. 4a) and somewhat more so when $\sigma_x = 10$ dB (Fig. 4b). For these cases, the error in the estimate of the variance as a function of the number of components is as shown in Table II. (There are negligible errors in estimates of the mean.) As indicated in the figures, the errors in the Wilkinson approach are substantial, ranging up to 74 percent when $\sigma_x = 10$ dB.

It should be observed that the situation with equal mean components and large dB spread is probably a worst-case situation. Indeed, from the above table we see for $K = 16$, $\sigma_x = 10$ dB, that the estimate of σ_p is off by 12.8 percent. In contrast, in Example 3 below, we deal with $K = 18$ components, and the same dB spread. There, the error in the estimate is less—about 6 percent. The only substantial difference in the two situations is the unequal mean values. These comments notwithstanding, further study is warranted for this boundary of parameter values, i.e., where the number of equal mean components is high ($K \geq 16$) and the dB spread is identical and large ($\sigma_x \geq 10$ dB).

Our technique was also tested on a number of examples with unequal components. We report on three that were chosen to illustrate the general applicability of the new method.

Example 1—Three components, equal means, different variances:

$$m_{x_i} = 0 \text{ dB}, \quad i = 1, 2, 3; \qquad \sigma_{x_1} = 6, \quad \sigma_{x_2} = 7, \quad \sigma_{x_3} = 9.5 \text{ dB}.$$

The Monte Carlo simulation gave $m_p = 8.08$, $\sigma_p = 5.356$. Our procedure provided the estimates $m_p = 8.05$, $\sigma_p = 5.273$, for a 0.03-dB error in the mean and 1.5 percent error in the variance.

Example 2—Nine components, taken in homogeneous groups of three:

$$m_{x_i} = -38 \text{ dB}; \qquad \sigma_{x_i} = 12 \text{ dB}, \quad i = 1, 2, 3$$

$$m_{x_i} = -18 \text{ dB}; \qquad \sigma_{x_i} = 10 \text{ dB}, \quad i = 4, 5, 6$$

$$m_{x_i} = -10 \text{ dB}; \qquad \sigma_{x_i} = 6 \text{ dB}, \quad i = 7, 8, 9.$$
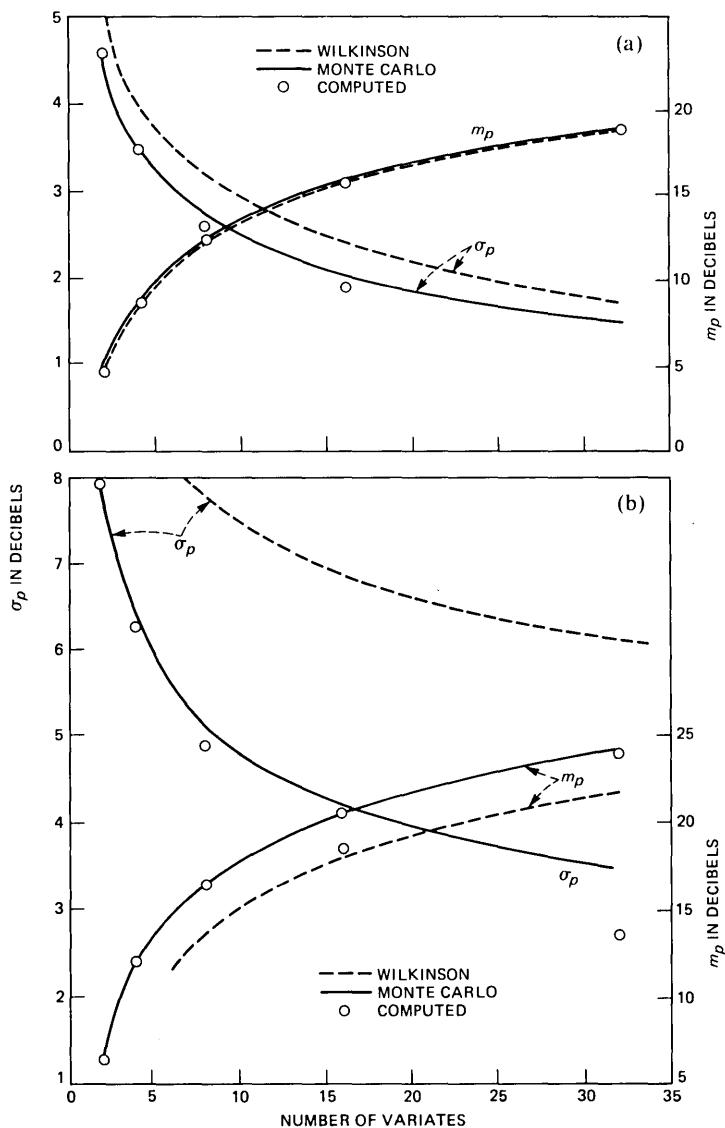
Fig. 4—Mean and standard deviation of power sum with varying number of identically distributed components. (a) Component mean, $m_x = 0$ and standard deviation, $\sigma_x = 6$ dB. (b) Component standard deviation $\sigma_x = 10$ dB.

Monte Carlo results gave $m_p = -0.61$, $\sigma_p = 3.90$, while our technique yielded $m_p = -0.6$, $\sigma_p = 3.79$. This gives an error of 0.01 dB in m_p and 2.8 percent in σ_p.

We now address the third issue raised at the beginning of this section. To show that the way in which we combine the variables has

Table II—Error in estimate of variance

Percent Error	No. of Components (K)				
	2	4	8	16	32
$\sigma_x = 10$ dB	0.13	1.4	5.4	12.8	21.4
$\sigma_x = 6$ dB	0.43	2.0	3.3	8.2	11.5

little effect, we permuted the order in combining the nine components. The resultant mean estimate varied between −0.59 and −0.64 dB, while the standard deviation varied between 3.66 and 3.89 dB. This example—and a number of others studied—illustrates the desired numerical robustness of the procedure.

Example 3—Eighteen components: This example would correspond to two tiers of interferers in a cellular mobile radio scheme.

Components 1 to 6: $m_x = 10$ dB, $\sigma_x = 10$ dB.
Components 7 to 12: $m_x = -2$ dB, $\sigma_x = 10$ dB.
Components 13 to 18: $m_x = -8$ dB, $\sigma_x = 10$ dB.

The Monte Carlo results are: $m_p = 27.07$, $\sigma_p = 4.54$, and our technique gave $m_p = 27.04$, $\sigma_p = 4.26$. The error is 0.03 dB in the mean estimate and 6.2 percent for σ_p.

V. CONCLUSIONS

In this study, we have verified once again, as others have, that the sum of a moderate number of log-normal random variables is well approximated by another log-normal variate, especially in the cdf range of 1 to 99 percent. Perhaps more important, we have been able to relate the mean and variance of the resultant (Gaussian) power sum to the first two moments of the individual underlying Gaussian components. Our method is highly accurate in the range of parameter values of most practical interest.

Based on our preliminary simulations, we may conclude that the analytical method presented in this paper is extremely accurate in evaluating the mean of the power sum for the complete range of parameter values investigated. This range was a dB spread of $2 \leq \sigma_x \leq 14$ dB and up to $K = 30$ components. It is also accurate in estimating the standard deviation with up to eight equal log-normal variates when σ_x is less than 10 dB. Outside this range, the approximation is slightly less accurate.

APPENDIX
Derivation of First and Second Moments

Our purpose is to provide enough detail so that an interested reader can rederive the formulae for the first and second moments, as given below by eqs. (48) and (73).

The expansions we use are

$$\ln(1 + x) = \sum_{k=1}^{\infty} C_k x^k, \quad |x| < 1 \quad \text{and} \quad C_k = \frac{(-1)^{k+1}}{k} \quad (36)$$

$$\ln^2(1 + x) = \sum_{k=1}^{\infty} b_k x^{k+1},$$

$$|x| < 1 \quad \text{and} \quad b_k = \frac{2(-1)^{k+1}}{k+1} \sum_{j=1}^{k} j^{-1}. \quad (37)$$

The density function of a normal random variable with arbitrary mean and variance is defined by

$$\Phi'(x; m, \sigma) = \frac{1}{\sqrt{2\pi}\sigma} e^{-(x-m)^2/2\sigma^2}. \quad (38)$$

The distribution function is a simple parameter function and is given by

$$\Phi\left(\frac{x - m}{\sigma}\right) = \int_{-\infty}^{x} \Phi'(t; m, \sigma)dt \equiv \frac{1}{\sqrt{2\pi}} \int_{-\infty}^{\frac{x-m}{\sigma}} e^{-t^2/2}dt. \quad (39)$$

The function $\Phi(x)$ is related to the error function by

$$\text{erf}(x) = \frac{2}{\sqrt{\pi}} \int_{0}^{x} e^{-t^2}dt \quad (40)$$

$$\Phi(x) = \tfrac{1}{2} + \tfrac{1}{2} \text{erf}(x/\sqrt{2}). \quad (41)$$

Three integrals which occur often in the development are

$$E\{e^{rx}\} = \int_{-\infty}^{+\infty} e^{rx}\Phi'(x; m, \sigma)dx = e^{mr+r^2\sigma^2/2} \quad (42)$$

$$\int_{-\infty}^{0} e^{rx}\Phi'(x; m, \sigma)dx = [e^{mr+r^2\sigma^2/2}]\Phi\left(\frac{-m - \sigma^2 r}{\sigma}\right)$$

$$\int_{0}^{\infty} e^{-rx}\Phi'(x; m, \sigma)dx = [e^{-mr+r^2\sigma^2/2}]\Phi\left(\frac{m - \sigma^2 r}{\sigma}\right). \quad (43)$$

We repeat the definitions introduced in Section III:

$$e^Z = L = L_1 + L_2 = e^{Y_1} + e^{Y_2}$$

$$Z = \ln(e^{Y_1} + e^{Y_2}),$$

with the Y_i Gaussian random variables. Let

$$w = Y_2 - Y_1$$

$$m_w = \bar{w} = E(w) = m_{y_2} - m_{y_1}$$

$$\sigma_w^2 = E(w - \bar{w})^2 = \sigma_{y_2}^2 + \sigma_{y_1}^2. \tag{44}$$

For convenience, we shall let $f(w)$ denote the particular Gaussian density function

$$f(w) = \Phi'(w; m_w, \sigma_w); \tag{45}$$

Z is rewritten as

$$Z = \ln(e^{Y_1} + e^{Y_2}) = \ln[e^{Y_1}(1 + e^w)]. \tag{46}$$

Taking the required expectations

$$E\{Z\} = m_z = m_{y_1} + E \ln(1 + e^w)$$

$$= m_{y_1} + \int_{-\infty}^{+\infty} \ln(1 + e^w)f(w)dw. \tag{47}$$

As discussed earlier, the integral is broken up into the intervals $(-\infty, 0)$ and $(0, \infty)$. Upon application of the series (36) and the averaging (42) and (43), we obtain the result

$$m_z = m_{y_1} + m_w\Phi\left(\frac{m_w}{\sigma_w}\right) - \frac{\sigma_w}{\sqrt{2\pi}} e^{-m_w^2/2\sigma_w^2}$$

$$+ \sum_{k=1}^{\infty} C_k e^{k^2\sigma_w^2/2}\left[e^{km_w}\Phi\left(\frac{-m_w - k\sigma_w^2}{\sigma_w}\right)\right. \tag{48}$$

$$\left. + e^{-km_w}\Phi\left(\frac{m_w - k\sigma_w^2}{\sigma_w}\right)\right].$$

All the terms, except m_{y_1}, are lumped together and denoted by $G_1(\sigma_w, m_w)$:

$$m_z = m_{y_1} + G_1(\sigma_w, m_w). \tag{49}$$

The function G_1 is shown graphically in Fig. 5.

The second moment is decomposed as

$$E(Z^2) = E\{[Y_1 + \ln(1 + e^w)]^2\}$$

$$= \sigma_{y_1}^2 + m_{y_1}^2 + E[2Y_1 \ln(1 + e^w)] + E[\ln^2(1 + e^w)]. \tag{50}$$

First, consider the cross term

$$A = E[2Y_1 \ln(1 + e^w)], \tag{51}$$

where Y_1 and $w = Y_2 - Y_1$ are jointly Gaussian with correlation coefficient
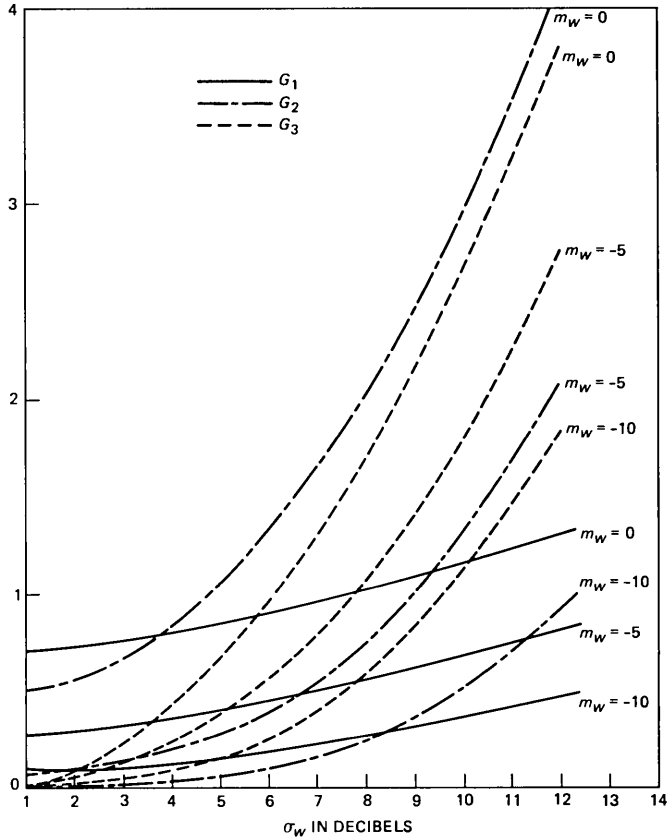
Fig. 5—The plots of G_i's as a function of σ_w with m_w as a parameter.

$$\rho = E\left[\frac{(Y_1 - m_{y_1})(w - m_w)}{\sigma_{y_1}\sigma_w}\right]$$

$$= -\frac{\sigma_{y_1}}{\sigma_w}$$

$$= -\sigma_{y_1}/\sqrt{\sigma_{y_1}^2 + \sigma_{y_2}^2} \ . \tag{52}$$

We utilize the conditional expectation property of jointly Gaussian random variables (see Ref. 17, Section 7-5):

$$E[(Y_1 - m_{y_1})|(w - m_w)] = \frac{\rho\sigma_{y_1}}{\sigma_w}(w - m_w) \tag{53}$$

or

$$E[(Y_1|w)] = m_{y_1} - \rho^2(w - m_w).$$

Then, (51) becomes

$$A = E[2Y_1 \ln(1 + e^w)]$$

$$= 2E_w[\ln(1 + e^w)E_{Y_1}|w(Y_1)]$$

$$= 2E_w\{\ln(1 + e^w)[m_{y_1} - \rho^2(w - m_w)]\}. \tag{54}$$

For convenience, we denote the first and second terms by A_1 and A_2, respectively:

$$A = A_1 - A_2. \tag{55}$$

Since

$$A_1 = 2m_{y_1}E[\ln(1 + e^w)]$$

$$= 2m_{y_1}(m_z - m_{y_1}) \tag{56}$$

from (47), we need only consider the second term A_2,

$$A_2 = 2\rho^2 E[(w - m_w) \ln(1 + e^w)]. \tag{57}$$

Integrate A_2 by parts:

$$A_2 = 2\rho^2 \int_{-\infty}^{+\infty} (w - m_w) \ln(1 + e^w)f(w)dw$$

$$= 2\rho^2\sigma_w^2 \int_{-\infty}^{+\infty} \frac{e^w}{1 + e^w} f(w)dw. \tag{58}$$

For negative w, we use the expansion

$$\frac{e^w}{1 + e^w} = \sum_{k=0}^{\infty} (-1)^k e^{(k+1)w} \tag{59}$$

to obtain

$$A_2' = 2\rho^2\sigma_w^2 \int_{-\infty}^{0} \frac{e^w}{1 + e^w} f(w)dw$$

$$= 2\rho^2\sigma_w^2 \sum_{k=0}^{\infty} (-1)^k e^{m_w(k+1)+(k+1)^2\sigma_w^2/2}$$

$$\Phi\left[\frac{-m_w - \sigma_w^2(k + 1)}{\sigma_w}\right]. \tag{60}$$

For the other part of (58), we have

$$A_2'' = 2\rho^2\sigma_w^2 \int_{0}^{\infty} \frac{e^w}{1 + e^w} f(w)dw$$

$$= 2\rho^2\sigma_w^2 \int_{0}^{\infty} \frac{1}{1 + e^{-w}} f(w)dw$$

$$= 2\rho^2\sigma_w^2 \int_0^\infty \sum_{k=0}^\infty (-1)^k e^{-kw}(f(w)dw$$

$$= 2\rho^2\sigma_w^2 \sum_{k=0}^\infty (-1)^k e^{-kmw+k^2\sigma_w^2/2}$$

$$\Phi\left[\frac{m_w - \sigma_w^{2k}}{\sigma_w}\right]. \tag{61}$$

Collecting the results for the cross term,

$$A = A_1 - A_2 = A_1 - (A_2' + A_2'')$$

$$= A_1 - 2\rho^2 G_3(\sigma_w, m_w)$$

$$= 2m_{y_1} G_1(\sigma_w, m_w) - 2\rho^2 G_3(\sigma_w, m_w). \tag{62}$$

The remaining term in $E(Z^2)$ to evaluate is the last expression in (50). We denote it by $G_2(\sigma_w, m_w)$.

$$G_2(\sigma_w, m_w) = E[\ln^2(1 + e^w)]$$

$$= \int_{-\infty}^0 \ln^2(1 + e^w)f(w)dw + \int_0^\infty \ln^2(1 + e^w)f(w)dw$$

$$= B_1 + B_2. \tag{63}$$

For the integration over the negative real line, we can use the expansion given by (37):

$$B_1 = \sum_{k=1}^\infty b_k \int_{-\infty}^0 e^{(k+1)w} f(w)dw$$

$$= \sum_{k=1}^\infty b_k e^{[(k+1)mw+(k+1)^2\sigma_w^2/2]}$$

$$\Phi\left[\frac{-m_w - \sigma^2(k + 1)}{\sigma_w}\right]. \tag{64}$$

The expression B_2 is rewritten as:

$$B_2 = \int_0^\infty \{\ln[e^w(1 + e^{-w})]\}^2 f(w)dw$$

$$= \int_0^\infty [\ln^2(1 + e^{-w}) + 2w \ln(1 + e^{-w}) + w^2]f(w)dw$$

$$= B_5 + B_4 + B_3. \tag{65}$$

The expressions for B_3 and B_5 are relatively straightforward:

$$B_3 = \int_0^\infty w^2 f(w)\, dw$$

$$= m_w^2 \left[1 - \Phi\left(\frac{-m_w}{\sigma_w}\right) \right]$$

$$+ \sqrt{2/\pi}\, m_w \sigma_w e^{-m_u^2/2\sigma_u^2}$$

$$+ \sigma^2 \left[1 - \Phi\left(\frac{-m_w}{\sigma_w}\right) \right] \frac{-m_w \sigma_w}{\sqrt{2\pi}} e^{-m_u^2/2\sigma_u^2} \tag{66}$$

$$B_5 = \int_0^\infty \ln^2(1 + e^{-w}) f(w)\, dw$$

$$= \int_{-\infty}^0 \ln^2(1 + e^{w}) f(-w)\, dw$$

$$= \int_{-\infty}^0 \sum_{k=1}^\infty b_k e^{(k+1)w} f(-w)\, dw$$

$$= \sum_{k=1}^\infty b_k e^{-(k+1)m_w + (k+1)^2 \sigma_u^2/2}$$

$$\Phi\left[\frac{m_w - \sigma_w^2(k+1)}{\sigma_w} \right]. \tag{67}$$

The final term to consider is

$$B_4 = \int_0^\infty 2w \ln(1 + e^{-w}) f(w)\, dw$$

$$= -2 \sum_{k=1}^\infty C_k \int_{-\infty}^0 w e^{kw} f(-w)\, dw. \tag{68}$$

Complete the square for the expression $e^{kw} f(-w)$ and integrate to obtain

$$B_4 = -2 \sum_{k=1}^\infty C_k e^{(-m_w k + k^2 \sigma_u^2/2)} \left[m_k \Phi\left(\frac{-m_k}{\sigma_w}\right) - \frac{\sigma_w}{\sqrt{2\pi}} e^{-m_k^2/2\sigma_u^2} \right], \tag{69}$$

where

$$m_k = -m_w + k\sigma_w^2. \tag{70}$$

Collecting the terms that make up $G_2(\sigma_w, m_w)$ in (63), we have

$$G_2(\sigma_w, m_w) = B_1 + B_2 = B_1 + (B_3 + B_4 + B_5) \tag{71}$$

as given by eqs. (64), (66), (69), and (67).

To summarize, the second moment is given by the expression

$$E(Z^2) = \sigma_{y_1}^2 + m_{y_1}^2 + 2\, m_{y_1} G_1(\sigma_w, m_w)$$

$$- 2\rho^2 G_3(\sigma_w, m_w) + G_2(\sigma_w, m_w), \qquad (72)$$

and, finally, the variance is

$$\sigma_z^2 = E(Z^2) - m_z^2$$

$$= \sigma_{y_1}^2 - G_1^2(\sigma_w, m_w) - 2\rho^2 G_3(\sigma_w, m_w) + G_2(\sigma_w, m_w). \qquad (73)$$

REFERENCES

1. L. F. Fenton, "The Sum of Log-Normal Probability Distributions in Scatter Transmission Systems," IRE Trans. Commun. Syst. *CS-8,* No. 1 (March 1960), pp. 57–67.
2. D. C. Cox, "Co-Channel Interference Considerations in Frequency-Reuse Small-Coverage-Area Radio Systems," IEEE Trans. Commun., *COM-30,* No. 1 (January 1982), pp. 9–15.
3. R. C. French, "The Effect of Fading and Shadowing on Channel Reuse in Mobile Radio," IEEE Trans. Vehicular Technology, *VT-28,* No. 3 (August 1979), pp. 171–81.
4. S. F. George, "The Detection of Nonfluctuating Targets in Log-Normal Clutter," NRL Report 6796, October 4, 1968.
5. G. V. Trunk and S. F. George, "Detection of Targets in Non-Gaussian Sea Clutter," IEEE Trans. Aerospace and Elect. Syst. *AES-6,* No. 5 (Sept. 1970), pp. 620–8.
6. J. Atchison and J. A. C. Brown, *The Lognormal Distribution,* Cambridge, Mass.: Cambridge University Press, 1957.
7. P. Bloomfield et al., "The Use of the Lognormal Distribution in Estimating Crude Oil Reserves," Technical Report, February 1979, Dept. of Statistics and Geology, Princeton University, Princeton, NJ.
8. N. L. Johnson and S. Kotz, *Continuous Univariate Distributions—1,* New York: Houghton Mifflin Co., 1970.
9. J. E. Farley, private communication.
10. W. A. Janos, "Tail of the Distribution of Sums of Log-Normal Variates," IEEE Trans. Inform. Theory, *IT-16,* No. 3 (May 1970), pp. 299–302.
11. I. E. O. Nasell, private communication.
12. I. Nasell, "Some Properties of Power Sums of Truncated Normal Random Variables," B.S.T.J., *46,* No. 9 (November 1967), pp. 2091–110.
13. N. A. Marlow, "A Normal Limit Theorem for Power Sums of Normal Random Variables," B.S.T.J., *46,* No. 9 (November 1967), pp. 2081–9.
14. N. A. Marlow, private communication.
15. J. I. Naus, "The Distribution of the Logarithm of the Sum of Two Log-Normal Variates," J. Amer. Statist. Assoc., *64,* No. 326 (June 1969), pp. 655–9.
16. M. A. Hamdan, "The Logarithm of the Sum of Two Correlated Log-Normal Variates," J. Amer. Statist. Assoc., *66,* No. 333 (March 1971), pp. 105–6.
17. A. Papoulis, *Probability, Random Variables, and Stochastic Processes,* New York: McGraw-Hill, 1965.

Piecewise Linear Approximation of Multivariate Functions

By G. S. LEE

To approximate functions of a single variable by using linear interpolation is routine in empirical studies. Here, we consider approximating functions of several variables in a similar piecewise linear manner. We focus on the nontrivial part of this technique, which is that of choosing the appropriate "pieces" for the piecewise linear approximation. Precisely, we seek to identify the best interpolants to use at a point of interpolation. This is not an issue for functions of a single variable, since the linear ordering of the number line leaves us with no choice. For functions of several variables, we propose several simple tools to help uncover undesirable choices. The techniques presented are useful in the empirical study of quantitatively complex functional relationships whose qualitative behavior is nevertheless known and simple. Response time relationships parametrized by workloads in computer performance modeling often fall into this category, and an actual bivariate function of this type is used to motivate the development.

I. INTRODUCTION

Linear approximation is a popular and economical way to gain appreciation of the behavior of functional relationships. Especially in higher dimensions, making sense out of a sample of data points in terms of the underlying multivariate relationship is greatly facilitated by some form of piecewise linear approximation. Such an approximation allows for estimation of the function at values not included in the sample, sheds light on the activity of the function at selected neighborhoods, and identifies regions where the relationship behaves interestingly.

For the sake of concreteness let us consider a typical problem. A simulation model of a computer system has been given. The workload driving the system is described by two variables giving the respective

percentages of two classes of users in the user population; there are three classes of users altogether. The two variables, then, form a bivariate parametrization of the workload. Six simulations were run, and the resulting mean response times are shown below. (This response time function will be denoted by h throughout this paper.)

$$h(60, 25) = 5.5$$

$$h(60, 7) = 2.1$$

$$h(40, 30) = 1.2$$

$$h(40, 7) = 1.0$$

$$h(20, 25) = 0.7$$

$$h(20, 15) = 0.7$$

It will be necessary to estimate the response times for many more workloads than for the six simulations already run. Yet, it would be inefficient to make a run for each possible parameter pair (x_1, x_2). It would also not be necessary, given the qualitatively simple relationship that generally exists between workloads and response times of computer systems. In this particular case, the function is expected to be monotone. Therefore, the six simulations not only give us the values of the function at those six points, but also the values between and around them, that is, at least approximately. For example, we could safely assert that $h(55, 10)$ should lie between 1.0 and 5.5. In fact, it would be reasonable to estimate the range to be from 1.8 to 5.5. This becomes obvious by plotting the six-parameter pairs used in the simulations, plus the point $P = (55, 10)$ on the (x_1, x_2) plane, as shown in Fig. 1. The points A through F are labeled in the order in which they were collected; point A is the oldest. Since the polygon with corners A, D, B, and E bound the point $(55, 10)$, it is reasonable to deduce that the values of h at A, D, B, and E bound the value of h at $(55, 10)$. This gives the interval $(1.0, 5.5)$. Furthermore, $h(55, 7)$ may be estimated as 1.8 by linear interpolation between $h(40, 7) = 1.0$ and $h(60, 7) = 2.1$. Since h is increasing in both x_1 and x_2, $h(55, 10) \geq h(55, 7)$. This gives the sharper interval $(1.8, 5.5)$.

As we will see, this approach can be continued until a numerical estimate for $h(55, 10)$ is reached. Two steps are required. The first step identifies the data points that contain relevant information about $h(55, 10)$. For example, we have already rejected C and F as irrelevant to P. This was simple and was done "by eye." Finer methods need be developed, however, to determine which one of A, B, D or E should be further discarded. The major part of this paper, starting with Section III, deals with this and related problems. The second step consists of fitting a linear function over the data points chosen as a result of the
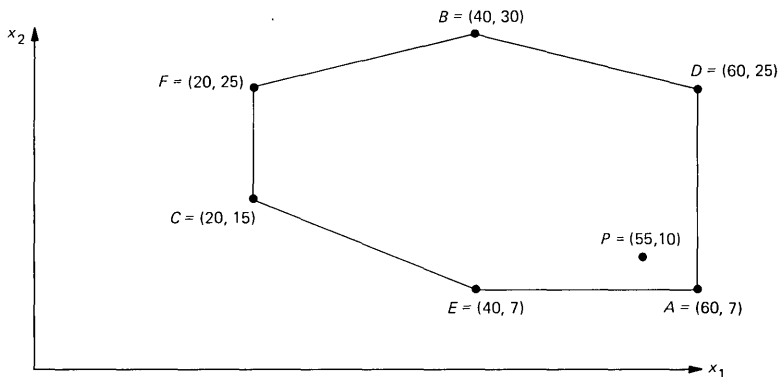
Fig. 1—Data points for case study.

first step; the mechanics of linear fitting will be reviewed in Section II. Together, the two steps produce the "best" way to fit the data points in a piecewise linear way. The concluding recapitulation gives an overview of the methodology in an iterative context.

Formulas used in our treatment are gathered in a sequence of propositions. Since they are rather straightforward and our interest is in their usage, only abbreviated arguments for their validity are included. All calculations may be easily carried out on a computer. Needed, aside from basic arithmetic, are routines to define and manipulate matrices, perform matrix multiplications and inversions, take determinants, and find eigenvectors of symmetric matrices. Computations for our examples have been carried out with relatively short programs in the S statistical package.[1]

Our proposed approach is not meant to replace the standard practice of fitting a single, global functional relationship to the data. The two procedures reveal different aspects of the data. Function fitting, being inherently global, is well suited for capturing the overall behavior of the relationship. This we hope to complement with the piecewise linear approach, which, being inherently local, is better suited for pinpointing places where interesting things happen to the function. This is especially relevant for iterative empirical studies, where it is useful to know where the function is active in the parameter space so that further experiments can be fruitfully specified.

II. THE BASIC INTERPOLATION

Linear interpolation for functions of a single variable is usually taught in high school in terms of such notions as similar triangles and slopes. For the purpose of generalization to higher dimensions, an alternative, though algebraically equivalent, viewpoint is preferred.

Specifically, let $f(x_1) = y_1$, $f(x_2) = y_2$, and $x_1 < x < x_2$. It can be shown that the usual linear interpolation gives the estimate

$$a_1 y_1 + a_2 y_2,$$

where α_1 and α_2 satisfy

$$a_1 x_1 + a_2 x_2 = x,$$

$$\alpha_1 + \alpha_2 = 1,$$

$$\alpha_1, \alpha_2 > 0.$$

In other words, to estimate $f(x)$ for some x in the interval $x_1 < x_2$, express x as a convex combination (weighted average) of x_1 and x_2, then estimate $f(x)$ as the same convex combination of $f(x_1)$ and $f(x_2)$.

Notations: As usual, $\mathbf{R}^n$ is the set of n-dimensional real column vectors. Also standard is the use of the prime notation for matrix transposition, as in $\mathbf{M}'$. If the jth column of matrix $\mathbf{M}$ is $\mathbf{m}_j$, we write $\mathbf{M} = (\mathbf{m}_1, \cdots, \mathbf{m}_k)$. The length of a vector $\mathbf{v} = (v_1, \cdots, v_n)'$ is denoted by

$$\|\mathbf{v}\| = \sqrt{(v_1^2 + \cdots + v_n^2)}.$$

For any $\mathbf{x} \in \mathbf{R}^n$, let $\mathbf{x}^* \in \mathbf{R}^{n+1}$ denote

$$\begin{pmatrix} \mathbf{x} \\ 1 \end{pmatrix},$$

i.e., the vector consisting of $\mathbf{x}$ followed by the singleton 1. If f is a function, $\hat{f}$ denotes its approximation by linear interpolation.

A higher dimensional analogue of having the points x_1, x_2 generate an interval in one dimension is having points $\mathbf{x}_1$, $\mathbf{x}_2$, $\mathbf{x}_3$ generate a triangle in two dimensions and having $\mathbf{x}_1$, $\mathbf{x}_2$, $\mathbf{x}_3$, $\mathbf{x}_4$ generate a pyramid in three dimensions. Just as we require that an interval in one dimension should not shrink to a point, we require that a triangle should contain area on a plane rather than reduce to a line segment, and that a pyramid should contain volume in solid space rather than collapse onto some plane. In general, we are concerned with the convex hull of $(n + 1)$ points $\mathbf{x}_1, \cdots, \mathbf{x}_{n+1} \in \mathbf{R}^n$, subject to the condition that these points do not lie in some lower $(<n)$ dimensional hyperplane. The matrix formulation of this geometric requirement is that the linear transformation $\mathbf{X}$ given by

$$\mathbf{X} = (\mathbf{x}_1 - \mathbf{x}_{n+1}, \cdots, \mathbf{x}_n - \mathbf{x}_{n+1})$$

should have the trivial kernel, or, by the rank-nullity theorem, satisfy $\det(\mathbf{X}) \neq 0$.

Definition: An n-dimensional pyramid is the convex hull of a set of $(n + 1)$ vectors $\{\mathbf{x}_1, \cdots, \mathbf{x}_{n+1}\} \subset \mathbf{R}^n$ such that

$$\det(\mathbf{x}_1 - \mathbf{x}_{n+1}, \cdots, \mathbf{x}_n - \mathbf{x}_{n+1}) \neq 0.$$

The points $\mathbf{x}_i$ are called its vertices, and any subset of n vertices forms a face of the pyramid.

We will often call a set of points a pyramid, rather than a convex hull generated by these points, as would be strictly correct; however, this makes no difference since there is a one-to-one correspondence between the set of vertices and the pyramid it generates.

Proposition 1: Let $f: \mathbf{R}^n \to \mathbf{R}$ be a function of n variables. Let $\{\mathbf{x}_1, \cdots, \mathbf{x}_{n+1}\} \subset \mathbf{R}^n$ be (i.e., generate) an n-dimensional pyramid containing $\mathbf{x} \in \mathbf{R}^n$, and let $f(\mathbf{x}_j) = y_j$. Then,

  (*i*) $\mathbf{X}^* = (\mathbf{x}_1^*, \cdots, \mathbf{x}_{n+1}^*)$ is an invertible $(n + 1) \times (n + 1)$ matrix, and

  (*ii*) the estimate $\hat{f}(\mathbf{x}) = (y_1, \cdots, y_{n+1})(\mathbf{X}^*)^{-1}\mathbf{x}^*$ is a higher dimensional generalization of linear interpolation for a single variable.

Proof:

  (*i*) If $\mathbf{X}^*$ were not invertible, its columns would be linearly dependent. Therefore, one of the vertices would be a convex (not necessarily positive) combination of the n remaining vertices, implying that the $n + 1$ points lie in $(n - 1)$-dimensional hyperplane at most. This contradicts the definition of a pyramid.

  (*ii*) Let $\alpha = (\mathbf{X}^*)^{-1}\mathbf{x}^* = (\alpha_1, \cdots, \alpha_{n+1})'$. Since $\mathbf{x}^* = \mathbf{X}^*\alpha$, it follows from the star (*) definition that

$$\mathbf{x} = \alpha_1\mathbf{x}_1 + \cdots + \alpha_{n+1}\mathbf{x}_{n+1},$$

$$\alpha_1 + \cdots + \alpha_{n+1} = 1.$$

Thus, α expresses $\mathbf{x}$ as a convex combination of $\{\mathbf{x}_1, \cdots, \mathbf{x}_{n+1}\}$. Since $\mathbf{x}$ is contained in the convex hull, $\alpha \geqq \mathbf{0}$. Hence, the linear interpolation at $\mathbf{x}$ should be

$$\hat{f}(\mathbf{x}) = \alpha_1 y_1 + \cdots + \alpha_{n+1} y_{n+1},$$

which is as proposed.

In practice, we will not know whether $\mathbf{x}$ is contained in the convex hull. Therefore, the vector of coefficients α should be explicitly computed to check that $\alpha \geqq \mathbf{0}$. The use of the procedure with negative components in α corresponds to linear extrapolation.

Example: Returning to the computer system response time function h, we see from the (x_1, x_2) plot in the previous section that

$$\{B, E, A\} = \left\{ \begin{pmatrix} 40 \\ 30 \end{pmatrix}, \begin{pmatrix} 40 \\ 7 \end{pmatrix}, \begin{pmatrix} 60 \\ 7 \end{pmatrix} \right\}$$

forms a two-dimensional pyramid, or triangle, containing

$$P = \begin{pmatrix} 55 \\ 10 \end{pmatrix}.$$

Alternatively, if plots are not feasible, as would be the case in higher dimensions, we calculate

$$\det\begin{pmatrix} 40\text{–}60 & 40\text{–}60 \\ 30\text{–} 7 & 7\text{–} 7 \end{pmatrix} = 460 \neq 0,$$

checking that a noncollapsing pyramid is obtained, and

$$\alpha = \begin{pmatrix} 40 & 40 & 60 \\ 30 & 7 & 7 \\ 1 & 1 & 1 \end{pmatrix}^{-1} \begin{pmatrix} 55 \\ 10 \\ 1 \end{pmatrix} = \begin{pmatrix} 0.13 \\ 0.12 \\ 0.75 \end{pmatrix} \geq 0,$$

checking that

$$\begin{pmatrix} 55 \\ 10 \end{pmatrix}$$

is contained in the pyramid. Interpolation according to the formula gives

$$(1.2 \quad 1.0 \quad 2.1) \begin{pmatrix} 0.13 \\ 0.12 \\ 0.75 \end{pmatrix} = 1.85.$$

Similarly,

$$\{E, A, D\} = \left\{ \begin{pmatrix} 40 \\ 7 \end{pmatrix}, \begin{pmatrix} 60 \\ 7 \end{pmatrix} \begin{pmatrix} 60 \\ 25 \end{pmatrix} \right\}$$

is a pyramid containing

$$\begin{pmatrix} 55 \\ 10 \end{pmatrix},$$

and interpolation using this pyramid gives

$$(1.0 \quad 2.1 \quad 5.5) \begin{pmatrix} 40 & 60 & 60 \\ 7 & 7 & 25 \\ 1 & 1 & 1 \end{pmatrix}^{-1} \begin{pmatrix} 55 \\ 10 \\ 1 \end{pmatrix} = 2.39.$$

III. THE SELECTION PROBLEM

We have just seen how two different choices of pyramids can lead to two markedly different approximations. Taking the average and approximating

$$\hat{h} \begin{pmatrix} 55 \\ 10 \end{pmatrix}$$

by $\frac{1}{2}(1.85 + 2.39) = 2.12$ is not justified. An average is appropriate when summarizing a batch of numbers that have been made different by random error, since the averaging process "zeroes out" the random errors. In our case, the difference between the two approximations

does not arise from random error. One of the choices is better than the other, and that is not a probabilistic phenomenon.

Another way to proceed is to put greater trust on closer interpolants than on further ones and choose the pyramid yielding the least-summed distance from its vertices to that point. Under this criterion, the pyramid ADE should be preferred over ABE, since D is closer to P than B is by nine units. Unfortunately, the notion of distance is not invariant to the choice of scales on the axes, and the criterion becomes sensitive to changes of units in the independent variables. The distance-type criteria have a further, more fundamental weakness, which they share with, among others, the criterion of Lawson.[2]

As used by Akima[3] in his algorithm for bivariate smooth interpolation, Lawson's criterion triangulates the (x_1, x_2) plane in such a way that minimum interior angles of triangles are maximized. The objective is to set up as many "fat" triangles as possible. Under such "fatness-type" criterion, ADE is again chosen over ABE, since ABE comes with the companion triangle ABD, which is too "skinny." An extremely skinny triangle is undesirable for two reasons. First, its X^* may be numerically unstable to invert. Second, it biases the estimation along a particular direction in the (x_1, x_2)-plane. (On the other hand, we will see in Section VI that thoughtful biasing may be beneficial.) It is not necessary, however, to make fatness an overall criterion just to avoid such excesses.

The problem with these distance- and fatness-type criteria is that only the configuration of the $\mathbf{x}$ variables is used in assessing pyramids. (With the curve-fitting approach that uses Lagrangian and trigonometric polynomials,[4] even this information is not taken into account.) This is an unnecessary restriction. Surely the values of the function at the interpolants, the $f(\mathbf{x})$'s, have much to say on the adequacy of an interpolation. Our basic working tool to tie $\mathbf{x}$ together with $f(\mathbf{x})$ is the notion of steepest ascent. Using it, we show that the correct pyramid to choose is ABE, rather than the pyramid ADE, favored by both criteria above. Incidentally, the ABE choice for (55, 10) was confirmed empirically by an actual simulation run which gave the result $h(55, 10) = 1.74$. Recall that interpolation with ABE gives 1.85, representing a 6.3 percent error, while interpolation with ADE gives 2.39, representing a 37.4 percent error. The fact that the interpolation overestimates could also have been predicted. See Section VII, where assumptions underlying our approach are discussed.

IV. STEEPEST ASCENT

Equipped with the mechanics of basic interpolation, we may analyze in detail the function's interpolated behavior on a given pyramid. We would like to know along which direction inside the pyramid the

function increases, and how fast that increase is. Because of the linearity of the interpolation, both questions have well-defined answers. The geometric way to derive an answer is to slice the pyramid into parallel "contour hyperplanes," which are systems of hyperplanes such that points on the same hyperplane have the same interpolated values.

Example: Figure 2 shows some contour hyperplanes (contour lines in two dimensions) corresponding to the pyramid (triangle) ABE. Points along the downward-sloping lines take the same interpolated values as labeled. Clearly, $\hat{h}$ increases most rapidly along the direction of the arrow, which is perpendicular to the contour lines.

Since the contour hyperplanes are parallel, a single vector perpendicular to all of them can be found. Actually, there will be many such vectors, but they can only have one of two opposite directions, one for increasing f and another for decreasing f. We agree to take the increasing direction. Being perpendicular to the contour hyperplanes, this direction has no component along which $\hat{f}$ does not increase. Therefore, it is the direction along which $\hat{f}$ increases the fastest. We define a unit vector in this direction to be the direction of steepest ascent of the function f in the pyramid. The rate of steepest ascent is the increase of $\hat{f}$ along the direction of steepest ascent per unit distance traveled.

It remains to formulate these geometric notions in matrix terms.

Proposition 2: Let $f: \mathbf{R}^n \to \mathbf{R}$ be a function of n variables, $\{\mathbf{x}_1, \cdots, \mathbf{x}_{n+1}\} \subset \mathbf{R}^n$ be a pyramid, $f(\mathbf{x}_i) = y_i$, and $\mathbf{X}^* = (\mathbf{x}_1^*, \cdots, \mathbf{x}_{n+1}^*)$. Let

$$(a_1, \cdots, a_{n+1}) = (y_1, \cdots, y_{n+1})(\mathbf{X}^*)^{-1}.$$

(i) The direction of steepest ascent in $\{\mathbf{x}_1, \cdots, \mathbf{x}_{n+1}\}$ is $(a_1, \cdots, a_n)/\|(a_1, \cdots, a_n)\|$, and

(ii) The rate of steepest ascent in $\{\mathbf{x}_1, \cdots, \mathbf{x}_{n+1}\}$ is $\|(a_1, \cdots, a_n)\|$.
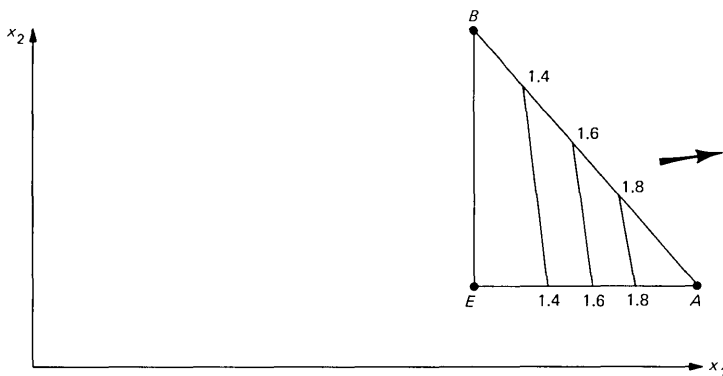
Fig. 2—Contour lines for ABE. Function increases in direction of arrow.

Proof: By definition of $(a_1, \cdots, a_{n+1})$, the interpolation fits the function

$$\hat{f}(x_1, \cdots, x_n) = a_1 x_1 + \cdots + a_n x_n + a_{n+1}$$

on the pyramid $\{\mathbf{x}_1, \cdots, \mathbf{x}_{n+1}\}$.

To show (*i*), note that $\hat{f}(\mathbf{u}) = \hat{f}(\mathbf{v})$ implies that $(a_1, \cdots, a_n)(\mathbf{u} - \mathbf{v}) = 0$. To show (*ii*), note that $\hat{f}((a_1, \cdots, a_n)/\|(a_1, \cdots, a_n)\|) - \hat{f}(0) = \|(a_1, \cdots, a_n)\|$.

Example: Table I lists some directions and rates of steepest ascent that we will use later.

V. A FIRST APPROACH: JUDGING BY FACES

Example: We are now ready to reject *ADE* in favor of *ABE*. Actually, since *ADE* and *BDE* form a companion pair, we will reject them both. This will be accomplished by analyzing the face *DE*. In Fig. 3, *ADE* and *BDE* are shown along with their respective directions of steepest ascent loosely placed about their centers. The two directions of steepest ascent make sense separately. Both show response time as an increasing function of x_1 and x_2. Together, however, they show that *DE* is a ridge, i.e., $\hat{h}$ increases as *DE* is approached from either side.

Table I—Some directions and rates
of steepest ascent

Pyramid	Direction of Steepest Ascent	Rate of Steepest Ascent
ADE	(0.29, 0.96)'	0.197
BDE	(0.99, 0.05)'	0.218
ABD	(0.81, 0.58)'	0.323
ABE	(0.98, 0.19)'	0.059
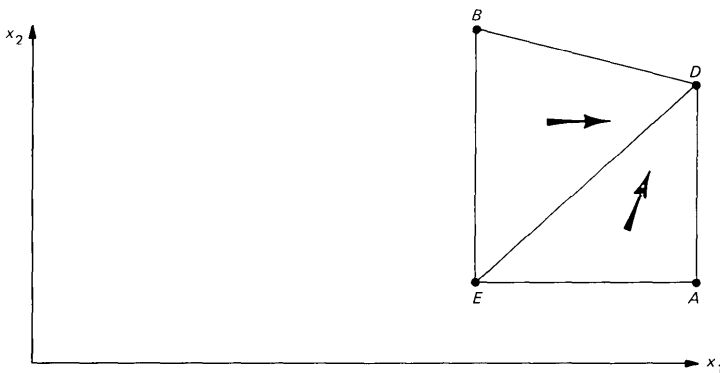
Fig. 3—ADE and BDE with their directions of steepest ascent.

Alternatively, a ridge indicates that $\hat{h}$ is not monotone along some direction on the (x_1, x_2) plane. From our knowledge of h, no such ridge should exist. The triangulation $\{ADE, BDE\}$ incorrectly shows a ridge because $h(D)$ is inordinately large. The triangulation allows D to pull up both triangles, causing their boundary to buckle. The correct way to picture h is shown in Fig. 4. For low values of x_1 and x_2, $\hat{h}$ grows moderately (rate of steepest ascent = 0.059 on ABE), with x_1 being mainly responsible for the increase. As x_1 and x_2 become large, $\hat{h}$ explodes (rate of steepest ascent = 0.323 on ABD), and x_2 begins to affect $\hat{h}$ seriously, although x_1 is still the major contributor. Because of the piecewise linearity of interpolation, AB has become an accelerating, refracting boundary but not a ridge. In Section VI, we will see another reason why ADE is a poor choice.

Note that specific knowledge about h was invoked to make the selection: We knew that response time as a function of workload had no ridges. In general, linear interpolation of functions with known major ridges, valleys, maxima, or minima should be avoided. An exception may be made if we are able to sprinkle such tricky terrain generously with further interpolants. Under finer resolution, the volatile formations should diminish. Of course, even if a ridge does exist, it is highly improbable that it should coincide with one of our faces.

Definition: A face is a bad face if there are two pyramids containing it, and their directions of steepest ascent either both point towards it or both point away from it.

Thus, we accept as likely those faces that may refract and/or accelerate steepest ascent vectors, but we question faces that gather or scatter them.

Matrix techniques are clearly needed to identify bad faces in higher dimensions, where graphs are not feasible. It is enough to find a technique to determine if a given steepest ascent approaches a given
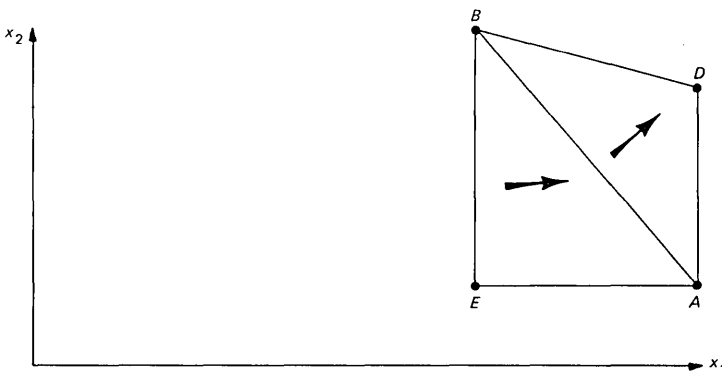
Fig. 4—ABE and ABD with their directions of steepest ascent.

face. Since approaching a face at 90 degrees is different from approaching it at 0.0001 degree, the angle of approach is also of interest. Note that knowledge of the angle alone does not tell us whether the ascent approaches; the ascent may be located on either side of the face.

Proposition 3: Let $\mathbf{a} \in \mathbf{R}^n$ be a steepest ascent for the pyramid $\{\mathbf{x}_1, \cdots, \mathbf{x}_{n+1}\} \subset \mathbf{R}^n$. Let $\{\mathbf{x}_1, \cdots, \mathbf{x}_n\} = F$ be the face of interest. Define the $n \times (n-1)$ matrix

$$\mathbf{X} = (\mathbf{x}_1 - \mathbf{x}_n, \mathbf{x}_2 - \mathbf{x}_n, \cdots, \mathbf{x}_{n-1} - \mathbf{x}_n).$$

Also define the $n \times n$ matrix

$$\mathbf{Y} = (-\mathbf{X}, \mathbf{a}) = (\mathbf{x}_n - \mathbf{x}_1, \mathbf{x}_n - \mathbf{x}_2, \cdots, \mathbf{x}_n - \mathbf{x}_{n-1}, \mathbf{a}).$$

(*i*) Let $\beta = (\beta_1, \cdots, \beta_n)' = \mathbf{Y}^{-1}(\mathbf{x}_n - \mathbf{x}_{n+1})$. If $\beta_n > 0$, $\mathbf{a}$ approaches F. If $\beta_n < 0$, $\mathbf{a}$ recedes from F. If $\mathbf{Y}$ is not invertible, $\mathbf{a}$ is parallel to F.

(*ii*) Let $\cos \theta = \sqrt{\mathbf{a}'\mathbf{X}(\mathbf{X}'\mathbf{X})^{-1}\mathbf{X}'\mathbf{a}}$. Then θ is the angle between $\mathbf{a}$ and F.

Proof:

(*i*) The trick here is to pull the vertex $\mathbf{x}_{n+1}$ to the origin so that we may examine the relationship between $\mathbf{a}$, now sitting at the origin, and F, now translated to $\{\mathbf{x}_1 - \mathbf{x}_{n+1}, \cdots, \mathbf{x}_n - \mathbf{x}_{n+1}\}$. For β as given above, let $\pi_i = \beta_i$ for $i = 1, \cdots, n-1$, $\pi_n = 1 - (\pi_1 + \cdots + \pi_{n-1})$, and $t = \beta_n$. The reader may check that

$$t\mathbf{a} = \sum_{i=1}^{n} \pi_i(\mathbf{x}_i - \mathbf{x}_{n+1}),$$

$$\sum_{i=1}^{n} \pi_i = 1.$$

The interpretation of the sign of β_n follows from the trick just described.

(*ii*) The trick is to translate the face to the origin by $\mathbf{x}_n$. We then regress $\mathbf{a}$ against the translated face $\{\mathbf{x}_1 - \mathbf{x}_n, \cdots, \mathbf{x}_{n-1} - \mathbf{x}_n\}$ so that its projection proj($\mathbf{a}$) onto the linear subspace spanned by the translated face may be found by the usual formula. Now take the inner product between $\mathbf{a}$ and proj($\mathbf{a}$), bearing in mind that $\mathbf{a}$ is a unit vector.

Example: Using the formulas above, we find the *DE* is approached by the direction of steepest ascent of *BDE* at 31 degrees, and *DE* is also approached by the direction of steepest ascent of *ADE* at 39 degrees. Thus, *DE* is a ridge.

VI. ANOTHER APPROACH: THE AXES CRITERION

Example: Let's consider again the selection problem with the response time function $y = h(x_1, x_2)$, but this time we consider the complementary pair of triangles *ABD* and *BDE*, shown in Fig. 5. While neither triangle is very skinny, we could roughly identify directions along

which they stretch out. For example, ADB stretches out in some direction along AB, which is quite perpendicular to its direction of steepest ascent. BDE, on the other hand, stretches somewhat along DE, which is not at all perpendicular to its direction of steepest ascent. This difference affords another basis for selection. Let's exaggerate somewhat and give the two triangles more definitive and mutually perpendicular directions of stretch; we also assume that the "direction of steepest ascent of the function" (a vague notion), denoted by $\mathbf{a}$, is perpendicular to the stretch of ABD. The situation is shown in Fig. 6. We may now rotate the configuration to new axes (x'_1, x'_2) so that the pair of triangles stretch in directions parallel to the new axes, as in Fig. 7. Because of our assumption, $\mathbf{a}$ becomes parallel to x'_1. This means that x'_2 has no effect on y, so we may plot y as a function of x'_1 alone.

a_1 = ASCENT IN ABD
a_2 = ASCENT IN BDE
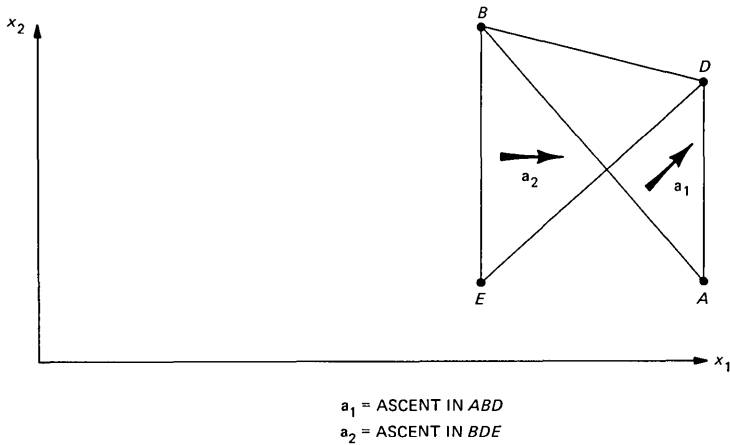
Fig. 5—Triangles ABD and BDE with directions of steepest ascent.
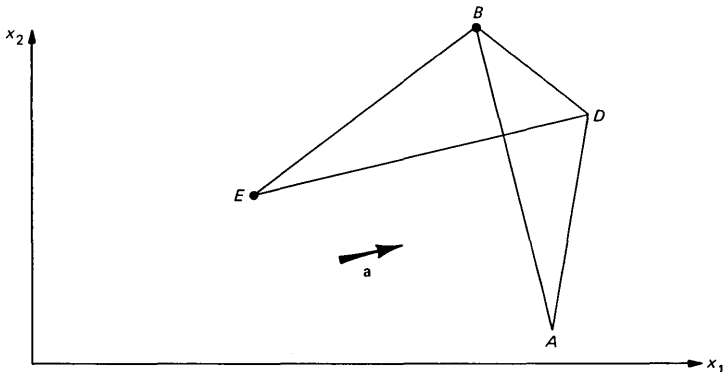
Fig. 6—ABD and BDE stretched in mutually perpendicular directions.

Since **a** points along x_1', y is an increasing function of x_1'. If y is a linear function of x_1', it will also be a linear function of (x_1, x_2), in which case it doesn't matter which triangle we select. Both will give perfect fit. However, for h, we must protect ourselves against nonlinearity. We actually know that h is concave downwards as a function of x_1'. (If h is concave upwards, the same argument below holds.) The elimination of x_2' leads to the (x_1', y) plot given in Fig. 8. Clearly, ABD hugs the function much better than BDE. By stretching linearly far along the direction of ascent, BDE loses touch of the underlying, nonlinear function. Here is the second reason why ABE is a better choice than ADE.

The moral is that triangles perpendicular to their directions of steepest ascent give better estimates. The same is true in higher dimensions, although in higher dimensions it is not appropriate to talk about the direction of stretch of a pyramid because a pyramid may stretch in several directions at once. In three dimensions, for example,
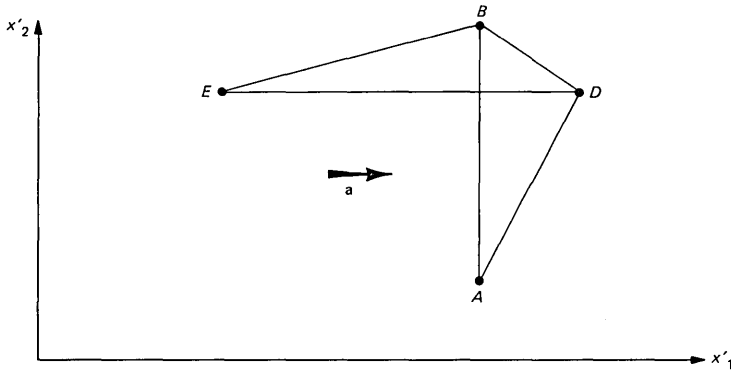
Fig. 7—Rotation of Fig. 6.
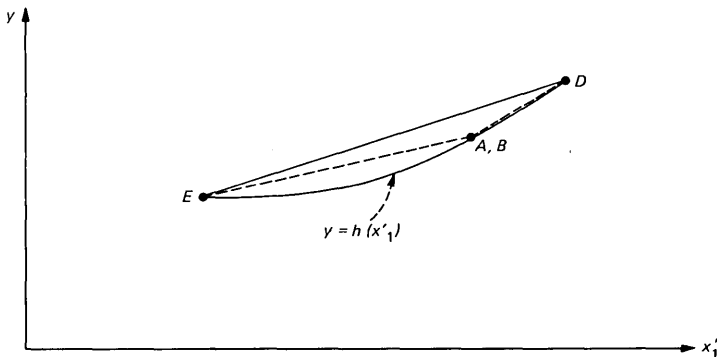
Fig. 8—Elimination of x_2.

a solid pyramid may stretch out in one single direction, as in a needle-like pyramid, or in two directions, as in a pancake-like pyramid. Therefore, we will appeal to the notion of the axes of a pyramid—the system of coordinates that best aligns with the vertices of the pyramid, such that the first coordinate aligns with the furthest stretch of the pyramid, $\cdots$, the last coordinate aligns with the shortest stretch of the pyramid. The coordinates (x_1', x_2') found above by rotation are an informal, visual example. Formally, it is necessary to define "best alignment." For convenience, we will define it in terms of least-squared distances. Then, we may use the principal component technique from multivariate statistical analysis.[5]

Definition: Let $\{x_1, \cdots, x_{n+1}\} \subset \mathbf{R}^n$ be a pyramid with mean vector

$$\bar{\mathbf{x}} = \frac{1}{n+1} (\mathbf{x}_1 + \cdots + \mathbf{x}_{n+1}).$$

Define the $n \times (n+1)$ matrices

$$\mathbf{X} = (\mathbf{x}_1, \cdots, \mathbf{x}_{n+1}), \qquad \bar{\mathbf{X}} = (\bar{\mathbf{x}}, \cdots, \bar{\mathbf{x}}).$$

Define the $n \times n$ covariance matrix

$$\mathbf{V} = \frac{1}{n} (\mathbf{X} - \bar{\mathbf{X}})(\mathbf{X} - \bar{\mathbf{X}})'.$$

Let $\mathbf{v}_1, \cdots, \mathbf{v}_n$ be the eigenvectors of V with eigenvalues $\lambda_1 \geqq \cdots \geqq \lambda_n$. (That is, $\mathbf{V}\mathbf{v}_i = \lambda_i \mathbf{v}_i$.) Then $\mathbf{v}_1$ is the first axis of the pyramid, $\mathbf{v}_2$ is the second axis of the pyramid, $\cdots$, $\mathbf{v}_n$ is the last axis.

The eigenvalue λ_i tells us how far the pyramid stretches along $\mathbf{v}_i$. Thus, a four-dimensional pyramid with eigenvalues $1000 \geqq 10 \geqq 10 \geqq 10$ stretches out mainly along $\mathbf{v}_1$, while a four-dimensional pyramid with eigenvalues $1000 \geqq 500 \geqq 10 \geqq 10$ stretches mainly along $\mathbf{v}_1$ and $\mathbf{v}_2$, with the stretch along $\mathbf{v}_1$ being significantly larger than the stretch along $\mathbf{v}_2$. A pyramid with identical eigenvalues does not stretch in any direction and is "fat." The eigenvalues cannot be 0 for pyramids.

The use of the axes $\mathbf{v}_1, \cdots, \mathbf{v}_n$ in evaluating a pyramid is as follows: if $\mathbf{a}$ is its direction of steepest ascent, then the ideal pyramid $\{x_1, \cdots, x_{n+1}\}$ satisfies

$$\mathbf{a}'\mathbf{v}_1 = 0$$
$$\cdot$$
$$\cdot$$
$$\cdot$$
$$\mathbf{a}'\mathbf{v}_{n-1} = 0.$$

Thus, its first $(n-1)$ axes are perpendicular to the direction of steepest ascent, leaving the last axis, the direction of shortest stretch of the pyramid, to coincide with its direction of steepest ascent. When comparing less-than-ideal pyramids, we choose the one where $|\mathbf{a}'\mathbf{v}_i|$ is close

to 0 for as many of the first $\mathbf{v}_1, \cdots, \mathbf{v}_m$ as possible. Note that $\mathbf{a}'\mathbf{v}_i$ is the cosine of the angle between $\mathbf{a}$ and $\mathbf{v}_i$.

Example: Using the formulas given above, Table II has been completed. Note that $\mathbf{v}_1$ and $\mathbf{v}_2$ are mutually perpendicular, as they must be. From the relatively high ratios of λ_1/λ_2, it follows that all four triangles have fairly prominent major (first) axes, i.e., they stretch along some distinct direction. *ABD* and *ABE* form the narrower pair of triangles. By comparing $|\mathbf{a}'\mathbf{v}_1|$, it follows that *ADE* and *BDE* tend to stretch along their respective directions of steepest ascent, while *ABD* and *ABE* are more perpendicular to their respective steepest ascents. Therefore, we chose the triangulation $\{ABD, ABE\}$ over the triangulation $\{ADE, BDE\}$.

VII. ASSUMPTIONS

Now we spell out some assumptions about the underlying function that are relevant to the validity of our linear interpolation.

The foremost assumption is that the function is reasonably smooth with respect to the mesh of the interpolants. Without such basic optimism, which is buttressed by the prerogative of adding further interpolants to refine the mesh, systematic investigation could not proceed. As described in Ref. 6: "The experimenter is like a person attempting to map the depth of the sea by making soundings at a limited number of places. $\cdots$ mapping a surface resembling a nest of stalagmites or the back of a porcupine would be impossible $\cdots$ since characteristics of the surface at one point would not be related to characteristics elsewhere." Under the smoothness assumption, the axis analysis presented in Section VI is valid, since it simply recommends, in quantitative terms, the prudence of spacing out the interpolants only where the function appears to behave uneventfully.

The face criterion of Section V applies when the function is monotone, in addition to being smooth. (Monotonicity as defined here is more stringent than what is usually required.)

Definition: A multivariate function $f: \mathbf{R}^n \to \mathbf{R}$ is monotone if one of the following holds for any $\mathbf{x}, \mathbf{y} \in \mathbf{R}^n$:

(*i*) For all $\alpha, \beta \in (0, 1)$, $\alpha > \beta \to f(\alpha\mathbf{x} + (1 - \alpha)\mathbf{y}) \geqq f(\beta\mathbf{x} + (1 - \beta)\mathbf{y})$, or

Table II—Axes analysis for typical problem

Triangle	Steepest Ascent α	Eigenvectors v_1, v_2	Eigenvalues λ_1, λ_2	$\alpha'v_1$
ADE	$(0.29, 0.96)'$	$(-0.78, -0.63)', (\ 0.63, -0.78)'$	182.0, 59.3	−0.83
BDE	$(0.99, 0.05)'$	$(-0.65, -0.76)', (\ 0.76, -0.65)'$	183.7, 96.0	−0.68
ABD	$(0.81, 0.58)'$	$(\ 0.68, -0.73)', (\ 0.73, \ 0.68)'$	233.4, 46.3	0.13
ABE	$(0.98, 0.19)'$	$(-0.60, \ 0.80)', (-0.80, -0.60)'$	234.5, 75.2	−0.44

(*ii*) For all α, $\beta \in (0, 1)$, $\alpha > \beta \to f(\alpha \mathbf{x} + (1 - \alpha)\mathbf{y}) \leqq f(\beta \mathbf{x} + (1 - \beta)\mathbf{y})$.

That is, f either increases or decreases consistently along whichever direction one travels in the $\mathbf{x}$-space.

Often, specific knowledge of the function includes its monotonicity. With our h, for example, it is unlikely that any direction should be singled out along which h "rollercoasts."

A further useful assumption is convexity (concavity).

Definition: A function $f: \mathbf{R}^n \to \mathbf{R}$ is convex on a convex region $A \subset \mathbf{R}^n$ if for any $\mathbf{x}$, $\mathbf{y} \in A$ and $\alpha \in (0, 1)$,

$$f(\alpha \mathbf{x} + (1 - \alpha)\mathbf{y}) \leqq \alpha f(\mathbf{x}) + (1 - \alpha) f(\mathbf{y}).$$

The function f is concave if

$$f(\alpha \mathbf{x} + (1 - \alpha)\mathbf{y}) \geqq \alpha f(\mathbf{x}) + (1 - \alpha) f(\mathbf{y}).$$

If f is convex on the region A, the interpolated function $\hat{f}$ satisfies

$$f(\mathbf{x}) \leqq \hat{f}(\mathbf{x}) \ (\mathbf{x} \in A).$$

(Similarly, if f is concave, we have $f \geqq \hat{f}$.) Hence, knowledge of the convexity (concavity) of f permits the conclusion that the interpolated approximations are the upper (lower) bounds to the true values of f. Since h appears to be convex on the hexagon $ABCDEF$, the response time estimates obtained from linear interpolation are likely to be worst-case estimates. This agrees with actual data:

$$h(55, 10) = 1.74 \leqq 1.85 = \hat{h}(55, 10).$$

Proposition 4: Let $\|\mathbf{a}\|$ be the rate of steepest ascent in pyramid $P = \{\mathbf{x}_1, \cdots, \mathbf{x}_{n+1}\} \subset \mathbf{R}^n$. Let $r_1, \cdots, r_i$ be the rates of steepest ascent in all pyramids that share some face F with P such that $\mathbf{a}$ recedes from F. Similarly, let $s_1, \cdots, s_j$ be the rates of steepest ascent in all pyramids sharing some face with P that is approached by $\mathbf{a}$. Then, for monotone f:

(*i*) It is consistent with the convexity of f on P that

$$r_1, \cdots, r_i \leqq \|\mathbf{a}\| \leqq s_1, \cdots, s_j.$$

(*ii*) It is consistent with the concavity of f on P that

$$r_1, \cdots, r_i \geqq \|\mathbf{a}\| \geqq s_1, \cdots, s_j.$$

Example: It follows from Fig. 9 that h is likely to be convex on ABE, since $0.025 < 0.059 < 0.323$.

VIII. MORE ON THE SECOND APPROACH: A GLOBAL METRIC

Selecting the "best" system of pyramids was straightforward in our example with ABE and ADE, since the number of triangles was few
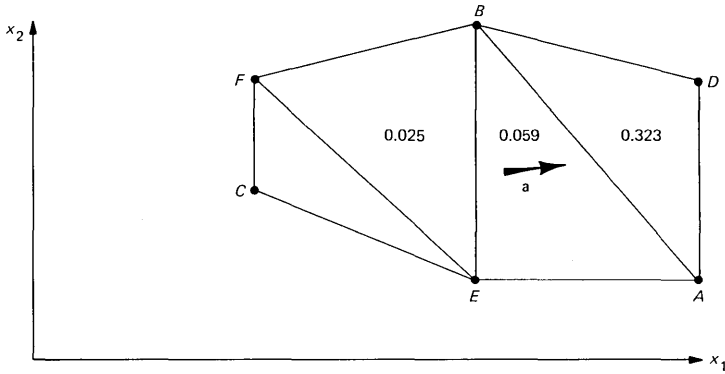
Fig. 9—Convexity of h.

and there was no trade-off between the two systems. When comparing systems of pyramids involving possibly dozens of pyramids each, and when each system contains both "good" and "bad" pyramids, individual assessments of pyramids must be combined into an overall measure to facilitate the comparison. A combined, global measure of the optimality of a system of pyramids is also necessary for the application of our procedure on a computer. We now derive such a metric under the principles discussed in Section VI.

Definition: Let $P = \{\mathbf{x}_1, \cdots, \mathbf{x}_{n+1}\} \subset \mathbf{R}^n$ be a pyramid with associated steepest ascent vector $\boldsymbol{\alpha}$. Let $\lambda_1 \geqq \cdots \geqq \lambda_n > 0$ be the eigenvalues derived from P as in Section VI, and let $\mathbf{v}_1, \cdots, \mathbf{v}_n$ be the corresponding eigenvectors. Define

$$m(P) = \frac{\sum\limits_{i=1}^{n} \lambda_i |\boldsymbol{\alpha}' \mathbf{v}_i|}{\sum\limits_{i=1}^{n} \lambda_i}.$$

In the above expression, $m(P)$ is intended to measure the departure of P from optimality. From the weighted-average form of its definition, it follows that a large value of $m(P)$ is caused by large values of $|\boldsymbol{\alpha}' \mathbf{v}_i|$ for the larger values of λ_i. Equivalently, it implies alignment of the major axes of P along $\boldsymbol{\alpha}$. An optimal P, of course, will do the opposite: As seen in Section VI, it will align its least-significant axes along $\boldsymbol{\alpha}$.

Definition: Let $\{P_1, \cdots, P_m\}$ be a system of pyramids. Let $\mathrm{Vol}(P_j)$ denote the volume of P_j. [Recall that $\mathrm{Vol}(\{\mathbf{x}_1, \cdots, \mathbf{x}_{n+1}\}) = \det(\{\mathbf{x}_1^*, \cdots, \mathbf{x}_{n+1}^*\})/n!$; see (Ref. 7, p. 331).] Define

$$M(\{P_1, \cdots, P_m\}) = \sum_{j=1}^{m} \mathrm{Vol}(P_j) m(P_j).$$

The expression $M(\{P_1, \cdots, P_m\})$ is the proposed overall metric of the departure of the system $\{P_1, \cdots, P_m\}$ from optimality. It sums the nonoptimality of each of its constituent pyramids, giving greater weight to the more voluminous pyramids. Note that it is not necessary to normalize M by the sum

$$\sum_{j=1}^{m} \text{Vol}(P_j),$$

since two comparable systems of pyramids will cover the same total volume.

Example: Applying the definitions above,

$$m(ADE) = (182.0*0.83 + 59.3*0.56)/(182.0 + 0.56) = 0.765,$$

$$\text{Vol}(ADE) = \det \begin{bmatrix} 60 & 60 & 40 \\ 7 & 25 & 7 \\ 1 & 1 & 1 \end{bmatrix} = 180.$$

$$m(BDE) = 0.695, \qquad \text{Vol}(BDE) = 230.$$

$$M(\{ADE, BDE\}) = 297.42;$$

$$m(ABD) = 0.269, \qquad \text{Vol}(ABD) = 180.$$

$$m(ABE) = 0.492, \qquad \text{Vol}(ABE) = 230.$$

$$M(\{ABD, ABE\}) = 161.85.$$

Since $M(\{ABD, ABE\}) < M(\{ADE, BDE\})$, our calculation with the metric M agrees with our earlier conclusion that $\{ABD, ABE\}$ is the preferred triangulation over $\{ADE, BDE\}$.

IX. BUILDING PYRAMIDS

One practical issue remains. In actual empirical studies, vertices become available one by one, and except when the first pyramid is formed, the pyramid building process is always applied to an existing system of pyramids. Especially in higher dimensions, we need an efficient and consistent method to incorporate new vertices into old systems of pyramids.

Example: Suppose the vertices A, B, C, D in our computer performance example have been satisfactorily triangulated, and E appears as a new vertex, as shown in Fig. 10. What new triangulations are generated so that they may be compared? If the new vertex is inside some triangle [e.g., $H = (55, 10)$ inside ABE], then an obvious reasonable answer exists (e.g., replace ABE by HBE, AHE, and ABH). In higher dimensions, the procedure is just as simple, so hereafter we will only consider new vertices not in the convex hull of the old vertices. We should specify that we start out with a minimal cover, that is, we start out
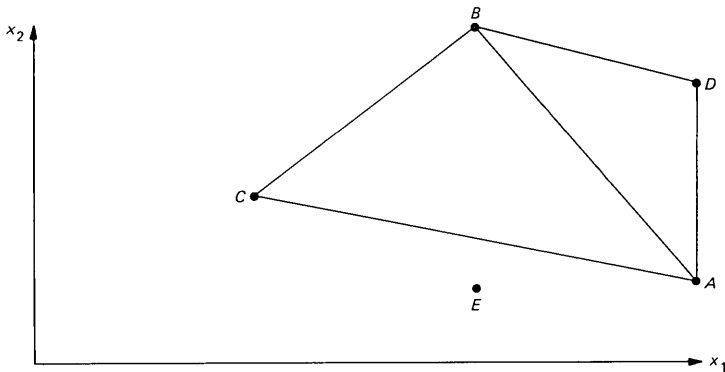
Fig. 10—Adding a new vertex to a system of pyramids.

from a system of pyramids containing the convex hull of the old points ("cover") in such a way that any point is in the interior of at most one pyramid ("minimal"). For example, if triangle BCD were added to the triangulation above, we would no longer have a minimal cover, since some points close to B would be inside two triangles. We would also like to end up with a minimal cover after incorporating the new point E. By going from minimal cover to minimal cover, the method we develop could be used again when a new vertex (e.g., F) comes around. For the sake of consistency, we do not want to add any pyramid implicitly rejected by the minimal cover we started out with, such as BCD. We call new covers satisfying this desideratum consistent. The appropriate building block for the new system of pyramids turns out to be faces.

Definition: Let $\{\mathbf{x}_1, \cdots, \mathbf{x}_K\} \subset \mathbf{R}^n$ be the set of vertices from the starting minimal cover, and let $\mathbf{p}$ be a point outside its convex hull. A new face is the convex hull of $\{\mathbf{p}, \mathbf{x}_{i_1}, \cdots, \mathbf{x}_{i_{n-1}}\}$ for any sequence $1 \leq i_1 < \cdots < i_{n-1} \leq K$ such that:

   (i) row rank of $(\mathbf{x}_{i_1} - \mathbf{p}, \cdots, \mathbf{x}_{i_{n-1}} - \mathbf{p}) = n - 1$, and
   (ii) no $\mathbf{x}_j$ $(j \neq i_1, \cdots, i_{n-1})$, is in the convex hull of $\{\mathbf{p}, \mathbf{x}_{i_1}, \cdots, \mathbf{x}_{i_{n-1}}\}$.

Condition (i) ensures that the new face does not collapse to some $<(n - 1)$ dimensional surface. It may be checked by counting the nonzero eigenvalues of the covariance matrix (see Section VI). Condition (ii) rules out pathologies such as face DE' in the two-dimensional case pictured in Fig. 11. (AE', of course, is legitimate.)

Proposition 5: Let F_0 be the set of old faces in the starting minimal cover, and N be the set of new faces. If S is any consistent minimal cover for the new convex hull whose set of faces is denoted by F, then

   (i) F is a subset of $F_0 \cup N$,

OLD VERTICES
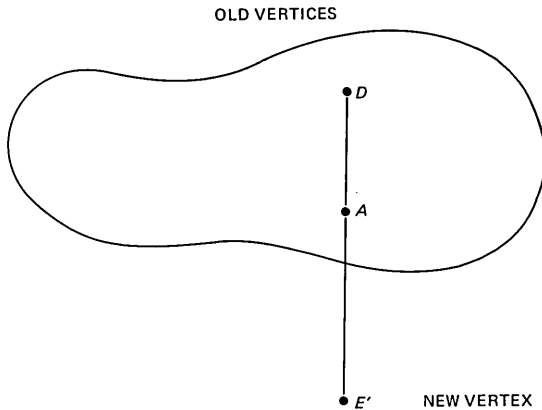
Fig. 11—The pathological triangle ADE'.

(ii) Any two faces from F do not intersect at interior points (though they may met at boundaries), and

(iii) F is a maximal set satisfying *(i)* and *(ii)*, i.e., any face not in F either is not in $F_0 \cup N$ or meets some face from F at interior points.

Proof: Check that the faces from any minimal cover must satisfy *(ii)*.

Thus, assuming that we can enumerate all sets of faces satisfying *(i)* through *(iii)*, we may proceed to reconstruct minimal covers from these sets, and Proposition 5 tells us that we would have captured all the consistent new minimal covers we want this way. Incidentally, Proposition 5 does not rule out the possibility that we may catch more than the new minimal covers or that some sets of faces may not be reconstructible into new minimal covers. These situations are dealt with by the converse to Proposition 5, which remains to be proven. Therefore, we should guard ourselves against the first possibility and not be surprised at the second.

The construction of all sets satisfying *(i)* to *(iii)* can be done neatly along a downward-growing binary tree whose branches enumerate the sets.

Example: Continuing the preceding example, it is clear that $F_0 = \{AB, AC, AD, BC, BD\}$ and $N = \{EA, EB, EC, ED\}$. Next, we list pairs of faces from $F_0 \cup N$ that meet at interior points in Table III. We now grow our tree. The trunk of our tree contains those faces meeting no others. Beyond that, we split the tree into two branches each time we choose between a face and any one of the faces it meets. We extend each branch as far as possible as long as it does not contain pairs of intersecting faces. At the end of each branch we reconstruct a new minimal cover from the faces listed on the branch; the result is displayed in Fig. 12. Thus, the leftmost branch $\{AD, BC, BD, EA, EC,$

Table III—Pairs of
intersecting faces for
typical problem

Face	Meets Face(s)
AB	ED
AC	EB, ED
AD	—
BC	—
BD	—
EA	—
EB	AC
EC	—
ED	AB, AC
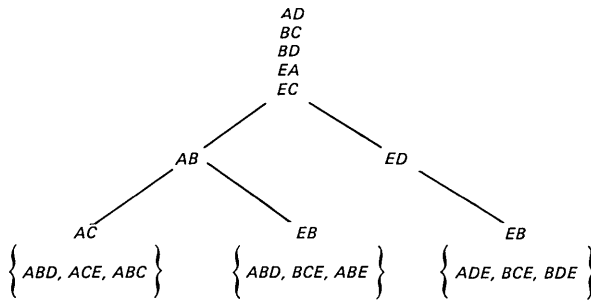
Fig. 12—Tree from new vertex E.

$AB, AC\}$ lists one of the possible sets of faces that contains as many faces as possible without including two that intersect at interior points. It is easy to see that the branch is an enumeration of all faces from the triangulation $\{ABD, ACE, ABC\}$. The other two branches are obtained similarly. Using the evaluation techniques from Sections V, VI, and VIII, the triangulation reconstructed from the faces listed in the middle branch was chosen.

The only step in this procedure, which is nontrivial in higher dimensions, is the tabulation of pairs of faces that intersect at interior points. Especially where there are many pairs of faces, making a pair-by-pair determination can be cumbersome.

Notation: Let $\mathbf{e}_i \in \mathbf{R}^n$ be the vector with 0 in every component except the ith, where it is 1.

Proposition 6: Let $F = \{\mathbf{x}_1, \cdots, \mathbf{x}_n\}$, $G = \{\mathbf{y}_1, \cdots, \mathbf{y}_n\} \subset \mathbf{R}^n$ be faces from $F_0 \cup N$. Choose any j such that $(\mathbf{x}_1 - \mathbf{x}_n, \cdots, \mathbf{x}_{n-1} - \mathbf{x}_n, \mathbf{e}_j)$ is invertible, and let

$$\mathbf{p}'(F) = \mathbf{e}'_n (\mathbf{x}_1 - \mathbf{x}_n, \cdots, \mathbf{x}_{n-1} - \mathbf{x}_n, \mathbf{e}_j)^{-1} \in \mathbf{R}^n.$$

(If F is a face, such j exists.) Similarly, define $\mathbf{p}'(G)$. Then F and G have empty interior intersections if and only if either

(i) $\mathbf{p}'(F)\mathbf{x}_1 < \min\{\mathbf{p}'(F)\mathbf{y}_1, \cdots, \mathbf{p}'(F)\mathbf{y}_n\}$ or $\mathbf{p}'(F)\mathbf{x}_1 > \max\{\mathbf{p}'(F)\mathbf{y}_1, \cdots, \mathbf{p}'(F)\mathbf{y}_n\}$, or

(ii) $\mathbf{p}'(G)\mathbf{y}_1 < \min\{\mathbf{p}'(G)\mathbf{x}_1, \cdots, \mathbf{p}'(G)\mathbf{x}_n\}$ or $\mathbf{p}'(G)\mathbf{y}_1 > \max\{\mathbf{p}'(G)\mathbf{x}_1, \cdots, \mathbf{p}'(G)\mathbf{x}_n\}$.

Proof: The clue is to recognize that $\mathbf{p}(F)$ is simply some vector perpendicular to F and $\mathbf{p}'(F)\mathbf{y}$ is the unscaled projection of $\mathbf{y}$ onto $\mathbf{p}(F)$. Clearly, two faces have disjoint interiors if and only if the two faces have disjoint projections along some direction perpendicular to one of them.

Example: We leave the response time function h so that we may illustrate application of Proposition 6 in three dimensions. We are given six vertices in $\mathbf{R}^3$, and we wish to determine how the 20 resulting faces intersect in pairs.

$$A = \begin{pmatrix} 20 \\ 1 \\ -1 \end{pmatrix} \quad B = \begin{pmatrix} 10 \\ 1 \\ -3 \end{pmatrix} \quad C = \begin{pmatrix} 10 \\ 2 \\ -2 \end{pmatrix}$$

$$D = \begin{pmatrix} 10 \\ 5 \\ -9 \end{pmatrix} \quad E = \begin{pmatrix} 10 \\ 6 \\ -4 \end{pmatrix} \quad F = \begin{pmatrix} 9 \\ 6 \\ -6 \end{pmatrix}.$$

Table IV contains the results of the calculations according to Proposition 6. The last column of the table, where filled, lists the pairs of faces with disjoint interiors that have been identified. There are five such pairs. For example, the first row shows, using a projection perpendicular to ABC, that ABC and DEF do not meet, since $30 < \min\{80, 60, 69\}$. Note that A, B, and C have the same projection, 30, since the projection is perpendicular to ABC. Note also that BCD and BCE yield the same rows on Table IV. This is because B, C, D, and E lie on the same plane. By Proposition 6, the five other pairs of faces must meet at interior points.

Because only six points were involved, each row in the table could only be used to separate two three-pointed faces. If more points were involved, more than one pair of faces could be found disjoint at once. For example, if we had two additional points G and H, and the first row read as in Table V, then the following pairs of faces may immediately be identified as disjoint:

$$ABC, DEF \quad ABH, DEF \quad AHC, DEF$$
$$ABC, EFG \quad ABH, EFG \quad AHC, EFG$$
$$ABC, DFG \quad ABH, DFG \quad AHC, DFG$$
$$ABC, DEG \quad ABH, DEG \quad AHC, DEG, \cdots$$

This method clearly beats having to test each pair separately.

Table IV—Determining how 20 faces meet in pairs

Face F	p'$(F)A$	p'$(F)B$	p'$(F)C$	p'$(F)D$	p'$(F)E$	p'$(F)F$	
ABC	30.0	30.0	30.0	80.0	60.0	69.0	*ABC, DEF*
ABD	17.5	17.5	5.0	17.5	−15.0	−6.0	*ABD, CEF*
ABE	24.0	24.0	18.0	50.0	24.0	33.0	
ABF	22.2	22.2	14.4	41.0	13.2	22.2	
ACD	30.0	5.0	30.0	30.0	85.0	6.9	
ACE	30.0	60.0	30.0	140.0	30.0	69.0	*ACE, BDF*
ACF	13.3	0.0	6.7	0.0	0.0	6.0	*ACF, BDE*
ADE	22.1	12.9	14.3	22.1	22.1	21.9	*ADE, BCF*
ADF	22.2	12.8	14.4	22.2	22.6	22.2	
AEF	22.2	13.2	14.4	23.0	22.2	22.2	
BCD	20.0	10.0	10.0	10.0	10.0	9.0	
BCE	20.0	10.0	10.0	10.0	10.0	9.0	
BCF	20.3	10.5	10.5	11.8	11.3	10.5	*ADE, BCF*
BDE	20.0	10.0	10.0	10.0	10.0	9.0	
BDF	20.1	9.7	10.2	9.7	11.1	9.7	*ACE, BDF*
BEF	20.4	11.4	10.8	14.0	11.4	11.4	
CDE	20.0	10.0	10.0	10.0	10.0	9.0	
CDF	20.3	9.9	10.5	10.5	11.9	10.5	
CEF	20.3	11.3	10.5	13.3	10.5	10.5	*ABD, CEF*
DEF	23.0	14.0	16.0	27.0	27.0	27.0	*ABC, DEF*

Table V—Separating many pairs of faces simultaneously

Face F	p'$(F)A$	p'$(F)B$	p'$(F)C$	p'$(F)D$	p'$(F)E$	p'$(F)F$	p'$(F)G$	p'$(F)H$
ABC	30	30	30	80	60	69	70	25
.								
.								
.								

X. RECAPITULATION

The cycle is now complete. We start out with some minimal cover—possibly consisting of a single pyramid—on the x-space of some function $y = f(\mathbf{x})$. The behavior of the function on the minimal cover may be explored by linear interpolation as discussed in Section II. If further information is subsequently found wanting, a new interpolant is chosen, and a new data point is empirically acquired. Using the technique from the preceding section, we are able to list *all* consistent ways to extend the starting minimal cover into a new minimal cover that incorporates the new interpolant. These new minimal covers should be evaluated both in terms of their faces and in terms of the axes of their pyramids. For either evaluation, the basic ingredient is the notion of steepest ascent. Through this notion the values of the function at the interpolants are taken into account. This distinguishes our approach from other schemes where only the x-space gets examined. Eventually, a best new minimal cover is chosen, and we are ready, once more, to interpolate and explore the function.

REFERENCES

1. R. A. Becker, and J. M. Chambers, "Design and Implementation of the *S* System for Interactive Data Analysis," Proc. Computer Software and Applications Chi-

cago, Illinois (November 13–16, 1978), pp. 626–9.
2. C. L. Lawson, "Generation of a Triangular Grid With Application to Contour Plotting," Tech. Memo. 299, Sect. 914, Jet Propulsion Lab., Calif. Inst. Tech. (February 1972).
3. H. A. Akima, "A Method of Bivariate Interpolation and Smooth Surface Fitting for Irregularly Distributed Data Points," ACM Trans. Math. Software, *4*, No. 2 (June 1978), pp. 148–59.
4. W. E. Milne et al., "Mathematics for Digital Computers," Vol. 1: Multivariate Interpolation, Wright Air Development Center Tech. Rep. 57–556, Aeronautical Research Laboratory (February 1958).
5. T. W. Anderson, *An Introduction of Multivariate Statistical Analysis*, New York: John Wiley, 1974.
6. G. E. P. Box, W. G. Hunter, and J. S. Hunter, *Statistics for Experimenters*: *An Introduction to Design, Data Analysis and Model Building*, New York: John Wiley, 1978.
7. G. Birkhoff and S. MacLane, *A Survey of Modern Algebra*, 4th ed., New York: McMillan Publishing Co., 1977.

A Traffic Overflow System With a Large Primary Queue

By J. A. MORRISON and P. E. WRIGHT*

(Manuscript received January 4, 1982)

We analyze a traffic overflow system that consists of two groups of trunks, with waiting spaces for each group, and some overflow capability from the primary to the secondary group. We consider the case in which the number of waiting spaces in the primary queue is large compared to the corresponding number in the secondary queue and to the number of trunks in the secondary group. The case of an infinite number of waiting spaces in the primary queue is also allowed. We contrast the approach presented with some previous approaches that are suitable when the number of waiting spaces in the primary queue is not comparatively large. As with previous approaches, the aim is to reduce the dimensions of the system of equations to be solved in order to calculate various steady-state quantities of interest. Our results include expressions for the loss probabilities, the probability of overflow from the primary to the secondary group, and the average waiting times in the queues. We also obtain the stability condition under which the results are valid when the number of waiting spaces in the primary queue is infinite.

I. INTRODUCTION

In this paper, a particular traffic overflow system with queueing is analyzed. The same system has been investigated previously where techniques were developed for reducing the dimensions of the system of equations to be solved in order to calculate various steady-state quantities of interest.[1,2] This analysis is a considerable improvement over the earlier study for the case when the number of waiting spaces in the primary queue is large compared to the corresponding number

---

in the secondary queue and to the number of secondary trunks.[1] A suitable analysis has already been made for the case when the number of waiting spaces in the secondary queue is large compared to the corresponding number in the primary queue and to the number of trunks in the two groups.[2]

In cases of interest, the sparse system of linear equations for determining the steady-state probabilities of the number of demands in the two groups may have very large dimensions. The reduced system of equations then has considerably fewer dimensions, but the system will be dense. Numerical results based on the solution of the original sparse system of equations by successive over-relaxation techniques, and on the solution of the reduced system of equations obtained earlier by Morrison,[1] were presented by Kaufman, Seery, and Morrison.[3] The numerical values of the various steady-state quantities of interest obtained by the two procedures agree to many significant figures. Other procedures for solving the original system of equations are discussed in Refs. 1 and 4.

The dimensions of the reduced system of equations obtained in this paper are independent of the number of waiting spaces in the primary queue. On the other hand, the dimensions of the reduced system of equations derived in Ref. 1 continue to increase as the number of waiting spaces in the primary queue increases. This is even more drastically the case for the original sparse system of equations. Consequently, the reduced system of equations that we derive is advantageous when the number of waiting spaces in the primary queue is large, and even more so when the number is infinite.

The traffic overflow system considered consists of two groups, a primary and a secondary, with $n_k > 0$ servers and q_k waiting spaces, which receive demands from independent Poisson sources S_k with arrival rates $\lambda_k > 0$, $k = 1$ and 2, respectively, as shown in Fig. 1. The service times of the demands are independent and exponentially distributed with mean service rate $\mu > 0$. If all n_2 servers in the secondary group are busy when a demand from S_2 arrives, the demand is queued if one of the q_2 waiting spaces is available; otherwise it is lost, that is, blocked and cleared from the system. Demands waiting in the secondary queue enter service, in some prescribed order, as servers in the secondary group become free.

If all n_1 servers in the primary group are busy when a demand from S_1 arrives, and there is a free server in the secondary group and no demands waiting in the secondary queue, the demand is served in the secondary. If there are no free servers, then the demand is queued in the primary queue, if one of the q_1 waiting spaces is available; otherwise it is lost. Previously, two different cases were considered for the treatment of demands waiting in the primary queue.[1,2] In case I, a
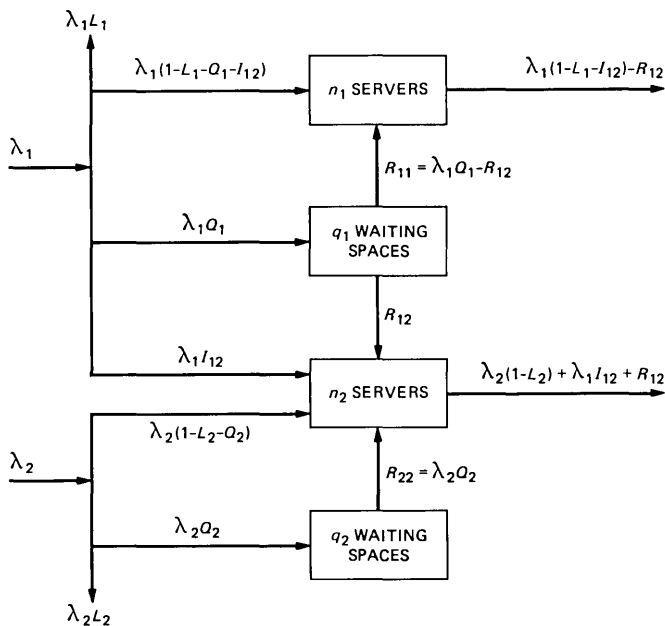
Fig. 1—Mean flow rates for an overflow system with queueing.

demand waiting in the primary queue may enter service either in the primary group, when a server becomes free, or in the secondary group, if a server becomes free and there are no demands waiting in the secondary queue. In case II, no overflow is permitted from the primary queue, so that a demand in the primary queue must wait for a server in the primary group to become free.

We consider only case I and use a different approach to analyze the overflow system. The new approach is preferable to the earlier approach[1] when q_1 is large compared to q_2 and n_2, or even infinite. The alternate earlier approach[2] is preferable when q_2 is large compared to q_1, n_1, and n_2, or even infinite.

Let p_{ij} denote the steady-state probability that there are i demands in the primary group and j demands in the secondary group, either in service or waiting. These probabilities satisfy a set of generalized birth-and-death equations, which take the form of partial difference equations connecting nearest neighboring states. The basic technique is to separate variables in regions away from certain boundaries of the state space, the elements of which are (i, j). These regions are shown in Fig. 2a. The analogous regions corresponding to the earlier analyses[1,2] are shown in Figs. 2b and 2c. The separation of variables leads to two sets of eigenvalue problems for the separation constant. The eigenvalues are roots of polynomial equations. The probabilities p_{ij} are then represented in terms of the corresponding eigenfunctions.
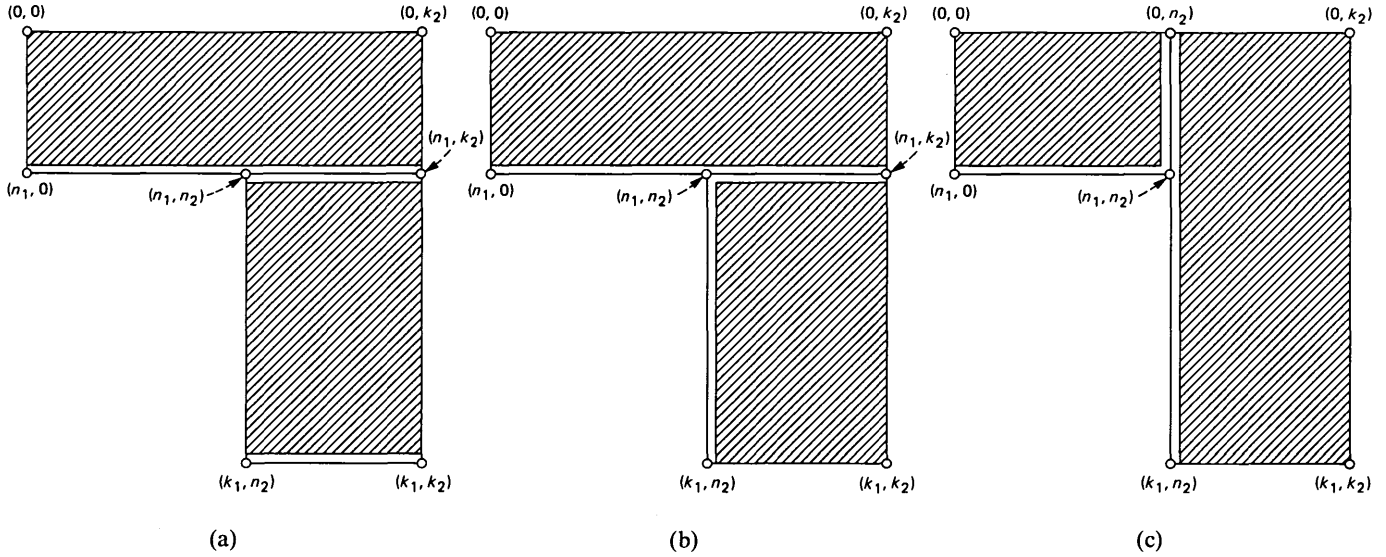
Fig. 2—Boundaries of regions in state space for the analysis of (a) this paper, and (b) and (c) the earlier papers.

The constant coefficients in these representations are determined from the boundary conditions and the normalization condition that the sum of the probabilities is unity. There are two sets of constants, corresponding to the representations of the probabilities p_{ij} in the two shaded regions in Fig. 2a. In general, these constants have to be evaluated numerically. However, we do show that the set of constants corresponding to the representation in the primary queueing region may be expressed explicitly in terms of the other set of constants. This further reduction leads to a problem of fewer dimensions than the one obtained in the first analysis,[1] regardless of the size of $q_1 > 0$.

Various steady-state quantities of interest may be expressed in terms of the probabilities p_{ij}. Among these are the loss (or blocking) probabilities, the probability of overflow from the primary to the secondary group, the probabilities that a demand is queued, and the average waiting times in the queues. These quantities may be expressed directly in terms of the constant coefficients occurring in the representations of the probabilities p_{ij}, averting the need to calculate the p_{ij}. This is a key advantage of the reduction in the dimensions of the problem.

The solution is built up in stages. In Section II, we consider solutions to the birth-and-death equations in the region $0 \le i \le n_1 - 1$, $0 \le j \le n_2 + q_2$ of state space. This corresponds to the case $q_1 = 0$, and was analyzed earlier as a special case.[1] Its inclusion here is for the sake of completeness. In Section III, we examine the solution in the region of state space corresponding to queueing in the primary, and give a heuristic derivation of the stability condition when $q_1 = \infty$. Section IV discusses the boundary and normalization conditions, while Section V is devoted to the calculation of various steady-state quantities of interest. In Section VI, we show how to achieve a further reduction in the dimensions of the problem by the introduction of a generating function. This reduction is obtained in another way in Section VII. Properties of the eigenfunctions that occur in the representations of the probabilities p_{ij} are given in Appendix A, the eigenvalues corresponding to the primary queueing region are discussed in Appendix B, and results pertaining to the generating function are derived in Appendix C.

II. REPRESENTATION OUTSIDE THE PRIMARY QUEUEING REGION

For convenience, we define

$$k_1 = n_1 + q_1, \qquad k_2 = n_2 + q_2. \tag{1}$$

Let p_{ij} ($0 \le i \le k_1$, $0 \le j \le k_2$) denote the steady-state probability that there are i demands in the primary, and j demands in the secondary. Define also the traffic intensities

$$a_1 = \lambda_1/\mu, \qquad a_2 = \lambda_2/\mu. \tag{2}$$

As usual, we let δ_{ij} denote the Kronecker delta, i.e.,

$$\delta_{ij} = \begin{cases} 1, & i = j, \\ 0, & i \neq j. \end{cases} \tag{3}$$

Finally, we introduce the function

$$\chi_l = \begin{cases} 1, & l \geq 0, \\ 0, & l < 0. \end{cases} \tag{4}$$

The probabilities p_{ij} satisfy a set of generalized birth-and-death equations. For case I, it may be shown[1] that

$$[a_1(1 - \delta_{ik_1}\chi_{j-n_2}) + a_2(1 - \delta_{jk_2}) + \min(i, n_1) + \min(j, n_2)]p_{ij}$$

$$= (1 - \chi_{i-n_1-1}\chi_{n_2-j-1})[a_1(1 - \delta_{i0})p_{i-1,j}$$

$$+ (1 - \delta_{jk_2})\min(j + 1, n_2)p_{i,j+1}] \tag{5}$$

$$+ (1 - \delta_{j0})[a_1\delta_{in_1}\chi_{n_2-j} + a_2(1 - \chi_{i-n_1-1}\chi_{n_2-j})]p_{i,j-1}$$

$$+ (1 - \delta_{ik_1})[(1 - \chi_{i-n_1}\chi_{n_2-j-1})\min(i + 1, n_1) + n_2\chi_{i-n_1}\delta_{jn_2}]p_{i+1,j},$$

for $0 \leq i \leq k_1$, $0 \leq j \leq k_2$. These equations were constructed to imply that

$$p_{ij} = 0, \, n_1 + 1 \leq i \leq k_1, \qquad 0 \leq j \leq n_2 - 1, \tag{6}$$

since there can be no queued demands in the primary when there is a free secondary server.

The normalization condition is

$$\sum_{i=0}^{n_1} \sum_{j=0}^{k_2} p_{ij} + \sum_{i=n_1+1}^{k_1} \sum_{j=n_2}^{k_2} p_{ij} = 1. \tag{7}$$

For $0 \leq i \leq n_1 - 1$ and $0 \leq j \leq k_2$, the variables in (5) may be separated,[1] and there are solutions of the form $\alpha_i\beta_j$, where

$$(a_1 + i + \rho)\alpha_i = a_1(1 - \delta_{i0})\alpha_{i-1} + (i + 1)\alpha_{i+1}, \tag{8}$$

for $0 \leq i \leq n_1 - 1$, and

$$[a_2(1 - \delta_{jk_2}) + \min(j, n_2) - \rho]\beta_j$$

$$= a_2(1 - \delta_{j0})\beta_{j-1} + (1 - \delta_{jk_2})\min(j + 1, n_2)\beta_{j+1}, \tag{9}$$

for $0 \leq j \leq k_2$, and ρ is a separation constant. The solution of (8) may be expressed in terms of Poisson-Charlier polynomials.[5,6] We denote here the solution of (8) for which $\alpha_0 = 1$ by $s_i(\rho, a_1)$. The properties of $s_i(\lambda, a)$ which we will need in the analysis are contained in Appendix A.

For $0 \leq j \leq n_2 - 1$, (9) becomes

$$(a_2 + j - \rho)\beta_j = a_2(1 - \delta_{j0})\beta_{j-1} + (j + 1)\beta_{j+1}, \tag{10}$$

and we see that there are solutions β_j proportional to $s_j(-\rho, a_2)$ for $0 \le j \le n_2$. For $n_2 \le j \le k_2$, we find that

$$[a_2(1 - \delta_{jk_2}) + n_2 - \rho]\beta_j = a_2\beta_{j-1} + n_2(1 - \delta_{jk_2})\beta_{j+1}. \tag{11}$$

To find a representation for solutions to (11), we define[1]

$$\Psi_l(\rho) = \left(\frac{n_2}{a_2}\right)^{l/2} U_l\left(\frac{a_2 + n_2 - \rho}{2\sqrt{a_2 n_2}}\right) \tag{12}$$

and

$$\phi_j(\rho) = \Psi_{k_2-j}(\rho) - \Psi_{k_2-j-1}(\rho), \tag{13}$$

where $U_l(x)$ denotes the lth Chebyshev polynomial of the second kind.[7] The properties of these functions are discussed in Appendix A. However, we note here that $U_0(x) \equiv 1$, $U_{-1}(x) \equiv 0$, and hence $\phi_{k_2}(\rho) \equiv 1$. From (11), and (134), it follows that β_j is proportional to $\phi_j(\rho)$ for $n_2 - 1 \le j \le k_2$.

Thus, as a basic solution to (9), we take

$$\beta_j = \begin{cases} s_j(-\rho, a_2)\phi_{n_2}(\rho), & 0 \le j \le n_2, \\ s_{n_2}(-\rho, a_2)\phi_j(\rho), & n_2 - 1 \le j \le k_2, \end{cases} \tag{14}$$

where

$$s_{n_2-1}(-\rho, a_2)\phi_{n_2}(\rho) = s_{n_2}(-\rho, a_2)\phi_{n_2-1}(\rho). \tag{15}$$

With the help of (13), (128), (129), and (133), (15) may be expressed in the form,

$$\rho[s_{n_2}(1 - \rho, a_2)\Psi_{q_2}(\rho) - s_{n_2-1}(1 - \rho, a_2)\Psi_{q_2-1}(\rho)] = 0. \tag{16}$$

The expression in the square brackets is a polynomial in ρ of degree k_2. It was shown[1] that its zeros are positive and distinct, and we denote them by ρ_m, $m = 1, 2, \cdots, k_2$. We adopt also the convention $\rho_0 = 0$. The calculation of the $\{\rho_m\}$ for $m > 0$ is related to an eigenvalue problem for a symmetric tridiagonal matrix.[1]

For the moment, we consider $q_1 = 0$, so that $k_1 = n_1$. This corresponds to the case of queueing in the secondary only, which has been analyzed as a special case.[1] In terms of the separated solutions to (5) for $0 \le i \le n_1 - 1$, a representation of the solution for $0 \le i \le n_1, 0 \le j \le k_2$ is

$$p_{ij} = \begin{cases} \displaystyle\sum_{m=0}^{k_2} d_m s_i(\rho_m, a_1)s_j(-\rho_m, a_2)\phi_{n_2}(\rho_m), & 0 \le j \le n_2, \\ \displaystyle\sum_{m=0}^{k_2} d_m s_i(\rho_m, a_1)s_{n_2}(-\rho_m, a_2)\phi_j(\rho_m), & n_2 \le j \le k_2. \end{cases} \tag{17}$$

The constants $\{d_m\}$ are determined only to within a multiplicative factor by the boundary conditions at $i = n_1$, $0 \leq j \leq k_2$, since the boundary condition at $j = n_2$ may be shown to be redundant.[1] The multiplicative factor is determined by the normalization condition (7). In general, the constants $\{d_m\}$ have to be calculated numerically.

For $q_1 > 0$, the representation (17) may still be used for $0 \leq i \leq n_1$, $0 \leq j \leq k_2$, but a different representation must be found for $n_1 + 1 \leq i \leq k_1$, $n_2 \leq j \leq k_2$. The earlier approach[1] was to find separated solutions to (5) in the region $n_1 + 1 \leq i \leq k_1$, $n_2 + 1 \leq j \leq k_2$, i.e., away from the boundary at $j = n_2$. This led to a representation of p_{ij} for $n_1 \leq i \leq k_1$, $n_2 \leq j \leq k_2$. Solutions were found that match those in (17) for $i = n_1$, $n_2 \leq j \leq k_2$, and an additional q_1 solutions were found that vanish at $i = n_1$. By the superposition of a suitable linear combination of these q_1 solutions, the boundary conditions at $j = n_2$, $n_1 + 1 \leq i \leq k_1$ could be satisfied, without disturbing the matching of the representations at $i = n_1$, $n_2 \leq j \leq k_2$. The constants $\{d_m\}$ are still available to satisfy the boundary conditions at $i = n_1$, $0 \leq j \leq k_2$, and again the condition at $j = n_2$ is redundant.

Since the number of additional constants to be determined in the above approach is q_1, this procedure is not suitable if q_1 is large. In the next section, we investigate an alternate approach that is suitable if q_1 is large or even infinite.

III. REPRESENTATION IN THE PRIMARY QUEUEING REGION

We now assume that $q_1 \geq 2$ and $q_2 \geq 1$, although these restrictions may be relaxed. For $n_1 + 1 \leq i \leq k_1 - 1$ and $n_2 \leq j \leq k_2$, the variables in (5) may be separated and there are solutions to the partial difference equations of the form

$$\sigma^{i-n_1} f_j, \qquad n_1 \leq i \leq k_1, \qquad n_2 \leq j \leq k_2,$$

where

$$\left[\left(n_1 - \frac{a_1}{\sigma} \right)(1 - \sigma) + a_2(1 - \delta_{jk_2}) + n_2(1 - \delta_{jn_2}\sigma) \right] f_j$$

$$= a_2(1 - \delta_{jn_2})f_{j-1} + n_2(1 - \delta_{jk_2})f_{j+1}, \qquad n_2 \leq j \leq k_2, \quad (18)$$

and σ is a separation constant. Since $a_1 \neq 0$, and we are interested in nontrivial solutions, $\sigma \neq 0$. In particular, for $n_2 + 1 \leq j \leq k_2$, we have

$$[a_2(1 - \delta_{jk_2}) + n_2 - \omega] f_j = a_2 f_{j-1} + n_2(1 - \delta_{jk_2})f_{j+1}, \qquad (19)$$

where

$$\omega = \left(\frac{a_1}{\sigma} - n_1 \right)(1 - \sigma). \qquad (20)$$

We see from (134) that a solution which satisfies the boundary condition at $j = k_2$ is

$$f_j = f_{k_2}\phi_j(\omega), \qquad n_2 \le j \le k_2, \tag{21}$$

with ϕ_j defined as in (13).

It remains to satisfy the boundary condition at $j = n_2$, namely,

$$[a_2 + n_2(1 - \sigma) - \omega]f_{n_2} = n_2 f_{n_2+1}. \tag{22}$$

With the help of (21) and (13), we obtain

$$n_2(1 - \sigma)\phi_{n_2}(\omega) + (a_2 - \omega)[\Psi_{q_2}(\omega) - \Psi_{q_2-1}(\omega)]$$
$$- n_2[\Psi_{q_2-1}(\omega) - \Psi_{q_2-2}(\omega)] = 0. \tag{23}$$

This reduces with the help of (20) and (133) to

$$(1 - \sigma)H(\sigma) = 0, \tag{24}$$

where

$$H(\sigma) = \left(n_1 - \frac{a_1}{\sigma}\right)\Psi_{q_2}(\omega) + n_2\phi_{n_2}(\omega), \tag{25}$$

with ω defined as in (20). Hence, $\sigma = 1$ or $H(\sigma) = 0$.

Now $\Psi_l(\omega)$ is a polynomial of degree l in ω. Hence, $\sigma^{q_2+1}H(\sigma)$ is a polynomial of degree $2q_2 + 1$ in σ, so that $H(\sigma) = 0$ has $2q_2 + 1$ roots. In Appendix B, we show that these roots are positive and distinct, and that at least q_2 of them lie between 0 and 1, and at least q_2 of them are greater than 1. More precisely, define

$$A_1 = n_1 + n_2\left[1 - \frac{\Psi_{q_2-1}(0)}{\Psi_{q_2}(0)}\right]. \tag{26}$$

Then, if $a_1 < A_1$, $q_2 + 1$ roots lie between 0 and 1, and q_2 roots exceed 1. If $a_1 > A_1$, then q_2 roots lie between 0 and 1, and $q_2 + 1$ roots exceed 1. Further, if $a_1 = A_1$, then $H(1) = 0$. We denote the roots of $H(\sigma) = 0$ by σ_r, $r = 1, \cdots, 2q_2 + 1$, with $0 < \sigma_1 < \cdots < \sigma_{2q_2+1}$. For convenience, we define $\sigma_0 = 1$. Then $\sigma_{q_2} < 1$ and $\sigma_{q_2+2} > 1$, and $\sigma_{q_2+1} < 1$ if $a_1 < A_1$, and $\sigma_{q_2+1} > 1$ if $a_1 > A_1$. Note that σ_r, $r = 0, \cdots, 2q_2 + 1$ are distinct if $a_1 \ne A_1$. On the other hand, $\sigma_0 = \sigma_{q_2+1}$ if $a_1 = A_1$.

For $q_1 < \infty$, we assume for simplicity that $a_1 \ne A_1$. We then have $2q_2 + 2$ distinct roots, and it follows that we may represent the probabilities in the form

$$p_{ij} = \sum_{r=0}^{2q_2+1} e_r \sigma_r^{i-n_1}\phi_j(\omega_r), \qquad n_1 \le i \le k_1, \qquad n_2 \le j \le k_2, \tag{27}$$

where

$$\omega_r = \left(\frac{a_1}{\sigma_r} - n_1\right)(1 - \sigma_r)$$

and the constants $\{e_r\}$ are to be determined. Consistency of the representations (27) and (17) at $i = n_1$ requires that

$$\sum_{r=0}^{2q_2+1} e_r\phi_j(\omega_r) = \sum_{m=0}^{k_2} d_m s_{n_1}(\rho_m, a_1)s_{n_2}(-\rho_m, a_2)\phi_j(\rho_m), \tag{28}$$

for $n_2 \le j \le k_2$.

For $q_1 = \infty$, we assume that $a_1 < A_1$; the reason for this will be apparent shortly. We use the representation (27), but the normalization condition (7) implies that $e_0 = 0$ and $e_r = 0$, $r = q_2 + 2, \cdots, 2q_2 + 1$ since $\sigma_0 = 1$ and $\sigma_r > 1$, $r = q_2 + 2, \cdots, 2q_2 + 1$. We thus have $q_2 + 1$ conditions to replace the $q_2 + 1$ boundary conditions lost on removal of the boundary at $i = k_1$. If $a_1 > A_1$, then $\sigma_{q_2+1} > 1$, and we would have to take $e_{q_2+1} = 0$ also. However, this would leave only q_2 constants e_r, $r = 1, \cdots, q_2$ to satisfy the $q_2 + 1$ conditions (28), which is insufficient.

The stability condition $a_1 < A_1$, for $q_1 = \infty$, may be derived heuristically as follows. Consider the situation when there are demands waiting in the primary queue. It follows that all n_2 servers in the secondary are busy. As the point of instability is reached, the primary queue will never be empty, and hence acts as an infinite source for the secondary servers. Demands from this source enter the secondary only when a server becomes available and there are no demands waiting in the secondary queue. Since the secondary system is a loss system, it is ergodic.

Let $P_j, j = n_2, \cdots, k_2$, be the steady-state probability that there are j demands in the secondary. Then the rate at which demands in the primary queue are served in the secondary is $n_2\mu P_{n_2}$, and the rate at which they are served in the primary is $n_1\mu$. Since $\lambda_1 = a_1\mu$, it follows that the stability condition is

$$a_1 < n_1 + n_2 P_{n_2}. \tag{29}$$

But, as for the system without the infinite source,[8]

$$P_j = \left(\frac{a_2}{n_2}\right)^{j-n_2} P_{n_2}, \qquad n_2 \le j \le k_2. \tag{30}$$

With the infinite source present, $P_j = 0, j = 0, \cdots, n_2 - 1$, and P_{n_2} is determined by

$$\sum_{j=n_2}^{k_2} P_j = 1. \tag{31}$$

From (30), (31), and (136), we obtain

$$P_{n_2} = \left[1 - \frac{\Psi_{q_2-1}(0)}{\Psi_{q_2}(0)} \right]. \tag{32}$$

From (26), (29), and (32), it follows that the stability condition for $q_1 = \infty$ is $a_1 < A_1$.

IV. BOUNDARY CONDITIONS

The constants $\{d_m\}$ and $\{e_r\}$ introduced in (17) and (27) must be chosen so as to satisfy the boundary conditions at $i = n_1$ and $i = k_1$. The boundary conditions at $i = k_1$ imply that

$$[a_2(1 - \delta_{jk_2}) + n_1 + n_2]p_{k_1,j}$$

$$= a_1 p_{k_1-1,j} + a_2(1 - \delta_{jn_2})p_{k_1,j-1} + n_2(1 - \delta_{jk_2})p_{k_1,j+1} \quad (33)$$

for $n_2 \leq j \leq k_2$. At $i = n_1$, we have

$$(a_1 + a_2 + n_1 + j)p_{n_1,j}$$

$$= a_1 p_{n_1-1,j} + (a_1 + a_2)(1 - \delta_{j0})p_{n_1,j-1} + (j + 1)p_{n_1,j+1} \quad (34)$$

for $0 \leq j \leq n_2 - 1$,

$$(a_1 + a_2 + n_1 + n_2)p_{n_1,n_2}$$

$$= a_1 p_{n_1-1,n_2} + (a_1 + a_2)p_{n_1,n_2-1} + n_2 p_{n_1,n_2+1} + (n_1 + n_2)p_{n_1+1,n_2}, \quad (35)$$

and

$$[a_1 + a_2(1 - \delta_{jk_2}) + n_1 + n_2]p_{n_1,j}$$

$$= a_1 p_{n_1-1,j} + a_2 p_{n_1,j-1} + n_1 p_{n_1+1,j} + n_2(1 - \delta_{jk_2})p_{n_1,j+1}, \quad (36)$$

for $n_2 + 1 \leq j \leq k_2$.

If we substitute (17) in (34), we find, on reduction with the help of (125), (128), and (129), that

$$\sum_{m=0}^{k_2} d_m \phi_{n_2}(\rho_m)[\rho_m s_{n_1}(1 + \rho_m, a_1)s_j(-\rho_m, a_2)$$

$$+ a_1 s_{n_1}(\rho_m, a_1)s_j(-1 - \rho_m, a_2)] = 0, \quad (37)$$

for $0 \leq j \leq n_2 - 1$. Similarly, if we substitute from (17) and (27), (36) implies, after reduction, that

$$\sum_{m=1}^{k_2} d_m \rho_m s_{n_1}(1 + \rho_m, a_1)s_{n_2}(-\rho_m, a_2)\phi_j(\rho_m)$$

$$- \sum_{r=0}^{2q_2+1} e_r(n_1\sigma_r - a_1)\phi_j(\omega_r) = 0, \quad (38)$$

for $n_2 + 1 \leq j \leq k_2$, and (33) implies, with the help of the fact that $f_j = \phi_j(\omega_r)$ satisfies (18) for $0 \leq r \leq 2q_2 + 1$, that

$$\sum_{r=0}^{2q_2+1} e_r \sigma_r^{q_1}[(n_1 + n_2\delta_{jn_2})\sigma_r - a_1]\phi_j(\omega_r) = 0, \tag{39}$$

for $n_2 \leq j \leq k_2$. Finally, (17), (27), (15), (125), (128), and (129) in (35) imply that

$$\sum_{m=0}^{k_2} d_m\phi_{n_2}(\rho_m)[\rho_m s_{n_1}(1 + \rho_m, a_1)s_{n_2}(-\rho_m, a_2)$$

$$+ a_1 s_{n_1}(\rho_m, a_1)s_{n_2}(-1 - \rho_m, a_2)]$$

$$- (n_1 + n_2)\sum_{r=0}^{2q_2+1} e_r \sigma_r \phi_{n_2}(\omega_r) = 0. \tag{40}$$

We will now show that the boundary condition at $i = n_1$, $j = n_2$ is redundant and may hence be dropped. Summing (39) from $j = n_2$ to k_2, we find that

$$\sum_{r=0}^{2q_2+1} e_r \sigma_r^{q_1}[(n_1\sigma_r - a_1)\Psi_{q_2}(\omega_r) + n_2\sigma_r\phi_{n_2}(\omega_r)] = 0. \tag{41}$$

For $r = 1, 2, \cdots, 2q_2 + 1$, it is true that

$$H(\sigma_r) \equiv \left(n_1 - \frac{a_1}{\sigma_r}\right)\Psi_{q_2}(\omega_r) + n_2\phi_{n_2}(\omega_r) = 0, \tag{42}$$

and $\sigma_0 = 1$ and $\omega_0 = 0$, so that (41) and (26) imply that

$$e_0(A_1 - a_1) = 0,$$

that is,

$$e_0 = 0, \tag{43}$$

since $a_1 \neq A_1$ by assumption. The redundancy of the boundary condition (40) may then be verified by summing (37) from $j = 0$ to $n_2 - 1$, (38) from $j = n_2 + 1$ to k_2, and (28) from $j = n_2$ to k_2, and by using the facts that ρ_m satisfies (16) for $m = 0, 1, 2, \cdots, k_2$, and $e_0 = 0$, together with the recurrence relations found in Appendix A.

Consider (39) for $j = n_2$. We note that $\phi_{n_2}(\omega_r)$ *is* nonzero; otherwise (22) with $f_j = \phi_j(\omega_r)$ would imply that $\phi_{n_2+1}(\omega_r) = 0$, and consequently that $\phi_j(\omega_r) \equiv 0$, in contradiction to the fact that $\phi_{k_2}(\omega_r) \equiv 1$. Further, since the roots of $H(\sigma)$ are distinct, it follows that not all of the square-bracketed terms are zero. Hence, the equation is nonvacuous. Since summation of (39) from $j = n_2$ to k_2 implies $e_0 = 0$, if we set $e_0 = 0$ in (38) and (39), then (39) for $j = n_2$ is redundant and accordingly may be dropped. We remark that even for $a_1 = A_1$, we are still free to take $e_0 = 0$ since $\sigma_{q_2+1} = 1$ in that case. As before, the boundary conditions

at $j = n_2$ $(i = n_1$ and $i = k_1)$ are redundant. Therefore, it follows that the constants $\{d_m\}$ and $\{e_r\}$ are determined by the boundary conditions at $i = n_1$ for $0 \le j \le n_2 - 1$ and $n_2 + 1 \le j \le k_2$, the consistency relationships at $i = n_1$, $n_2 \le j \le k_2$, the boundary conditions at $i = k_1$, $n_2 + 1 \le j \le k_2$ if q_1 is finite, and the normalization condition (7).

We summarize the results of the last three sections as follows:

$$p_{ij} = \left\{ \begin{array}{ll} \displaystyle\sum_{m=0}^{k_2} d_m s_i(\rho_m, a_1) s_j(-\rho_m, a_2)\phi_{n_2}(\rho_m), & 0 \le j \le n_2, \\[1.5em] \displaystyle\sum_{m=0}^{k_2} d_m s_i(\rho_m, a_1) s_{n_2}(-\rho_m, a_2)\phi_j(\rho_m), & n_2 \le j \le k_2, \end{array} \right. \tag{44}$$

for $0 \le i \le n_1$ and,

$$p_{ij} = \sum_{r=1}^{2q_2+1} e_r \sigma_r^{i-n_1}\phi_j(\omega_r), \qquad n_2 \le j \le k_2, \tag{45}$$

for $n_1 \le i \le k_1$, $(q_1 < \infty)$, where

$$\rho_m[s_{n_2}(1 - \rho_m, a_2)\Psi_{q_2}(\rho_m) - s_{n_2-1}(1 - \rho_m, a_2)\Psi_{q_2-1}(\rho_m)] = 0, \tag{46}$$

for $m = 0, 1, 2, \cdots, k_2$ and

$$H(\sigma_r) = 0, \qquad r = 1, 2, 3, \cdots, 2q_2 + 1 \tag{47}$$

with $\omega_r \equiv \left(\dfrac{a_1}{\sigma_r} - n_1 \right)(1 - \sigma_r)$.

The $k_2 + 2q_2 + 2$ constants $\{d_m\}$ and $\{e_r\}$ are determined, with $e_0 = 0$, by (28) and (37) to (39) only to within a multiplicative constant, which is determined by the normalization condition. From (44), (46), (13), (130), it follows that

$$\sum_{j=0}^{k_2} p_{ij} = d_0 s_i(0, a_1)[s_{n_2}(1, a_2)\Psi_{q_2}(0) - s_{n_2-1}(1, a_2)\Psi_{q_2-1}(0)], \tag{48}$$

for $0 \le i \le n_1$, so that (7), (13), (45), and (130) imply that

$$d_0 s_{n_1}(1, a_1)[s_{n_2}(1, a_2)\Psi_{q_2}(0) - s_{n_2-1}(1, a_2)\Psi_{q_2-1}(0)]$$
$$+ \sum_{r=1}^{2q_2+1} e_r\Gamma_{q_1}(\sigma_r)\Psi_{q_2}(\omega_r) = 1, \tag{49}$$

where

$$\Gamma_q(\xi) = \sum_{l=0}^{q-1} \xi^{q-l} = \left\{ \begin{array}{ll} \xi(1 - \xi^q)/(1 - \xi), & \xi \ne 1, \\ q, & \xi = 1. \end{array} \right. \tag{50}$$

We point out that the special case $q_1 \ge 1$, $q_2 = 0$ has previously been analyzed.[1] In the primary queue region, solutions of the form

$$p_{i,n_2} = \left(\frac{a_1}{n_1 + n_2} \right)^{i-n_1} p_{n_1,n_2}, \qquad n_1 \le i \le k_1, \tag{51}$$

where

$$p_{n_1,n_2} = \sum_{m=0}^{k_2} d_m s_{n_1}(\rho_m, a_1) s_{n_2}(-\rho_m, a_2) \phi_{n_2}(\rho_m), \tag{52}$$

were found. We note that since $k_2 = n_2$ for $q_2 = 0$, $\phi_{n_2}(\rho) = \phi_{k_2}(\rho) \equiv 1$, above. For $q_1 = \infty$, the stability condition was found to be $a_1 < n_1 + n_2$. It is readily verified that the representations (44) and (45), and the stability condition $a_1 < A_1$, produce the same result.

For $q_1 = \infty$ and $q_2 \geq 1$, we must set $e_r = 0$ for $r = q_2 + 2, \cdots,$ $2q_2 + 1$, as well as $e_0 = 0$, as discussed in Section III. The remaining $k_2 + q_2 + 2$ constants $\{d_m\}$ and $\{e_r\}$ are then determined by (28), (37), and (38) to within a multiplicative constant, which is determined by the normalization condition. But, from (50),

$$\Gamma_\infty(\xi) \equiv \lim_{q_1 \to \infty} \Gamma_{q_1}(\xi) = \frac{\xi}{(1 - \xi)}, \qquad 0 \leq \xi < 1. \tag{53}$$

Hence, for $q_1 = \infty$, the normalization condition (49) is

$$d_0 s_{n_1}(1, a_1)[s_{n_2}(1, a_2)\Psi_{q_2}(0) - s_{n_2-1}(1, a_2)\Psi_{q_2-1}(0)]$$

$$+ \sum_{r=0}^{q_2+1} \frac{e_r \sigma_r}{(1 - \sigma_r)} \Psi_{q_2}(\omega_r) = 1. \tag{54}$$

V. SOME STEADY-STATE QUANTITIES

We now proceed with the calculation of various steady-state quantities of interest. These quantities are shown in Fig. 1, which depicts mean flow rates. The loss probabilities are, for the primary and secondary, respectively,

$$L_1 = \sum_{j=n_2}^{k_2} p_{k_1,j}, \qquad L_2 = \sum_{i=0}^{k_1} p_{i,k_2}, \tag{55}$$

while the probabilities that a demand from the primary, or secondary, source is queued on arrival are

$$Q_1 = \sum_{i=n_1}^{k_1-1} \sum_{j=n_2}^{k_2} p_{ij}, \, (q_1 \geq 1), \qquad Q_2 = \sum_{i=0}^{k_1} \sum_{j=n_2}^{k_2-1} p_{ij}, \, (q_2 \geq 1). \tag{56}$$

The probability that a demand arriving from the primary source overflows immediately is

$$I_{12} = \sum_{j=0}^{n_2-1} p_{n_1,j}. \tag{57}$$

Since the mean service rate is μ for each server, the mean departure rate from the primary queue to the primary servers is

$$R_{11} = n_1\mu \sum_{i=n_1+1}^{k_1} \sum_{j=n_2}^{k_2} p_{ij}, \qquad (q_1 \geq 1), \tag{58}$$

while the mean departure rate from the secondary queue is

$$R_{22} = n_2\mu \sum_{i=0}^{k_1} \sum_{j=n_2+1}^{k_2} p_{ij}, \qquad (q_2 \geq 1). \tag{59}$$

The mean rate at which queued demands in the primary overflow to the secondary servers is

$$R_{12} = n_2\mu \sum_{i=n_1+1}^{k_1} p_{i,n_2}, \qquad (q_1 \geq 1). \tag{60}$$

The average queue populations are, for the primary and secondary, respectively,

$$V_1 = \sum_{i=n_1+1}^{k_1} \sum_{j=n_2}^{k_2} (i - n_1)p_{ij}, \qquad (q_1 \geq 1), \tag{61}$$

and

$$V_2 = \sum_{i=0}^{k_1} \sum_{j=n_2+1}^{k_2} (j - n_2)p_{ij}, \qquad (q_2 \geq 1). \tag{62}$$

Also, the average number of demands in service in the two groups are

$$X_1 = \sum_{i=0}^{n_1} \sum_{j=0}^{k_2} ip_{ij} + n_1(1 - \delta_{q_1,0}) \sum_{i=n_1+1}^{k_1} \sum_{j=n_2}^{k_2} p_{ij}, \tag{63}$$

and

$$X_2 = \sum_{i=0}^{n_1} \sum_{j=0}^{n_2-1} jp_{ij} + n_2 \sum_{i=0}^{k_1} \sum_{j=n_2}^{k_2} p_{ij}. \tag{64}$$

An application of Little's theorem[8] to the primary and secondary queues shows that the average waiting times of the queued demands in the primary and secondary are given by

$$W_1 = \frac{V_1}{\lambda_1 Q_1}, \, (q_1 \geq 1), \qquad W_2 = \frac{V_2}{\lambda_2 Q_2}, \, (q_2 \geq 1), \tag{65}$$

respectively, independently of the service order within each queue. Also, if we apply Little's theorem to the primary and secondary groups of servers, we obtain

$$\lambda_1(1 - L_1 - I_{12}) - R_{12} = \mu X_1, \quad \lambda_2(1 - L_2) + \lambda_1 I_{12} + R_{12} = \mu X_2, \tag{66}$$

since the mean service rate is μ.

The steady-state quantities of interest may be expressed directly in terms of the constants $\{d_m\}$ and $\{e_r\}$, with the help of the representations (44) and (45). From (55), with the help of (13), we find that

$$L_1 = \sum_{r=1}^{2q_2+1} e_r\sigma_r^{q_1}\Psi_{q_2}(\omega_r), \tag{67}$$

and with the help of (130) and the fact that $\phi_{k_2}(\rho) \equiv 1$, we find that

$$L_2 = \sum_{m=0}^{k_2} d_m s_{n_1}(1 + \rho_m, a_1) s_{n_2}(-\rho_m, a_2) + \sum_{r=1}^{2q_2+1} e_r \Gamma_{q_1}(\sigma_r), \qquad (68)$$

where $\Gamma_q(\xi)$ is as defined in (50). Similarly, it follows from (57) and (130) that

$$I_{12} = \sum_{m=0}^{k_2} d_m s_{n_1}(\rho_m, a_1) s_{n_2-1}(1 - \rho_m, a_2) \phi_{n_2}(\rho_m). \qquad (69)$$

Next, we find from (56), (50), and (13) that

$$Q_1 = \sum_{r=1}^{2q_2+1} \left(\frac{e_r}{\sigma_r}\right) \Gamma_{q_1}(\sigma_r) \Psi_{q_2}(\omega_r). \qquad (70)$$

Also, (58), (50), and (13) imply that

$$R_{11} = n_1 \mu \sum_{r=1}^{2q_2+1} e_r \Gamma_{q_1}(\sigma_r) \Psi_{q_2}(\omega_r), \qquad (71)$$

while from (60) and (50) it follows that

$$R_{12} = n_2 \mu \sum_{r=1}^{2q_2+1} e_r \Gamma_{q_1}(\sigma_r) \phi_{n_2}(\omega_r). \qquad (72)$$

It may be shown directly from (5) that

$$R_{11} + R_{12} = \lambda_1 Q_1, \qquad (73)$$

and, using (42), it is readily verified that this is consistent with the representations (70) to (72).

At this point, we define

$$r_j = \sum_{i=0}^{k_1} p_{ij}, \qquad n_2 \leq j \leq k_2. \qquad (74)$$

If we sum on i in (5), we obtain

$$[a_2(1 - \delta_{jk_2}) + n_2] r_j = a_2 r_{j-1} + n_2(1 - \delta_{jk_2}) r_{j+1}, \qquad (75)$$

for $n_2 + 1 \leq j \leq k_2$. It follows that

$$n_2 r_j = a_2 r_{j-1}, \qquad n_2 + 1 \leq j \leq k_2. \qquad (76)$$

Hence, since $L_2 = r_{k_2}$, from (55) and (74), we find that

$$r_j = \left(\frac{n_2}{a_2}\right)^{k_2-j} L_2, \qquad n_2 \leq j \leq k_2. \qquad (77)$$

Then, it follows from (50) and (59) that

$$R_{22} = \lambda_2 \Gamma_{q_2}\left(\frac{n_2}{a_2}\right) L_2. \qquad (78)$$

Also, from (56) and (77), we deduce that

$$Q_2 = \Gamma_{q_2}\left(\frac{n_2}{a_2}\right)L_2. \tag{79}$$

These representations satisfy $R_{22} = \lambda_2 \dot{Q}_2$. We remark that this latter result, as well as (73), hold since, in the steady state, the average arrival and departure rates are equal, for both the primary and secondary queues.

From (61) and (13), we find that

$$V_1 = \sum_{r=1}^{2q_2+1} e_r \Lambda_{q_1}(\sigma_r)\Psi_{q_2}(\omega_r), \tag{80}$$

where

$$\Lambda_q(\xi) = \sum_{l=1}^{q} l\xi^l = \begin{cases} \xi[1 - (q+1)\xi^q + q\xi^{q+1}]/(1-\xi)^2, & \xi \neq 1, \\ \tfrac{1}{2}q(q+1), & \xi = 1. \end{cases} \tag{81}$$

We note in passing that

$$\Gamma_q(\xi) = q\xi^{q+1} + (1-\xi)\Lambda_q(\xi), \tag{82}$$

a formula that may be numerically useful. From (62), (74), (77), and (81), it follows that

$$V_2 = \left(\frac{n_2}{a_2}\right)^{q_2} \Lambda_{q_2}\left(\frac{a_2}{n_2}\right)L_2. \tag{83}$$

Finally, from (63), with the help of (7), (48), and (131), we find that

$$X_1 = n_1 - d_0 s_{n_1-1}(2, a_1)[s_{n_2}(1, a_2)\Psi_{q_2}(0) - s_{n_2-1}(1, a_2)\Psi_{q_2-1}(0)], \tag{84}$$

and, from (64), with the help of (7), (17), (130), and (131),

$$X_2 = n_2 - \sum_{m=0}^{k_2} d_m s_{n_1}(1 + \rho_m, a_1)s_{n_2-1}(2 - \rho_m, a_2)\phi_{n_2}(\rho_m). \tag{85}$$

We remark that in view of (67) to (69), (72), (84), and (85), the relations presented in (66) provide a useful numerical check.

We point out that the results of this section up to this point are valid for $q_1 < \infty$. We recall that for $q_1 = \infty$, $e_r = 0$ for $r = q_2 + 2, \cdots$, $2q_2 + 1$, since $\sigma_r > 1$ for these values of r. In addition, the stability condition $a_1 < A_1$, with A_1 defined in (26), is necessary. Under these assumptions, since $0 < \sigma_r < 1$ for $r = 1, \cdots, q_2 + 1$, we find, analogously to (67), that

$$L_1|_{q_1=\infty} = 0, \tag{86}$$

as expected. Also, with the help of (53), we obtain, analogously to (68) and (70) to (72),

$$L_2\big|_{q_1=\infty} = \sum_{m=0}^{k_2} d_m s_{n_1}(1+\rho_m, a_1)s_{n_2}(-\rho_m, a_2) + \sum_{r=1}^{q_2+1} \frac{e_r \sigma_r}{(1-\sigma_r)}, \quad (87)$$

and

$$Q_1\big|_{q_1=\infty} = \sum_{r=1}^{q_2+1} \frac{e_r}{(1-\sigma_r)} \Psi_{q_2}(\omega_r), \quad (88)$$

$$R_{11}\big|_{q_1=\infty} = n_1\mu \sum_{r=1}^{q_2+1} \frac{e_r \sigma_r}{(1-\sigma_r)} \Psi_{q_2}(\omega_r), \quad (89)$$

and

$$R_{12}\big|_{q_1=\infty} = n_2\mu \sum_{r=1}^{q_2+1} \frac{e_r \sigma_r}{(1-\sigma_r)} \phi_{n_2}(\omega_r). \quad (90)$$

Similarly, from (81), we have

$$\Lambda_\infty(\xi) = \lim_{q_1\to\infty} \Lambda_{q_1}(\xi) = \frac{\xi}{(1-\xi)^2}, \quad 0 < \xi < 1. \quad (91)$$

Hence, corresponding to (80), we obtain

$$V_1\big|_{q_1=\infty} = \sum_{r=1}^{q_2+1} \frac{e_r \sigma_r}{(1-\sigma_r)^2} \Psi_{q_2}(\omega_r). \quad (92)$$

The expressions for I_{12}, R_{22}, Q_2, V_2, X_1, and X_2, given by (69), (78), (79), and (83) to (85), still hold. Of course, the constants $\{d_m\}$ and $\{e_m\}$, which occur in these expressions, (87) to (90) and (92), are those pertaining to $q_1 = \infty$, and are determined in the manner discussed at the end of Section IV.

VI. ELIMINATION OF ONE SET OF CONSTANTS

We will now show how to determine the constants $\{e_r\}$ in the representation (27) of the probabilities p_{ij} for $n_1 \le i \le k_1$, $n_2 \le j \le k_2$, in terms of the constants $\{d_m\}$ in the representation (17) of the probabilities p_{ij} for $0 \le i \le n_1$, $0 \le j \le k_2$. For $n_1 \le i < k_1$, $n_2 \le j \le k_2$ we have, from (5),

$$[a_1 + a_2(1 - \delta_{jk_2}) + n_1 + n_2]p_{ij}$$

$$= a_1 p_{i-1,j} + [(a_1 + a_2)\delta_{in_1}\delta_{jn_2} + a_2(1 - \delta_{jn_2})]p_{i,j-1}$$

$$+ (n_1 + n_2\delta_{jn_2})p_{i+1,j} + n_2(1 - \delta_{jk_2})p_{i,j+1}. \quad (93)$$

We consider this equation for $n_1 \le i < \infty$, and introduce the generating function

$$G_j(z) = \sum_{i=n_1}^{\infty} p_{ij}z^{i-n_1}. \quad (94)$$

The series will be convergent for sufficiently small $|z|$.

We consider $z \neq 0$ and define

$$\zeta = (1 - z)\left(\frac{n_1}{z} - a_1\right). \tag{95}$$

Then, from (93) to (95), it follows that

$$\left[a_2(1 - \delta_{jk_2}) + n_2\left(1 - \frac{1}{z}\delta_{jn_2}\right) - \zeta\right]G_j(z)$$

$$- a_2(1 - \delta_{jn_2})G_{j-1}(z) - n_2(1 - \delta_{jk_2})G_{j+1}(z)$$

$$= a_1 p_{n_1-1,j} + (a_1 + a_2)\delta_{jn_2}p_{n_1,j-1} - \frac{1}{z}(n_1 + n_2\delta_{jn_2})p_{n_1,j}, \quad (96)$$

for $n_2 \leq j \leq k_2$. We now define $G_j^{(l)}(z)$ for $n_2 \leq l \leq k_2$ as the solutions of the equations

$$\left[a_2(1 - \delta_{jk_2}) + n_2\left(1 - \frac{1}{z}\delta_{jn_2}\right) - \zeta\right]G_j^{(l)}(z)$$

$$- a_2(1 - \delta_{jn_2})G_{j-1}^{(l)}(z) - n_2(1 - \delta_{jk_2})G_{j+1}^{(l)}(z) = -\frac{1}{z}\delta_{jl}, \quad (97)$$

for $n_2 \leq j \leq k_2$. Then, from (96) and (97), we have

$$G_j(z) = \sum_{l=n_2}^{k_2}(n_1 p_{n_1,l} - a_1 z p_{n_1-1,l})G_j^{(l)}(z)$$

$$+ [n_2 p_{n_1,n_2} - (a_1 + a_2)z p_{n_1,n_2-1}]G_j^{(n_2)}(z). \quad (98)$$

We define

$$\Upsilon_j(z) = \left(\frac{a_2}{n_2}\right)^{j-n_2}\left[\Psi_{j-n_2}(\zeta) - \frac{n_2}{a_2 z}\Psi_{j-n_2-1}(\zeta)\right], \tag{99}$$

where $\Psi_l(\rho)$ is as defined in (12). It is shown in Appendix C that the solution of (97) is

$$G_j^{(l)}(z) = \begin{cases} \left(\dfrac{n_2}{a_2}\right)^{l-n_2} \dfrac{\phi_l(\zeta)\Upsilon_j(z)}{(1-z)H(1/z)}, & n_2 \leq j \leq l, \\[3mm] \left(\dfrac{n_2}{a_2}\right)^{l-n_2} \dfrac{\Upsilon_l(z)\phi_j(\zeta)}{(1-z)H(1/z)}, & l \leq j \leq k_2, \end{cases} \tag{100}$$

for $n_2 \leq l \leq k_2$, where $\phi_j(\rho)$ and $H(\sigma)$ are as defined in (13) and (25), respectively, with ω as defined in (20). We know that $H(\sigma_r) = 0$, $r = 1, \cdots, 2q_2 + 1$, with $0 < \sigma_1 < \cdots < \sigma_{2q_2+1}$. As discussed in Section III, $\sigma_{q_2} < 1$, $\sigma_{q_2+2} > 1$, and $\sigma_{q_2+1} < 1$ if $a_1 < A_1$, and $\sigma_{q_2+1} > 1$ if $a_1 > A_1$, where A_1 is given by (26). We assume that $a_1 \neq A_1$, so that $\sigma_{q_2+1} \neq 1$.

Now, from (12), (13), (20), (25), (95), and (99), $z^{q_2}H(1/z)$, $z^{k_2-j}\phi_j(\zeta)$ and $z^{j-n_2}\Upsilon_j(z)$ are polynomials in z of degrees $2q_2 + 1$, $2(k_2 - j)$ and

$2(j - n_2)$, respectively. It follows from (100) that $zG_j^{(l)}(z) \to 0$ as $z \to \infty$, for $n_2 \le j \le k_2$, $n_2 \le l \le k_2$. Hence, from (98), we have $G_j(z) \to 0$ as $z \to \infty$, for $n_2 \le j \le k_2$. It follows that we may expand $G_j(z)$ in partial fractions in the form

$$G_j(z) = \sum_{r=0}^{2q_2+1} \frac{g_{jr}}{(z - 1/\sigma_r)}, \qquad n_2 \le j \le k_2, \tag{101}$$

where $\sigma_0 = 1$, and

$$g_{jr} = \lim_{z \to 1/\sigma_r} [(z - 1/\sigma_r)G_j(z)]. \tag{102}$$

From (93), for $n_1 \le i < k_1$, (94), and (101), we deduce that

$$p_{ij} = - \sum_{r=0}^{2q_2+1} \sigma_r^{i+1-n_1} g_{jr}, \qquad n_1 \le i \le k_1, \qquad n_2 \le j \le k_2. \tag{103}$$

We proceed with the explicit calculation of g_{jr}. Let

$$g_{jr}^{(l)} = \lim_{z \to 1/\sigma_r} [(z - 1/\sigma_r)G_j^{(l)}(z)]. \tag{104}$$

Then, from (98), (102), and (104), we obtain

$$\sigma_r g_{jr} = \sum_{l=n_2}^{k_2} (n_1 \sigma_r p_{n_1,l} - a_1 p_{n_1-1,l}) g_{jr}^{(l)}$$

$$+ [n_2 \sigma_r p_{n_1,n_2} - (a_1 + a_2) p_{n_1,n_2-1}] g_{jr}^{(n_2)}. \tag{105}$$

As we noted in Section IV, $\phi_{n_2}(\omega_r) \ne 0$. It is shown in Appendix C that

$$\Upsilon_j(1/\sigma_r) = \frac{\phi_j(\omega_r)}{\phi_{n_2}(\omega_r)}, \qquad n_2 \le j \le k_2, \tag{106}$$

with ω_r given by (47). Hence, from (100), (104), and (106), since $\sigma_0 = 1$, we obtain

$$g_{j0}^{(l)} = - \left(\frac{n_2}{a_2} \right)^{l-n_2} \frac{\phi_l(0)\phi_j(0)}{\phi_{n_2}(0)H(1)} = - \frac{\phi_j(0)}{H(1)} \tag{107}$$

from (137). We note that $H(1) \ne 0$, since we have assumed that $a_1 \ne A_1$. We also obtain

$$g_{jr}^{(l)} = \left(\frac{n_2}{a_2} \right)^{l-n_2} \frac{\phi_l(\omega_r)\phi_j(\omega_r)}{\sigma_r(1 - \sigma_r)H'(\sigma_r)\phi_{n_2}(\omega_r)}, \qquad r = 1, \cdots, 2q_2 + 1, \tag{108}$$

where the prime denotes derivative.

From (27), (103), (105), and (107), since $\sigma_0 = 1$, it follows that

$$H(1)e_0 = \sum_{l=n_2}^{k_2} (n_1 p_{n_1,l} - a_1 p_{n_1-1,l}) + n_2 p_{n_1,n_2} - (a_1 + a_2) p_{n_1,n_2-1}. \tag{109}$$

If we substitute for $p_{n_1,l}$ and $p_{n_1-1,l}$, $n_2 \le l \le k_2$, and p_{n_1,n_2-1} from (17), and sum on l, and use (13) and (128), we obtain

$$H(1)e_0 = \sum_{m=0}^{k_2} d_m [\rho_m s_{n_1-1}(1 + \rho_m, a_1) s_{n_2}(-\rho_m, a_2) \Psi_{q_2}(\rho_m)$$

$$+ n_2 s_{n_1}(\rho_m, a_1) s_{n_2}(-\rho_m, a_2) \phi_{n_2}(\rho_m)$$

$$- (a_1 + a_2) s_{n_1}(\rho_m, a_1) s_{n_2-1}(-\rho_m, a_2) \phi_{n_2}(\rho_m)]. \quad (110)$$

After reduction with the help of (46) and some recurrence relations, we deduce from (110) that

$$H(1)e_0 = - \sum_{m=0}^{k_2} d_m \phi_{n_2}(\rho_m)[\rho_m s_{n_1}(1 + \rho_m, a_1) s_{n_2-1}(1 - \rho_m, a_2)$$

$$+ a_1 s_{n_1}(\rho_m, a_1) s_{n_2-1}(-\rho_m, a_2)]. \quad (111)$$

But, summation of (37) from $j = 0$ to $n_2 - 1$ shows that the term on the right-hand side of (111) is zero, so that

$$H(1)e_0 = 0. \quad (112)$$

Since $H(1) \ne 0$ for $a_1 \ne A_1$, it follows that $e_0 = 0$, as was shown in Section IV.

Next, from (27), (103), (105), and (108), we deduce that

$$\sigma_r(1 - \sigma_r)H'(\sigma_r)\phi_{n_2}(\omega_r)e_r$$

$$= \sum_{l=n_2}^{k_2} (a_1 p_{n_1-1,l} - n_1 \sigma_r p_{n_1,l})\left(\frac{n_2}{a_2}\right)^{l-n_2} \phi_l(\omega_r)$$

$$+ [(a_1 + a_2)p_{n_1,n_2-1} - n_2 \sigma_r p_{n_1,n_2}]\phi_{n_2}(\omega_r), \quad (113)$$

for $r = 1, \cdots, 2q_2 + 1$. If we substitute for $p_{n_1,l}$ and $p_{n_1-1,l}$, $n_2 \le l \le k_2$, and p_{n_1,n_2-1} from (17), we obtain

$$\sigma_r(1 - \sigma_r)H'(\sigma_r)e_r = \sum_{m=0}^{k_2} d_m [a_1 s_{n_1-1}(\rho_m, a_1) - n_1 \sigma_r s_{n_1}(\rho_m, a_1)]$$

$$\cdot s_{n_2}(-\rho_m, a_2) \sum_{l=n_2}^{k_2} \left(\frac{n_2}{a_2}\right)^{l-n_2} \phi_l(\rho_m)\phi_l(\omega_r)/\phi_{n_2}(\omega_r) + \sum_{m=0}^{k_2} d_m s_{n_1}(\rho_m, a_1)$$

$$\cdot [(a_1 + a_2)s_{n_2-1}(-\rho_m, a_2) - n_2 \sigma_r s_{n_2}(-\rho_m, a_2)]\phi_{n_2}(\rho_m), \quad (114)$$

for $r = 1, \cdots, 2q_2 + 1$. The sums on l are given explicitly by (144), or by (145) if $\rho_m = \omega_r$.

If we set $\sigma_r = 1$ in the right-hand side of (114), so that $\omega_r = 0$ from (47), it is found after reduction that the expression reduces to $-H(1)e_0$, as given by (111), and hence is zero, from (112). It follows that $(1 - \sigma_r)$ may be factored from both sides of (114). Consequently, we

may consider the limiting case $a_1 \to A_1$, and obtain a finite expression for e_{q_2+1}, even though $\sigma_{q_2+1} \to 1$ as $a_1 \to A_1$.

Now that we have determined the constants $\{e_r\}$ in terms of the constants $\{d_m\}$, it remains to determine the latter. These are determined from (37) for $0 \le j \le n_2 - 1$, (39) for $n_2 + 1 \le j \le k_2$ and (49). The redundancy of (39) for $j = n_2$ was discussed in Section IV, and follows from the fact that $H(1)e_0 = 0$. Thus, the constants $\{d_m\}$ are determined from the boundary conditions at $i = n_1$, $0 \le j \le n_2 - 1$ and at $i = k_1$, $n_2 + 1 \le j \le k_2$, and from the normalization condition, the boundary condition at $i = k_1$, $j = n_2$ being redundant. The constants $\{d_m\}$ have to be calculated numerically.

VII. AN ALTERNATE DERIVATION

In this final section, we will give another derivation of the expressions for e_0 and e_r, $r = 1, \cdots, 2q_2 + 1$, given in (109) and (113). This derivation is more direct, but somewhat obscure, and was not evident until the results had been established with the help of the generating function approach.

We make use of the representation (27) for the probabilities p_{ij}, which holds for $n_1 \le i \le k_1$ and $n_2 \le j \le k_2$, and the boundary conditions at $i = n_1$, $n_2 \le j \le k_2$, as given by (35) and (36). In particular, from (27) we have

$$p_{n_1,j} = \sum_{r=0}^{2q_2+1} e_r \phi_j(\omega_r), \qquad n_2 \le j \le k_2. \tag{115}$$

Next, from (27) and (36), with the help of (47) and (134), we obtain

$$p_{n_1-1,j} = \sum_{r=0}^{2q_2+1} \frac{e_r}{\sigma_r} \phi_j(\omega_r), \qquad n_2 + 1 \le j \le k_2. \tag{116}$$

Also, from (27) and (35), with the help of (47) and (140), we find that

$$a_1 p_{n_1-1,n_2} + (a_1 + a_2) p_{n_1,n_2-1} = a_1 \sum_{r=0}^{2q_2+1} \frac{e_r}{\sigma_r} \phi_{n_2}(\omega_r). \tag{117}$$

From (115) to (117), it follows that

$$\sum_{j=n_2}^{k_2} (a_1 p_{n_1-1,j} - n_1 \sigma_m p_{n_1,j}) \left(\frac{n_2}{a_2}\right)^{j-n_2} \phi_j(\omega_m)$$

$$+ [(a_1 + a_2) p_{n_1,n_2-1} - n_2 \sigma_m p_{n_1,n_2}] \phi_{n_2}(\omega_m)$$

$$= \sigma_m \sum_{r=0}^{2q_2+1} e_r \left[\left(\frac{a_1}{\sigma_r \sigma_m} - n_1\right) \sum_{j=n_2}^{k_2} \left(\frac{n_2}{a_2}\right)^{j-n_2} \phi_j(\omega_m)\phi_j(\omega_r) \right.$$

$$\left. - n_2 \phi_{n_2}(\omega_m)\phi_{n_2}(\omega_r) \right]. \tag{118}$$

Now, from (47),

$$(\omega_r - \omega_m) = (\sigma_m - \sigma_r)\left(\frac{a_1}{\sigma_r\sigma_m} - n_1\right). \tag{119}$$

But, for $a_1 \neq A_1$, we know that $\sigma_r \neq \sigma_m$ for $r \neq m$. Hence, if we set $\rho = \omega_m$ in (143), and make use of (119) and (142), we obtain

$$\left(\frac{a_1}{\sigma_r\sigma_m} - n_1\right) \sum_{j=n_2}^{k_2} \left(\frac{n_2}{a_2}\right)^{j-n_2} \phi_j(\omega_m)\phi_j(\omega_r)$$

$$= n_2\phi_{n_2}(\omega_m)\phi_{n_2}(\omega_r), \qquad r \neq m, \qquad r, m = 0, \cdots, 2q_2 + 1. \tag{120}$$

This implies that all the terms on the right-hand side of equation (118), except the ones corresponding to $r = m$, are zero.

Next, from (13), (20), (25), and (133), it follows that

$$(1 - \sigma)H(\sigma) = a_2\phi_{n_2-1}(\omega) - n_2\sigma\phi_{n_2}(\omega), \tag{121}$$

and

$$\frac{d}{d\sigma}[(1 - \sigma)H(\sigma)]$$

$$= \left(n_1 - \frac{a_1}{\sigma^2}\right)[a_2\phi'_{n_2-1}(\omega) - n_2\sigma\phi'_{n_2}(\omega)] - n_2\phi_{n_2}(\omega). \tag{122}$$

Hence, from (145) we obtain

$$\left(\frac{a_1}{\sigma_r^2} - n_1\right) \sum_{j=n_2}^{k_2} \left(\frac{n_2}{a_2}\right)^{j-n_2} [\phi_j(\omega_r)]^2 - n_2[\phi_{n_2}(\omega_r)]^2$$

$$= \phi_{n_2}(\omega_r)\left\{\frac{d}{d\sigma}[(1 - \sigma)H(\sigma)]\right\}_{\sigma=\sigma_r}, \qquad r = 0, \cdots, 2q_2 + 1. \tag{123}$$

But, $\sigma_0 = 1$ and $\omega_0 = 0$, and $H(\sigma_r) = 0, r = 1, \cdots, 2q_2 + 1$, so that

$$\left\{\frac{d}{d\sigma}[(1 - \sigma)H(\sigma)]\right\}_{\sigma=\sigma_r} = \begin{cases} -H(1), & r = 0 \\ (1 - \sigma_r)H'(\sigma_r), & r = 1, \cdots, 2q_2 + 1. \end{cases} \tag{124}$$

The expressions in (109) and (113) for e_0 and e_r, $r = 1, \cdots, 2q_2 + 1$, respectively, follow directly from (118), if we set $m = 0$ and $m = 1, \cdots, 2q_2 + 1$, respectively, and make use of (120), (123), (124), and (137).

APPENDIX A
Properties of the Eigenfunctions

We define $s_i(\lambda, a)$ by the recurrence relation

$$(a + i + \lambda)s_i(\lambda, a)$$

$$= a(1 - \delta_{i0})s_{i-1}(\lambda, a) + (i + 1)s_{i+1}(\lambda, a); \quad s_0(\lambda, a) = 1, \tag{125}$$

for $i = 0, 1, \cdots$. Thus, $s_n(\lambda, a)$ is a polynomial of degree n in both λ and a, and it may be related to a Poisson-Charlier polynomial.[5,6] However, we will give here the properties of $s_n(\lambda, a)$ that we will need. An explicit formula is[1]

$$s_i(\lambda, a) = \sum_{r=0}^{i} \frac{(\lambda)_r a^{i-r}}{r!(i-r)!}, \tag{126}$$

where

$$(\lambda)_0 = 1, \qquad (\lambda)_r = \lambda(\lambda + 1) \cdots (\lambda + r - 1), \qquad r = 1, 2, \cdots. \tag{127}$$

It was also shown[1] that

$$(i + 1)s_{i+1}(\lambda, a) = as_i(\lambda, a) + \lambda s_i(\lambda + 1, a), \tag{128}$$

and

$$s_i(\lambda, a) = s_i(\lambda + 1, a) - (1 - \delta_{i0})s_{i-1}(\lambda + 1, a). \tag{129}$$

From (129), it follows that

$$\sum_{i=0}^{n} s_i(\lambda, a) = s_n(\lambda + 1, a), \tag{130}$$

and, from (128) and (130), we deduce that

$$\sum_{i=0}^{n} (n - i)s_i(\lambda, a) = (1 - \delta_{n0})s_{n-1}(\lambda + 2, a). \tag{131}$$

We now turn our attention to the Chebyshev polynomials of the second kind,[7] $U_l(x)$. They may be defined by the recurrence relation

$$2xU_l(x) = U_{l+1}(x) + U_{l-1}(x); \qquad U_{-1}(x) \equiv 0, \qquad U_0(x) \equiv 1, \tag{132}$$

for $l = 0, 1, \cdots$. From (12) and (132), it follows that

$$(a_2 + n_2 - \rho)\Psi_l(\rho) = a_2\Psi_{l+1}(\rho) + n_2\Psi_{l-1}(\rho);$$

$$\Psi_{-1}(\rho) \equiv 0, \qquad \Psi_0(\rho) \equiv 1. \tag{133}$$

From (13) and (133), we deduce that

$$[a_2(1 - \delta_{jk_2}) + n_2 - \rho]\phi_j(\rho) = a_2\phi_{j-1}(\rho) + n_2(1 - \delta_{jk_2})\phi_{j+1}(\rho), \tag{134}$$

for $j \leq k_2$. Since[7]

$$U_l\left[\frac{1}{2}\left(\xi + \frac{1}{\xi}\right)\right] = \sum_{r=0}^{l} \xi^{2r-l}, \tag{135}$$

it follows that

$$\Psi_l(0) = \left(\frac{n_2}{a_2}\right)^{l/2} U_l\left(\frac{a_2 + n_2}{2\sqrt{a_2 n_2}}\right) = \sum_{r=0}^{l} \left(\frac{n_2}{a_2}\right)^r. \tag{136}$$

Hence, from (13), we have

$$\phi_j(0) = \left(\frac{n_2}{a_2}\right)^{k_2 - j}. \tag{137}$$

If we set $\rho = \omega_r$ in (134), and also use (134) as it stands, we obtain

$$(\omega_r - \rho)\phi_j(\rho)\phi_j(\omega_r) = a_2[\phi_{j-1}(\rho)\phi_j(\omega_r) - \phi_j(\rho)\phi_{j-1}(\omega_r)]$$
$$- n_2(1 - \delta_{jk_2})[\phi_j(\rho)\phi_{j+1}(\omega_r) - \phi_{j+1}(\rho)\phi_j(\omega_r)]. \tag{138}$$

If we now multiply (138) by $(n_2/a_2)^{j-n_2}$, and sum on j, we deduce that

$$(\omega_r - \rho) \sum_{j=n_2}^{k_2} \left(\frac{n_2}{a_2}\right)^{j-n_2} \phi_j(\rho)\phi_j(\omega_r)$$
$$= a_2[\phi_{n_2-1}(\rho)\phi_{n_2}(\omega_r) - \phi_{n_2}(\rho)\phi_{n_2-1}(\omega_r)]. \tag{139}$$

But, from (21) and (22),

$$[a_2 + n_2(1 - \sigma_r) - \omega_r]\phi_{n_2}(\omega_r) = n_2\phi_{n_2+1}(\omega_r), \tag{140}$$

for $r = 0, \cdots, 2q_2 + 1$. Also, from (134), since $q_2 \geq 1$,

$$(a_2 + n_2 - \omega_r)\phi_{n_2}(\omega_r) = a_2\phi_{n_2-1}(\omega_r) + n_2\phi_{n_2+1}(\omega_r). \tag{141}$$

From (140) and (141), it follows that

$$a_2\phi_{n_2-1}(\omega_r) = n_2\sigma_r\phi_{n_2}(\omega_r), \qquad r = 0, \cdots, 2q_2 + 1. \tag{142}$$

Hence, from (139) and (142), we have

$$(\omega_r - \rho) \sum_{j=n_2}^{k_2} \left(\frac{n_2}{a_2}\right)^{j-n_2} \phi_j(\rho)\phi_j(\omega_r)$$
$$= \phi_{n_2}(\omega_r)[a_2\phi_{n_2-1}(\rho) - n_2\sigma_r\phi_{n_2}(\rho)], \qquad r = 0, \cdots, 2q_2 + 1. \tag{143}$$

If we set $\rho = \rho_m$ in (143) and make use of the fact that ρ_m, $m = 0, \cdots, k_2$, are the roots of equation (15), we deduce that

$$(\omega_r - \rho_m)s_{n_2}(-\rho_m, a_2) \sum_{j=n_2}^{k_2} \left(\frac{n_2}{a_2}\right)^{j-n_2} \phi_j(\rho_m)\phi_j(\omega_r)$$
$$= \phi_{n_2}(\rho_m)\phi_{n_2}(\omega_r)[a_2 s_{n_2-1}(-\rho_m, a_2) - n_2\sigma_r s_{n_2}(-\rho_m, a_2)]. \tag{144}$$

Also, if we divide (143) by $(\omega_r - \rho)$ and let $\rho \to \omega_r$, and use (142) and L'Hospital's rule, we find that

$$\sum_{j=n_2}^{k_2} \left(\frac{n_2}{a_2}\right)^{j-n_2} [\phi_j(\omega_r)]^2$$
$$= \phi_{n_2}(\omega_r)[n_2\sigma_r\phi'_{n_2}(\omega_r) - a_2\phi'_{n_2-1}(\omega_r)], \qquad r = 0, \cdots, 2q_2 + 1, \tag{145}$$

where the prime denotes derivative.

APPENDIX B

Eigenvalues Corresponding to the Primary Queueing Region

We consider here the zeros of

$$H(\sigma) \equiv \left(n_1 - \frac{a_1}{\sigma}\right)\Psi_{q_2}(\omega) + n_2\phi_{n_2}(\omega), \tag{146}$$

where

$$\omega = \left(\frac{a_1}{\sigma} - n_1\right)(1 - \sigma). \tag{147}$$

As may be seen from (12) and (13), $\Psi_{q_2}(\omega)$ and $\phi_{n_2}(\omega)$ are both polynomials in ω of degree q_2. It follows that $\sigma^{q_2+1}H(\sigma)$ is a polynomial in σ of degree $2q_2 + 1$, so that $H(\sigma) = 0$ has $2q_2 + 1$ roots. Now[7]

$$U_l(\cos \theta) = \frac{\sin(l + 1)\theta}{\sin \theta}. \tag{148}$$

We define

$$\alpha_m = a_2 + n_2 - 2\sqrt{a_2 n_2} \cos\left(\frac{m\pi}{q_2 + 1}\right), \qquad m = 1, \cdots, q_2, \tag{149}$$

and we note that $0 < \alpha_1 < \cdots < \alpha_{q_2}$. From (12), it follows that

$$\Psi_{q_2}(\alpha_m) = 0, \qquad m = 1, \cdots, q_2. \tag{150}$$

Next, we consider

$$\phi_{n_2}(\omega) \equiv \Psi_{q_2}(\omega) - \Psi_{q_2-1}(\omega), \tag{151}$$

and we note from (137) that $\phi_{n_2}(0) > 0$. If $q_2 = 1$, then $\phi_{n_2}(\alpha_1) = -1$, and the unique zero β_1 of $\phi_{n_2}(\omega)$ satisfies $0 < \beta_1 < \alpha_1$. For $q_2 \geq 2$, we define

$$\zeta_s = a_2 + n_2 - 2\sqrt{a_2 n_2}\cos\left(\frac{s\pi}{q_2}\right), \qquad s = 1, \cdots, q_2 - 1, \tag{152}$$

and we note that

$$0 < \alpha_1 < \zeta_1 < \cdots < \alpha_{q_2-1} < \zeta_{q_2-1} < \alpha_{q_2}. \tag{153}$$

From (12) and (148), it follows that

$$\Psi_{q_2-1}(\zeta_s) = 0, \qquad s = 1, \cdots, q_2 - 1. \tag{154}$$

Then, from (150), (151), (153), and (154), we deduce that

$$\phi_{n_2}(\alpha_1) = -\Psi_{q_2-1}(\alpha_1) < 0, \qquad \phi_{n_2}(\zeta_1) = \Psi_{q_2}(\zeta_1) < 0,$$

$$\phi_{n_2}(\alpha_2) = -\Psi_{q_2-1}(\alpha_2) > 0, \cdots. \tag{155}$$

We let

$$\phi_{n_2}(\beta_m) = 0, \qquad m = 1, \cdots, q_2, \tag{156}$$

with $\beta_1 < \beta_2 < \cdots < \beta_{q_2}$. Then, it follows that

$$0 < \beta_1 < \alpha_1 < \zeta_1 < \beta_2 < \alpha_2 < \cdots < \zeta_{q_2-1} < \beta_{q_2} < \alpha_{q_2}. \quad (157)$$

Now, from (147), it is seen that ω decreases from $+\infty$ to 0 as σ increases from $0+$ to $\min(1, a_1/n_1)$, and ω increases from 0 to $+\infty$ as σ increases from $\max(1, a_1/n_1)$ to $+\infty$. Hence γ_m and δ_m, $m = 1, \cdots, q_2$, are determined uniquely by the relations

$$\left(\frac{a_1}{\gamma_m} - n_1\right)(1 - \gamma_m) = \alpha_m, \qquad 0 < \gamma_m < \min\left(1, \frac{a_1}{n_1}\right),$$

$$\left(\frac{a_1}{\delta_m} - n_1\right)(1 - \delta_m) = \beta_m, \qquad 0 < \delta_m < \min\left(1, \frac{a_1}{n_1}\right). \quad (158)$$

It follows from (157) that

$$0 < \gamma_{q_2} < \delta_{q_2} < \cdots < \gamma_1 < \delta_1 < \min(1, a_1/n_1). \quad (159)$$

Now, from (146) and (147), since $\phi_{n_2}(0) > 0$, we have $H(a_1/n_1) > 0$. But, from (150) and (156) to (158),

$$H(\delta_1) = \left(n_1 - \frac{a_1}{\delta_1}\right)\Psi_{q_2}(\beta_1) < 0, \qquad H(\gamma_1) = n_2\phi_{n_2}(\alpha_1) < 0. \quad (160)$$

Also, for $q_2 \geq 2$,

$$H(\delta_2) = \left(n_1 - \frac{a_1}{\delta_2}\right)\Psi_{q_2}(\beta_2) > 0, \qquad H(\gamma_2) = n_2\phi_{n_2}(\alpha_2) > 0, \quad (161)$$

and so on. Finally, consideration of the sign of $\Psi_{q_2}(\omega)$ for $\omega \to +\infty$ leads to

$$H(0+) = \begin{cases} -\infty, & \text{if } q_2 \text{ is even,} \\ +\infty, & \text{if } q_2 \text{ is odd.} \end{cases} \quad (162)$$

From the above results, it follows that there are roots of $H(\sigma) = 0$ in the intervals $(0, \gamma_{q_2})$, $(\delta_{q_2}, \gamma_{q_2-1})$, $\cdots$, (δ_2, γ_1) and $(\delta_1, a_1/n_1)$. Since $\delta_1 < 1$, there are at least q_2 roots in the interval $(0, 1)$.

Next, from (159), we have

$$\max\left(1, \frac{a_1}{n_1}\right) < \frac{a_1}{n_1\delta_1} < \frac{a_1}{n_1\gamma_1} < \cdots < \frac{a_1}{n_1\delta_{q_2}} < \frac{a_1}{n_1\gamma_{q_2}}. \quad (163)$$

Also, from (146), (147), (150), and (156) to (158), we obtain

$$H\left(\frac{a_1}{n_1\delta_1}\right) = n_1(1 - \delta_1)\Psi_{q_2}(\beta_1) > 0, \quad H\left(\frac{a_1}{n_1\gamma_1}\right) = n_2\phi_{n_2}(\alpha_1) < 0, \quad (164)$$

and, for $q_2 \geq 2$,

$$H\left(\frac{a_1}{n_1\delta_2}\right) = n_1(1 - \delta_2)\Psi_{q_2}(\beta_2) < 0, \quad H\left(\frac{a_1}{n_1\gamma_2}\right) = n_2\phi_{n_2}(\alpha_2) > 0, \quad (165)$$

and so on. Hence there are q_2 roots of $H(\sigma) = 0$ in the intervals

$$\left(\frac{a_1}{n_1\delta_1}, \frac{a_1}{n_1\gamma_1}\right), \cdots, \left(\frac{a_1}{n_1\delta_{q_2}}, \frac{a_1}{n_1\gamma_{q_2}}\right).$$

These q_2 roots are greater than 1, and we have seen that at least q_2 of the remaining $q_2 + 1$ roots lie in the interval $(0, 1)$. It is evident that the $2q_2 + 1$ roots of $H(\sigma) = 0$ are positive and distinct.

It remains to consider the root that lies in the interval $(\delta_1, a_1/n_1)$. But, from (146) and (147), with the help of (13), we obtain

$$H(1) = \Psi_{q_2}(0)(A_1 - a_1), \tag{166}$$

where A_1 is as defined in (26). Also, we have shown that $H(\delta_1) < 0$ and $H(a_1/n_1) > 0$. Hence, if $a_1 < A_1$ this root lies in the interval $(\delta_1, 1)$, and there are $q_2 + 1$ roots in the interval $(0, 1)$, and q_2 roots greater than 1. If $a_1 > A_1$, then $a_1/n_1 > 1$ and the root lies in the interval $(1, a_1/n_1)$, and there are q_2 roots in the interval $(0, 1)$, and $q_2 + 1$ roots greater than 1. If $a_1 = A_1$, then one root is unity, and there are q_2 roots in the interval $(0, 1)$, and q_2 roots greater than 1.

APPENDIX C
Results Pertaining to the Generating Function

We derive here the solutions of (97), and we first consider $l = n_2$. Then,

$$[a_2(1 - \delta_{jk_2}) + n_2 - \zeta]G_j^{(n_2)}(z)$$
$$= a_2 G_{j-1}^{(n_2)}(z) + n_2(1 - \delta_{jk_2})G_{j+1}^{(n_2)}(z), \tag{167}$$

for $n_2 + 1 \leq j \leq k_2$. It follows from (134) that

$$G_j^{(n_2)}(z) = G_{k_2}^{(n_2)}(z)\phi_j(\zeta), \qquad n_2 \leq j \leq k_2, \tag{168}$$

since $\phi_{k_2}(\zeta) \equiv 1$. If we set $j = n_2$ in (97), and substitute from (168), we obtain

$$\left\{\left[a_2 + n_2\left(1 - \frac{1}{z}\right) - \zeta\right]\phi_{n_2}(\zeta) - n_2\phi_{n_2+1}(\zeta)\right\}G_{k_2}^{(n_2)}(z) = -\frac{1}{z}. \tag{169}$$

With the help of (13), (95), and (133), we deduce that

$$\left[a_2 + n_2\left(1 - \frac{1}{z}\right) - \zeta\right]\phi_{n_2}(\zeta) - n_2\phi_{n_2+1}(\zeta)$$
$$= \left(1 - \frac{1}{z}\right)[(n_1 - a_1 z)\Psi_{q_2}(\zeta) + n_2\phi_{n_2}(\zeta)] = \left(1 - \frac{1}{z}\right)H(1/z), \tag{170}$$

from (20) and (25). Hence,

$$(1 - z)H(1/z)G_{k_2}^{(n_2)}(z) = 1. \tag{171}$$

Since $\Upsilon_{n_2}(z) \equiv 1$, from (99), we have established (100) for $l = n_2$.

Next, we consider $l = k_2$. Then, from (97)

$$\left[a_2 + n_2\left(1 - \frac{\delta_{jn_2}}{z}\right) - \zeta \right] G_j^{(k_2)}(z)$$
$$= a_2(1 - \delta_{jn_2})G_{j-1}^{(k_2)}(z) + n_2 G_{j+1}^{(k_2)}(z), \quad (172)$$

for $n_2 \leq j \leq k_2 - 1$. But, it may be verified from (95), (99), and (133), that

$$\left[a_2 + n_2\left(1 - \frac{\delta_{jn_2}}{z}\right) - \zeta \right] \Upsilon_j(z)$$
$$= a_2(1 - \delta_{jn_2})\Upsilon_{j-1}(z) + n_2\Upsilon_{j+1}(z), \quad (173)$$

for $j \geq n_2$. It follows that

$$G_j^{(k_2)}(z) = G_{n_2}^{(k_2)}(z)\Upsilon_j(z), \qquad n_2 \leq j \leq k_2, \quad (174)$$

since $\Upsilon_{n_2}(z) \equiv 1$. If we set $j = k_2$ in (97), and substitute from (174), we obtain

$$[(n_2 - \zeta)\Upsilon_{k_2}(z) - a_2\Upsilon_{k_2-1}(z)]G_{n_2}^{(k_2)}(z) = -\frac{1}{z}. \quad (175)$$

With the help of (13), (95), (99), and (133), this may be written in the form

$$\left(\frac{a_2}{n_2}\right)^{q_2} (1 - z)[(n_1 - a_1 z)\Psi_{q_2}(\zeta) + n_2\phi_{n_2}(\zeta)]G_{n_2}^{(k_2)}(z) = 1. \quad (176)$$

It follows from (170) that

$$\left(\frac{a_2}{n_2}\right)^{q_2} (1 - z)H(1/z)G_{n_2}^{(k_2)}(z) = 1. \quad (177)$$

Since $\phi_{k_2}(\zeta) \equiv 1$, we have established (100) for $l = k_2$.

Finally, we consider $n_2 < l < k_2$. Then, from (97),

$$\left[a_2 + n_2\left(1 - \frac{\delta_{jn_2}}{z}\right) - \zeta \right] G_j^{(l)}(z)$$
$$= a_2(1 - \delta_{jn_2})G_{j-1}^{(l)}(z) + n_2 G_{j+1}^{(l)}(z), \quad (178)$$

for $n_2 \leq j \leq l - 1$, and

$$[a_2(1 - \delta_{jk_2}) + n_2 - \zeta]G_j^{(l)}(z) = a_2 G_{j-1}^{(l)}(z) + n_2(1 - \delta_{jk_2})G_{j+1}^{(l)}(z), \quad (179)$$

for $l + 1 \leq j \leq k_2$. It follows from (134) and (173) that

$$G_j^{(l)}(z) = \begin{cases} G_{n_2}^{(l)}(z)\Upsilon_j(z), & n_2 \leq j \leq l, \\ G_{k_2}^{(l)}(z)\phi_j(\zeta), & l \leq j \leq k_2, \end{cases} \quad (180)$$

since $\Upsilon_{n_2}(z) \equiv 1$ and $\phi_{k_2}(\zeta) \equiv 1$. The consistency of the representations for $j = l$ requires that

$$G_{n_2}^{(l)}(z)\Upsilon_l(z) = G_{k_2}^{(l)}(z)\phi_l(\zeta). \tag{181}$$

Also, if we set $j = l$ in (97), and substitute from (180), we obtain

$$(a_2 + n_2 - \zeta)G_{k_2}^{(l)}(z)\phi_l(\zeta) - a_2 G_{n_2}^{(l)}(z)\Upsilon_{l-1}(z)$$
$$- n_2 G_{k_2}^{(l)}(z)\phi_{l+1}(\zeta) = -\frac{1}{z}. \tag{182}$$

It remains to solve (181) and (182) for $G_{n_2}^{(l)}(z)$ and $G_{k_2}^{(l)}(z)$.

Now, since $l < k_2$, it follows from (134) and (182) that

$$a_2[G_{k_2}^{(l)}(z)\phi_{l-1}(\zeta) - G_{n_2}^{(l)}(z)\Upsilon_{l-1}(z)] = -\frac{1}{z}. \tag{183}$$

If we eliminate $G_{n_2}^{(l)}(z)$ with the help of (181), we find that

$$a_2 z G_{k_2}^{(l)}(z)[\Upsilon_l(z)\phi_{l-1}(\zeta) - \phi_l(\zeta)\Upsilon_{l-1}(z)] = -\Upsilon_l(z). \tag{184}$$

But, from (134) and (173), for $n_2 < j < k_2$,

$$(a_2 + n_2 - \zeta)\phi_j(\zeta) = a_2\phi_{j-1}(\zeta) + n_2\phi_{j+1}(\zeta), \tag{185}$$

and

$$(a_2 + n_2 - \zeta)\Upsilon_j(z) = a_2\Upsilon_{j-1}(z) + n_2\Upsilon_{j+1}(z). \tag{186}$$

Hence,

$$a_2[\Upsilon_j(z)\phi_{j-1}(\zeta) - \phi_j(\zeta)\Upsilon_{j-1}(z)]$$
$$= n_2[\Upsilon_{j+1}(z)\phi_j(\zeta) - \phi_{j+1}(\zeta)\Upsilon_j(z)], \tag{187}$$

for $n_2 < j < k_2$. Since $n_2 < l < k_2$, it follows that

$$\Upsilon_l(z)\phi_{l-1}(\zeta) - \phi_l(\zeta)\Upsilon_{l-1}(z)$$
$$= \left(\frac{a_2}{n_2}\right)^{l-n_2-1}[\Upsilon_{n_2+1}(z)\phi_{n_2}(\zeta) - \phi_{n_2+1}(\zeta)\Upsilon_{n_2}(z)]. \tag{188}$$

But, from (99) and (133),

$$n_2[\Upsilon_{n_2+1}(z)\phi_{n_2}(\zeta) - \phi_{n_2+1}(\zeta)\Upsilon_{n_2}(z)]$$
$$= \left[a_2 + n_2\left(1 - \frac{1}{z}\right) - \zeta\right]\phi_{n_2}(\zeta) - n_2\phi_{n_2+1}(\zeta). \tag{189}$$

Hence, from (170), (188), and (189), we obtain

$$a_2[\Upsilon_l(z)\phi_{l-1}(\zeta) - \phi_l(\zeta)\Upsilon_{l-1}(z)] = \left(\frac{a_2}{n_2}\right)^{l-n_2}\left(1 - \frac{1}{z}\right)H\left(\frac{1}{z}\right). \tag{190}$$

It follows from (184) that

$$\left(\frac{a_2}{n_2}\right)^{l-n_2}(1 - z)H\left(\frac{1}{z}\right)G_{k_2}^{(l)}(z) = \Upsilon_l(z). \tag{191}$$

In view of (180), (181), and (191), we have established (100) for $n_2 < l < k_2$.

We will now establish the relationship (106). From (21) and (22), it follows that

$$[a_2 + n_2(1 - \sigma_r) - \omega_r]\phi_{n_2}(\omega_r) = n_2\phi_{n_2+1}(\omega_r). \tag{192}$$

Hence, from (47), (95), and (189), since $\Upsilon_{n_2}(z) \equiv 1$, we have

$$\Upsilon_{n_2+1}(1/\sigma_r)\phi_{n_2}(\omega_r) = \phi_{n_2+1}(\omega_r). \tag{193}$$

As we noted in Section IV, $\phi_{n_2}(\omega_r) \neq 0$. Since $\Upsilon_{n_2}(1/\sigma_r) \equiv 1$, we see that (106) holds for both $j = n_2$ and $j = n_2 + 1$. But, from (47), (95), (185), and (186), $\phi_j(\omega_r)$ and $\Upsilon_j(1/\sigma_r)$ are both solutions of

$$(a_2 + n_2 - \omega_r)h_j = a_2 h_{j-1} + n_2 h_{j+1}, \qquad n_2 < j < k_2. \tag{194}$$

It follows that (106) holds for $n_2 \leq j \leq k_2$.

REFERENCES

1. J. A. Morrison, "Analysis of Some Overflow Problems with Queuing," B.S.T.J. *59*, No. 8 (October 1980), pp. 1427–1462.
2. J. A. Morrison, "Some Traffic Overflow Problems with a Large Secondary Queue," B.S.T.J. *59*, No. 8 (October 1980), pp. 1463–1482.
3. L. Kaufman, J. B. Seery, and J. A. Morrison, "Overflow Models for Dimension® PBX Feature Packages," B.S.T.J. *60*, No. 5 (May–June 1981), pp. 661–676.
4. L. Kaufman, unpublished work.
5. A. Erdélyi, et al., *Higher Transcendental Functions*, Vol. II, New York: McGraw-Hill, 1953, p. 226.
6. J. Riordan, *Stochastic Service Systems*, New York: John Wiley, 1962.
7. W. Magnus, F. Oberhettinger, and R. P. Soni, *Formulas and Theorems for the Special Functions of Mathematical Physics*, New York: Springer-Verlag, 1966, p. 256.
8. L. Kleinrock, *Queueing Systems, Volume I: Theory*, New York: John Wiley, 1975.

Memoryless Nonlinearities With Gaussian Inputs: Elementary Results

By H. E. ROWE

The distortion-to-signal power ratio at the output of a memoryless nonlinearity is determined by simple calculations. This is done by application of Bussgang's theorem, which may also be obtained as a special case of Price's theorem. Specific results are given for hard and soft instantaneous and envelope limiters.

I. INTRODUCTION

We present elementary derivations of some useful results for memoryless nonlinearities driven by Gaussian noise. The present relations may be obtained as special cases of more general results,[1] but the present methods are elementary and give physical understanding.

Let a nonlinearity have input x, output z, and nonlinear characteristic $h(x)$;

$$z = h(x). \tag{1}$$

Let $x(t)$ be a stationary, Gaussian random noise. Then it is well-known (Bussgang's theorem) that the cross-correlation between input and output has the same shape as the autocorrelation of the input,

$$\langle x(t + \tau)z(t) \rangle = \alpha \cdot \langle x(t + \tau)x(t) \rangle. \tag{2}$$

This may be seen as a special case of Price's theorem,[2,3] or directly as outlined in the appendix.

From (2) we can write the output $z(t)$ of any instantaneous nonlinearity with Gaussian input $x(t)$ as

$$z(t) = \alpha \cdot x(t) + y(t), \tag{3}$$

where $y(t)$ will be uncorrelated with $x(t)$;

$$\langle x(t + \tau)y(t) \rangle = 0. \tag{4}$$

The constant α in eq. (3) is given as follows:

$$\alpha = \frac{1}{\sqrt{2\pi\phi(0)}} \int_{-\infty}^{\infty} \frac{x}{\phi(0)} e^{-\frac{x^2}{2\phi(0)}} h(x) dx$$

$$= \frac{1}{\sqrt{2\pi\phi(0)}} \int_{-\infty}^{\infty} e^{-\frac{x^2}{2\phi(0)}} h'(x) dx, \tag{5}$$

where

$$\langle x(t) \rangle = 0, \qquad \phi(\tau) = \langle x(t + \tau)x(t) \rangle. \tag{6}$$

II. NARROW-BAND INPUT

If $x(t)$ is narrow-band, it is useful to write

$$x(t) = R(t)\cos[\omega_c t + \theta(t)]$$

$$= \frac{1}{2} R(t)e^{-j\theta(t)}e^{-j\omega_c t} + \frac{1}{2} R(t)e^{j\theta(t)}e^{j\omega_c t}, \tag{7}$$

where $R(t)$ and $\theta(t)$, the envelope and angle, slowly varying compared to $\omega_c t$, are defined in terms of $x(t)$ and is Hilbert transform $\hat{x}(t)$ in the usual way:

$$R(t)e^{j\theta(t)}e^{j\omega_c t} = x(t) + j\hat{x}(t). \tag{8}$$

The output of the nonlinearity may then be written[4]

$$z(t) = \sum_{n=0}^{\infty} A_n(R)\cos(n\omega_c t + n\theta), \tag{9}$$

where R and θ are understood to be functions of t. The different terms of (9) occupy separate narrow bands, centered around their respective midband frequencies $n\omega_c$. The output envelopes $A_n(R)$ are nonlinear functions of the input envelope R.[4]

We regard the first term of (3) as the undistorted, or signal, component of the nonlinearity output, and the second term of (3) as distortion. Thus, the signal component of (9) resides exclusively in the $n = 1$ term, to which we subsequently restrict our attention. We redefine $z(t)$ to be the response to (9) of a zonal filter centered on ω_c, and drop the subscript 1 on the coefficient of the $n = 1$ term of (9), to yield

$$z(t) = A(R)\cos(\omega_c t + \theta) \tag{10}$$

as the output to be investigated. In eq. (10), $A(R)$ is given by[5]

$$A(R) = \frac{2}{\pi} \int_0^{\pi} h(R \cos \beta)\cos \beta d\beta, \tag{11}$$

in terms of the instantaneous nonlinear characteristic $h(\ )$ of (1).

The output [eqs. (10) and (11)] contains both signal and distortion components. For Gaussian input $x(t)$, $R(t)$ is Rayleigh, and α of (5) is given in terms of envelope by

$$\alpha = \frac{(1/2)\langle R \cdot A(R)\rangle}{\phi(0)}$$

$$= \frac{1}{2\phi(0)} \int_0^\infty RA(R) \cdot \frac{R}{\phi(0)} e^{-\frac{R^2}{2\phi(0)}} dR$$

$$= \frac{\sqrt{\pi}}{2} \frac{1}{\sqrt{2\phi(0)}} \int_0^\infty \left[\operatorname{erfc} \frac{R}{\sqrt{2\phi(0)}} + \frac{2}{\sqrt{\pi}} \frac{R}{\sqrt{2\phi(0)}} e^{-\frac{R^2}{2\phi(0)}}\right] A'(R) dR, \quad (12)$$

where

$$\operatorname{erfc} u = \frac{2}{\sqrt{\pi}} \int_u^\infty e^{-t^2} dt. \quad (13)$$

The output signal power S is given by

$$S = \alpha^2 \cdot \phi(0). \quad (14)$$

The constant α in eq. (14) may be calculated from either (5) or (12), whichever is more convenient. The second line of (12) is equivalent to the $m = 1$ case of eq. (9) of Ref. 1.

In eq. (10), $z(t)$ contains both the signal component

$$\alpha \cdot x(t) = \alpha \cdot R(t)\cos[\omega_c + \theta(t)] \quad (15)$$

and a distortion component, of power D. To find this, we determine the total power $S + D$ in $z(t)$ of (10), and subtract S. We have

$$S + D = \frac{1}{2}\langle A^2(R)\rangle = \frac{1}{2}\int_0^\infty A^2(R) \cdot \frac{R}{\phi(0)} e^{-\frac{R^2}{2\phi(0)}} dR. \quad (16)$$

Since $S \leq S + D$, we must have from (12), (14), and (16)

$$\langle R \cdot A(R)\rangle^2 \leq 2\phi(0) \cdot \langle A^2(R)\rangle. \quad (17)$$

Noting that

$$2\phi(0) = \langle R^2\rangle, \quad (18)$$

(17) is simply the Schwarz inequality.

III. HARD (INSTANTANEOUS OR ENVELOPE) LIMITER

The instantaneous nonlinear characteristic of (1) is:

$$h(x) = \operatorname{sgn} x = \begin{matrix} 1, & x > 0. \\ -1, & x < 0. \end{matrix} \quad (19)$$

The corresponding envelope characteristic of (11) is:

$$A(R) = \frac{4}{\pi}, \qquad R > 0. \tag{20}$$

The signal gain α of (3) is, by the second relation of either (5) or (12):

$$\alpha = \sqrt{\frac{2}{\pi\phi(0)}} \tag{21}$$

The output signal power S is by (14):

$$S = \frac{2}{\pi}. \tag{22}$$

Finally, the total power in the first zone is given by (16):

$$S + D = \frac{8}{\pi^2}. \tag{23}$$

Therefore,

$$\frac{D}{S+D} = 1 - \frac{\pi}{4}. \tag{24}$$

IV. SOFT INSTANTANEOUS LIMITER

The instantaneous nonlinear characteristic of (1) is:

$$h(x) = \begin{matrix} x, & |x| \leq X. \\ 1, & |x| \geq X. \end{matrix} \tag{25}$$

This signal gain α is from the second relation of (5):

$$\alpha = \frac{2}{\sqrt{\pi}} \cdot \text{erf} \frac{X}{\sqrt{2\phi(0)}}, \tag{26}$$

where

$$\text{erf } u = \frac{2}{\sqrt{\pi}} \int_0^u e^{-t^2} dt = 1 - \text{erfc } u. \tag{27}$$

V. SOFT ENVELOPE LIMITER

The envelope nonlinear characteristic of (11) is:

$$A(R) = \begin{matrix} R, & 0 \leq R \leq A. \\ A, & A \leq R \leq \infty. \end{matrix} \tag{28}$$

The signal gain α is, by the second relation of (12):

$$\alpha = \frac{\sqrt{\pi}}{2} \frac{A}{\sqrt{2\phi(0)}} \cdot \text{erfc} \frac{A}{\sqrt{2\phi(0)}} + 1 - e^{-\frac{A^2}{2\phi(0)}}. \tag{29}$$

By (14), the output signal power is:

$$S = \phi(0) \cdot \left[\frac{\sqrt{\pi}}{2} \frac{A}{\sqrt{2\phi(0)}} \cdot \mathrm{erfc} \frac{A}{\sqrt{2\phi(0)}} + 1 - e^{-\frac{A^2}{2\phi(0)}} \right]^2. \tag{30}$$

This is equivalent to eq. (24a) of Ref. 1. The total power in the first zone is by (16):

$$S + D = \phi(0) \cdot \left[1 - e^{-\frac{A^2}{2\phi(0)}} \right]. \tag{31}$$

Therefore, for the soft envelope limiter (28):

$$\frac{D}{S+D} =$$

$$1 - \left[\frac{\sqrt{\pi}}{2} \frac{A}{\sqrt{2\phi(0)}} \, \mathrm{erfc} \, \frac{A}{\sqrt{2\phi(0)}} + 1 - e^{-\frac{A^2}{2\phi(0)}} \right]^2 \Bigg/ \left[1 - e^{-\frac{A^2}{2\phi(0)}} \right]. \tag{32}$$

Asymptotically:

$$\frac{D}{S+D} \sim \frac{1}{2} e^{-\frac{A^2}{2\phi(0)}} \Bigg/ \left[\frac{A^2}{2\phi(0)} \right], \qquad \frac{A^2}{2\phi(0)} \gg 1. \tag{33}$$

VI. ACKNOWLEDGMENT

APPENDIX

Derivation of Eq. (2)

A special case of Price's theorem[2] may be stated as follows.[3] Let x_1 and x_2 be jointly Gaussian random variables with first and second moments given as follows:

$$\langle x_1 \rangle = \langle x_2 \rangle = 0.$$

$$\langle x_1^2 \rangle = \langle x_2^2 \rangle = R_{11}. \tag{34}$$

$$\langle x_1 x_2 \rangle = R_{12}.$$

The normalized covariance is

$$\rho_{12} = \frac{R_{12}}{R_{11}}. \tag{35}$$

Let x_1 and x_2 be passed through two different instantaneous nonlinearities with characteristics h_1 and h_2, yielding outputs $h_1(x_1)$ and $h_2(x_2)$ with output cross-variance

$$\psi = \langle h_1(x_1) h_2(x_2) \rangle. \tag{36}$$

Then

$$\frac{\partial \psi}{\partial \rho_{12}} = \langle h_1'(x_1) h_2'(x_2) \rangle, \tag{37}$$

where

$$h_1'(x_1) = \frac{dh_1(x)}{dx}\bigg|_{x=x_1}, \qquad h_2'(x_2) = \frac{dh_2(x)}{dx}\bigg|_{x=x_2}. \tag{38}$$

To derive Bussgang's theorem set:

$$h_1(x) = h(x).$$

$$h_2(x) = x.$$

$$x_1 = x(t).$$

$$x_2 = x(t + \tau). \tag{39}$$

$$x(t) = \text{stationary Gaussian noise.}$$

$$\phi(\tau) = \langle x(t + \tau)x(t) \rangle; \qquad \rho(t) = \frac{\phi(\tau)}{\phi(0)}.$$

Substituting (39) into (34) to (38),

$$\frac{\partial \psi}{\partial \phi} = \frac{1}{\phi(0)} \langle h'(x) \rangle = \text{constant.} \tag{40}$$

Integrating,

$$\psi(\tau) = \langle x(t + \tau)h(x) \rangle = \text{constant} \cdot \phi(\tau), \tag{41}$$

the result given in (2).

The following alternative derivation, without using Price's theorem, was given by Jack Salz. From (2)

$$\alpha = \frac{\langle x(t + \tau)z(t) \rangle}{\langle x(t + \tau)x(t) \rangle}. \tag{42}$$

Express the nonlinear characteristic of (1) as the contour integral of its transform;[4]

$$z = h(x) = \frac{1}{2\pi} \int_C F(ju)e^{jxu}du. \tag{43}$$

Write

$$x = \frac{1}{j}\frac{d}{dv} e^{jvx}\bigg|_{v=0}. \tag{44}$$

Then,

$$\langle x(t+\tau)z(t)\rangle = \frac{1}{2\pi j}\lim_{v\to 0}\frac{d}{dv}\int_C F(ju)\langle e^{j(ux(t)+vx(t+\tau))}\rangle du$$

$$= \phi(\tau)\cdot\frac{j}{2\pi}\int_C F(ju)u e^{-u^2\phi(0)/2}du, \tag{45}$$

the same result as (41). Substituting in (42),

$$\alpha = \frac{j}{2\pi}\int_C F(ju)u e^{-u^2\phi(0)/2}du. \tag{46}$$

Equation (46) is readily shown to be equivalent to (5), by substituting the transform relation (43) into (5) and interchanging the order of integration.

REFERENCES

1. A. A. M. Saleh, "Intermodulation Analysis of FDMA Satellite Systems Employing Compensated and Uncompensated TWT's," IEEE Trans. Commun., *COM-30* (May 1982), pp. 1233–42.
2. R. Price, "A Useful Theorem for Nonlinear Devices Having Gaussian Inputs," I.R.E. Trans. Inform. Theory, *IT-4* (June 1958), pp. 69–72.
3. Ralph Deutsch, "Nonlinear Transformations of Random Processes," Englewood Cliffs, New Jersey: Prentice-Hall, 1962; pp. 15–21.
4. S. O. Rice, "Mathematical Analysis of Random Noise," B.S.T.J. *23* (July 1944), pp. 282–332, and *24* (January 1945), pp. 46–156. Reprinted in "Noise and Stochastic Processes," N. Wax, Editor, New York: Dover Publications, Inc., 1954, Section 4.3.
5. N. Blachman, "Detectors, Bandpass Nonlinearities, and Their Optimization: Inversion of the Chebyshev Transform," IEEE Trans. Inform. Theory, *IT-17* (July 1971), pp. 398–404.

A Variation on CSMA/CD That Yields Movable TDM Slots in Integrated Voice/Data Local Networks

By N. F. MAXEMCHUK

(Manuscript received January 6, 1982)

A variation on the carrier-sense, multiple-access/collision-detection (CSMA/CD) protocol for local-area, random-access broadcast networks is presented. The new protocol supports any mix of voice and data traffic, and has an upper bound on the delay of periodic traffic. In conventional CSMA/CD systems, statistical fluctuations in the transmission delay may cause disruptions in reconstructed voice waveforms. This does not occur with the new protocol. With this protocol, data sources use conventional CSMA/CD techniques to access the channel, while voice sources use a subset of these protocols, and appear to acquire a time-division multiplexed (TDM) slot. As in TDM systems, the entire system capacity can be used by the periodic sources. Unlike TDM systems, periodic slots are repositioned when other transmissions interfere with them, timing discrepancies between sources can be tolerated, and a centralized controller is not required to assign slots. Simulations are used to compare the delays in this system with those in conventional CSMA/CD systems. It is shown that at link utilizations of 0.9, voice sources can operate in a time-assignment, speech-interpolation mode. The effect of periodic traffic on conventional CSMA/CD protocols is also determined.

I. INTRODUCTION

There are basic differences between the requirements for data and voice transmission. There are also differences between the capabilities of local networks and the functions that should be performed on these networks, and general global networks. A protocol is described for integrating data and voice in a local-area, random-access broadcast network. It enables a single system, with similar interfaces for voice and data, to be used for both. The protocol satisfies the transmission

1527

requirements of both media, and takes advantage of the characteristics of local networks. This protocol can be applied to any system with periodic and aperiodic sources, as long as all of the periodic sources have the same transmission requirements.

In general, transmission capacity is less expensive in a local environment than in the global environment. This has resulted in significant differences in the types of networks implemented for data transmission in the two situations. In global networks, expensive access and switching techniques have been used to minimize the network capacity required to effect communications, whereas in local networks simpler switching techniques and less costly access nodes have been used. Several global networks, which use store-and-forward and packet-switching techniques to reduce the transmission requirements, are described in Chapters 1 and 2 of Ref. 1. A survey of techniques used in local networks, and an extensive bibliography is given in Ref. 2. Many of these local networks are configured as loops or random-access channels. Switching is simplified, but high-bandwidth communications channels are required.

The proximity of nodes in local networks leads to smaller propagation delays than those that occur in global networks. This has resulted in the development of more efficient random-access broadcast techniques for local networks[3,4] than have been developed for global networks (see Ref. 5 for a survey of random-access techniques and additional references).

Most proposals for integrated digital voice and data networks have applied to global networks. A survey of this work and an extensive bibliography can be found in Ref. 6. These proposals use variable-rate speech-coding techniques,[7,8] packet-switching techniques,[9,10] or complex strategies for combining circuit and packet switching.[11] These techniques are expensive to implement and should not be considered for local area communications. As in local data networks, integrated networks should take into account the reduced transmission costs and propagation delays in a local environment. In addition, only simple speech-coding techniques should be considered.

The requirements for digital voice transmission, both in terms of capacity and delay, are significantly different from those of data. The distribution of data traffic on local networks is typically bimodal,[12] comprising short interactive messages and long file transfers. The traffic from these sources arrives sporadically. If the message is divided into packets, a variance in the packet delay can be tolerated, providing the entire message delay is not excessive.

Uncompressed, digitized telephone calls require a large number of bits to be transferred, with much more stringent delay requirements than data sources have. Using a 32-kb/s speech coder, and transmitting

only during active speech intervals, over 4-½ Mb of data must be transmitted during a 3-minute telephone call. The data cannot be accumulated over the entire call and then transmitted as a large file transfer between computers, because the participants interact. The maximum delay allowed in current telephone connections is on the order of a few hundred milliseconds. However, in a local network, the maximum delay must be significantly less than this, since the connection may also use an outside facility.

In a packet voice system, overhead bits must be transmitted in addition to the information from the digitized voice source. The more voice samples included in this packet, the higher the ratio of information to total bits in the packet, and the higher the transmission efficiency of the channel. However, the more voice samples included in a packet, the greater the delay between the time a sample is generated and the time it is delivered to the receiving telephone. As a compromise, packets consisting of several tens of milliseconds of speech are used in the systems described in this paper.

The variance of the delay in digital speech systems must also be constrained. The digital-to-analog converter at the receiver uses samples at a fixed rate. If a packet of samples is delayed to the extent that the previously transmitted samples are completely used up before it arrives, a discontinuity occurs in the speech. The probability of this occurring can be reduced by delaying the first packet of voice samples that arrives at the receiver and buffering future packets until they are needed. If the maximum delay is not constrained, this technique can reduce, but not eliminate, the problem. This delay adds to the overall delay between the speaker and the listener, and must be kept small.

In the global networks referenced earlier, packets of voice that do not arrive in time are lost. It is argued that if a small percentage of voice packets are discarded at random, the resultant distortion is tolerable. This same argument is used in proposals to integrate voice and data on local networks.[13,14] It may be valid to assume that voice packets are lost at random when aperiodic data sources generate most of the network requirements, or when the periodicity of speech sources is reduced by variable-rate speech-coding techniques. However, this assumption will probably not hold in a local network.

Based upon the measured data utilization of local networks[12] and the anticipated transmission requirements of digital voice, voice packets will most likely dominate integrated local networks. Since voice packets are generated periodically, if packets from voice sources collide, they are likely to continue colliding on successive transmissions. Therefore, successive delays from the same source will be correlated. Voice sources that do not contend with other sources may have a small average and variance of delay, while those that contend with a large

number of voice sources may have a large average and variance of delay. If networks are designed based upon an acceptable average level of lost packets, and these packets are concentrated among a small number of connections during a small period of time, rather than being distributed randomly, the resultant service may not be acceptable.

Instead of reducing the periodicities to achieve fair packet losses, the periodicities can be used to eliminate lost packets entirely. This is accomplished by a variation on the carrier-sense, multiple-access/collision-detection (CSMA/CD) transmission protocol defined in Section II. This protocol transmits data by conventional CSMA/CD techniques, but uses only a subset of these techniques to transmit voice. The periodic sources do not detect collisions. In addition, periodic packets are tailored as described in Section III, the length of data packets is constrained, and periodic packets are given a higher retransmission priority. In Section IV, we show that this protocol limits the delay of voice packets to one data packet transmission time.

Periodic sources using this protocol operate as if a time-division multiplexed (TDM) channel has been assigned to each source. The difference between this channel and standard TDM channels is that it is not locked solidly into a time slot. The time slot may be shifted slightly back in time. When this occurs, the voice samples that arrive during the shift are transmitted in an expanded information area. An interesting characteristic of this system is that a periodic source can gain access to a system that does not appear to have the capacity to handle another periodic source. The system does not fail, but begins to operate as a completely utilized TDM system, with a slightly longer slot period. This phenomenon is explained in Section V. Another result of the time slot mobility is that timing discrepancies can exist between periodic sources without time slots being overwritten. This type of operation is described in Section VI.

In this system, if a periodic source and an aperiodic source are waiting to use a busy channel, the periodic source has a higher access priority and acquires the channel first. Typically, in queueing systems, when the delay of one class of users is reduced by raising its priority, the delay of the remaining users must increase. A simulator, which is described in Section VII, has been written to study the delays in this type of system. The model for the sources in the simulations is explained in Section VIII. The delays of periodic and aperiodic sources in this system are compared with the delays incurred when all sources use the same access protocol. These results are reported in Section IX. In Section X, alternative protocols are described.

II. TRANSMISSION PROTOCOL

In this protocol, all of the packets from an aperiodic source, and the

first packet from a periodic source that is beginning to transmit, use a CSMA/CD protocol. Before transmitting, the source listens to the channel and refrains from transmitting if the channel is busy. While transmitting, the source also listens to the channel and stops transmitting if a collision with another source is detected. If the channel is busy, or if a collision occurs, the source tries again after the channel becomes idle. This protocol is not dependent upon the specific retry strategy these sources use to resolve contention. Any of the conventional strategies will work.

After the first transmission, a periodic source transmits all of the data it has accumulated whenever it acquires the channel. The source schedules its next transmission attempt at a fixed time T_p after the last successful transmission. In the first description of the transmission protocol, it will be assumed that T_p is the same for all sources. The effect of timing errors will be investigated in Section VI.

A periodic source listens before transmitting and defers transmission rights to terminals that are currently transmitting. However, this source does not listen while transmitting, and never terminates transmission prematurely. Instead, the packet structure for a periodic source is designed to allow aperiodic sources to detect a collision and terminate transmission before the periodic source begins transmitting useful data. When busy channels are encountered, the periodic source begins transmitting as soon as the channel becomes idle. This protocol, in conjunction with a constraint on the packet size from aperiodic sources, prevents packets from periodic sources from colliding.

As periodic traffic enters a system, the system becomes a TDM system. A periodic source acquires the channel and periodically uses a slot starting at this time until it is delayed by aperiodic traffic, or another periodic source starting to transmit. At this time, the periodic slot scheduled for the periodic source is shifted slightly. Additional data are transmitted in the first delayed slot to compensate for the shift.

III. PACKET STRUCTURE

The packets from aperiodic sources, Fig. 1a, consist of overhead bits and data bits. The overhead bits contain synchronization bits, source and destination addresses, packet-length counts, packet sequence numbers, error-control bits, and any other functions required by the communications protocols. These are variable-length packets. They are constrained to be less than or equal in length to the packets from the periodic sources.

Packets from periodic sources, Fig. 1b, consist of preempt bits, overhead bits, data bits, and overflow bits. During the preempt interval, the periodic source places a signal on the transmission media but

OVERHEAD (H_A BITS)	DATA (I_A BITS)

(a)

PREEMPT (P_p BITS)	OVERHEAD (H_p BITS)	DATA (I_p BITS)	OVERFLOW (O_p BITS)
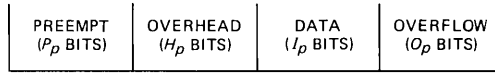
(b)

Fig. 1—(a) Packets from aperiodic sources. (b) Packets from periodic sources.

does not send information. This interval is long enough for an aperiodic source to detect a collision, stop transmitting, and have the effects of the transmission removed from the system before the periodic source begins transmitting useful data.

The length of the preempt interval, τ_p, is

$$\tau_p = 2\tau_t + \tau_{on} + \tau_I + \tau_{off},$$

where

τ_t is the maximum one-way propagation delay in the medium,

τ_{on} is the time required for a signal to be detected once it has propagated to a position on the channel,

τ_I is the time before the hardware reacts to a collision,

and

τ_{off} is time for a signal that is turned off to stop affecting a receiver, after the end of signal has propagated to the receiver.

Times τ_{on} and τ_{off} take into account electronics delays in the receivers and distortion in the received waveform caused by finite bandwidth channels which may not be correctly terminated. The preempt interval in a 3-Mb, 1-km simulated system is 38 bits long.

The overhead segment for periodic packets will be smaller than the overhead segment for aperiodic packets. An error-control strategy may not be used for periodic sources, since retransmitted packets will probably arrive too late to be used, and a greater error rate can be tolerated in sampled voice than in data. Packets will not arrive out of sequence; therefore, sequence numbers are not necessary. In addition, the number of bits of data in packets from these sources is deterministic, so that the length field is not required. In the simulations, $H_A = 100$ bits and $H_p = 40$ bits.

When a periodic source acquires the channel, it transmits all the data it has accumulated. The source schedules its next transmission T_p seconds after a successful transmission. If the channel is not busy at this time, the samples it has collected fit in the data area. If the channel is busy, it waits before transmitting. The samples that arrive

during this time are transmitted in the overflow area. Even when there are no overflow samples to be transmitted, the source transmits carrier during the overflow time. This guarantees that a periodic source takes no more time to transmit when it is delayed than when it acquires the channel immediately.

The size of the overflow area is determined by the maximum delay a periodic source can experience. This transmission protocol guarantees that the maximum delay for a periodic source will not exceed a packet transmission time. In the system simulated, the periodic sources generate 8000 4-bit samples per second, and T_p is 30 ms. A maximum of four samples arrive during a packet transmission interval; therefore, the overflow area is 16 bits.

The first packet from a periodic source may be shorter than successive packets since it does not include a preempt interval or an overhead interval. However, the same packet size will be maintained for this packet as for all other periodic packets. This guarantees that the scheduled interval between the next packet from this source and a packet from another periodic source is at least a periodic packet transmission time, X_p.

IV. CHANNEL CONTENTION

Delay is incurred in CSMA/CD networks when the channel is busy and when transmitting sources collide. Systems with periodic and aperiodic sources are being considered. Therefore, a periodic source can be delayed because

(i) the channel is busy transmitting an aperiodic packet,

(ii) a collision with an aperiodic source occurs,

(iii) the channel is busy transmitting a periodic packet, or

(iv) a collision with a periodic source occurs.

In this section, it is shown that only the first and third of these four mechanisms delay periodic sources, and that the maximum delay is less than X_p. It is assumed that every periodic source has the same T_p. The effects of timing inaccuracies are investigated in Section VI.

Whenever a periodic source and an aperiodic source collide, the aperiodic source detects the collision and stops transmitting before the periodic source begins transmitting useful data. Therefore, a periodic source is not delayed by a collision with an aperiodic source.

Whenever a periodic source and an aperiodic source are waiting for an idle channel, the periodic source obtains the channel. The periodic source begins transmitting as soon as the channel becomes idle. If an aperiodic source waits, it detects a busy channel and does not transmit. If an aperiodic source begins transmitting immediately, it detects a collision and stops transmitting. Therefore, a periodic source can only be delayed by an aperiodic source whose transmission is already in

progress. This delay is at most the packet transmission time for an aperiodic source, X_a, which is constrained to be less than X_p.

Consider a sequence of k periodic sources scheduled to transmit at times

$$t_{1,1}, \; t_{2,2}, \; \cdots, \; t_{k,k}.$$

Let

$t_{i,j}$ be the time the transmission from source i is scheduled to appear at the location of source j ($t_{i,j} - t_{i,i}$ is the propagation delay from the ith to the jth source),

$t'_{i,j}$ be the time the transmission from source i actually appears at location j (this takes into account the channel acquisition delay for the ith source),

and,

$D_i = t'_{i,j} - t_{i,j}$ be the delay of the ith source. (Since the propagation time is independent of the delay, the delay between the scheduled and actual arrival is the same for each destination j, and the second subscript is not needed.)

The transmission from each periodic source lasts X_p, and each periodic source schedules its next transmission T_p after its last successful transmission. Therefore,

$$t_{i+1,i+1} - t_{i,i+1} \geq X_p.$$

If $D_i = 0$, the ith periodic source does not delay the $(i + 1)$th periodic source, and, as long as

$$D_i < X_p$$

these two sources will not collide.

Periodic sources cannot be delayed by periodic sources which have not been delayed. Therefore, the first periodic source to be delayed must be delayed by an aperiodic source. The delay incurred by the first periodic source is less than X_p. The effect of this delay may propagate and effect a sequence of periodic sources. In a general sequence of periodic sources, if

$$D_i < X_p,$$

then,

$$t'_{i,i+1} < t_{i+1,i+1},$$

and, the ith and $(i + 1)$th do not collide. The transmission time required by the ith source is X_p, even though it is delayed, and must transmit more samples. If

$$t'_{i,i+1} + X_p \leq t_{i+1,i+1},$$

then the $(i + 1)$th is not delayed by the ith periodic source. This source may be delayed by an aperiodic source, and start a new sequence of delayed periodic sources, but the delay it incurs will be less than X_p. If

$$t'_{i,i+1} + X_p > t_{i+1,i+1},$$

the delay incurred by the $(i + 1)$th source is

$$D_{i+1} = t'_{i,i+1} + X_p - t_{t+1,i+1}.$$

Since the $(i + 1)$th source is waiting for the channel, this delay cannot be increased by an aperiodic source. The delay can be written as

$$D_{i+1} = D_i + t_{i,i+1} - t_{i+1,i+1} + X_p.$$

Since

$$t_{i,i+1} - t_{i+1,i+1} + X_p \le 0,$$

$$D_{i+1} \le D_i.$$

Therefore, the delay incurred by a sequence of periodic sources is a nonincreasing function, the maximum delay incurred by a periodic source is less than X_p, and periodic sources do not collide.

V. OVERLOAD TRAFFIC

Consider a system operating in a mode in which the channel capacity is nearly completely used by periodic sources. Assume that a time gap remains that is large enough for another source to begin transmitting, but not large enough to transmit an entire packet. Let another periodic source acquire the channel at this time. Is a failure mode created? Do delays build up until periodic sources start colliding? Is data lost? No. Instead, the system begins to operate without time gaps. The period between channel acquisitions increases, and some or all of the overflow bits in every packet are always used. Whenever a periodic source can acquire the channel, its ability to transmit is guaranteed.

Let a periodic source begin transmitting in a small time gap, such as that described in the hypothetical example. The periodic source it delays is delayed less than X_p. This source transmits the data accumulated during the delay in its overflow area and schedules its next transmission T_p seconds after it successfully acquires the channel. Successive periodic sources are delayed by an amount less than or equal to the delay incurred by the preceding source, as shown in the previous section.

The original interfering source becomes just another source in the sequence of interfering sources. It can be delayed by no more than the delay it originally caused, and can delay the source following it by no more than it did originally. Since the delay is a nonincreasing function,

and it cannot go to zero for the over-utilized channel, it must stabilize at some positive time, ϵ, which is the same for all sources. The delay, ϵ, is equal to X_p, minus the sum of the idle channel times for a period T_p before the overflow source entered the channel. Using the terminology from the preceding section:

$$\epsilon = X_p - \sum_{t_{i,i+1}\epsilon T_p} [t_{i+1,i+1} - (t_{i,i+1} + X_p)].$$

When the stable situation occurs, each periodic source transmits a packet every $T_p + \epsilon$ seconds. It transmits the samples that have arrived in this period of time in the data and overflow area. At the end of each transmission, there is a periodic source that has been waiting ϵ seconds. This source acquires the channel before an aperiodic source or the first packet from another periodic source can. Until one of the sources ends its transmission, and channel capacity becomes available, the system operates as a TDM system with a slot period of $T_p + \epsilon$ seconds. No data are lost, and the slot delays do not grow indefinitely.

VI. TIMING CONSIDERATIONS

In a sampled data communication system, it is necessary for the transmitter and receiver to be frequency locked, so that samples are used at the same rate at which they are generated. In broadcast networks, this can be achieved by sending a clock signal outside of the data band or by using a modulation rule with a clock component. The former technique provides accurate timing, but requires that one unit be responsible for inserting the clock on the system. In the latter technique, there is no centralized control, every transmitting unit is identical, but timing discrepancies may exist between the transmitters, particularly when very little data are being transmitted.

Timing discrepancies result in the periodic terminals having different estimates of the interpacket interval T_p. Let the interpacket interval for the ith periodic terminal $T_{i,p}$ be within ϵ of T_p, so that

$$|T_{i,p} - T_p| \leq \epsilon.$$

Let the ith and $(i + 1)$th periodic terminals transmit at

$$t_{i,i+1} = t,$$

and,

$$t_{i+1,i+1} = t + X_p,$$

so that there is no separation of the packets at the $(i + 1)$th source. The next packets from these terminals are scheduled at

$$t_{i,i+1} = t + T_{i,p},$$

and,

$$t_{i+1,i+1} = t + X_p + T_{i+1,p}.$$

These two times may be separated by as little as $X_p - 2\epsilon$. If the first packet in this sequence is delayed by a packet from an aperiodic source, it may be delayed until

$$t'_{i,i+1} < t + T_{i,p} + X_a.$$

With the constraint $X_a \leq X_p$, it is possible that both periodic sources will be waiting for the channel and will collide. This situation cannot be resolved by the protocol. It can be prevented by constraining the length of aperiodic packets to

$$X_a \leq X_p - 2\epsilon.$$

With this constraint, it can be shown, as in Section IV, that sequences of periodic sources do not collide, and that the delay of a periodic source does not exceed X_p.

This length constraint cannot be used to solve all of the problems that arise because of timing inconsistencies. The first packet from a periodic source must have length X_p to reserve an entire slot, but must enter the system like a periodic packet. This can be resolved by allowing periodic sources to recognize and preempt the first packet from a periodic source that begins transmitting within 2ϵ of the periodic source's scheduled transmission. Now, the maximum delay caused by the first packet from a periodic source is not greater than that caused by a packet from an aperiodic source.

VII. SIMULATION

A general-purpose simulator has been written to determine the characteristics of broadcast networks. In this simulator, the protocols used by sources, the traffic generated by a source, the physical position of a source on a channel, the parameters that define a transmission channel, and the interconnection of channels can be varied.

In the simulator, time jumps between the occurrence of significant events, rather than continuously moving forward by small increments. Functions such as wait for idle channel and listen while transmitting are implemented by giving the channel the characteristics of an active device. The channel notifies a source when the state of the channel, at the location of the source, has changed. Actually, the channel in this type of system is passive and sources that perform these functions examine the channel continuously. However, the interval of time in which the state of the channel can change and a significant event can occur is small compared to the average time between significant events. A simulator that models the continuous operation of the sources would

have to examine the channel at small intervals, and would be much less efficient, in terms of processing, than the technique selected.

In this simulator, the channel maintains lists of sources that are transmitting, listening while transmitting, and listening for an idle channel. When the state of the channel changes, channel maintenance routines notify the terminals in the lists at the appropriate times. These routines take into account the propagation delays between terminals, and the detection time of terminals.

Queues of messages and packets waiting to be transmitted from the sources are maintained without creating physical queues. Instead, the clocks associated with packet and message generation are allowed to run independent of the simulation clock. Each source keeps track of the time the packet and message it is transmitting were generated. When the transmission is complete, this time is updated to determine the next packet or message arrival at this source. If this time is less than the simulation time, this object has been waiting in a queue, and can be transmitted immediately. If it is greater than the simulation time, the queue is empty, and the message or packet is scheduled to arrive in the future.

The periodic terminals approximate voice terminals that only transmit during active speech intervals. For the parameters selected in the simulations, the speech interval durations are more than three orders of magnitude greater than the packet transmission time, and more than six orders of magnitude greater than certain of the channel-related events. The simulator tracks the fine structure of channel-related events. Because of the different time scales, the simulations could not be conducted for a long enough time to guarantee that all combinations of active and inactive intervals occur with the proper probabilities. To compensate for this, a different random-number generator is used to generate active and silent intervals than is used to generate the other random events in the simulation. This allows different protocols for periodic sources to be compared when the same active and silent intervals occur.

The systems simulated have the following characteristics:
   (i) Sources are uniformly distributed along a single cable.
   (ii) Channel length is 1 km.
   (iii) Transmission rate is 3 Mb/second.
   (iv) Time to detect the presence and removal of carrier, τ_{on} and τ_{off}, is 1 μs.
   (v) Time to detect interference, τ_I, is 4 μs.
   (vi) Time the channel must remain idle between transmissions is one-third of a microsecond.

These parameters do not correspond to a particular hardware realization of a system, but are indicative of what might be expected.

VIII. SOURCE MODELS

Aperiodic and periodic terminals are simulated. They correspond to a number of data sources sharing a store and forward node, and a two-way voice conversation. Some of the parameters associated with these terminals are selected to study specific characteristics of the system or to facilitate programming, rather than to accurately model the source. The results of the simulations provide an indication of how the system operates and not precisely how many terminals of a specific type can be supported.

The model for the sources in this system is shown in Fig. 2. In the remainder of this paper, the packets from the various sources are referred to as follows:

Type A—all of the packets from aperiodic sources.

Type F—the first packets in active intervals from periodic sources.

Type P—all other packets from periodic sources.

Type X—a composite of all of the packets from periodic sources.

Type T—a composite of all of the packets from all sources.

The protocols for periodic sources are referred to as follows:

Π_A—Periodic sources use the protocol proposed in this paper.

Π_L—Periodic sources use the same protocol as data traffic and transmit enough overhead bits to have the same packet size as Π_A.

Π_S—Periodic sources use the same protocol as data traffic, but transmit fewer overhead bits than Π_L.

Π_X—Either Π_L or Π_S. This symbol is used when describing the intersection set of these two protocols.

The doublet (x, y) refers to packets of type x, when the periodic sources use protocol y.

In the model, all of the sources test the state of the transmission medium before transmitting (LBT). If the channel is currently being used (B), they wait until it is idle (WIC), then schedule a transmission retry according to a source-specific strategy (SRB). Transmission priorities can be established by using different strategies for different sources. For instance, if one type of source can retry sooner than another, these sources are more likely to find the channel idle and will have a smaller average delay. For this set of simulations, all of the sources begin transmitting as soon as the channel becomes idle. If the channel is not heavily used, there is seldom more than one source waiting, and this will lead to the smallest possible delay. If more than one source is waiting, they collide and the collision retry strategy determines which source obtains the channel.

Transmitting sources may or may not listen while transmitting. In this set of simulations, sources listen while transmitting type A, (F, Π_A), and (X, Π_X) packets. When a collision is detected, a source-

Fig. 2—Model of the transmission strategies used by the sources in the simulations.

◇ TEST–TAKES NO TIME.

▭ EVENT WHICH MAY TAKE NONZERO TIME.

○ CONDUCTS A TEST WHILE AN EVENT IS IN PROGRESS.
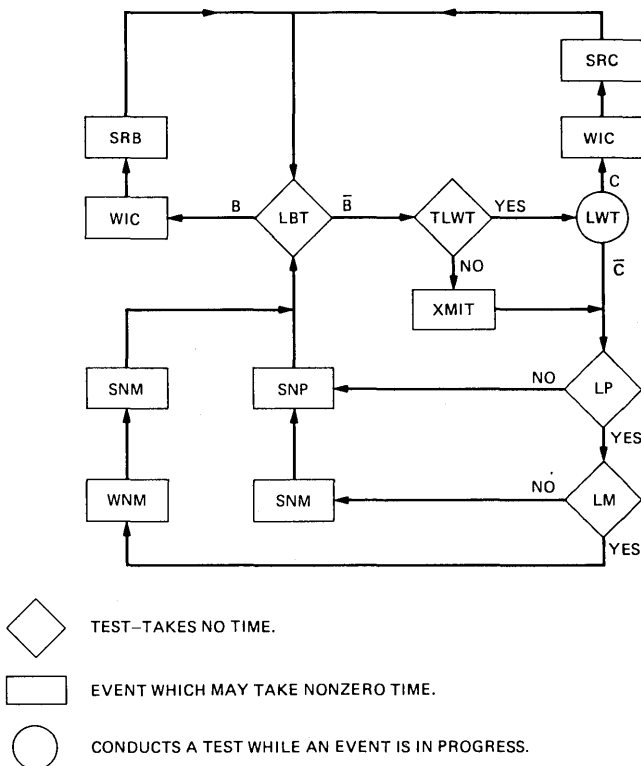
 LBT – LISTEN TO THE CHANNEL BEFORE TRANSMITTING.
 LWT – LISTEN TO THE CHANNEL WHILE TRANSMITTING.
XMIT – TRANSMIT.
 WIC – WAIT FOR IDLE CHANNEL.
 SRB – SCHEDULE A RETRY AFTER A BUSY CHANNEL.
 SRC – SCHEDULE A RETRY AFTER A COLLISION.
 SNP – SCHEDULE TRANSMISSION OF NEXT PACKET.
 SNM – SCHEDULE TRANSMISSION OF NEXT MESSAGE.
   B – CHANNEL BUSY.
   $\bar{B}$ – CHANNEL NOT BUSY.
   C – COLLISION DURING TRANSMISSION.
   $\bar{C}$ – NO COLLISION DURING TRANSMISSION.
  LP – TEST IF THE TRANSMITTED PACKET WAS THE LAST PACKET IN THE MESSAGE.
  LM – TEST IF THE TRANSMITTED MESSAGE WAS THE LAST MESSAGE IN THE QUEUE.
 WNM – WAIT FOR NEXT MESSAGE.
TLWT– TEST IF THIS TERMINAL IS TO LISTEN WHILE TALKING.

dependent retry strategy (SRC) is initiated. The sources do not listen while transmitting type (P, Π_A) packets.

The algorithm, SRC, provides another opportunity to assign transmission priorities. Sources generating type A and (X, Π_X) packets distribute their retrys uniformly over an interval $2^i\Delta\tau$, where i is the number of collisions this packet has experienced, and $\Delta\tau$ is two round-

trip transmissions delays. The value of i is limited to ten, so the retry interval varies from two to 1024 round-trip delays. Sources generating type (F, Π_A) packets distribute their retrys uniformly over an interval $\Delta\tau$. Under heavy-load conditions, these souces retry sooner than those generating type A packets and have a smaller average delay. The periodic sources model voice terminals that only transmit during active speech intervals. Type (F, Π_A) packets are given a higher priority because they must acquire the channel in less than 50 ms more than 98 percent of the time.[15,16] It is shown in Section IX that this requirement is met at channel utilizations of 0.9.

In this model, after a packet is successfully transmitted the source determines if this is the last packet in a message. If it is not, the next packet transmission is scheduled. If it is, the next message is scheduled. For the periodic sources, a message corresponds to an active interval during which packets are generated. After the last packet in an active interval is transmitted, there is never a message waiting. Instead, a silent interval is generated, and lasts until the next message arrives. Type (P, Π_X) packets are generated every T_p seconds after the first packet successfully acquires the channel. These packets are queued until they can be transmitted. Type (P, Π_A) packets are generated T_p seconds after the last successful channel acquisition.

The aperiodic sources generate variable-length messages. The messages arrive independently and are queued until they can be transmitted. The message length determines the number of packets in the message and the length of the last packet. The source transmits all of the packets in a message before determining if another message is waiting. The packet scheduling algorithm (SNP) waits before transmitting successive packets from this source. This enables other sources to acquire the channel.

The aperiodic sources in these simulations have the following characteristics:

(*i*) The message interarrival process is a negative exponential distribution with a mean of 33.47 ms.

(*ii*) The packet size is 1050 bits, 90 overhead bits, and 960 data bits.

(*iii*) The message length is deterministic—it is 960 bits. (Each message generates a single maximum-size packet.)

(*iv*) The minimum time between successive packets from the same source is four round-trip transmission delays.

These characteristics do not correspond to any known data source. They are selected to allow comparisons between systems with different mixes of periodic and aperiodic sources. The average number of bits transmitted by one of these sources is equal to the average number of bits transmitted by a periodic source. This allows the network utiliza-

tion to remain constant, while the mixture of periodic and aperiodic sources is varied. From this, the effect of periodic rather than aperiodic requirements on a broadcast network is determined. Using these characteristics, type A packets are almost the same size as type (X, Π_A) packets. This causes the largest possible delay to be incurred by the periodic sources.

The periodic sources have the following characteristics:

(i) For all of the sources, T_p is set to 30 ms. This results in 960 data bits per packet.

(ii) The duration of silent and active intervals are exponentially distributed with means of 0.185 and 1.31 seconds, respectively.

(iii) For type (X, Π_A) packets, $H_p = 40$ bits, $O_p = 16$ bits, and $P_p = 38$ bits. This results in 1054-bit packets.

(iv) For type (X, Π_L) packets, $H_p = 94$ bits. This retains the same link utilization as aperiodic sources and periodic sources using the new protocol.

(v) For protocol Π_s, $H_p = 40$ bits. This shows the effect of increasing the link utilization in the new protocol.

The mean values of the distributions are selected so that the total active time, the average active interval, and the number of active intervals correspond to those in a two-way telephone conversation.[17] This model assumes that the two speakers in a conversation do not talk simultaneously. It ignores the 0.07 probability of double talk. This model is easier to implement than one which allows double talk and should provide a reasonable indication of the system delays.

IX. SIMULATION RESULTS

Simulations have been conducted for protocols Π_A, Π_s, and Π_L. The fraction of the requirements generated by periodic sources was set to 0, 10, 25, 50, 75, 90, and 100 percent of the total requirements and the nominal offered utilization, S, to 0.7, 0.8, and 0.9. For protocols Π_A and Π_L, the actual values of S are very close to the nominal values. For protocol Π_s, the utilization generated by aperiodic sources and the number of periodic packets is the same as for the other protocols. However, the overhead associated with periodic packets is reduced. Therefore, the actual value of S is less than the nominal value.

Statistics were taken for 10 seconds of elapsed time after a 2-second initialization period. As the utilization varied from 0.7 to 0.9, the total number of packets in the simulations varied from about 20,000 to 25,500. The time between successive starts of active intervals for the periodic traffic is on the order of a second or two. It is unlikely that all combinations of active and inactive periodic terminals are witnessed in a 10-second interval. However, the same active intervals occurred for each of the protocols, and the data show definite trends. The

average and standard deviation of the channel access delay are plotted as a function of the percentage of the load generated by periodic sources in Figs. 3 and 4.

For Π_L, the periodic and aperiodic sources use the same transmission protocol and have the same packet lengths. For this protocol, the network utilization remains constant as the load shifts from aperiodic to periodic sources. All of the curves (T, Π_L) display the same characteristic. For a small fraction of periodic load, the delay measures increase. As the fraction of the load generated by periodic sources becomes large, the delay measures decrease.

This behavior can be accounted for by characteristics of periodic sources. As the periodic sources change between the active and inactive mode, the short-term utilization changes. The delay versus utilization curve for this type of system is concave upward so that the delay averaged over a number of utilizations is greater than the delay associated with the average utilization. This accounts for the initial increase in the curves. The periodic sources transmit packets at a multiple of T_p after the first successful transmission. This separates sources so that a large number of sources do not collide. Since it takes longer to resolve contention between larger numbers of sources, the average delay decreases as the number of sources that may be separated increases. This accounts for the decrease in the delay measures when the fraction of the load generated by periodic sources exceeds ten percent.

Curves (T, Π_A) show the delay characteristics for all of the packets in a system that uses the new protocol. The total utilization is the same as for Π_L. The delays for (T, Π_A) are less than those for (T, Π_L). Protocol Π_A guarantees that periodic sources do not collide with each other and that they successfully acquire the channel when they collide with aperiodic sources. Since there are fewer collisions, and fewer of the collisions that occur result in unsuccessful transmissions, less of the channel capacity is wasted. The decrease in delay is a result of the reduced-channel contention.

Comparing Π_A and Π_L demonstrates the favorable characteristics of the new protocol but not the unfavorable characteristics. Protocol Π_A requires additional bits to be transmitted in the preempt and overflow areas of the message. To show the effect of these bits, Π_s is examined. This protocol is the same as Π_L, except the overhead in periodic packets is reduced. As the fraction of the load generated by periodic sources increases, the average channel utilization decreases. Curves (T, Π_s) are below (T, Π_L), but are still above (T, Π_A). The latter result is due to the ratio of data bits to packet length in the system simulated. The preempt header is dependent upon the propagation delay in the system. As the channel becomes longer, or the transmission rate
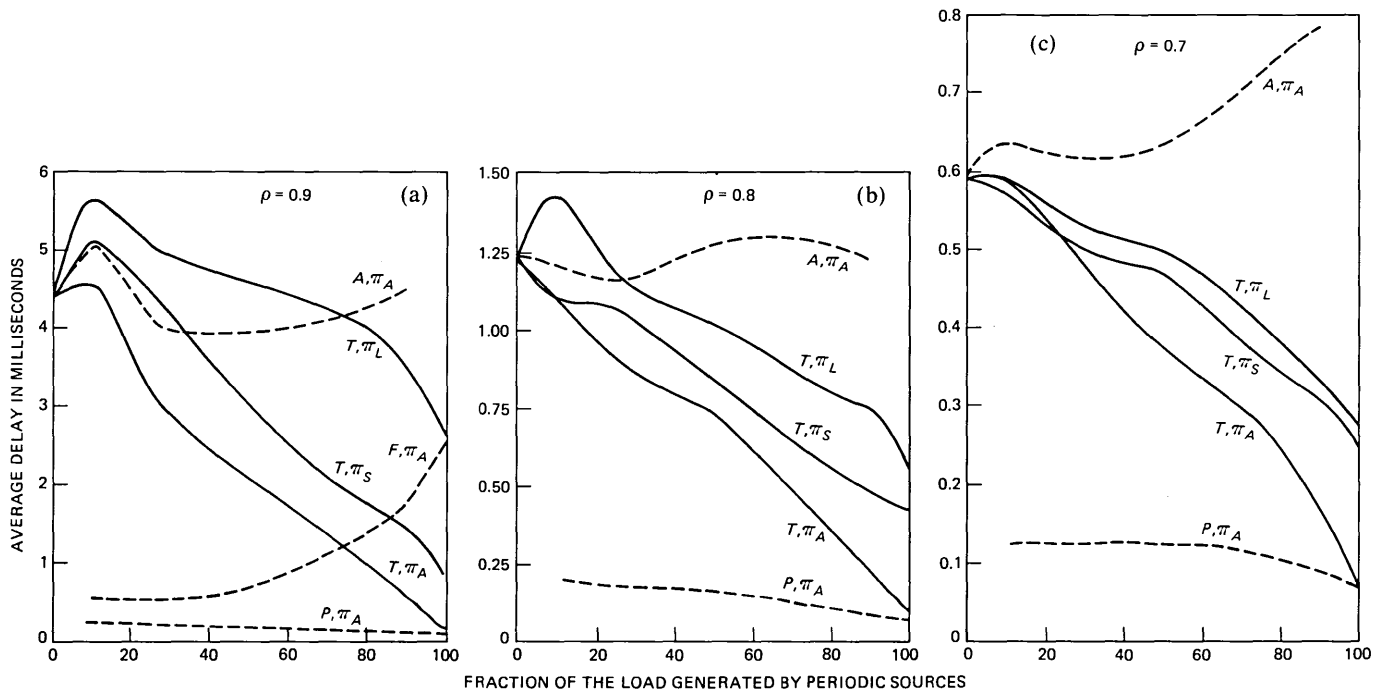
Fig. 3—Average delay versus the fraction of the load generated by periodic sources for several types of sources with protocols at the following utilizations: (a) $\rho = 0.9$; (b) $\rho = 0.8$; (c) $\rho = 0.7$.
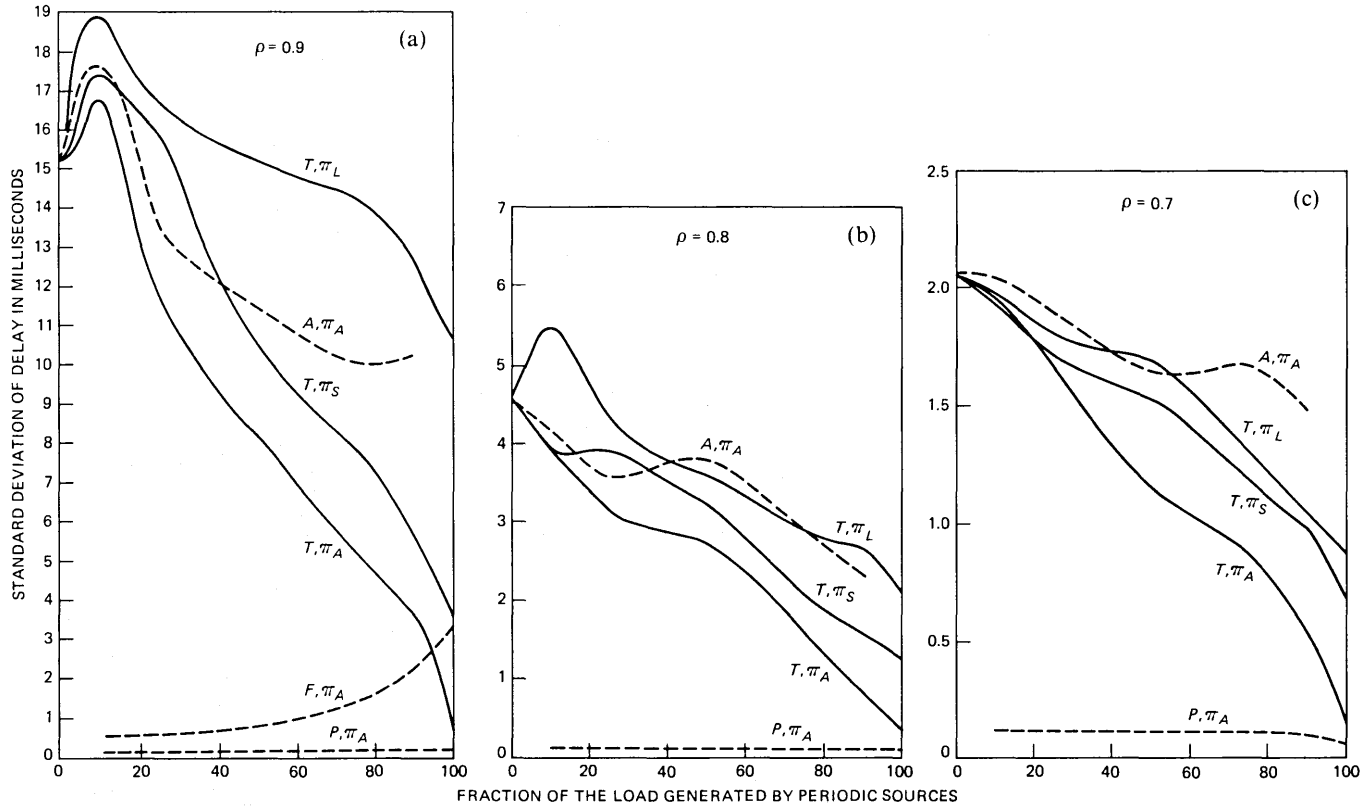
Fig. 4—Standard deviation of delay versus the fraction of the load generated by periodic sources for several types of sources with protocols at the following utilizations: (a) $\rho = 0.9$; (b) $\rho = 0.8$; (c) $\rho = 0.7$.

increases, this will comprise a larger fraction of the packet in Π_A, and the operation of Π_s will improve with respect to Π_A. A similar improvement will occur if T_p is decreased.

Protocol Π_A establishes an upper bound on the delay experienced by periodic traffic by giving this traffic a higher priority than aperiodic traffic. The dashed curves (A, Π_A) and (P, Π_A) represent the components of (T, Π_A) generated by aperiodic and periodic traffic, respectively. As expected, curves (A, Π_A) are above (T, Π_A), while (P, Π_A) are below. However, there are some interesting effects noted on these curves. As the fraction of the load generated by periodic sources increases, the number of sources that have a higher priority than the aperiodic sources increases. The delay experienced by the aperiodic sources is expected to increase. However, at utilizations of 0.8 or 0.9, there is not a significant increase in the average delay, and the standard deviation of the delay decreases.

From curves (T, Π_L), it can be concluded that it is definitely beneficial for aperiodic sources to share a channel with periodic sources. From curves (A, Π_A), it may even be beneficial for aperiodic sources to share a channel with higher priority periodic sources.

It has been stated that speech-activated systems should have a channel-acquisition delay less than 50 ms at least 98-percent of the time. From curves (A, Π_A), it should be possible to meet this constraint up to utilizations of 0.9, even if the first packet of speech is given the same transmission priority as aperiodic traffic, assuming that the 98-percent point corresponds to two standard deviations beyond the mean. In Π_A, the first packet from a periodic source is given a higher priority than packets from aperiodic sources. Using this strategy, it should be possible to lose no samples, not even those used to detect the presence of energy. For instance, if the transmitter stores the last 30 ms of speech samples, and it takes 10 ms to detect the presence of energy, no active samples are lost when the channel is acquired within 20 ms. At utilizations of 0.9, this appears to be well within the capability of the system.

X. ALTERNATIVE PROTOCOLS

Several other protocols for periodic traffic were considered. These protocols did not operate as well as the protocol described here and were not completely characterized. However, it is instructive to describe two of these protocols and their perceived shortcoming.

One possible approach to reduce the average and variance of the delay for periodic traffic is to give the periodic traffic a higher retransmission priority than aperiodic traffic. This approach is used in Π_A to reduce the delay for the first packet in a periodic sequence. Note in Figs. 3 and 4 that this strategy works best when the high-priority

traffic is a very small fraction of the total traffic. Priority systems do not reduce contention between high-priority users. In a local network designed to handle data and voice requirements, the voice transmission requirements are expected to far exceed the data requirements. A priority system will not provide significant improvements in this type of an environment.

In addition, the priority system may reduce delay problems, but it does not eliminate them. The delay is still an unbounded statistical variable. The probability of exceeding a specified delay is nonzero, and packets will be lost. This probability may be acceptable for moderate utilizations, but as the utilization approaches one, it will increase and become significant. Because of the high transmission requirements of voice, it is expected that a voice and data system will have to operate at much higher utilizations than data only systems.

Another protocol, which was tried, gives periodic traffic absolute preemptive right to the network. The periodic packets have a preempt header. They begin transmitting without listening to the network and interrupt any terminals that are transmitting. The preempt header is long enough for the nonpreemptive terminals to detect a collision and stop transmitting before useful data are transmitted by the preemptive terminals. This protocol results in zero transmission delay for periodic packets once they have acquired a slot. They acquire the slot for the first packet by behaving like an aperiodic terminal, as in the recommended protocol.

This protocol requires exact timing synchronization between periodic terminals and does not operate well at high-channel utilizations. Since the periodic terminals do not listen to the channel before transmitting and transmit periodically at what they perceive to be T_p seconds, if there is a discrepancy between various terminals' estimates of T_p, they will eventually interfere with one another. In addition, when the utilization for periodic sources is slightly greater than 50 percent, it is possible for these sources to be spaced in such a way that no new sources can obtain a time slot.

When this protocol was simulated, it was found that when the channel utilization from periodic sources exceeded 0.7, the channel efficiency decreased rapidly and the access time for the first packets from periodic sources and packets from aperiodic sources became intolerably long. The channel efficiency is the fraction of time the channel is being used to transmit data that are successfully received, over the total time that data are being transmitted. The unsuccessfully transmitted data occurs when packets are interrupted by collisions. The propagation delay in local networks is small compared with the packet transmission time, and terminals listen before transmitting. Therefore, for the previously defined protocols, collisions only occur

near the beginning of transmission. In this protocol, a packet can be interrupted at any time. As the fraction of time that preempt terminals use the system increases, the probability of interrupting a terminal that has completed a significant portion of its transmission increases and the channel efficiency decreases. As the channel efficiency decreases, the fraction of the channel capacity remaining for successful transmissions decreases and the delays increase. When the channel utilizations generated by periodic sources approached 0.7, the delay experienced by first periodic transmissions and aperiodic transmissions ranged from several tenths of a second to a second. This is an intolerable delay.

XI. CONCLUSIONS

When periodic and aperiodic data are transmitted on the same network, using conventional CSMA/CD protocols, the average and variance of the delay can be reduced by the periodicities in the data. By requiring periodic sources to begin generating periodic packets after they have successfully acquired the channel, the periodic requirements are separated in time, and collisions are reduced. This results in a decrease in the network delay. Channel contention is further reduced by requiring periodic sources to transmit all of the data they have acquired whenever they transmit and to schedule their next transmission a fixed time after their last successful channel acquisition.

If, in addition, periodic sources are only delayed by aperiodic sources with transmissions in progress, the size of packets from aperiodic sources is less than that from periodic sources, and the size of packets from periodic sources is not increased by the delay, then packets from periodic sources do not collide. The maximum channel acquisition delay experienced by periodic sources in this mode of operation is a packet transmission time.

By delaying the use of the first packet from a periodic source by a packet transmission time, the next packet is always received before all of the samples in previous packets are used. There are no discontinuities caused by the late arrival of samples in the reconstructed waveform, and packets of samples are never discarded because of excessive transmission delays.

In this mode of operation, periodic sources appear to have a dedicated TDM channel. There is a difference between the bandwidth allocation in this type of system and that of a true TDM system. In a TDM system, the time slots for a particular channel always carry the same number of bits and are fixed with respect to the beginning of a periodically recurring frame. In this system, the time slot for a particular channel may be moved back with respect to a hypothetical start of frame when the channel is busy. When this occurs, the number of

bits of data being carried by the slot increases. In the extreme, when the channel is overutilized, the slot is shifted back by the same amount every time it occurs. The slot period and the amount of data in the slot increases.

The mobility of time slots, in conjunction with the access protocol, allows all of the excess capacity that is not being used to transmit periodic packets to be used by aperiodic sources, even if the excess capacity is dispersed in small intervals throughout the TDM frame. The system can shift between any mix of periodic and aperiodic traffic without a central controller reallocating the bandwidth.

In conventional TDM systems, all of the transmitters must be able to accurately determine the location of their assigned slots to avoid transmitting simultaneously with other sources. In this system, a periodic source is willing to wait for a communication in progress to be completed. Therefore, timing inaccuracies between periodic sources can be tolerated, as long as the inaccuracy is not long enough to cause two periodic sources to simultaneously initiate communications.

Finally, the simulation results indicate that periodic sources can acquire a channel quickly enough to operate in a time-assignment, speech-interpolation mode. Storage and delay in the system may be used to reduce, and possibly eliminate, clipping which normally occurs at the beginning of active intervals in this type of system.

REFERENCES

1. M. Schwartz, *Computer-Communication Network Design and Analysis*, New York: Prentice-Hall, 1977.
2. J. F. Hayes, "Local Distribution in Computer Communications," IEEE Communications Magazine, *19*, No. 2 (March 1981), pp. 5–14.
3. R. M. Metcalfe and D. R. Boggs, "Ethernet: Distributed Packet Switching for Local Computer Networks," Commun. of the ACM, *19*, No. 7 (July 1976), pp. 395–404.
4. R. C. Crane and E. A. Taft, "Practical Considerations in Ethernet Local Network Design," Hawaii Int. Conf. Syst. Sciences, (January 1980), pp. 166–75.
5. F. A. Tobagi, "Multiaccess Protocols in Packet Communication Systems," IEEE Trans. Commun., *COM-28*, No. 4 (April 1980), pp. 468–88.
6. T. Bailly, A. J. McLaughlin, and C. J. Weinstein, "Voice Communication in Integrated Digital Voice and Data Networks," IEEE Trans. Commun., *COM-28*, No. 9 (September 1980), pp. 1478–89.
7. T. Bailly, B. Gold, and S. Seneff, "A Technique for Adaptive Voice Flow Control in Integrated Packet Networks," IEEE Trans. Commun., *COM-28*, No. 3 (March 1980), pp. 325–33.
8. D. Cohen, "A Protocol for Packet-Switching Voice Communication," North-Holland Publishing Co., Computer Networks, *2*, No. 4–5, (September–October 1978), pp. 320–31.
9. G. J. Coviello, "Comparative Discussion of Circuit vs Packet Switched Voice," IEEE Trans. on Commun., *COM-27*, No. 8 (August 1979), pp. 1153–9.
10. O. A. Mowafi and W. J. Kelly, "Integrated Voice/Data Packet Switching Techniques for Future Military Networks," IEEE Trans. Commun., *COM-28*, No. 9 (September 1980), pp. 1655–62.
11. M. J. Fisher and T. C. Harris, "A Model for Evaluating the Performance of an Integrated Circuit- and Packet-Switched Multiplex Structure," IEEE Trans. Commun., *COM-24*, No. 2 (February 1976), pp. 195–202.
12. J. F. Shoch and J. A. Hupp, "Measured Performance of an Ethernet Local Network," Commun. of the ACM, *23*, No. 12 (December 1980), pp. 711–21.

13. J. F. Shoch, "Carrying Voice Traffic Through an Ethernet Local Network—A General Overview," IFIP WG 6.4 International Workshop on Local-Area Computer Networks, Zurich (August 1980), pp. 429–46.
14. D. H. Johnson and G. C. O'Leary, "A Local Access Network for Packetized Digital Voice Communication," IEEE Trans. Commun., *COM-29*, No. 5 (May 1981), pp. 679–88.
15. S. I. Campanella, "Digital Speech Interpolation," Comsat Tech. Rev., *6*, No. 1 (Spring 1976), pp. 127–58.
16. K. Bullington and I. M. Fraser, "Engineering Aspects of TASI," B.S.T.J., *38*, No. 2 (March 1959), pp. 353–64.
17. P. T. Brady, "A Technique for Investigating On-Off Patterns of Speech," B.S.T.J., *44*, No. 1 (January 1965), pp. 1–22.

CONTRIBUTORS TO THIS ISSUE

Bernard C. De Loach, Jr., B.S. (Physics) 1951, M.S. (Physics), 1952, Auburn University; Ph.D. (Physics), 1956, Ohio State University; Bell Laboratories, 1956—. After joining Bell Laboratories, Mr. De Loach was a member of the Radio Research Department. Presently, he is engaged in the development of semiconductor lightwave devices and superconducting Josephson Junctions. He has been granted eleven patents. From 1955 to 1956, he was an Ohio State University Fellow. In 1972, he received the IEEE Fellow Award and in 1975, the IEEE David Sarnoff Award and the Stuart Ballentine Medal. Member, IEEE, Pi Mu Epison, Sigma Xi, Sigma Pi Sigma.

Christopher Flores, B.Tech. (Electrical Engineering), 1978, Indian Institute of Technology, Kanpur; M.S. (Operations Research), 1981, University of California, Berkeley; Ph.D. candidate (Electrical Engineering), 1978—, University of California, Berkeley. Mr. Flores' dissertation topic involves encoding of bursty services under a delay criterion. His other research interests include stochastic networks, multiple-access channels, and spread spectrum systems.

Bryon L. Kasper, B.Sc. (E.E.), University of Alberta, 1973; Alberta Government Telephones, 1973–1975; Ph.D. (E.E.), University of Alberta, 1981; Bell Laboratories, 1981—. Mr. Kasper worked for Alberta Government Telephones on acceptance testing of light-route microwave, mobile radio, and customer services equipment. At the University of Alberta, he conducted research on real-time digital signal processing for use in removing terrestrial radio interference from decametric radio astronomy observations. Since joining the Guided Wave Research Laboratory of Bell Laboratories, he has been involved in the equalization of optical transmission systems and in various aspects of high-speed, single-mode optical systems. Member, IEEE.

Richard B. Lawry, Associate in Electronics Technology, 1968, Penn Technical Institute; Bell Laboratories, 1968—. Mr. Lawry has worked in acousto-optic modulator fabrication and design, in automated charge-coupled device testing, and in dc sputtering of thin metal films for laser machining. His current work concerns p-type contact studies on InP.

George S. Lee, B.A. (Mathematics and Philosophy), 1975, Yale University; M.S. (Statistics), Ph.D. (Mathematics), 1980, University of

Wisconsin at Madison; Bell Laboratories, 1980—1982; American Bell, 1982—. Mr. Lee is a member of the Performance Analysis Group in the Advanced Information Systems/Net 1 project. His primary field of interest is in computer performance modeling. Member, American Mathematical Society, American Statistical Association.

John O. Limb, B.E.E., 1963, Ph.D. (Electrical Engineering), 1967, University of Western Australia, Nedlands; Research Laboratory, Australian Post Office, 1966 to 1967; Bell Laboratories, 1967—. At Bell Laboratories, Mr. Limb worked for a number of years on the coding of color and monochrome picture signals to reduce channel capacity requirements and has published widely in this area. He currently heads the Distributed Computer Systems Research Department, and has been studying the application of new telecommunications services in the office environment. His current research interest is wideband, local-area networks. Fellow, Institute of Electrical Engineers. Member, IEEE (Editor of IEEE Transactions on Communications), Association for Computing Machinery, Association for Research in Vision and Opthalmology, Optical Society of America.

Nicholas F. Maxemchuk, B.S.E.E., 1968, City College of New York; M.S.E.E., 1970, Ph.D., 1975, University of Pennsylvania. RCA David Sarnoff Research Center 1968–1976; Bell Laboratories 1976—; Adjunct Faculty of Computer and Information Sciences Department and Systems Engineering Department at the University of Pennsylvania. Mr. Maxemchuk is a member of the technical staff of the Distributed Computer Systems Research Department. Since joining Bell Labs he has done research on computer-communication networks, virtual and speech editing, and picture processing. He teaches courses on computer-communication networks, and he is Associate Editor for Data Communication for the IEEE Transactions on Communications. Member, Eta Kappa Nu, Tau Beta Pi.

Robert C. Miller, B.A. (Mathematics), 1949, University of Chicago; Ph.D. (Physics), 1957, University of Illinois; Bell Laboratories, 1957—. At Bell Laboratories, Mr. Miller has worked on electron device designs, diagnostic studies of gaseous laser systems, laser microrecording systems, and photovoltaic device applications. He is currently studying chemical diffusion in III–V semiconductors.

John A. Morrison, B.Sc., 1952, King's College, University of London; Sc.M., 1954 and Ph.D., 1956, Brown University; Bell Laboratories,

1956—. Mr. Morrison has done research in a number of different areas of applied mathematics and mathematical physics. He has recently been interested in probability theory, and various queueing problems in particular. He was a Visiting Professor of Mechanics at Lehigh University during the Fall semester 1968. He is currently the Managing Editor of SIAM Review. Member, American Mathematical Society, SIAM, IEEE, Sigma Xi.

Vasant K. Prabhu, B.E. (Dist.), 1962, Indian Institute of Science, Bangalore, India; S.M., 1963, Sc.D., 1966, Massachusetts Institute of Technology; Bell Laboratories, 1966—. Mr. Prabhu has been concerned with various theoretical problems in solid-state microwave devices and digital and optical communication systems. Member, IEEE, Eta Kappa Nu, Sigma Xi, Tau Beta Pi, Commission 6 of URSI.

Harrison E. Rowe, B.S., 1948, M.S., 1950, Sc.D., 1952 (Electrical Engineering), Massachusetts Institute of Technology; U. S. Navy, 1945–1946; Bell Laboratories, 1952—. Early in his career at Bell Laboratories, Mr. Rowe worked in the Radio Research Laboratory. Presently, he is a member of the technical staff of the Radio Physics Research Department. His publications include numerous papers and one textbook, spanning a variety of fields including parametric amplifiers, noise and communication theory, propagation in random media, and related problems in waveguide, radio, and optical communication systems. He is the joint author of five patents. Mr. Rowe is a Fellow of the IEEE, and a co-recipient of the 1977 David Sarnoff Award and the 1972 Microwave Prize. Member, Commission C of URSI, Sigma Xi, Tau Beta Pi, Eta Kappa Nu.

Stuart C. Schwartz, B.S., M.S. (Aeronautical Engineering), 1961, Massachusetts Institute of Technology; Ph.D. (Information and Control Engineering), 1966, The University of Michigan; Jet Propulsion Laboratory, Pasadena, California, 1961–1962; The Technion, Haifa, Israel, 1972–1973; Bell Laboratories, 1980–1981; Princeton University 1966—. At Bell Laboratories, Mr. Schwartz was a member of the Radio Research Laboratory's technical staff. At Technion, he was a John S. Guggenheim Fellow and a Visiting Professor, Department of Electrical Engineering. His principal research interests are in the application of probability and stochastic processes to problems in statistical communication and system theory. He has served as an editor of the SIAM Journal of Applied Mathematics. Member, Sigma Gamma Tau, Eta Kappa Nu, Sigma Xi, Institute of Mathematical Statistics.

Thomas S. Stakelon, B.S. (Physics), 1967, Manhattan College; M.S., 1969, Ph.D., 1974 (Physics), University of Illinois, Urbana; Post-doctoral Assistant, 1974–1976, The Ohio State University; Bell Laboratories, 1976—. At Bell Laboratories, Mr. Stakelon is Technical Supervisor of the Wavelength Division Multiplexing Group. He has been engaged in the exploratory and specific development of devices and components for wavelength multiplexing in fiber optic sytems since 1979. Prior to that he worked on ferrite materials development and testing.

Raymond Steele, B.S., 1959, Ph.D. (Electrical Engineering), 1975, Durham University, Durham, England; E. K. Cole, Ltd., 1959–1961; Cossor Radar, Electronics, Ltd., 1961–1962; The Marconi Company, 1962–1965; Royal Naval College, 1965–1968; Loughborough University of Technology, 1968–1979; Bell Laboratories, 1979—. At E. K. Cole, Ltd., Cossor Radar, Electronics, Ltd., and The Marconi Company, all located in Essex, England, Mr. Steele was engaged in research and development. As a member of the Lecturing Staff at the Royal Naval College in London, he lectured on telecommunications for the NATO and external London University degree courses. At the Loughborough University of Technology in Loughborough, England, he directed a research group in digital encoding of speech and television signals, in addition to serving as Senior Lecturer. Before joining Bell Laboratories on a full-time basis, Mr. Steele served as part-time consultant to the Laboratories' Acoustics Research Department. Presently, he is a member of the Communications Methods Research Department. He is the author of *Delta Modulation Systems*, published in 1975.

Paul E. Wright, A.B. (Mathematics/Physics), 1982, Cornell University. Mr. Wright was a Summer Research Associate at Bell Laboratories, 1981–1982. He is currently in a Ph.D. program at Cornell and is interested in Mathematical Physics. Member, Phi Beta Kappa, Alpha Lambda Delta, Alpha Chi Sigma.

Yu S. Yeh, B.S.E.E., 1961, National Taiwan University; M.S. (Electrical Engineering), 1964, Ph.D. (Electrical Engineering), 1966, University of California at Berkeley; Chinese Navy 1961–1962; Harvard University, 1966–1967; Bell Laboratories, 1967-. Mr. Yeh was engaged in mobile radio research from 1967 to 1972. Since that time he has worked on communication satellite systems and digital radio systems.

PAPERS BY BELL LABORATORIES AUTHORS

COMPUTING/MATHEMATICS

Barta S. M., **Capital Accumulation in a Stochastic Decentralized Economy.** J Econ Theo 26(1):124–142, 1982.

Benes V. E., Karatzas I., **Optimal Stationary Linear-Control of the Wiener Process.** J Optim Th 35(4):611–633, 1981.

Bertocci G. et al., **An Approach to the Implementation of a Discrete Cosine Transform.** IEEE Commun 30(4):635–641, 1982.

Boggs P. T., Tolle J. W., Wang P., **On the Local Convergence of Quasi-Newton Methods for Constrained Optimization.** Siam J Con 20(2):161–171, 1982.

Calderbank A. R., Wales D. B., **A Global Code Invariant Under the Higman-Sims Group.** J Algebra 75(1):233–260, 1982.

Carlson C. R., Arora A. K., Carlson M. M., **The Application of Functional Dependency Theory to Relational Databases.** Computer J 25(1):68–73, 1982.

Chang G. J., Hwang F. K., Lin S., **Group-Testing With Two Defectives.** Discr App M 4(2):97–102, 1982.

Cleveland W. S. et al., **Graphical Methods for Seasonal Adjustment.** J Am Stat A 77(377):52–62, 1982.

Conway J. H., Sloane N. J. A., **Fast Quantizing and Decoding Algorithms for Lattice Quantizers and Codes.** IEEE Info T 28(2):227–232, 1982.

Conway J. H., Parker R. A., Sloane N. J. A., **The Covering Radius of the Leech Lattice.** P Roy Soc A 380(1779):261–290, 1982.

Conway J. H., Sloane N. J. A., **Voronoi Regions of Lattices, 2nd Moments of Polytopes, and Quantization.** IEEE Info T 28(2):211–226, 1982.

Doshi B., **Optimal Switching Among a Finite Number of Markov Processes.** J Optim Th 35(4):581–610, 1981.

Fishburn P. C., **Monotonicity Paradoxes in the Theory of Elections.** Discr App M 4(2):119–134, 1982.

Fishburn J. P., Finkel R. A., **Quotient Networks.** IEEE Comput 31(4):288–295, 1982.

Fishburn P. C., **Restricted Thresholds for Interval Orders—A Case of Nonaxiomatizability by a Universal Sentence.** J Math Psyc 24(3):276–283, 1981.

Foschini G. J., **Equilibria for Diffusion Models of Pairs of Communicating Computers—Symmetric Case.** IEEE Info T 28(2):273–284, 1982.

Freed D. S., Shepp L. A., **A Poisson-Process Whose Rate is a Hidden Markov Process.** Adv Appl P 14(1):21–36, 1982.

Hawkins D. T., Wagers R., **Online Bibliographic Search Strategy Development.** Online 6(3):12–19, 1982.

Heffler M. J., **Description of a Menu Creation and Interpretation System.** Software 12(3):269–281, 1982.

Heyman D. P., **On Ross Conjectures About Queues With Nonstationary Poisson Arrivals.** J Appl Prob 19(1):245–249, 1982.

Hopfield J. J., **Neural Networks and Physical Systems With Emergent Collective Computational Abilities.** P NAS Biol 79(8):2554–2558, 1982.

Hsuan F., Hwang F. K., Parnes M., **A Class of Selection Problems for Which More Sampling Is More Informative.** Biometrika 69(1):280–283, 1982.

Hunt J. W., **Tutorial Series. 15. Programming Languages.** Computer 15(4):70–88, 1982.

Hwang F. K., **Complete Balanced Howell Rotations for $8K+5$ Teams.** Discr Math 39(2):145–151, 1982.

Hwang F. K., **New Concepts in Seeding Knockout Tournaments.** Am Math Mo 89(4):235–239, 1982.

Jain A. K., **Estimation in Stratified Random Sampling—Adjustment for Changes in Strata Composition.** Ann I Stat 34(1):91–103, 1982.

Lien Y. E., **On the Equivalence of Database Models.** J ACM 29(2):333–362, 1982.

Lloyd S. P., **Least-Squares Quantization in PCM.** IEEE Info T 28(2):129–137, 1982.

Morris R. J. T., Kaufman J. S., **Performance Comparison of I/O Access Disciplines for Transaction-Processing Systems.** Computer J 25(1):74–83, 1982.

Newman D. J., **The Hexagon Theorem.** IEEE Info T 28(2):137–139, 1982.

Papadimitriou C. H. et al., **The Complexity of Restricted Spanning Tree Problems.** J ACM 29(2):285–309, 1982.

Pruzansky S., Tversky A., Carroll J. D., **Spatial Versus Tree Representations of Proximity Data.** Psychometri 47(1):3–24, 1982.

Rosenthal R. W., **A Model of Far-Sighted Electoral Competition.** Math Soc SC 2(3):289–297, 1982.

Sethi R., **Useless Actions Make a Difference—Strict Serializability of Database Updates.** J ACM 29(2):394–403, 1982.

Simen D., **RK Actions on Manifolds.** Am J Math 104(1):1–7, 1982.

Topkis D. M., **A Cutting-Plane Algorithm With Linear and Geometric Rates of Convergence.** J Optim Th 36(1):1–22, 1982.

Whitt W., **Existence of Limiting Distributions in the GI/G/S Queue.** Math Oper R 7(1):88–94, 1982.

Whitt W., **On the Heavy-Traffic Limit-Theorem for GI/G/Infinity Queues.** Adv Appl P 14(1):171–190, 1982.

ENGINEERING

Antler M., Sproles E. S., **Effect of Fretting on the Contact Resistance of Palladium.** IEEE Compon 5(1):158–166, 1982.

Auston D. H., Smith P. R., **Picosecond Optical Electronics for High-Speed Instrumentation.** Laser Focus 18(4):89–93, 1982.

Bayruns R. J., Suciu P. I., Wittwer N. C., Fraser D. L., Fuls E. N., Kushner R. A., Ashley F. R., Gere E. A., **A Fine-Line NMOS IC for Raster-Scan Control of a 500-MHz Electron-Beam Deflection System.** IEEE Device 29(4):737–744, 1982.

Buck T. M. et al., **Round Robin Comparison of Low-Energy Ion Scattering by ESA, Time-of-Flight, Stripping Technique and Computer Simulation.** Nucl Instru 194(1–3):649–653, 1982.

Cherin A. H., Head E. D., Lovelace C. R., Gardner W. B., **Selection of Mandrel Wrap Mode Filters for Optical Fiber Loss Measurements.** Fiber In Op 4(1):49–65, 1982.

Cline T. W., Jander R. B., **Wavefront Aberration Measurements on Grin-Rod Lenses.** Appl Optics 21(6):1035–1041, 1982.

Dasgupta S., **Contact Force Analysis of Slotted Beam Connectors.** IEEE Compon 5(1):153–158, 1982.

Dasgupta S., Kohl R. W., **Cutting Force Analysis of Split Beam Connectors.** IEEE Compon 5(1):180–185, 1982.

Easton R. L., Hutchison P. T., Kolor R. W., Mondello R. C., Muise R. W., **TASI-E Communications System.** IEEE Commun 30(4):803–807, 1982.

Furuya K., Miller B. I., Coldren L. A., Howard R. E., **Novel Deposit Spin Wave-Guide Interconnection (DSWI) Technique for Semiconductor Integrated-Optics.** Electr Lett 18(5):204–205, 1982.

Gaarder N. T., Slepian D., **On Optimal Finite-State Digital Transmission Systems.** IEEE Info T 28(2):167–186, 1982.

Gray E. W., Harrington D. J., **Surface Topography of Printed Wiring Boards and Its Effect on Flashover.** IEEE Compon 5(1):142–146, 1982.

Ibbotson D. E., Flamm D. L., **Chemical and Discharge Effects in Plasma Etching With Freons and Other Electronegative Gases.** IEEE El Ins 17(2):163–167, 1982.

Lanzerotti L. J., Meloni A., Medford L. V., Gregori G. P., **Induction in a Transatlantic Cable at Periods Between 20 Minutes and One Day.** Geophys R L 9(4):439–441, 1982.

Leamy H. J., **Laser Processing in Silicon Microelectronics Technology.** IEEE Compon 5(1):112–117, 1982.

Lum R. M., Feinstein L. G., **Thermal-Degradation of Polymers for Molded Integrated-Circuit (IC) Devices—The Effect of a Flame-Retardant.** ACS Symp S 1982(184):213–232, 1982.

Manzione L. T., Paek U. C., Tu C. F., Gillham J. K., **Characterization of Polymer-Coated Optical Fibers Using a Torsion Pendulum.** J Appl Poly 27(4):1301–1311, 1982.

Nahory R. E., Leheny R. F., **In0.53Ga0.47As Field-Effect Transistor (FETS) and PIN-FETS.** P Soc Photo 272:32–35, 1981.

Nelson R. J., **Long-Wavelength Lasers for Optical Communications.** P Soc Photo 269:13–16, 1981.

Patel C. K. N., **Potential and Application of Infrared Optical Fibers.** P Soc Photo 266:22–30, 1981.

Runge P. K., **High-Capacity Optical-Fiber Undersea Cable System.** P Soc Photo 266:86–92, 1981.

Tsong I. S. T., Tolk N. H., Buck T. M., Kraus J. S., Pian T. R., Kelly R., **Outer-Shell Electronic Processes in Ne+ Collisions With a Ni(110) Surface.** Nucl Instru 194(1–3):655–658, 1982.

Tyson J. A., Lee R. W., **Charge-Coupled Device (CCD) Imaging Polarimeter.** P Soc Photo 290:144–149, 1981.

Wagner R. E., Sandahl C. R., **Interference Effects in Optical Fiber-Connections.** Appl Optics 21(8):1381–1385, 1982.

Wilson L. O., **Numerical Simulation of Gate Oxide Thinning in MOS Devices.** J Elchem SO 129(4):831–837, 1982.

Zacharias A., **X-Ray Lithography for Integrated-Circuit Development and Manufacturing.** IEEE Compon 5(1):118–121, 1982.

MANAGEMENT/ECONOMICS

Fishburn, P. C., **An Axiomatic Characterization of Skew-Symmetric Bilinear Functionals, With Applications to Utility-Theory.** Econ Lett 8(4):311–313, 1981.

PHYSICAL SCIENCES

Ahlers G. et al., **Nonlinear Renormalization-Group Analysis of the Thermal Conductivity of He-4 for Tau Greater-than-or-Equal-to-Tau-Lambda.** Phys Rev B 25(5):3136–3167, 1982.

Anderson P. W., Alpar M. A., Pines D., Shaham J., **The Rheology of Neutron Stars Vortex-Line Pinning in the Crust Superfluid.** Phil Mag A 45(2):227–238, 1982.

Antler M., Preece C. M., Kaufmann E. N., **The Effect of Boron Implantation on the Sliding Wear and Contact Resistance of Palladium, 60Pd40Ag, and a CuNiSn Alloy.** IEEE Compon 5(1):81–85, 1982.

Armentrout P. B. et al., **Reaction of Cr+, Mn+, Fe+, Co+, and Ni+ With O-2 and N2O—Examination of the Translational Energy-Dependence of the Cross-Sections of Endothermic Reactions.** J Chem Phys 76(5):2449–2457, 1982.

Aumiller G. D., **Broadly Tunable Near IR CW Dye-Laser Using Propylene Carbonate as a Solvent.** Opt Commun 41(2):115–116, 1982.

Azbel M. Y., **Random Elastic-Scattering—Long-Range. Correlation and Localization.** Phys Rev B 25(2):849–862, 1982.

Bachelet G. B., Schluter M., **Relativistic Norm-Conserving Pseudopotentials.** Phys Rev B 25(4):2103–2108, 1982.

Bachelet G. B., Tanner C., Schluter M., **Static Atomic Polarizabilities From Norm-Conserving Pseudopotentials.** Phys St S-B 110(1):313–322, 1982.

Bally J., Langer W. D., **Isotope-Selective Photodestruction of Carbon-Monoxide.** Astrophys J 255(1):143–148, 1982.

Bally J., Scoville N. Z., **Structure and Evolution of Molecular Clouds Near H II Regions. 2. The Disk Constrained H II Region, S106.** Astrophys J 255(2):497–509, 1982.

Baraff G. A., Kane E. D., Schluter M., **Enfeebled Oxygen Bonding and Metastability in GaP-O.** Phys Rev B 25(2):548–560, 1982.

Barker R. A., Mayer T. M., Burton R. H., **Surface-Composition and Etching of III-V Semiconductors in Cl-2 Ion-Beams.** Appl Phys L 40(7):583–586, 1982.

Beck S. M., Brus L. E., **Transient Intermediates in the Photo Fries Isomerization of Phenyl Acetate via Spontaneous Raman-Spectroscopy.** J Am Chem S 104(7):1805–1808, 1982.

Bedzyk M. J. et al., **X-Ray Standing Wave Analysis for Bromine Chemisorbed on Silicon.** J Vac Sci T 20(3):634–637, 1982.

Bethea C. G. et al., **Opto-Electronic Picosecond Sampling System Utilizing a Modulated Barrier Photo-Diode.** Appl Phys L 40(7):591–594, 1982.

Bokor J., Freeman R. R., Cooke W. E., **Autoionization-Pumped Laser.** Phys Rev L 48(18):1242–1245, 1982.

Bondybey V. E. et al., **Infrared-Spectra and Isomerization of CHNO Species in Rare-Gas Matrices.** J Mol Spect 92(2):431–442, 1982.

Bondybey V. E., English J. H., **Laser Excitation Spectra and Lifetimes of Pb-2 and Sn-2 Produced by YAG Laser Vaporization.** J Chem Phys 76(5):2165–2170, 1982.

Bovey F. A., **The C-13 NMR-Study of Polymer Structure and Dynamics.** Pur A Chem 54(3):559–568, 1982.

Bridges T. J., **Single-Crystal Infrared Fibers.** P Soc Photo 266:69–71, 1981.

Brown B. L., Mills A. P., Tyson J. A., **Real-Time Analysis System for a Gravitational-Wave Antenna.** Rev Sci Ins 53(4):479–484, 1982.

Cais R. E., Spencer C. P., **The Dechlorination of Polyvinyl-Chloride by Zinc and Tributyl Tin Hydride—Characterization of the Product Microstructures by C-13 NMR.** Eur Polym J 18(3):189–198, 1982.

Canter K. F., Mills A. P., **Slow Positron Beam Design Notes.** Can J Phys 60(4):551–557, 1982.

Capasso F., Williams G. F., **A Proposed Hydrogenation Nitridization Passivation Mechanism for GaAs and Other III-V Semiconductor Devices, Including InGaAs Long Wavelength Photodetectors.** J Elchem So 129(4):821–824, 1982.

Chabal Y. J. et al., **Laser Quenched and Impurity Induced Metastable Si(111)1X1 Surfaces.** J Vac Sci T 20(3):763–769, 1982.

Chandan H. C., Kalish D., **Temperature-Dependence of Static Fatigue of Optical Fibers Coated with a UV-Curable Polyurethane Acrylate.** J Am Ceram 65(3):171–173, 1982.

Chen C. Y. et al., **GaAs AlXGa1-X As Depletion Stop Photo-Transistor Grown by Molecular-Beam Epitaxy.** Appl Phys L 40(6):510–512, 1982.

Chen C. Y. et al., **Quasi-Schottky Barrier Diode on N-Ga-0.47In-0.53 as Using a Fully Depleted P+-Ga-0.47In-0.53 As Layer Grown by Molecular-Beam Epitaxy.** Appl Phys L 40(5):401–403, 1982.

Chen H. S., **On Mechanisms of Structural Relaxation in a $Pd_{48}Ni_{32}P_{20}$ Glass.** J Non-Cryst 46(3):289–305, 1981.

Chen H. S., Aust K. T., Waseda Y., **Structural Investigation of Amorphous Fe-Zr, Co-Zr and Ni-Zr Alloys With Low Zirconium Concentration.** J Non-Cryst 46(3):307–319, 1981.

Cheng K. Y. et al., **Measurement of the Gamma-L Separation in Ga-0.47In-0.53 As by Ultraviolet Photoemission.** Appl Phys L 40(5):423–425, 1982.

Chu S., Mills A. P., **Excitation of the Positronium $1^3S_1 \rightarrow 2^3S_1$ Two-Photon Transition.** Phys Rev L 48(19):1333–1337, 1982.

Chu S. N. G., **Screw Dislocation in a Two-Phase Isotropic Thin Film.** J Appl Phys 53(4):3019–3023, 1982.

Chui S. T., **Grain-Boundary Theory of Melting in Two Dimensions.** Phys Rev L 48(14):933–935, 1982.

Cladis P. E., Goodby J. W., **Pressure Study of a Hexatic-B and Crystal B-Phase.** Molec Cryst 72(9–10):307–312, 1982.

Cladis P. E., Goodby J. W., **Pressure Temperature Phase Diagram of Some Tilted Smectic Phases.** Molec Cryst 72(9–10):313–317, 1982.

Cohen E., Sturge M.D., **Fluorescence Line Narrowing, Localized Exciton-States, and Spectral Diffusion in the Mixed Semiconductor CDSXSE1-X.** Phys Rev B 25(6):3828–3840, 1982.

Cohen L. G., Mammel W. L., Lumish S., **Tailoring the Shapes of Dispersion Spectra to Control Bandwidths in Single-Mode Fibers.** Optics Lett 7(4):183–185, 1982.

Cohen M. L., Heine V., Phillips J. C., **The Quantum-Mechanics of Materials.** Sci Am 246(6):82+, 1982.

Coldren L. A. et al., **Combined Dry and Wet Etching Techniques to Form Planar (011) Facets in GaInAsP/InP Double Heterostructures.** Electr Lett 18(5):235–237, 1982.

Craighead H. G., Howard R. E., Liao P. F., Tennant D. M., Sweeney J. E., **Textured Germanium Optical Storage Medium.** Appl Phys L 40(8):662–664, 1982.

Craighead H. G., Howard R. E., Sweeney J. E., Tennant D. M., **Textured Surfaces— Optical Storage and Other Applications.** J Vac Sci T 20(3):316–319, 1982.

Dahlberg, S. C. et al., **Photochromic Switching in Semiconducting Films of Triphenylformazan.** J Chem Phys 76(5):2731–2733, 1982.

Dautremont-Smith W. C., **Transition-Metal Oxide Electrochromic Materials and Displays—A Review. 2. Oxides With Anodic Coloration.** Displays 3(2):67–80, 1982.

Davis G. T. et al., **Structural and Dielectric Investigation on the Nature of the Transition in a Copolymer of Vinylidene Fluoride and Trifluoroethylene (52/ 48 Mol Percent).** Macromolec 15(2):329–333, 1982.

Dicenzo S. B., Basu S., Wertheim G. K., Buchanan D. N., Fischer J. E., **In-Plane Charge-Distribution in Potassium-Intercalated Graphite.** Phys Rev B 25(2): 620–626, 1982.

Digregorio S. et al., **An Electron-Spin-Resonance and Optical Study of V4+ in Zircon-Type Crystals.** J Chem Phys 76(6):2931–2937, 1982.

Dingle R., Weisbuch C., Stormer H. L., Morkoc H., Cho A. Y., **Characterization of High-Purity GaAs Grown by Molecular-Beam Epitaxy.** Appl Phys L 40(6):507–510, 1982.

Duguay M. A., Damen T. C., **Picosecond Measurement of Spontaneous and Stimulated Emission From Injection Lasers.** Appl Phys L 40(8):667–669, 1982.

Dutta N. K., Nelson R. J., **Light Saturation of InGaAsP-InP LEDs.** IEEE J Q El 18(3):375–381, 1982.

Ekholm D. T., Bonyhard P. I., Muehlner D. J., Nelson T. J., **NDRO Detector for Ion-Implanted Bubble Devices.** J Appl Phys 53(3):2525–2527, 1982.

Farrow L. A., Richton R. E.,, **Photo-Acoustic Applications to Chemical Kinetics.** P Soc Photo 286:18–23, 1981.

Fisher M. E., Fisher D. S., **Wall Wandering and the Dimensionality Dependence of the Commensurate-Incommensurate Transition.** Phys Rev B 25(5):3192–3198, 1982.

Fujimura O., Haskin M. E., **X-Ray Microbeam System With a Discrete-Spot Target.** P Soc Photo 273:244–253, 1981.

Ghate B. B., Holmes R. J., Pass C. E., **Environmentally Induced Permeability Degradation in Ferrite Powders.** Am Ceram S 61(4):484+, 1982.

Gibbs H. M. et al., **Optical Bistable Devices—The Basic Components of All-Optical Systems.** P Soc Photo 269:75–80, 1981.

Glarum S. H., Marshall J. H., **The AC Response of Nickel-Oxide Electrode Films.** J Elchem So 129(3):535–542, 1982.

Gold A., Allen S. J., Wilson B. A., Tsui D. C., **Frequency-Dependent Conductivity of a Strongly Disordered Two-Dimensional Electron-Gas.** Phys Rev B 25(6):3519–3528, 1982.

Goldfarb R. B., Rao K. V., Chen H. S., Patton C. E., **Further Evidence for a Spin-Glass Phase-Transition in Amorphous Fe-Mn-P-B-Al Alloys.** J Appl Phys 53(3):2217–2219, 1982.

Gossard A. C. et al., **Electric Properties of Unipolar GaAs Structures with Ultrathin Triangular Barriers.** Appl Phys L 40(9):832–833, 1982.

Gossard A. C., Brown W., Allyn C. L., Weigmann W., **Molecular-Beam Epitaxial Growth and Electrical Transport of Graded Barriers for Nonlinear Current Conduction.** J Vac Sci T 20(3):694–700, 1982.

Graedel T. E., McRae J. E., **Total Organic-Component Data—A Study of Urban Atmospheric Patterns and Trends.** Atmos Envir 16(5):1119–1132, 1982.

Green M. L., Sherwood R. C., Wong C. C., **Powder-Metallurgy Processing of CrCoFe Permanent-Magnet Alloys Containing 5–25 Wt.-Percent Co.** J Appl Phys 53(3):2398–2400, 1982.

Gregori G. P. et al., **Electrical Conductivity Structure in the Lower Crust.** Geophys Sur 4(4):467–499, 1982.

Greywall D. S., Busch P.A., **He-3-Melting-Curve Thermometry.** J L Temp Ph 46(5–6):451–465, 1982.

Griffiths J. E., Espinosa G. P., Remeika J. P., Phillips J. C., **Reversible Quasi-Crystallization in GeSe₂ Glass.** Phys Rev B 25(2):1272–1286, 1982.

Guelin M., Langer W. D., Wilson R.W., **The State of Ionization in Dense Molecular Clouds.** Astron Astr 107(1):107–127, 1982.

Gyorgy E. M., Lecraw R. C., Luther L. C., **Rapid Diffusion in Garnets Doped with Si, Ge, or Ca.** J Appl Phys 53(3):2492–2494, 1982.

Harmon B. N., Weber W., Hamann D. R., **Total-Energy Calculations for Si With a 1st-Principles Linear Combination of Atomic Orbitals Method.** Phys Rev B 25(2):1109–1115, 1982.

Harris T. D., **High-Sensitivity Spectrophotometry.** Analyt Chem 54(6):A741, 1982.

Hasegawa A., Sato T., **Existence of a Negative Potential Solitary-Wave Structure and Formation of a Double-Layer.** Phys Fluids 25(4):632–635, 1982.

Hauser J. J., Rodgers J. W., **Variable Range Hopping in Al Implanted Sapphire.** Appl Phys L 40(8):707–708, 1982.

Havener C. C. et al., **Observation of a Large Electric-Dipole Moment Produced in Electron-Transfer Collisions of H+ on He.** Phys Rev L 48(14):926–929, 1982.

Herriott D. R., **Electron-Beam Lithography.** J Vac Sci T 20(3):781–785, 1982.

Hodeau J. L., Marezio M., Remeika J. P., Chen C. H., **Structural Distortion in the Primitive Cubic Phase of the Superconducting Magnetic Ternary Rare-Earth Rhodium Stannides.** Sol St Comm 42(2):97–102, 1982.

Jean Y. C., DiSalvo F. J., **Positron Lifetimes of the 2H-TAsE2 Crystal as a Function of Temperature.** Molec Cryst 81(1–4):149–154, 1982.

Johnson L. F. et al., **Planarization of Patterned Surfaces by Ion-Beam Erosion.** Appl Phys L 40(7):636–638, 1982.

Jones W. R., **Computer Analysis of Arrott Plots of Compositionally Modulated Materials.** J Appl Phys 53(3):2442–2444, 1982.

Kelleher P. G., Wentz R. P., Falcone D. R., **Hydrolysis of Poly(butylene Terephthalate).** Polym Eng S 22(4):260–264, 1982.

Kelso S. M., **Energy-Dependent and Stress-Dependent Hole Masses in Germanium and Silicon.** Phys Rev B 25(2):1116–1125, 1982.

Keramidas V. G., Temkin H., Bonner W. A., **Growth of InP and InGaAsP (EG-Greater-Than-or-Equal-to-1.15EV) Layers by Liquid-Phase Epitaxy Under Phosphorus Overpressure.** Appl Phys L 40(8):731–733, 1982.

Khanarian G., **The Non-Linear Dielectric Effect of Alpha, Omega-Dibromoalkanes.** J Chem Phys 76(6):3186–3188, 1982.

Kodama Y., Ablowitz M. J., Satsuma J., **Direct and Inverse Scattering Problems of the Nonlinear Intermediate Long-Wave Equation.** J Math Phys 23(4):564–576, 1982.

Kolodner P., Tyson J. A., **Microscopic Fluorescent Imaging of Surface-Temperature Profiles With 0.01°C Resolution.** Appl Phys L 40(9):782–784, 1982.

Kwan J., Linke R. A., **Circumstellar Molecular Emission of Evolved Stars and Mass Loss—IRC+10216.** Astrophys J 254(2):587–593, 1982.

Kwo J., Wertheim G. K., Gurvitch M., Buchanan D. N., **X-Ray Photoemission Spectroscopy Study of Surface Oxidation of Nb/Al Overlayer Structures.** Appl Phys L 40(8):675–677, 1982.

Lamola A. A., Flores J., **Effect of Buffer Viscosity on the Fluorescence of Bilirubin Bound to Human-Serum Albumin.** J Am Chem S 104(9):2530–2534, 1982.

Lang D. V., Cohen J. D., Harbison J. P., Sergent A. M., **Observation of Photoinduced Changes in the Bulk-Density of GaP States in Hydrogenated Amorphous Silicon.** Appl Phys L 40(6):474–476, 1982.

Lasser R., Smith N. V., **Empirical Band Calculations of the Optical Properties of D-Band Metals.3. Rh and Pd.** Phys Rev B 25(2):806–814, 1982.

Laughlin R. B., **Helium Diffraction From the GaAs(110) Surface and the Generation of Helium-Surface Potentials.** Phys Rev B 25(4):2222–2247, 1982.

Lazarov C., Shulman H., **Obstructions to Foliation-Preserving Vector Fields** J Pure Appl 24(2):171–178, 1982.

Leamy H. J. et al., **Direct Observation of Grain-Boundary Effects in Polycrystalline Silicon Thin-Film Transistors.** Appl Phys L 40(7):598–600, 1982.

Lecraw R. C., Luther L. C., Gyorgy E. M., **Growth-Induced Anisotropy and Damping Versus Temperature in Narrow Linewidth, 1-μm YLG(BI, CA, SI) Bubble Films.** J Appl Phys 53(3):2481–2482, 1982.

Lemons R. A. et al., **Laser Crystallization of Si Films on Glass.** Appl Phys L 40(6):469–471, 1982.

Lemons R. A., Bosch M. A., **Microscopy of Si Films During Laser Melting.** Appl Phys L 40(8):703–706, 1982.

Loponen M.T. et al., **Measurements of the Time-Dependent Specific Heat of Amorphous Materials.** Phys Rev B 25(2):1161–1173, 1982.

Lovinger A. J. et al., **Crystalline Forms in a Copolymer of Vinylidene Fluoride and Trifluoroethylene (52/48 Mol-Percent).** Macromolec 15(2):323–328, 1982.

Luther L. C., Lecraw R. C., Dillon J. F., Wolfe R., **An Improved BIYIG Composition for One-Micron Bubbles.** J Appl Phys 53(3):2478–2480, 1982.

Lyons K. B. et al., **Incommensurate Structural Phase-Transition in $BaMnF_4$—Light-Scattering From Phasons.** Phys Rev B 25(3):1791–1804, 1982.

Maan J. C., Englert T., Tsui D. C., Gossard A. C., **Observation of Cyclotron-Resonance in the Photoconductivity of Two-Dimensional Electrons.** Appl Phys L 40(7):609–610, 1982.

Marcus M. A., Goodby J. W., **Cholesteric Pitch and Blue Phases in a Chiral-racemic Mixture.** Molec Cryst 72(9–10):297–305, 1982.

Mayer T. M., Barker R. A., **Reactive Ion-Beam Etching With CF_4—Characterization of a Kaufman Ion-Source and Details of SiO_2 Etching.** J Elchem So 129(3):585–591, 1982.

MacCraith B. D., Glynn T. J., Imbusch G. F., Remeika J. P., Wood D. L., **Exchange Interactions in Nearest-Neighbor Cr^{3+} Ion-Pairs in $LiGa_5O_8:Cr^{3+}$.** Phys Rev B 25(6):3572–3575, 1982.

Marcus M., **Crystallography of Blue Phase 1 and Phase 2.** Phys Rev A 25(4):2272–2275, 1982.

Marcus M., **Relative Order Parameters of Cholesteric and Blue Phases.** Phys Rev A 25(4):2276–2280, 1982.

Matheson T. G., Higgins R.J., **Tunneling in Tilted Si Inversion Layers.** Phys Rev B 25(4):2633–2644, 1982.

Mattheiss L. F., Weber W., **Electronic Structure of Cubic V_3Si and Nb_3Sn.** Phys Rev B 25(4):2248–2269, 1982.

Mcafee S. R., Lang D. V., Tsang W. T., **Observation of Deep Levels Associated with the GaAs AlXGa1-X As Interface Grown by Molecular-Beam Epitaxy.** Appl Phys L 40(6):520–522, 1982.

Miller D. A. B., **Bistable Optical Devices—Physics and Operating Characteristics.** Laser Focus 18(4):79–84, 1982.

Miller R. C., Gossard A. C., Tsang W. T., Munteanu O., **Extrinsic Photo-Luminescence From GaAs Quantum Wells.** Phys Rev B 25(6):3871–3877, 1982.

Mitchell J. W., **Trace Analysis and Ultrapurification of Materials for Optical Wave-Guide Technology.** Pur A Chem 54(4):819–834, 1982.

Mitchell J. W., **State-of-the-Art Contamination Control Techniques for Ultra-trace Elemental Analysis.** J Rad Chem 69(1–2):47–105, 1982.

Mollenauer L. F., Stolen R. H., **Solitons in Optical Fibers.** Laser Focus 18(4):193–198, 1982.

Mucha J. A., **Tunable Diode-Laser Measurements of Water-Vapor Line Parameters in the 6-μm Spectral Region.** Appl Spectr 36(2):141–147, 1982.

Nassau K., Chadwick D. L., **Glass-Formation in the System GeO_2-Bi_2O_3-Tl_2O.** J Am Ceram 65(4):197–202, 1982.

Odagaki T., Lax M., **Hopping Conduction in Positionally Disordered Chains.** Phys Rev B 25(4):2301–2306, 1982.

Odagaki T., Lax M., **Low-Frequency Hopping Conductivity of Random Chains.** Phys Rev B 25(4):2307–2309, 1982.

Osheroff D. D., **Nuclear Magnetic Ordering in Solid He-3.** J Appl Phys 53(3):1843–1844, 1982.

Paalanen M. A. et al., **Stress Tuning of the Metal-Insulator Transition at Millikelvin Temperatures.** Phys Rev L 48(18):1284–1287, 1982.

Papaefthymiou G. C. et al., **Anti-Ferromagnetic Exchange Interactions in [Fe₄S₄(SR)₄]²⁻, ³⁻Clusters.** Inorg Chem 21(5):1723–1728, 1982.

Pearson D. S., Raju V. R., **Configurational and Viscoelastic Properties of Branched Polymers.** Macromolec 15(2):294–298, 1982.

Pei S. S., **Logic Delays of 5-μm Current-Switched Josephson Gates.** Appl Phys L 40(8):739–741, 1982.

Pessa M., Lindroos M., Asonen H., **Photoemission Spectra and Band Structures of D-Band Metals. 9. Triangulation Analysis of Angle-Resolved Data on Copper.** Phys Rev B 25(2):738–744, 1982.

Phillips J. C., **Localization of Octahedral-Tetrahedral Coordination Energy Differences with S-P Bonding.** Phys Rev B 25(4):2310–2314, 1982.

Pian T. R., Tolk N., Kraus J., Traum M. M., Tully J., Collins W. E., **Electron Stimulated Desorption of Excited Alkali Atoms From Alkali-Halide Surfaces.** J Vac Sci T 20(3):555–558, 1982.

Pitetti R. C., Keller H. N., Morabito J. M., **High-Pressure Steam Stabilization of Tantalum Thin-Film Resistors.** Thin Sol Fi 87(1):1–11, 1982.

Poate J. M., **Diffusion and Reactions in Gold-Films.** Sol St Tech 25(4):227–234, 1982.

Preece C. M., Kaufmann E. N., **The Effect of Boron Implantation on the Cavitation Erosion Resistance of Copper and Nickel.** Corros Sci 22(4):267–281, 1982.

Purcell F. J. et al., **Compositional Analysis of a Terpolymer Photoresist by Raman-Spectroscopy.** ACS Symp S 1982(184):45–59, 1982.

Raghavachari K., **An Abinitio Study of the Harmonic Force-Field and Vibrational Frequencies of Thionylimide—Basis Set and Electron Correlation Effects.** J Chem Phys 76(7):3668–3672, 1982.

Raines R. D., Heffner W. R., Cladis P. E., Marcus M., **The Dielectric-Constant of a Cyanophenyl-Thiobenzoate.** Molec Cryst 72(9–10):263–269, 1982.

Reichmanis E., Wilkins C. W., **Poly(Methyl Methacrylate-CO-3-Oximino-2-Butanone Methacrylate-CO-Methacrylonitrile)—A Deep-UV Photoresist.** ACS Symp S 1982(184):29–43, 1982.

Reinhart F. K., **Prospects of Monolithic Optical Integration.** P Soc Photo 272:66–75, 1981.

Reynolds A. H., **Kinetics and Temperature-Dependence of Carboxymyoglobin Ligand Photo-Dissociation.** Biophys J 38(1):15–18, 1982.

Rice C. E., Jackel J. L., **HNbO₃ and HTaO₃—New Cubic Perovskites Prepared From LiNbO₃ and LiTaO₃ Via Ion-Exchange.** J Sol St Ch 41(3):308–314, 1982.

Rummel H., Cohen R. L., Gutlich P., West K. W., **Ni-61 Mossbauer Measurements of Nickel Microprecipitates Produced in LaNi₅ by Cyclic Hydrogen Absorption and Desorption.** Appl Phys L 40(6):477–479, 1982.

Schwartz G. P. et al., **Influence of Interface Composition on Al-GaAs Schottky Barriers.** J Vac Sci T 20(3):674–679, 1982.

Shah J. et al., **Hot-Carrier Relaxation in P-InO.53Ga0.47As.** Appl Phys L 40(6):505–507, 1982.

Shank C. V. et al., **Compression of Femtosecond Optical Pulses.** Appl Phys L 40(9):761–763, 1982.

Slusher R. E., Surko C. M., Schuss J. J., Parker R. R., Hutchinson I. H., Overskei D., Scaturro L. S., **Study of Driven Lower-Hybrid Waves in the Alcator A Tokamak Using CO-2 Laser Scattering.** Phys Fluids 25(3):457–472, 1982.

Smith N. V., Lasser R., Chiang S., **Empirical Band Calculations of the Optical Properties of D-Band Metals. 4. Optical-Absorption, Photoemission, and Magneto-Optical Properties of Ferromagnetic Nickel.** Phys Rev B 25(2):793–805, 1982.

Smith N. V., Woodruff D. P., **Influence of k-Conservation in Ultraviolet Isochromat Spectra From Ni.** Phys Rev B 25(5):3400–3403, 1982.

Smith N. V., Woodruff D. P., **Surface Spectroscopies with Synchrotron Radiation.** Science 216(4544):367–372, 1982.

Snell R. L., Langer W. D., Frerking M. A., **Determination of Density Structure in Dark Clouds From CS Observations.** Astrophys J 255(1):149–159, 1982.

Stillinger F. H., Weber T. A., David C. W., **Application of the Polarization Model to the Study of Phosphoric-Acid Media.** J Chem Phys 76(6):3131–3143, 1982.

Stillinger F. H., Weber T. A., **Polarization Model Study of Isotope Effects in the**

Gas-Phase Hydronium-Hydroxide Neutralization Reaction. J Chem Phys 76(8):4028-4036, 1982.

Stillwagon L., **Radiation Degradation and Film Solubility Rates of Poly(Butene-1-Sulfone).** ACS Symp S 1982(184):19-27, 1982.

Stormer H. L., Gossard A. C., Wiegmann W., **Observation of Intersubband Scattering in a Two-Dimensional Electron-System.** Sol St Comm 41(10):707-709, 1982.

Szmanda C. R., McAfee K. B., Hozack R. S., **Nonradiative Charge-Exchange Between N+ and CO_2.** J Phys Chem 86(7):1217-1221, 1982.

Tamari N. et al., **High- to Low-Threshold Crescent InGaAsP Mesa-Substrate Buried Heterojunction Lasers.** Electr Lett 18(4):177-178, 1982.

Temkin H. et al., **Optically Induced Catastrophic Degradation in InGaAsP/InP Layers.** Appl Phys L 40(7):562-565, 1982.

Tompkins H. G., Frank R. A., Allara D. L., **Sputter Yield Measurements on Simulated Adventitious Carbonaceous Contamination.** J Vac Sci T 20(3):400-402, 1982.

Tompkins H. G., Augis J. A., **The Oxidation of Cobalt in Air From Room Temperature to 467°C.** Oxid Metal 16(5-6):355-369, 1981.

Tonelli A. E., **Conformational Characteristics of Polyvinyl Bromide and Ethylene Vinyl Bromide Copolymers.** Macromolec 15(2):290-293, 1982.

Tsang W. T., **Reliable (AlGa)As DH Lasers Grown by Molecular-Beam Epitaxy for Optical Communication Systems.** P Soc Photo 269:17-24, 1981.

Tung R. T., Bean J. C., Gibson J. M., Poate J. M., Jacobson D. C., **Growth of Single-Crystal $CoSi_2$ on Si (111).** Appl Phys L 40(8):684-686, 1982.

Valdes F., Welch W. J., Haber D., **The Jovian Ammonia Abundance From Interferometric Observations of Limb Darkening at 3.4 mm.** Icarus 49(1):17-26, 1982.

Vanuitert, L. G., **Melting-Point Relations for Simple Halides, Oxides, and Chalcides.** J Appl Phys 53(4):3034-3039, 1982.

Wagner A., **The Hydrodynamics of Liquid-Metal Ion Sources.** Appl Phys L 40(5):440-442, 1982.

Wannier P. G., Penzias A. A., Jenkins E. B., **The CO-12/CO-13 Abundance Ratio Toward Zeta-Ophiuchi.** Astrophys J 254(1):100-107, 1982.

Washington, M. A., Fulton I. A., **Observation of Flux Trapping Threshold in Narrow Superconducting Thin-Films.** Appl Phys L 40(9):848-850, 1982.

Weber T. A. et al., **Reactive Collisions of H_3O+ and OH- Studied With the Polarization Model.** J Phys Chem 86(8):1314-1318, 1982.

Weber W., Mattheiss, L. F., **Electronic Structure of Tetragonal Nb_3Sn.** Phys Rev B 25(4):2270-2284, 1982.

Wertheim G. K., Dicenzo S. B., Buchanan D. N. **Core-Electron Spectroscopy of Adsorbate Ions—Iodine On Ag(111).** Phys Rev B 25(5):3020-3025, 1982.

White J. C., Henderson D., **Tunable, 178-nm Iodine Anti-Stokes Raman Laser.** Optics Lett 7(5):204-206, 1982.

Wokaun A., Gordon J. P., Liao P. F., **Radiation Damping in Surface-Enhanced Raman-Scattering.** Phys Rev L 48(14):957-960, 1982.

Wright P. D., Joyce W. B., Craft D. C., **Electrical Derivative Characteristics of InGaAsP Buried Heterostructure Lasers.** J Appl Phys 53(3):1364-1372, 1982.

Yan M. F., Rhodes W. W., **Preparation and Properties of TiO_2 Varistors.** Appl Phys L 40(6):536-537, 1982.

Zellers E. T., Roedel R. J., Wudl F., **Organocopper Thin-Film Structures Exhibiting Threshold Switching With Short-Term Memory.** J Non Cryst 46(3):361-369, 1981.

Zipfel C. L., Saul R. H., Chin A. K., Keramidas V. G., **Competing Processes in Long-Term Accelerated Aging of Double Heterostructure Gal-xAlxAs Light-Emitting Diodes.** J Appl Phys 53(3):1781-1786, 1982.

SOCIAL AND LIFE SCIENCES

Friedman J. M. et al., **Ligation and Quaternary Structure Induced Changes in the Heme Pocket of Hemoglobin—A Transient Resonance Raman Study.** Biochem 21(9):2022-2028, 1982.

Ondrias M. R., Rousseau D. L., Simon S. R., **Resonance Raman Detection of Structural Dynamics At the Active-Site in Hemoglobin.** P Nas Biol 79(5):1511-1514, 1982.

Patel D. J., Pardi A., Itakura K., **DNA Conformation, Dynamics, and Interactions in Solution.** Science 216(4546):581–590, 1982.

Patel D. J. et al., **Right-Handed and Left-Handed DNA—Studies of B-DNA and Z-DNA by Using Proton Nuclear Overhauser Effect and P NMR.** P Nas Biol 79(5):1413–1417, 1982.

SPEECH AND ACOUSTICS

Atal B. S., **Predictive Coding of Speech at Low Bit Rates.** IEEE Commun 30(4):600–614, 1982.

Bias R. G. et al., **Generation(s) of Phonological Codes in Reading—A Reply.** Psychol B 91(2):369–371, 1982.

Crochiere R. E., Cox R. V., Johnston J. D., **Real-Time Speech Coding.** IEEE Commun 30(4):621–634, 1982.

Daumer W. R., **Subjective Evaluation of Several Efficient Speech Coders.** IEEE Commun 30(4):655–662, 1982.

Flanagan J. L., **Talking With Computers—Synthesis and Recognition of Speech by Machines.** IEEE Biomed 29(4):223–232, 1982.

Gilbert E. N. **Reverberation Between Concentric Spheres.** IEEE Acoust 30(2):162–166, 1982.

Goodman D. J., Nash R. D., **Subjective Quality of the Same Speech Transmission Conditions in Seven Different Countries.** IEEE Commun 30(4):642–654, 1982.

Myers C. S., Rabiner L. R., **An Automated Directory Listing Retrieval System Based on Recognition of Connected Letter Strings.** J Acoust So 71(3):716–727, 1982.

Shashaty A. J., **The Effective Lengths for Flow Noise of Hydrophones in a Ship-Towed Linear-Array.** J Acoust So 71(4):886–890, 1982.

Tartter V. C., **Vowel and Consonant Manipulations and the Dual Coding Model of Auditory Storage—A Re-Evaluation.** J Phonetics 10(2):217–223, 1982.

Worley R. D., Walker R. A., **Low-Frequency Ambient Ocean Noise and Sound Transmission Over a Thinly Sedimented Rock Bottom.** J Acoust So 71(4):863–870, 1982.

CONTENTS, OCTOBER 1982

Implementing and Testing New Versions of a Good 48-Bit Pseudo-random Number Generator
    C. S. Roberts

Some Extremal Markov Chains
    J. E. Mazo

Quality Evaluation Plan Using Adaptive Kalman Filtering
    M. S. Phadke

B.S.T.J. BRIEF

Low-Elevation-Angle Propagation Effects on COMSTAR Satellite Signals

By J. M. TITUS* and H. W. ARNOLD

I. INTRODUCTION

Little information exists on earth-space propagation at lower elevation angles. One earlier experiment[1] has shown greater fluctuation in signal levels over low-elevation paths. This signal fluctuation likely results from focusing and defocusing by inhomogeneities in the atmosphere's index of refraction caused by turbulence. The fluctuation increases at lower elevation angles, then, because the signal must pass through more atmosphere.

The opportunity existed during 1976 to make more low-elevation observations at 19 GHz as the COMSTAR satellites were placed into position. This paper describes the acquisition and analysis of the low-elevation propagation data. Results are presented showing the fluctuation intensity of the received signal at several elevation angles.

II. EXPERIMENT

Two satellites were launched carrying 19-GHz beacon transmitters, COMSTAR I in May 1976, and COMSTAR II in June 1976. As they were placed in their final positions, they drifted upward from the horizon at a rate of 1 to 2 degrees per day. Original data were taken at 19 GHz on Crawford Hill for elevation angles from 1 to 10 degrees above the horizon with a 3.7-meter diameter antenna and an interim receiver.[2] Signals received on vertical and horizontal polarizations (relative to the Crawford Hill horizon) were recorded on analog magnetic tape.

---

* This work was performed while Ms. Titus was a summer student.

The satellites were rotating slowly; therefore, the directional antenna on the satellites caused the received signal level to vary. There was very little variation over a period of a few minutes, however. Weather throughout the initial experiment was generally cloudy and overcast, but there was no significant precipitation. The 0.3-degree beamwidth of the Crawford Hill antenna precluded ground-reflected signals. Since both transmitter and receiver had excellent amplitude stability, atmospheric turbulence was the only reasonable source of the signal-amplitude fluctuations observed. These fluctuations occurred almost all the time, as contrasted with the more infrequent multipath fading observed on terrestrial paths.

On the analog magnetic tape, data samples were taken once every hour for ten consecutive minutes. For each 10-minute interval (corresponding to a particular elevation angle), three sets of 256 points, sampled at a rate of 5 points per second, were digitized and recorded under control of an HP 9830 calculator. Signal amplitudes for the two polarizations were sampled simultaneously. The three 51-second samples of digitized signals were taken from the beginning of the ten-minute run unless some readily apparent problem existed on the chart data.

III. RESULTS

After data samples were digitized from all magnetic tapes, an analysis was made to determine how elevation angle affected signal fluctuation. For each sample set, the mean and standard deviation of the received signal amplitude for each polarization and the correlation coefficient between the vertically and horizontally polarized signals were calculated.

Some sample sets were unusable because of low signal levels, so a method was devised to locate and delete them. It was assumed that the receiver noise level was the same as that existing later in the experiment, when the signal-to-noise ratio was approximately 46 dB in clear air. From this assumption a graph was constructed that gave, as a function of mean receiver output in volts, the standard deviation-to-mean ratio expected from receiver noise alone. Each sample set was checked and deleted if its fluctuation was not at least two standard deviations higher than that expected from receiver noise alone.

For all remaining sample sets, scatter plots of fluctuation (defined as the ratio of the standard deviation to the mean) vs. elevation angle were printed. Figure 1 shows an example for COMSTAR I using horizontal polarization. Results for the horizontal polarization from COMSTAR II and for the vertical polarization from both satellites were also plotted, and were very similar to the results shown. Multiple data exist
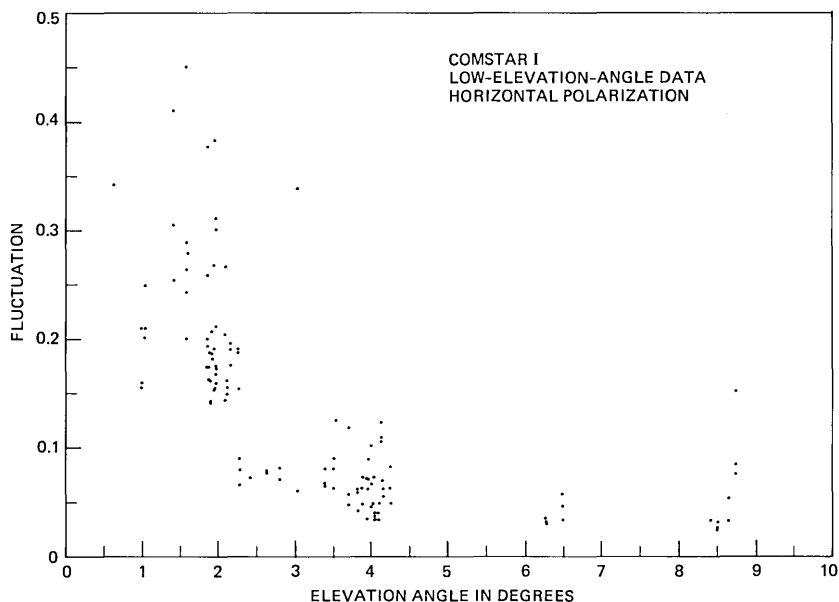
Fig. 1—19-GHz signal amplitude fluctuation vs. path elevation angle for COMSTAR I using horizontal polarization.

for certain elevation angles, because in those cases the satellites were at nearly the same elevation angles for more than one hour.

Figure 1 indicates that signal fluctuation increases dramatically as the path elevation angle decreases. A simple theory to explain this trend involves the notion that the strength of the fluctuation is dependent on the number of air masses through which the propagation path passes. The number of air masses is proportional to the integral of the density (kg/m³) of the atmosphere along the path. One air mass is defined as the density integral along a vertical path.

The number of air masses as a function of elevation angle was calculated in two ways: (i) by assuming that the atmosphere can be modeled as evenly distributed over a height up to nine km, and (ii) by modeling the atmosphere as six layers from altitudes of 0 to 30 km with different densities.[3] The latter was done for both evenly spaced layers (steps of 5 km/layer) and unevenly spaced layers (steps of 2, 3, 5, 6, 6 and 8 km/layer) to observe the effect of the higher density of the lower atmosphere at the very low angles. The results for the two methods are compared in Fig. 2 and show no significant differences. Therefore, the simpler method was used for the following results. Both methods depart radically from the cosecant angular dependence seen
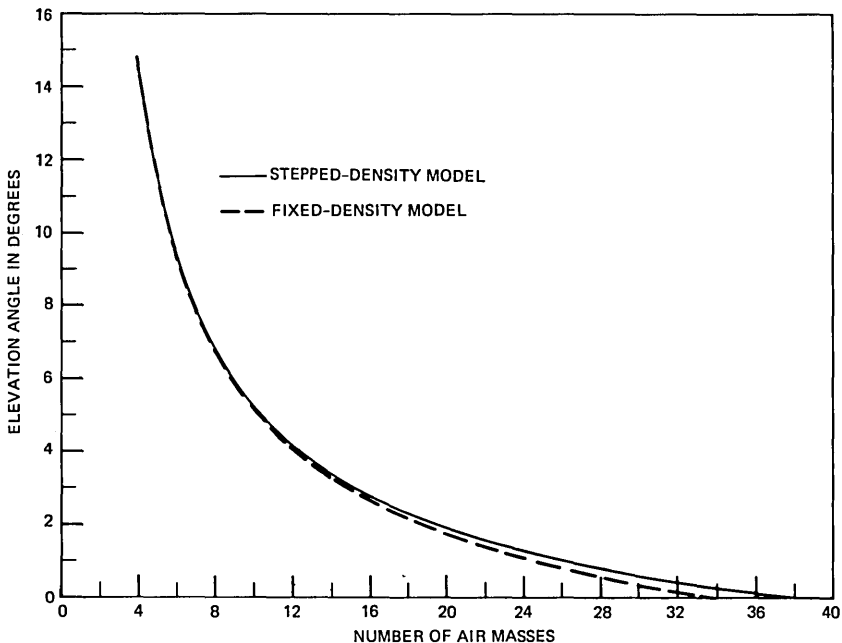
Fig. 2—Path elevation angle vs. number of air masses for stepped-density and fixed-density atmospheric models.

at higher elevation angles,[4] owing to the earth's curvature.

Figure 3 shows a scatter plot of signal fluctuation vs. number of air masses for the combined data from COMSTAR I and COMSTAR II. This figure shows that the fluctuation of the signal increases rapidly as the number of air masses increases. The functional form of this dependence cannot be determined from the available data, but appears to be at least linear. For very low-elevation-angle paths (1 to 1.25 degrees) traversing a large number of air masses (24), the signal fluctuation varies about 0.25. For a significantly smaller number of air masses (i.e., below 8), and relatively higher elevation angles (above 6.50 degrees), the fluctuation decreases to around 0.05.

Results for both received polarizations show that fluctuations with number of air masses for the two polarizations are nearly identical. Instantaneous correlation coefficients between the polarizations were typically above 0.95 when the fluctuations were also large compared with the receiver noise level (i.e., at low-elevation angles). It thus appears that the cause of the fluctuation is not dependent on the state of the polarization—vertical or horizontal. This is the first known observation of this polarization independence for elevation angles below 5 degrees.
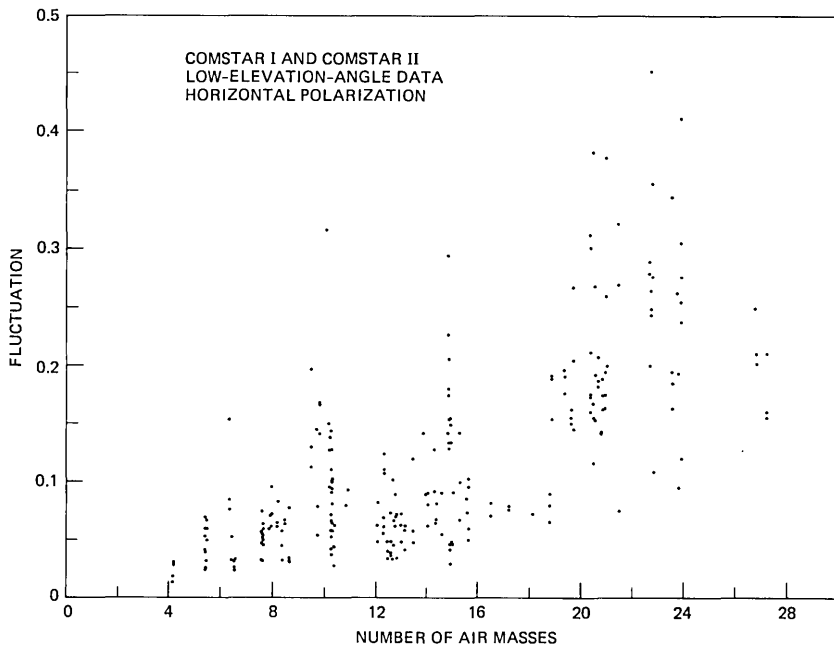
Fig. 3—19-GHz signal amplitude fluctuation vs. number of air masses along path for combined COMSTAR I and COMSTAR II data using horizontal polarization.

IV. CONCLUSIONS

Two conclusions can be drawn from this experiment. One is that the signal fluctuation is independent of polarization. Two facts lead to this conclusion: (i) there is a very high correlation between signal strengths at the two polarizations; and (ii) the results for fluctuation vs. number of air masses were nearly identical for the two polarizations. The second conclusion is that fluctuation intensity increases at lower elevation angles. This increase is consistent with the increase in the number of air masses along the path.

REFERENCES

1. W. J. Vogel, A. W. Straiton, and B. M. Fannin, "ATS-6 Ascending: Near Horizon Measurements over Water at 30 GHz," Radio Science, *12* (September–October 1977), pp. 757–65.
2. H. W. Arnold, D. C. Cox, and D. A. Gray, "The 19 GHz Receiving System for an Interim COMSTAR Beacon Propagation Experiment at Crawford Hill," B.S.T.J., *57,* No. 5 (May–June 1978), pp. 1331–39.
3. Kenneth Davies, *Ionospheric Radio Propagation,* Chapter 6, Washington, D.C.: U.S. Government Printing Office, 1965.

4. H. W. Arnold, D. C. Cox, and A. J. Rustako, Jr., "Rain Attenuation at 10–30 GHz Along Earth-Space Paths: Elevation Angle, Frequency, Seasonal and Diurnal Effects," IEEE Trans. Commun., *COM-29* (May 1981), pp. 716–21.